THIRTY-FIRST QUARTERLY
AND EIGHTH ANNUAL REPORT

to Sponsors of

The Institute for the Study of Metals

THE UNIVERSITY OF CHICAGO

FOR PRIVATE CIRCULATION ONLY

DECEMBER 1953

All articles contained herein have been submitted for publication in some professional journal, as indicated under the title of each article. It is urgently requested that no public reference to these articles be made until after their publication and that reference then be made to the appropriate periodical.

* * *

Acknowledgment is made to the following organizations for their sponsorship of the Institute for the Study of Metals as a whole:

Aluminum Company of America
Aluminium Laboratores, Ltd.
American Can Company
Bethlehem Steel Company
Copper and Brass Research Association
Crane Company
E. I. DuPont de Nemours and Company
General Motors Corporation
Inland Steel Company
International Harvester Company
Motorola, Inc.
Pittsburgh Plate Glass Company
Standard Oil Company (Indiana)
Standard Oil Development Company of New Jersey
Union Carbide and Carbon Corporation
United States Steel Corporation
Westinghouse Electric Corporation

Acknowledgment is also made to the following:

The U. S. Office of Naval Research for sponsorship of a program on the deformation of metals [Contract No. N-6ori-02004, NR 019 302 and War Department Contract No. TB4-2] and on high pressure research [Contract No. N-6ori-20-XX];

The U. S. Air Research and Development Command for their support of our metal surface reaction research [Contract No. AF33(616)-2090] and of our boron in steel program [Contract No. AF18(600)-12];

The U. S. Atomic Energy Commission for their support of research on graphite [Contract No. AT(1101)-96];

Office of Ordnance Research, U. S. Army for its support of research on grain boundaries [Contract No. DA-11-022-ORD-834].

CONTENTS

I

CONSTITUTION OF IRON-BORON ALLOYS IN THE LOW BORON RANGE*

M. E. Nicholson

(Submitted to Trans. A.I.M.E.)

Abstract

The solid solubility of boron in iron has been determined by saturating iron with respect to Fe_2B at several temperatures from 870° to 1135°C. In alpha-iron the maximum solubility was found to be 0.002 per cent B and in gamma-iron the solubility varied from 0.001 per cent at 915°C to 0.020 per cent B at 1165°C. The eutectic and peritectoid temperatures were found to be 1165° and 911°C respectively and the gamma-iron solidus was located approximately at 0.020 per cent B.

Recent investigations of boron-treated steels[1,2] indicate that the solubility of boron in austenite is of the order of 0.003 per cent at 900°C. This has led to the general belief that the solubility of boron in alpha and gamma iron is considerably less than that indicated by Wever and Müller.[3] Therefore the solid solubilities of boron in alpha and gamma iron have been redetermined. The eutectic and peritectoid temperatures were also remeasured and the gamma-iron solidus was studied in some detail.

In 1929 Weber and Müller investigated the phase equilibria of iron-boron alloys. Figure 1 shows the solid solubility region of the iron-boron diagram based on their investigation. They found that boron lowered the A_4 transformation temperature to 1381°C where saturated delta solid solution "which must contain about 0.15 per cent B" and "gamma solid solution containing about 0.10 per cent B" are in equilibrium with liquid containing 1.9 per cent B. At the eutectic temperature of 1174°C, gamma solid solution was found to contain "about 0.15 per cent B." A peritectoid relation was found to exist between alpha and gamma iron with an invariant temperature at 915°C, where the boron solubility in gamma iron was "about 0.10 per cent B" and the solid solubility in alpha iron "did not exceed 0.15 per cent B." Although most of their investigation was made using thermal analysis and metallography, the solid solubility of boron in alpha iron was established using X-ray lattice parameter measurements.

Because of the apparent success of Wever and Müller in using the X-ray lattice parameter technique as a means of determining the limit of solid solubility in alpha iron, several precision lattice parameter measurements were made of a decarburized high-purity iron and an iron-0.011 per cent boron alloy.

The iron-boron alloy was prepared by boronizing (as described below) a rod of decarburized iron to produce a case of iron boride, Fe_2B, and annealing it in vacuo at 1100°C until the core was saturated with boron. The iron-boron alloy was then annealed a second time in vacuo for 60 hours at 905°C and quenched into oil. 350-mesh filings of this alloy and of the specimen of iron were then mixed with fine alundum powder to prevent sintering

* This work was partially supported by the Aeronautical Research Laboratory, Wright-Patterson Air Force Base, Ohio, under Contract AF 18(600)-12.

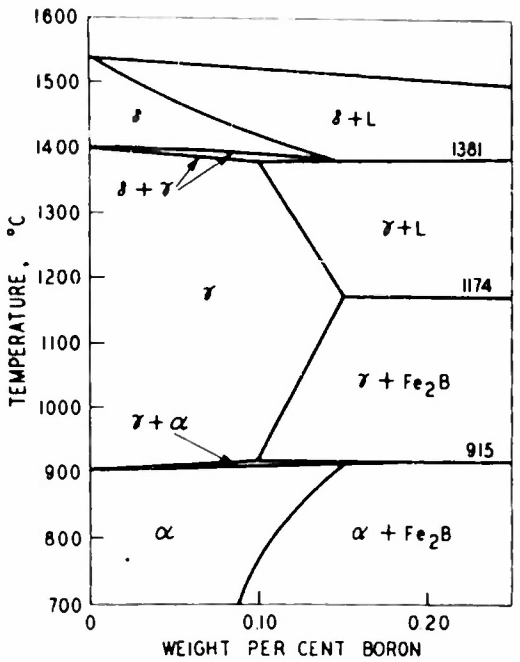

Fig. 1. Portion of iron-boron equilibrium diagram after Weber and Muller.[3]

and grain growth during the final heat treatment. The powders were finally heated in purified helium for 15 min at 905°C and quenched into brine, after which the metal filings and alundum were separated magnetically. Lattice parameter measurements were made of the two samples, using a 50 mm back reflection focusing camera and unfiltered cobalt and chromium characteristic radiations. The lattice parameters of the alloys were computed by using Cohen's least squares method, yielding the following values:

$$\text{Iron at } 20^{\circ}\text{C} = 2.8664 \pm 0.0001\text{Å}$$

$$\text{Fe-B alloy at } 20^{\circ}\text{C} - 2.8665 \pm 0.0001\text{Å}$$

Since the difference between these values was so small, it was concluded that the X-ray method was unsatisfactory for studying the variation of the solid solubility of boron in iron with temperature.

A more suitable method for investigating the extremely limited solid solubility of boron in iron was considered to be by means of a chemical analysis of the saturated solid solution. In addition to the investigation of the solid solubility of boron in iron, the peritectoid and eutectic temperatures were measured by standard thermal analysis. Metallographic techniques were used to establish the location of the gamma solidus line and to verify the eutectic temperature.

Experimental Details and Results

Determination of Solid Solubility of Boron in Alpha and Gamma Iron: In a two-component system the solid solubility of a terminal solid solution may be determined by allowing diffusion to occur between a pure metal and the intermediate phase which may co-exist until equilibrium is reached,

and then analyzing the saturated solid solution for the solute element. For determining solid solubility of boron in iron, the diffusion couple should consist of iron and iron boride, Fe_2B.

To make the couples, pieces of vacuum-melted high-purity iron cut from a 3 in. diameter ingot obtained from the National Research Corporation of Cambridge, Mass., were swaged into rods about 1/4 in. in diameter. The iron ingot had the following analysis: 0.0035 per cent C, 0.001 per cent Mn, 0.008 per cent Si, 0.054 per cent Ni, 0.001 per cent Mg, 0.001 per cent Cu, 0.005 per cent O, and 0.00015 per cent N. Three-inch lengths of the iron rods were placed in an alundum boat and surrounded with boron powder obtained from the Cooper Metallurgical Associates, Cleveland, Ohio, designated as Grade A 325 mesh powder. This boron contained 0.22 per cent C and 0.38 per cent Fe and 99.30 per cent B. The specimens were then heated in a dry hydrogen atmosphere at a temperature of 900°C for 2 or 3 hr. As a result of this treatment* an iron boride case approximately 0.005 in. thick was produced on the surface of the iron rods, such as shown in Fig. 2.

Fig. 2. Microstructure of a high purity iron boronized 3 hours at 900°C showing iron boride, Fe_2B, case. Etched with picral-nital duplex etch, X150.

X-ray diffraction of the case showed it was completely Fe_2B. Thus this technique, which will be referred to as boronizing, was suitable for producing the desired couples for the solid solubility studies. The method had two advantages over the normal welding technique for producing diffusion couples. First, it produced an iron-iron boride interface which was continuous and free from contaminants such as B_2O_3; second, as chemical analysis showed, the case was formed without measurable carbon pickup. Thus the contaminant which had been considered a major cause of error in earlier determinations of Fe-B phase equilibria was eliminated.

Although no detailed study has been made of the gas transfer process, several characteristics of the process were noted. It was found that virtually

---

* Previous work at this Institute by S. Harper had shown the feasibility of this method.

no boron was transferred to the iron if the treatment was carried out in vacuum or in helium. Even in a hydrogen atmosphere, boron transfer was negligible unless the iron was intimately surrounded with boron powder.

The iron-iron boride specimens were annealed in vacuo for periods listed in Table I. Calculated from data of Wells,[4] all specimens were annealed for periods sufficient to saturate the iron. The sample shape and size were chosen so that (1) after boronizing and annealing to saturation a metallographic specimen could be taken for determining the iron boride case depth; (2) the iron boride case could be easily and completely removed;

TABLE I

Data for Solid Solubility Determination

Saturation Anneal		Spec.	Analysis, Weight Per Cent			
Temp. °C	Time Hrs.	Dia., In.	Boron	Oxygen	Equiv. B.	"O Free" B
1135	6.0	0.06 +	0.019	---	---	---
1125	48	0.25	0.015	0.0036	0.0016	0.0134
1125	48	0.25	0.015	0.0058	0.0026	0.012
1100	30	0.18	0.013	0.0043	0.002	0.010
1100	30	0.18	0.012	0.0038	0.0017	0.011
1100	30	0.18	0.011	Al treated		
1100	30	0.18	0.010	" "		
1075	72	0.25	0.0095	0.0036	0.0016	0.0081
1075	72	0.25	0.010	0.0053	0.0024	0.0076
1000	85	0.18	0.0044	0.0046	0.0021	0.0023
1000	85	0.18	0.0057	0.0047	0.0021	0.0036
1000	85	0.18	0.0031	Al treated		
1000	85	0.18	0.0032	" "		
925	165	0.18	0.0032	0.0044	0.0020	0.0012
925	165	0.18	0.0033	0.0048	0.0022	0.0012
925	165	0.18	0.0036	Al treated		
900	72	0.18	0.0043	0.0046	0.0021	0.0022
900	72	0.18	0.0039	0.0045	0.0020	0.0019
900	72	0.18	0.0020	Al treated		
900	72	0.18	0.0017	" "		
870	175	0.18	0.0038	0.0050	0.0022	0.0016
870	175	0.18	0.0038	0.0046	0.0021	0.0017
870	175	0.18	0.0022	Al treated		
800	D	---	0.0022	0.0017	0.0008	0.0014

+ Flat Specimen

and (3) samples could be prepared for chemical analysis without contamination. After the saturation anneal, a metallographic specimen from the middle of the rod was examined to determine the maximum depth of case. Generally, 0.005 in. more than the maximum case depth was removed by grinding to completely remove the iron boride case. After removing the case, an additional 0.005 in. was turned off on a lathe to remove any metal which may have had embedded Fe_2B particles. A sample of about 100 milligrams was then carefully turned off for chemical analysis.

Boron analyses were made using the colorimetric (quinalizarin) technique developed by the Youngstown Sheet and Tube Company and described by Dean and Silkes.[5] However, it was modified to the extent that a photodensitometer was used for measuring densities of the final solution. The densities were measured at a wavelength of 610 millimicrons. Using boron-steel samples obtained from the National Bureau of Standards, the colorimetric method was found to have an accuracy of about 10 per cent at concentrations of 0.004 per cent B and about 20 per cent at concentrations of 0.001 per cent B. The results of saturation experiments are shown in Table I and are presented graphically in Fig. 3. The 800°C data were obtained from diffusion data of boron in iron.[6]

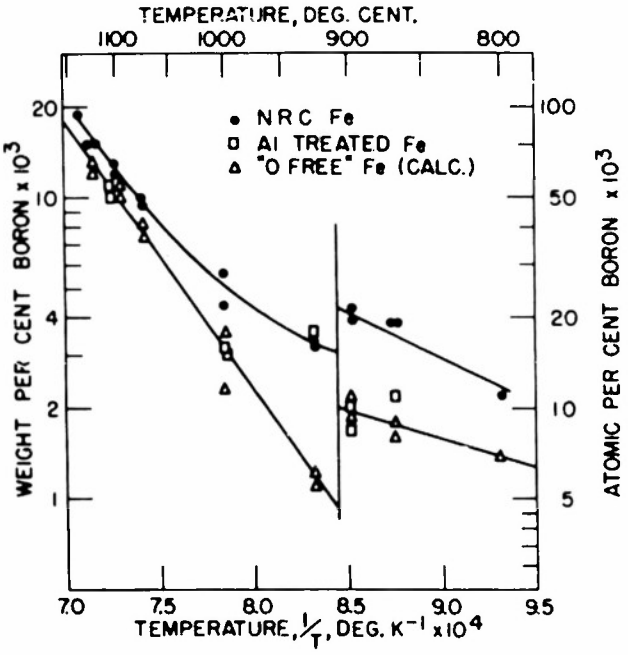

Fig. 3. Logarithm of boron content of saturated iron specimens and corrected boron content plotted as a function of reciprocal temperature.

To determine whether the calculated annealing times were sufficient to saturate the core of the solid solubility specimens, chemical samples were taken from the outside of the core (after removing the case) and the center from several annealed rods. Analysis of these samples showed the boron content of the center was higher than that of the outside. It was suspected that an impurity such as oxygen which was more concentrated at the center than at the outside was precipitating as a boron compound.

To determine whether oxygen was affecting the boron content of the iron, several solid solubility samples of low oxygen iron were prepared

from an aluminum-treated iron. To prepare this alloy, 150 grams of high purity iron was induction-melted in vacuo in a recrystallized alumina crucible. When the iron was molten, 5 g of an Fe-10 per cent Al alloy was added. The ingot was homogenized in vacuum and finally swaged to 0.180 in. diameter. Analysis of this ingot showed 0.124 per cent free aluminum and 0.028 per cent Al_2O_3. The boron analyses of the aluminum-treated specimens are included in Table I and Fig. 3 and shown graphically in Fig. 4, where the boron content of several alloys is plotted as a function of oxygen content. The uncombined oxygen of the aluminum-treated specimens

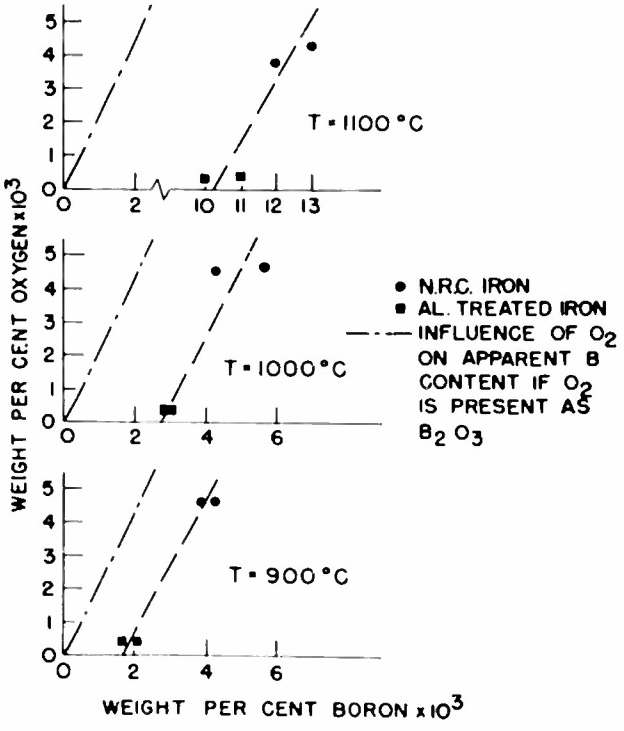

Fig. 4. Influence of oxygen content on boron content of saturated iron specimens.

was assumed to be less than 0.0005 per cent. At the left a line has been drawn which has for its slope the combining ratio of oxygen to boron in B_2O_3. This slope equals 2.18 wt. % O/wt. % B. From these data which indicate that oxygen in the iron combines stoichiometrically with boron to form B_2O_3, it was apparent that to obtain the solid solubility of boron in iron, the boron contents of the iron specimens would have to be corrected for the influence of oxygen. The oxygen content of the solid solubility specimens was measured by vacuum fusion analysis. These data are shown in Table I as well as the corrected or oxygen-free boron contents.

Determination of the Eutectic and Peritectoid Temperatures: The eutectic temperature was determined by thermal analysis, using a vacuum-melted iron 3.5 per cent boron alloy which was remelted in vacuo in a recrystallized alumina crucible. The temperature was measured by means of a platinum-platinum-10 per cent rhodium thermocouple which was protected by an alundum protection tube. The alloy was heated to 1250°C and allowed to cool at about 0.3°C per min. Although the sample was not stirred during cooling, only a slight super-cooling occurred. At 1159°C the temperature remained invariant for 15 min.

The eutectic temperature was also checked metallographically using alloy iron-0.6 per cent boron alloy. The alloy was first cold-worked and homogenized at 1100°C to destroy the eutectic structure of the ingot. Quarter-inch diameter wafers 1/8 in. thick were heated at the desired temperature in purified helium for from 10 to 30 min and then slowly cooled. Furnace temperatures were measured with a calibrated platinum-platinum-10 per cent rhodium thermocouple. At 1160°C no melting was observed. At 1165°C, after 10 min, some melting occurred as indicated by small areas of a eutectic in the microstructure of the sample. The sample heated for 10 min at 1170°C showed a complete eutectic network. Thus the eutectic temperature was considered to be 1165° ± 5°C.

The influence of boron on the A_3 transformation of iron was studied using a differential method of thermal analysis in which the transformation of an iron-boron alloy was compared with the transformation of iron. A sample of decarburized iron 1/4 in. in diameter and 5/8 in. long was used as a reference material. The iron was decarburized by treating in wet hydrogen for 24 hr at 850°C followed by a 48-hr treatment in dry hydrogen at the same temperature. A hole 1/10 in. in diameter and 5/16 in. long was drilled on the axis of the sample to accommodate a thermocouple. The iron-boron alloy was made of a similar sample of iron which had been boronized and annealed to saturation at 1125°C, producing an alloy containing about 0.015 per cent B. The samples were placed in contact with 26-gage chromel-alumel thermocouples in a cylindrical block of steel 1 in. in diameter and 3-1/2 in. long which had been split in half longitudinally and machined to accommodate the specimens and thermocouples. The block was supported on a tripod so that it would be centered in the 3-1/2 in. diameter quartz furnace tube. The thermal analysis was performed in vacuo. Instead of using a 3-wire differential thermocouple arrangement, 2 wires were substituted for the common one so that the couples were electrically separate. Temperature measurements of the 2 specimens were made simultaneously, using Type B Rubicon potentiometers. After making several heating and cooling curves, the specimens were interchanged and the measurements repeated. The heating and cooling rate of about 1/4°C per min was controlled using a Wheelco program controller in conjunction with an Exactline.

As a check of the method, an additional run was made using 2 specimens of the decarburized iron. Since iron was used as a reference, the couples were not calibrated. The results are shown in Table II. The tem-

TABLE II

Temperature of α - γ Transformation of Iron and Iron-Boron Alloy Determined by Termal Analysis

Spec.	Direction	Temp. °C	
		T. C. 1	T. C. 2
Fe-B	Heating	913.2	913.5
Fe	"	911.7	912.6
Fe(check)	"	911.8	912.5
Fe-B	Cooling	910.6	911.0
Fe	"	908.5	909.9
Fe(check)	"	909.0	909.9

perature variation between successive runs, made without changing specimen positions, was 0.1°C or less; therefore, data listed are the average of several runs to the nearest 0.1°C. From these data the average temperature difference between Fe-B alloy and the reference iron was:

Heating: 1.2 ± 0.25°C
Cooling: 1.5 ± 0.4°C

The Fe-B alloy transformed at a higher temperature than the transformation of iron, both on heating and cooling.

Determination of the Solidus: The solidus line was determined metallographically at 1185°, 1250°, and 1350°C, using several arc-melted iron-boron alloys. The oxygen content and corrected boron content of these alloys is shown in Table III. The samples were treated at the desired tem-

TABLE III

Analyses of Arc-Melted Iron-Boron Alloys Weight Per Cent

Boron	Oxygen	Corr. Boron
0.021	0.0055	0.018
0.025	0.0061	0.022
0.029	0.0047	0.027
0.035	0.0060	0.032

perature 1/2 hr in purified helium and quenched into brine. Fig. 5 shows the resulting microstructures of iron-boron alloys containing 0.021, 0.025, 0.029, 0.035 per cent B respectively. The top row (Figs. 5a-5d shows the structures of alloys quenched from 1350°C and the lower row (Figs. 5e-5h) shows the structures of the alloys quenched from 1185°C. In the 0.029 and 0.035 per cent B alloys the grain boundary constituent indicates liquid was formed during annealing both at 1185° and 1350°C. On the other hand, the 0.021 per cent B alloy shows no evidence of liquid but only a fine discontinuous grain boundary precipitate typical of iron-boron alloys quenched from high temperatures. The microstructures of the 0.025 per cent B alloy are intermediate between the structures of 0.021 per cent B alloy on one hand and 0.029 and 0.035 per cent B on the other. The grain boundary constituent is more continuous than in the 0.021 per cent B alloy, however it does not exhibit the characteristic appearance of liquids shown in the 0.029 and 0.035 per cent B alloy. It would therefore appear that the 0.025 per cent B alloy must approximate the solidus composition both at 1185° and 1350°C. Microstructures of specimens treated at 1250°C simply served to show that no significant curvature existed in the solidus between 1185° and 1350°C. All of these specimens were first etched with 2 per cent picral and then etched in 2 per cent nital. The picral etches boron-rich phases, but tends to stain ferrite. The nital removes this stain and delineates more clearly the grain boundaries.

Discussion

In Fig. 3 the logarithm of the boron content is plotted as a function of the reciprocal of the absolute temperature. All of the data presented are in reasonable agreement within the error of the analytical method except

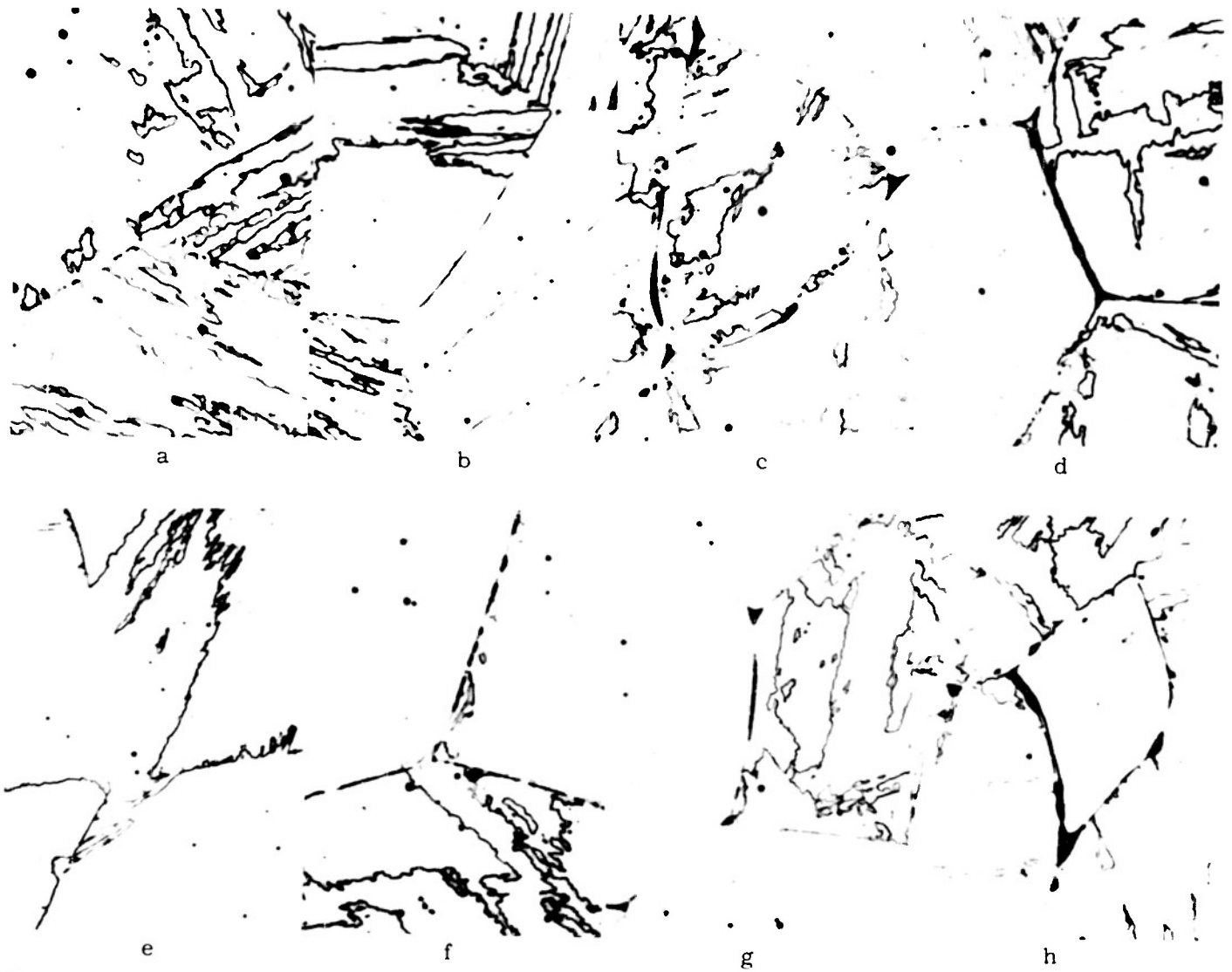

Fig. 5. Microstructures of four iron-boron alloys heated one-half hour at the temperatures indicated and quenched in brine. Left to right: 0.021, 0.025, 0.029, and 0.035 per cent B. Top row: Quenched from 1350°C. Bottom row: Quenched from 1185°C. Etched with picral-nital duplex etch, X300.

that for an aluminum-treated iron saturated at 925°C. This value which is even greater than that for high purity iron at the same temperature appears to be obviously erroneous. For this reason this value was not used in establishing the location of the oxygen-free solubility line. From the figure is is clear that in gamma iron a reasonably linear relation between temperature and composition exists for the oxygen-free solid solubilities, while it does not for the uncorrected ones. This would indicate that the hypothesis regarding the influence of oxygen was correct and that solid solubility of boron in gamma follows the behavior of dilute solutions. The maximum solubility of boron in oxygen-free gamma iron at the eutectic temperature is 0.021 per cent and minimum solubility at the peritectoid temperature is 0.001 per cent. In alpha the maximum solubility which occurs at the peritectoid temperature is 0.002 per cent. The solubility of boron in alpha iron shows a much smaller concentration variation with temperature than in gamma iron.

In considering such limited solubilities as those in the iron-boron system, the question arises whether the data represent bulk solubilities or grain boundary concentrations of solute. If the grain boundary concentration of boron is considerably higher than that of the bulk, then it would be expected that the determined concentrations should vary with the ratio of grain boundary area to volume. A measurement of this ratio using the method of Smith and Guttman[7] for all of the alloys treated below the peritectoid temperature showed the variation of this ratio was from 4.9 mm^{-1} to 13.5 mm^{-1}. For this variation in surface-to-volume ratio there was no observed change in boron content. However, grain boundary absorption of considerable magnitude could exist for such surface-to-volume ratios and still have any related variation in boron content obscured by the error of the analytical method. Using 0.0003 per cent boron as being the minimum variation which could be considered significant and the above surface-to-volume ratios, a simple calculation shows that 10 per cent of the boron in the sample would have to be absorbed at grain boundaries to be detectable. This absorption is sufficient to form a monolayer of boron at the grain boundary.

The solubility data indicate that a peritectoid relationship exists between alpha and gamma iron-boron solid solutions. From the solubilities which exist at the transformation, one may calculate approximately the change in the transformation temperature produced by the solid solution of boron. Using a modification of the Van't Hoff equation,[9]

$$\Delta T = -\frac{RT^2}{H_{Tr}}\frac{\Delta[B]}{100}$$

where ΔT is the change in temperature of transformation; T, the transformation temperature of pure iron; ΔB the difference between the boron content of gamma iron and boron content of alpha iron in equilibrium with it, in atomic per cent; and H_{Tr} the heat of transformation of iron. Using the following values, T = 1183, B = 0.005 $\pm$ 0.0015, H = 212 $\pm$ 30, one obtains the value of T = 0.7 $\pm$ 0.3°C. Thus the theoretical value of ΔT agrees fairly well with the experimental one, considering the error in both of these values. The fact that in every determination both on heating and cooling (at 1/4°C/min), the iron-boron alloy transformed at a temperature above that of the reference iron clearly supports the solid solubility evidence that a peritectoid relation exists between alpha and gamma iron-boron solid solutions. With reference to the temperature of the A_3 of pure iron, 910°C, as determined by Wells et al,[10] the peritectoid becomes 911.3 $\pm$ 0.4°C.

In connection with the location of the solidus line, as in locating the solid solubility line, it was necessary to appraise the influence of oxygen of the liquid-solid equilibrium and what fraction of the total boron was effective as a solute element. In view of the fact that the oxygen content was small in these alloys, it was assumed that it did not affect the equilibrium relations, but that it only reduced that effective boron content of the alloys by combining with boron as B_2O_3. Therefore the position of the solidus was drawn using the calculated oxygen-free boron contents of the 0.025 per cent B alloy, i.e., 0.021 per cent B. When the solidus was so constructed, the triple point as determined by the intersection of the solidus and the eutectic temperature falls slightly (0.001 per cent B) to the right of the triple point determined by the intersection of the solid solubility line and the eutectic temperature.

The phase relations of iron-boron alloys based on this work are shown in Fig. 6.

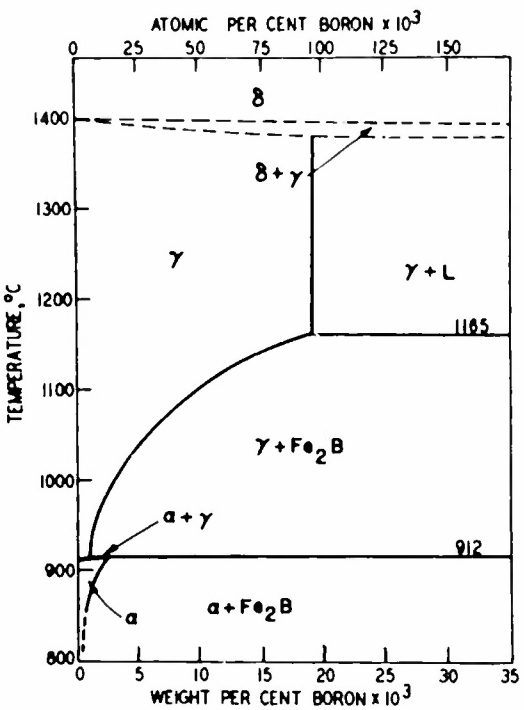

Fig. 6. Iron-boron constitution diagram in the low boron range based on this investigation.

Acknowledgments

The author appreciates very much the helpful discussions which he had with many members of the Institute for the Study of Metals and wishes to thank those who so willingly cooperated in the preparation and analysis of these alloys. Special thanks are due Mr. Adolph A. Roman who performed the colorimetric analyses, Mr. K. K. Ikeuye who prepared some of the alloys, and Mrs. Betty Nielsen who prepared the photomicrographs.

References

1. C. Wells, Private Communication.
2. R. A. Grange and T. M. Garvey, Factors Affecting the Hardenability of Boron-Treated Steels. Trans. A. S. M. (1946) 37, 136-191.
3. F. Wever and A. Müller, The Binary System, Iron-Boron, etc. Mitt. K. W. I. Eisenforsch.(1929) 11, 193-223.
4. C. Wells, In press A.I.M.E.
5. R. S. Dean and B. Silkes, Boron in Iron and Steel. U. S. Bureau of Mines Inf. Cir. 7363, Sept. 1946.
6. P. Gordon, Private Communication.
7. C. S. Smith and L. Guttman, Measurement of Internal Boundaries in Three-Dimensional Structures by Random Sectioning. Trans. A.I.M.E. (1953) 197, 81-87.
8. C. Kubaschewski, The Atomic Heats of Several Metals, Zeit. f. Metallkunde (1950) 41, 445.
9. G. N. Lewis and M. Randall, Thermodynamics, McGraw-Hill, New York (1923) 238.
10. C. Wells, R. A. Ackley, and R. F. Mehl, A Dilatometric Study of the Alpha-Gamma Transformation in High Purity Iron. Trans. A. S. M. (1936) 24, 46-66.

II

LIGHT SCATTERING IN LIQUID HELIUM

A. W. Lawson and Lothar Meyer
(Submitted to The Physical Review)

Abstract

Classical formulas appear to describe adequately the data reported here on the relative scattering of light by liquid and gaseous helium. Anomalous scattering at the λ-point, if present, is less than the relatively large experimental error of about 20 per cent.

The light scattering of liquid helium has been discussed theoretically by Goldstein,[1] Schiff,[2] Galanin,[3] and Ginsburg.[4] The lowest predicted value for the scattering is given by Rayleigh's classical theory of density fluctuations.[5]

According to this approach, the fraction of light scattered per unit volume, per unit solid angle, is given by

$$i/I = \frac{\pi^2}{18 \mu_o^4 \lambda_o^4} (\mu_o^2 - 1)(\mu_o^2 + 2)^2 kT\chi \qquad (1)$$

where μ_o is the index of refraction corresponding to the wavelength λ_o of the scattered light, k is the Boltzmann constant, T the absolute temperature, and χ is the isothermal compressibility. Despite the fact that the temperature of liquid helium is considerably less than its Debye temperature, Brillouin* has demonstrated that Eq. (1) is still valid in this temperature range for optical wavelengths. If, however, the λ-point phenomena are related to the condensation of an ideal Bose-Einstein gas, the scattering below the λ-point should be by orders of magnitude higher and critical opalescence should be expected at the λ-point itself.

Two experimental observations of the light scattering in liquid helium are recorded in the literature: one by McLennan, Smith, and Wilhelm[6] and the other by Jakovlev.[7]

McLennan, Smith, and Wilhelm found that the intensity of the light scattered by liquid helium could not be distinguished from the background in their experiment, which indicates that the scattering is of the order of magnitude given by Eq. (1). Jakovlev, comparing visually the scattering of air with that of liquid helium, came to the same conclusion.

We have measured the light scattering of liquid helium in a more quantitative manner. The apparatus is shown schematically in Fig. 1. The scattering chamber consisted of the lower end of a thin-walled stainless steel tube 1 in. o.d., with a quartz window on top and another at the side.

---

* Brillouin's theory (Annales de Physique 17, 88 (1922)) does not include zero-point energy as it is based on classical quantum theory. Introduction of the zero-point correction into his theory affects the values computed by Eq. (1) by less than 5 per cent.

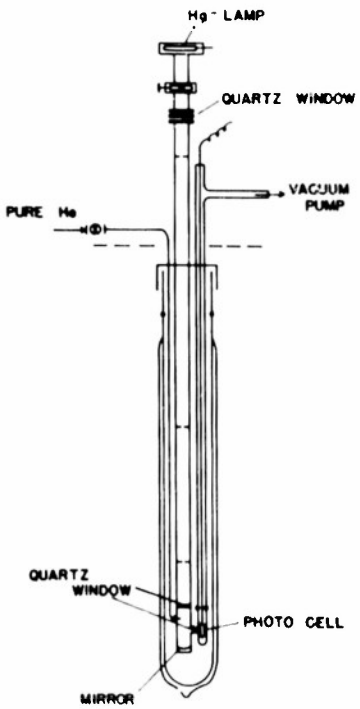

Fig. 1. Apparatus for measuring the scattering of light by liquid helium.

These windows were mounted on the metal with "Araldyte" plastic.* A concave surface mirror on the bottom of the scattering chamber reflected the light beam back out of the cryostat. A high pressure H-4 mercury arc lamp mounted outside the cryostat at the top of the stainless steel tube served as light source. A metal stopcock was used as light switch. No effort was made to use monochromatic light, as the available intensity at all wavelengths was needed to achieve adequate sensitivity. The scattered light was measured with a photomultiplier tube #P-28 mounted immediately in front of the side window of the scattering chamber. It was separated by a quartz bulb and by high vacuum from the helium bath.# The photo current was measured with a galvanometer arrangement with a sensitivity of 3×10^{-11} amps/mm deflection. The scattering chamber could be filled with helium via a stainless steel capillary. The purification of the helium used for the scattering experiments required extreme care. The helium was first purified under 2000 lbs/sq in. over charcoal at 80°K, and then once more led over well degassed charcoal in a liquid nitrogen bath before entering the vacuum system connected with the scattering chamber. During filling, the gas flow rate had to be kept below 1 liter per minute. The liquid used for the scattering experiments was condensed from this highly purified gas.

The standard equipment for transferring liquid helium into the cryostat, for pumping on the helium bath, etc., are not shown in Fig. 1, nor is the dewar with liquid nitrogen surrounding the helium dewar.

As the measurement of the absolute ratio of intensity of the primary beam to that of the light scattered under a 90° angle seemed rather complicated, we preferred to calibrate the system by determining the light scattered by helium gas under 1 atmosphere at its boiling point. By taking the ratio of the light scattered by the liquid at different temperatures, $S_L(T)$, to the light scattered by the gas at the boiling point under the same conditions, $S_g(BP)$, the necessity of knowing the intensity of the primary

* "Araldyte"—trade name of Ciba Company for ethoxyline resins.

\# Originally the photocell was placed directly in the liquid helium surrounding the scattering chamber. Under these conditions the sensitivity of the cell became extremely low and the results were erratic. This behavior is probably due to the fact that the Cs-Sb surfaces of these cells are semi-conductors with an extremely small gap between the valence and conduction bands, and so become practically insulators at helium temperatures. Surrounding the photomultiplier tube with high vacuum was sufficient to keep it at a temperature around 50°K in spite of the fact that the quartz vacuum chamber was covered for more than 10 inches with He II. The latter temperature seemed to provide nearly optimum working conditions for this type of photo-tube, because then the sensitivity was unimpaired and the noise level low.

beam, the geometric factors, etc., is eliminated. Eq. (1) then reduces to

$$\frac{S_L(T)}{S_g(BP)} = \frac{(\varepsilon_L - 1)^2}{(\varepsilon_g - 1)^2} \frac{T}{4.2} \chi_L P_g^* \qquad (2)$$

The results of a typical run are given in Table I.

Within our accuracy of about 20 per cent, the light scattering of liquid helium is in experimental agreement with Eq. (2) if one uses the experimentally determined values for μ_o^2 or ε and χ.[8] No excess scattering larger than our experimental error is observed at the λ-point. This conclusion was confirmed by several runs in which the temperature of the bath was allowed to warm up slowly from 2.1 to 2.2°K during an interval of from 10 to 20 minutes. The galvanometer readings remained constant within the experimental accuracy and did not deviate perceptibly from the normal value as the λ-point was passed.#

It should be emphasized that the principal source of error in this experiment is from impurities. Although it might be presumed that it would be relatively simple to purify helium, our experience indicates that extraordinary precautions must be taken to avoid the introduction of miniscule particles of dust. Any deviation from our strict routine in handling the helium gas inevitably led to a considerably enhanced background scattering.

The results reported here are consistent with those of Taconis[9] and Reekie[10] who were unable to detect any change in the X-ray diffraction pattern of liquid helium at the λ-point.

References

1. L. Goldstein, Phys. Rev. 57, 241 (1940).
2. L. Schiff, Phys. Rev. 57, 844 (1940).
3. A. Galanin, J. Exptl. Theor. Phys. 10, 1267 (1940).
4. V. L. Ginsburg, J. Phys. (U.S.S.R.) 7, 305 (1943).
5. See, for instance, R. H. Fowler, Statistical Mechanics (Macmillan Company, N. Y., 1936) 2nd edition, p. 768.
6. J. C. McLennan, H. D. Smith, and J. O. Wilhelm, Phil. Mag. 14, 161 (1932).
7. I. A. Jakovlev, J. Phys. (U.S.S.R.) 7, 307 (1948).
8. See W. H. Keesom, Helium (Elzevier, Amsterdam, 1942), pp. 136, 319, 134, 236.
9. W. H. Keesom and K. W. Taconis, Physica 5, 270 (1938).
10. J. Reekie, T. S. Hutchison, C. F. A. Beaumont, Proc. Phys. Soc. A 66, 409 (1953).

---

* Eq. (2) is derived by using the ideal gas law. Actually, the deviation from the ideal gas law at the helium BP is about 25 per cent. However, using the second virial coefficient B as measured by Keesom and Walstra (Physica 7, 985, 1940), not only χ_g, but also the value of ε changes, since it has to be calculated from the values given for -191° and 0°C by means of the gas density at 4.2°K. Both corrections cancel each other within 10 per cent, which does not exceed accuracy of our measurements and the accuracy to which the compressibility of the liquid is known.

\# The liquid in the scattering chamber was kept under 1 atmosphere pressure to avoid bubble formation during warming or cooling of the bath, so the λ-point of the liquid helium in the chamber was a few thousandths of a degree lower than that in the bath. In some runs the temperature of the bath was kept as near as possible ($\pm$ 0.003° to the λ-point of the liquid helium in the scattering chamber. Even then there was not the slightest indication of an increase in scattering.

TABLE I

Comparison of observed and calculated values of $S_L(T)/S_g(BP)$

1	2	3	4	5	6	7	8
T °K	P atmos.	Phase	Galv. deflect. in cm	Background deflection in cm	4 minus 5	$S_L(T)/S_g(BP)$ obs.	$S_L(T)/S_g(BP)$ calc. Eq. (2)
4.2	1	gas	3.0_0	2.8_0	0.2_0	$1._0$	
4.2	1	liq.	3.6_0	2.8_0	0.8_0	$4._0$	3.8
2.1	1	liq.	3.0_0	2.8_0	0.2_0	$1._0$	1.0
1.5	1	liq.	2.9_5	2.8_0	0.1_5	0.7_5	0.7

III

THERMAL ANOMALIES ASSOCIATED WITH THE ANTIFERROMAGNETIC ORDERING OF FeF_2, CoF_2, AND NiF_2

J. W. Stout and Edward Catalano*
(To be published in The Physical Review)

From measurements of the magnetic susceptibility of powdered materials Bizette[1] concluded that MnF_2 and FeF_2 are antiferromagnetic, but that the isomorphous compounds CoF_2 and NiF_2 are not. The neutron diffraction studies of Erickson[2] show, however, that at low temperatures all four compounds are antiferromagnetically ordered and magnetic anisotropy measurements[3] on a single crystal of CoF_2 indicate an antiferromagnetic behavior. We have measured the heat capacity of FeF_2, CoF_2, and NiF_2 over the temperature range 12-300°K. Each of these salts shows a pronounced thermal anomaly of the lambda shape characteristic of processes where there is cooperative ordering. The experimental heat capacity data in the neighborhood of the anomalies are shown in Figs. 1, 2, and 3 for

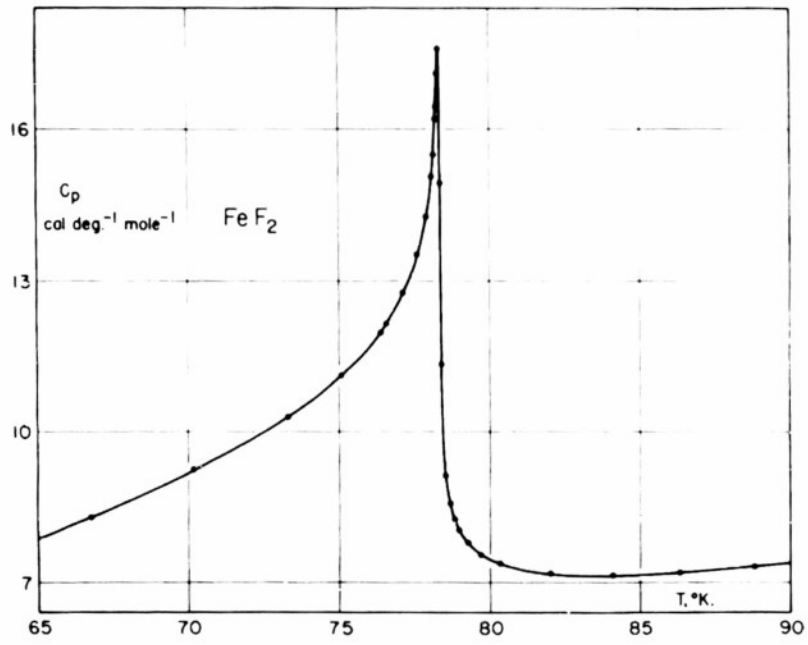

Fig. 1. Molal heat capacity of ferrous fluoride versus temperature.

FeF_2, CoF_2, and NiF_2 respectively. In order to determine the shape of the curves, the points in the regions of rapidly changing heat capacity were

* Eastman Kodak Company Fellow 1951-52; Allied Chemical and Dye Corporation Fellow 1952-53.

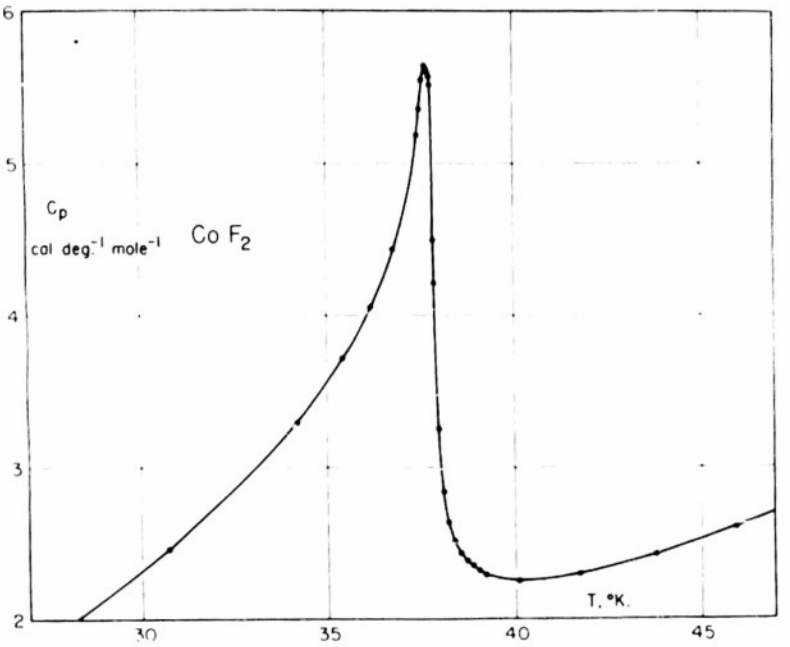

Fig. 2. Molal heat capacity of cobalt fluoride versus temperature.

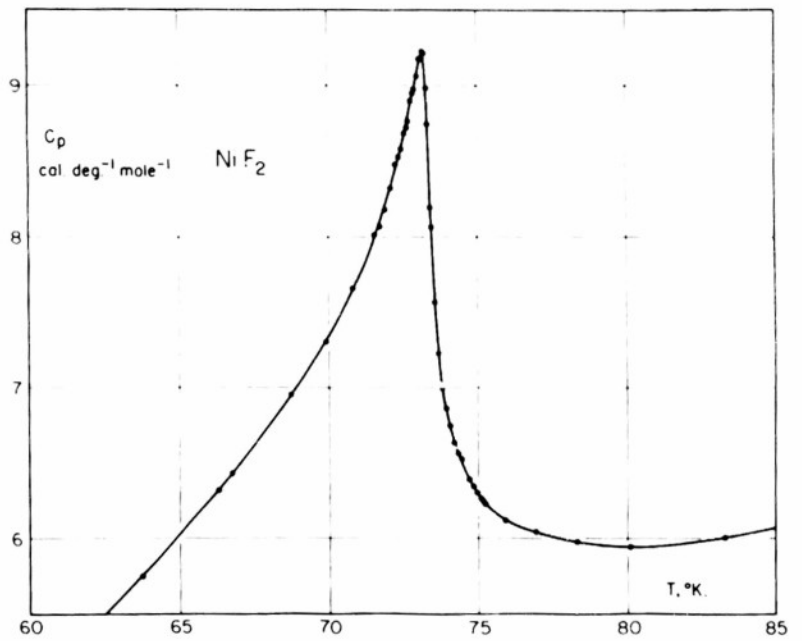

Fig. 3. Molal heat capacity of nickel fluoride versus temperature.

taken with small temperature increments (about 0.1°). The temperatures of the heat capacity maximum are: FeF_2, 78.3°K; CoF_2, 37.7°K; NiF_2, 73.2°K. A similar anomaly in MnF_2 with a heat capacity maximum at 66.5°K has been reported previously.[4] There seems to be no doubt that these anomalies represent the loss in entropy upon passing from the disordered paramagnetic state to the ordered antiferromagnetic state.

The antiferromagnetic Curie temperatures deduced by Erickson[2] from the temperature variation of the magnetic structure factor are higher than those of the maximum in heat capacity by factors ranging from 1.1 to 1.3. However, the neutron diffraction measurements are a relatively imprecise method for determining the Curie temperature and also it seems probable that near the Curie point the magnetic form factor is varying much more rapidly with temperature than the Brillouin function used by Erickson in his extrapolation. We do not believe, therefore, that there is a significant disagreement.

We have also made heat capacity measurements on the diamagnetic salt ZnF_2, which is isomorphous with the four antiferromagnetic fluorides. The data on ZnF_2 will permit an estimate of the entropy and heat capacity arising from lattice vibrations in the antiferromagnetic salts and thus enable the separation of the thermal effects due to the magnetic ordering. The data and calculations will be published in detail elsewhere.

References

1. H. Bizette, Ann. Phys. [12] 1, 295 (1946).
2. R. A. Erickson, Phys. Rev. 90, 779 (1953).
3. J. W. Stout and L. M. Matarrese, Revs. Modern Phys. 25, 338 (1953).
4. J. W. Stout and H. E. Adams, J. Am. Chem. Soc. 64, 1535 (1942).

IV

THE OPTICAL CONSTANTS OF Ag, Au, Cu, AND Al

I. THE ABSORPTION COEFFICIENT k

L. G. Schulz

(Submitted to The Journal of the Optical Society of America)

Abstract

A description is given of a comparison method for determining the values of the absorption coefficient k of a metal relative to previously determined values for Ag. In this method transmission interference filters are constructed which have mica as the dielectric and have reflecting layers of Ag and of the metal x being studied. On adjacent areas of a single sheet of mica, pairs of filters are formed, one with a Ag-mica-Ag combination and the other with a Ag-mica-x combination. Components of a filter pair will have identical mica thicknesses. For a given filter pair the wavelengths transmitted by one combination are compared with those transmitted by the other. Values of k are then calculated from the change in phase accompanying the reflection of light at normal incidence at mica-metal interfaces. The method was found to have special advantages in the wavelength region of 0.65μ to 0.95μ for metals with high reflectivities. Results are given for Au, Cu, and Al in the range of 0.45μ to 0.95μ. The new values of k tend to agree closely with older values obtained by other methods. A discussion is included concerning the validity of surface measurements for determining the bulk properties of metals.

Introduction

In a previous paper[1] an interference method was described for the determination of the absorption coefficient k, and results given for Ag and Al. In the present paper a modification of that method is presented and experimental values given for Au, Cu, and Al. Many of the evaporation and optical procedures which were used are similar to those employed in previous experiments.[1,2,3] Part II of this paper[4] will present the procedure and the results of experiments to determine the index of refraction n.

In the past, with the Drude[5] procedure, both optical constants n and k were determined at the same time on a single sample. In the procedures here employed two rather distinct types of experiments are performed and the results combined to give n and k. In the first type the phase change accompanying reflection at normal incidence is determined, and in the second type the intensity of reflection is measured. In general, since n and k are involved in both types of experiments, it is necessary to carry through the calculations associated with each more or less simultaneously. This separation of the measurements into two types of experiments proved highly advantageous, especially in connection with heat treatment and ageing of samples. It was found that the k values determined in the past are essentially the same as the new values but that the old values of n are often very much higher than the new ones.

The need for the redetermination of the optical constants of metals has been pointed out several times recently.[1,3] These constants, in addition to

being of practical importance in the optical use of evaporated films, are of interest in connection with the theory of solids.[6,7,8] It is this latter interest which has led to the study of the optical properties of metals reported in part in these two papers. The methods developed here, principally for use in the visible region, have been extended to the infra-red where the results are more directly related to the predictions of the free electron theory of metals. These results will be given later.

Description of the Method

Pairs of transmission interference filters[9] having a single mica sheet as the common dielectric for each pair were made with the components arranged as shown in Fig. 1A. On one side of a mica sheet a nearly opaque

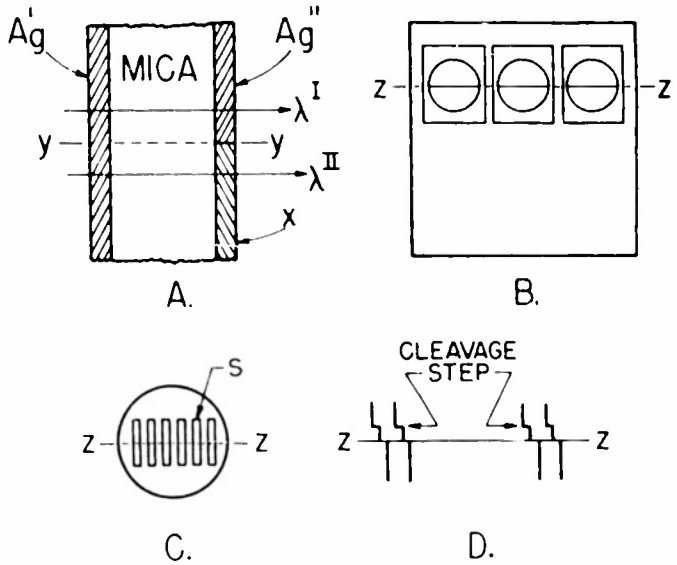

Fig. 1. Details of the filter construction and the arrangement for wavelength measurements. Drawing A shows the arrangement of components in a filter pair; B shows how three such pairs were mounted over holes in a sheet of metal. Drawing C indicates how a survey was made of each sample by moving it with respect to the slit S of the spectrograph to a new position for each photograph. In D the discontinuities in the interference bands of the upper filter reveal the presence of cleavage steps in the mica dielectric.

film of silver, Ag', was formed by evaporation and deposition in a vacuum. Part of the opposite side was covered with silver, Ag", and the remainder with the metal x under investigation. The upper filter with the Ag-mica-Ag sequence will be designated as filter I and the lower, with the Ag-mica-x sequence, as filter II. The transmitted wavelengths λ^{I} and λ^{II} of such a pair were measured, and from these values the absorption coefficient k_x of the metal x was calculated.

The calculation procedure employed was similar to that used earlier,[1] but complications arose here because of the dispersion of the mica. Eq. (1) gives the relation of the wavelengths λ^{I} to the mica thickness t, the mica index of refraction n_o, the order of interference N, and the phase change ψ_{Ag} occurring during the mica-Ag-mica reflection.

$$2n_o^{I} t + \frac{\psi_{Ag}^{I} \lambda^{I}}{2\pi} + \frac{\psi_{Ag}^{I} \lambda^{I}}{2\pi} = N\lambda^{I} \qquad (1)$$

Eq. (2) is a similar equation for λ^{II}.

$$2n_o^{II} t + \frac{\psi_{Ag}^{II} \lambda^{II}}{2\pi} + \frac{\psi_{x}^{II} \lambda^{II}}{2\pi} = N\lambda^{II} \qquad (2)$$

Subtracting Eq. (2) from Eq. (1) and rearranging gives Eq. (3).

$$N(\lambda^{II} - \lambda^{I}) - \left[\frac{\psi_{x}^{II} \lambda^{II}}{2\pi} - \frac{\psi_{Ag}^{I} \lambda^{I}}{2\pi}\right] = \left[\frac{\psi_{Ag}^{II} \lambda^{II}}{2\pi} - \frac{\psi_{Ag}^{I} \lambda^{I}}{2\pi}\right] + 2t\,(n_o^{II} - n_o^{I}) \qquad (3)$$

In Eq. (3) the principal terms are to the left; those to the right are correction terms. The relation of ψ to the index of refraction of the dielectric n_o and the optical constants of the metal, n and k, is given in Eq. (4).

$$\tan\psi = \frac{2k\,n_o}{k^2 + n^2 - n_o^2} \qquad (4)$$

To use Eqs. (3) and (4) it is necessary to have a knowledge of the dispersion of the mica. This was obtained in a preliminary experiment using filters of the type Ag-mica-Ag with the thickness varying from 1μ to 30μ. The results[10] shown in Fig. 2 are in good agreement with those of Einsporn.[11]

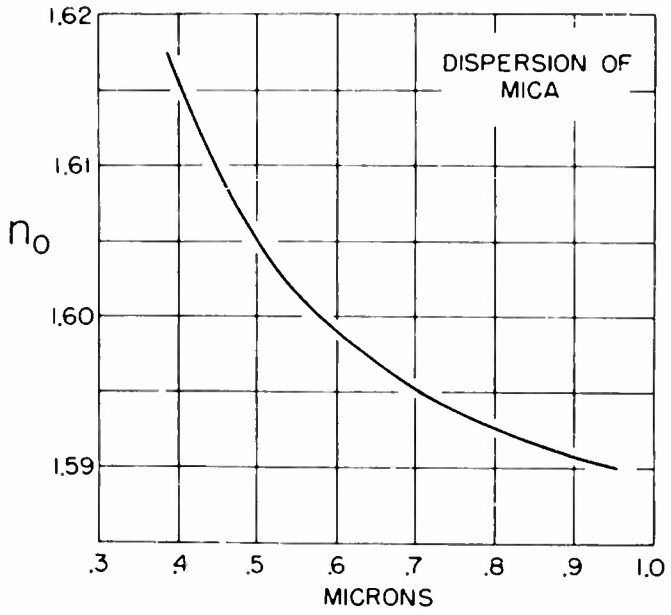

Fig. 2. Graph showing the dispersion of mica. The values shown are for the larger of the two indices of refraction.

(In the calculations the k values of Ag were those found earlier.[1]) For a given wavelength the value of n_o varied slightly from sample to sample, but the dispersion remained unchanged within the experimental error. With the help of Fig. 2 and the experimental values of λ^{I} and λ^{II}, Eq. (3) was used to obtain ψ_x and then Eq. (4) used to calculate k_x. Both n and k appear in Eq. (4), but for wavelengths above about 0.65 microns k^2 is far greater than n^2. Consequently, in the long wavelength region the phase change angle ψ becomes insensitive to n and, accordingly, the interference method can by itself give values of k. In the short wavelength region, however, it is necessary to know n rather accurately; the values used were obtained from the experiments in Part II which were carried out concurrently.

TABLE I

Principal Factors in the Evaluation of the Interference Method. The Drude method was taken as the standard for comparison.

Advantages	Disadvantages
1. No special optical equipment, such as a polarizing spectrometer, is required.	1. A definite lower limit is set by mica transmission at about 0.35 μ and an upper limit is set by available photographic plates.
2. The interface between the mica and metal is ideally smooth.	2. The mica-metal interface must have a reflectivity above about 0.5.
3. Samples can be exposed to air without damaging the metal surface being studied.	3. The metal must be formable as an evaporated film.
4. The method is easily adaptable to photographic procedures.	4. Samples cannot be used for n determinations.

In Eq. (4) the phase change angle ψ is associated with reflections on metal layers of at least opaque thicknesses. Since the experimental method employed here requires that there be transmission of some light through the metal films, a correction is necessary for the error resulting from using non-opaque layers. Convenient graphical methods had been worked out in previous experiments[2] for determining the variation in ψ as the film thickness is changed. In Fig. 3 are shown values of the deviation of ψ from the opaque thickness values for several wavelengths for the case of Au. Since the properties of Au and Cu are similar to those of Ag above about 0.65μ, the thicknesses of x and Ag'' were made nearly equal when studying Au or Cu, thereby causing the phase change corrections to cancel. Below about 0.55μ, for Au and Cu, the correction changes sign and varies with thickness in a way difficult to predict. It is then necessary to know the thickness of the film rather accurately if the proper correction is to be made. In general, the uncertainty in the correction was kept below that resulting from experimental errors in measuring transmitted wavelengths.

It was found possible to modify the method to permit the use of reflection as well as transmission filters. In such a modification, light is incident and is reflected from the Ag' side. The films Ag'' and x of Fig. 1A were opaque in thickness, such films being easier to make than semi-transparent ones. Also, the necessity of corrections of the kind discussed in connection

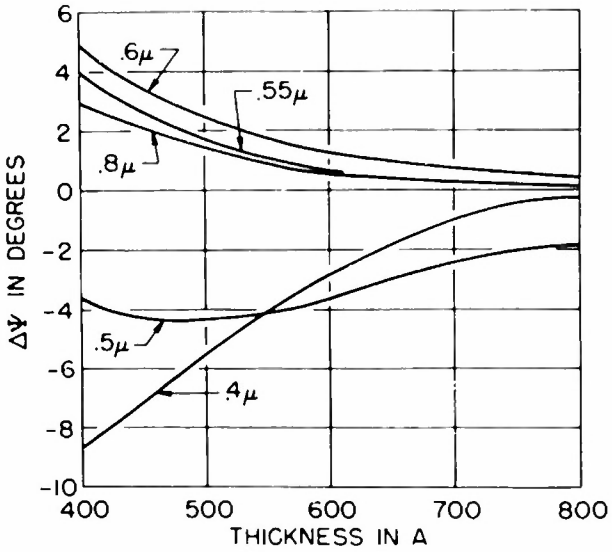

Fig. 3. Graph showing the deviation $\Delta\Psi$ of the phase change angle from the opaque thickness value as the film thickness is varied. For Au the films were usually 500A to 600A thick.

with Fig. 3 are avoided. Great difficulty was experienced, however, in keeping the mica sufficiently plane and, in addition, a more complex optical set-up was required to illuminate the sample.

Although the method has not been used enough to permit a complete evaluation, the comparison with the Drude method[5] given in Table I provides a starting point. There is often a tendency to over-estimate the difficulties of the Drude method, but these difficulties are partly compensated by over fifty years of development, both in experimental techniques and in methods of calculation. It seems clear, however, that the interferometric method has special advantages in the near infrared, 0.65μ to 0.95μ for metals with high reflectivity. The fact that a reference metal, Ag, must be used is not a handicap because there is good agreement among various determinations of the k for Ag.

Experimental Details

The mica used for the dielectric spacer was selected from a large supply of high grade India ruby mica. It was cleaved in air under a binocular microscope, a procedure which avoided the necessity of any subsequent cleaning. Usually three filter pairs were prepared at the same time by mounting three mica pieces covering a range of thicknesses on a holder of the kind shown in Fig. 1B. Experience showed that the optimum thickness was about 5 microns, a thickness which was easy to handle but not so thick as to make inconveniently difficult the measurements of wavelength shifts $\lambda^{II} - \lambda^{I}$ which are inversely proportional to thickness.

The evaporations were made in an 18 in. bell jar unit which could be evacuated to about 10^{-5} mm Hg. The charge to be evaporated was prefused in a preliminary evacuation. In a second evacuation, during which deposition on the mica occurred, a barrier shielded the mica from the initial stream of vapor. Formation of films Ag" and x were made in a single evacuation—suitable mechanical manipulations in the vacuum having been worked out for

this purpose. The deposition of Ag' was made in a third evacuation. Thicknesses of the deposits could be controlled to about ± 50A by weighing the charge. The films were made as thick as possible consistent with reasonable transmission. For Ag'', Au, and Cu this was usually near 600A, for Al near 400A. The thickness of Ag' was usually near 500A, that is, somewhat less than Ag''. It was permissible to have Ag' rather thin since phase changes at mica-Ag'-mica reflections enter only in a dispersion term, the first correction term on the right of Eq. (3).

The wavelengths λ^{I} and λ^{II} were determined photographically with the help of a 21-foot grating (manufactured by Jarrel Ash) in a manner already described.[1] Eastman Kodak plates, types F, N, and M, were used. Since the dispersion of the spectrograph was nearly constant, the wavelength separation $\Delta\lambda = \lambda^{I} - \lambda^{II}$ was easily determined as the product of the linear separation on the plate and the dispersion at that wavelength region. The accuracy was such that the uncertainty in $N\Delta\lambda$ was about 10A in the region of 0.6 to 0.9 microns. Below 0.6μ the uncertainty increased to about 20A for Au and Cu. Because the spectrometer was a grating instrument, the second order of the region 0.35μ to 0.45μ occurred with the first order above 0.7μ. This result was a great help in determining the order number N.

Although the mica was selected to be free from detectable cleavage steps, there was no absolute certainty that some were not overlooked. If a step should run along the line zz which divides filter I from II as shown in Fig. 1B, then an error would result since it was assumed that the thickness t was a constant across zz, or yy of drawing A. To avoid such an error, photographs were taken through each filter pair at many different points along zz as shown in C. The presence of a step would be indicated by a discontinuity in the fringe pattern as shown in drawing D. From a sequence of photographs it was possible to map out the positions of any cleavage step, thereby making it possible to select a fringe system at a point on zz not close to the step.

Results

The values of k which were obtained are given in tabular form in Table II and in graphical form in Figs. 4, 5, 6, and 7 for Ag, Au, Cu, and Al respectively. Also shown on the graphs are some of the most quoted of previous determinations, including values down to 0.25μ. The solid curves represent the new results, whereas broken lines are used to connect sets of earlier results. For the latter, the wavelengths used were often the strong emission lines of Hg.

Silver

Although this metal (which was used as the standard) had been studied earlier,[12] the k values obtained are repeated here for completeness and to enable a comparison to be made with previously determined values. As shown in Fig. 4, in the very much studied visible region of about 0.45μ to 0.65μ, there is excellent agreement with the values obtained by Minor[13] (1903) and Hass[14] (1946), both using a Drude procedure. Whereas the samples of Minor were prepared by chemical methods, those of Hass were formed by evaporation and condensation in a vacuum. The good agreement of the values of Minor with recent values is probably due to the freedom of Ag from oxide films,[1] a circumstance tending to make Ag a suitable metal for a standard. The values of Kretzman[15] are included because there seem to be no others particularly concerned with the region of 0.6μ to 1.0μ.

TABLE II

Values of the Absorption Coefficient k as a Function of Wavelength for Ag, Au, Cu, and Al

λ (μ)	Ag	Au	Cu	Al
.40	1.93	-	-	3.92
.45	2.42	1.88	2.20	4.32
.50	2.87	1.84	2.42	4.80
.55	3.32	2.37	2.42	5.32
.60	3.75	2.97	3.07	6.00
.65	4.20	3.50	3.65	6.60
.70	4.62	3.97	4.17	7.00
.75	5.05	4.42	4.62	7.12
.80	5.45	4.84	5.07	7.05
.85	5.85	5.30	5.47	7.15
.90	6.22	5.72	5.86	7.70
.95	6.56	6.10	6.22	8.50

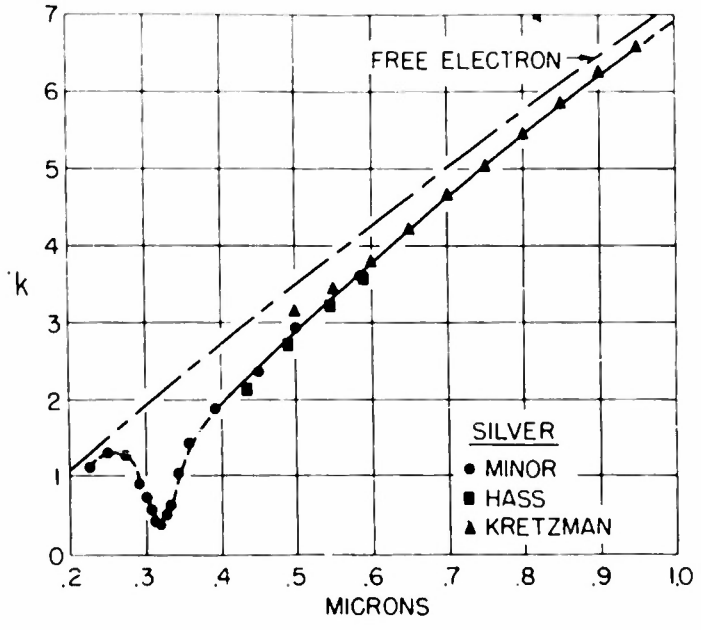

Fig. 4. Values of the absorption coefficient k as a function of wavelength for Ag.

Gold

The values obtained are in fair agreement with those of Meier[16] who used a Drude procedure on metallurgically prepared samples and who worked in the same laboratory as Minor.[13] Also included for comparison in the visible region are the results of Tool[17] who made a particularly careful study of Au and Cu. In contrast to this good agreement in the visible region is the rather large deviation from the values of Kretzman[15] in the infrared. The results in Table II and Fig. 5 are based on measurements made on four samples.

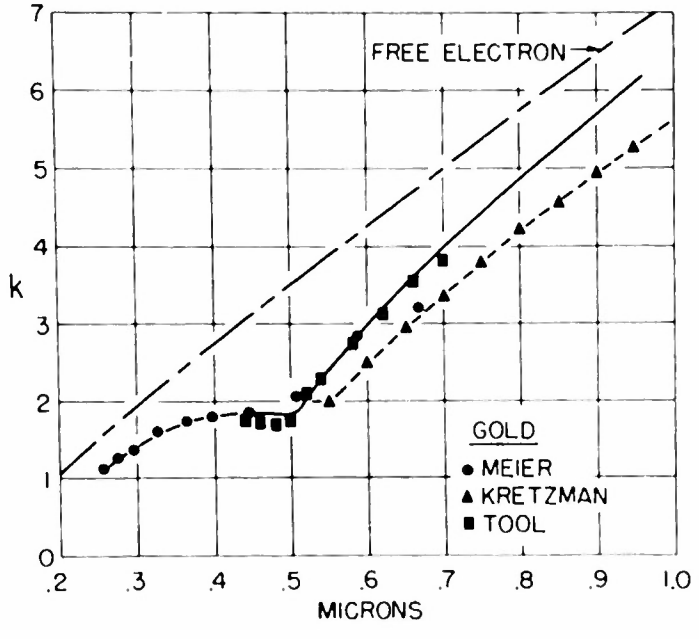

Fig. 5. Values of the absorption coefficient k as a function of wavelength for Au.

Copper

The new values in the visible region are in close agreement with those given by Tool.[17] Minor's values, on the other hand, tend to be low, especially in the red region. (For a summary of many of the older measurements see Nathanson.[18]) The results in Table II and Fig. 6 are based on measurements of four samples.

Aluminum

The broken line refers to an earlier determination with an interferometric method.[1] There is good agreement in the visible region but a wide difference in the infrared. This difference is partly explained by the difficulties in the earlier determination arising from uncertainties in n and from the fall in reflectivity in this region. Also included are two sets of values[14,19] obtained by the Drude method. The results in Table II and Fig. 7 are based on measurements of two samples.

Neither ageing nor annealing produced any change in the experimental values of k for these four metals. This is in contrast to the observed changes in n values which will be discussed in Part II.

Discussion of the Results

It is a satisfaction to find that there is good agreement between the results obtained by two such different methods as the one used here and the

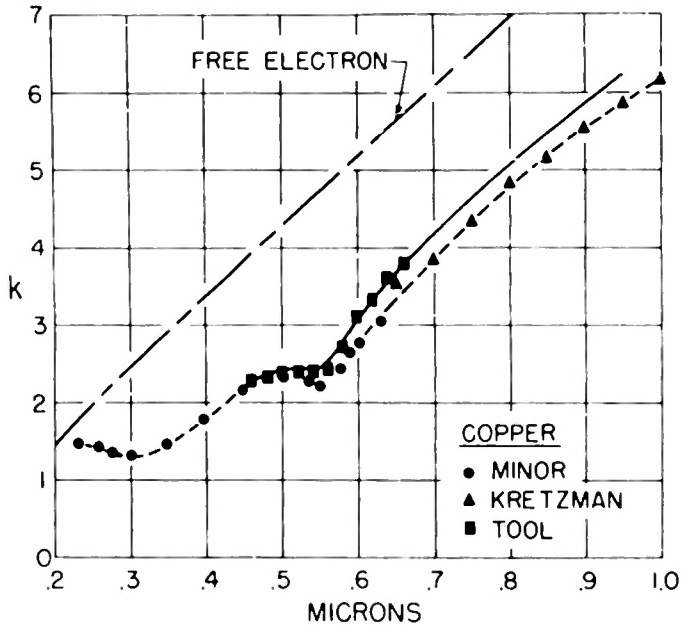

Fig. 6. Values of the absorption coefficient k as a function of wavelength for Cu.

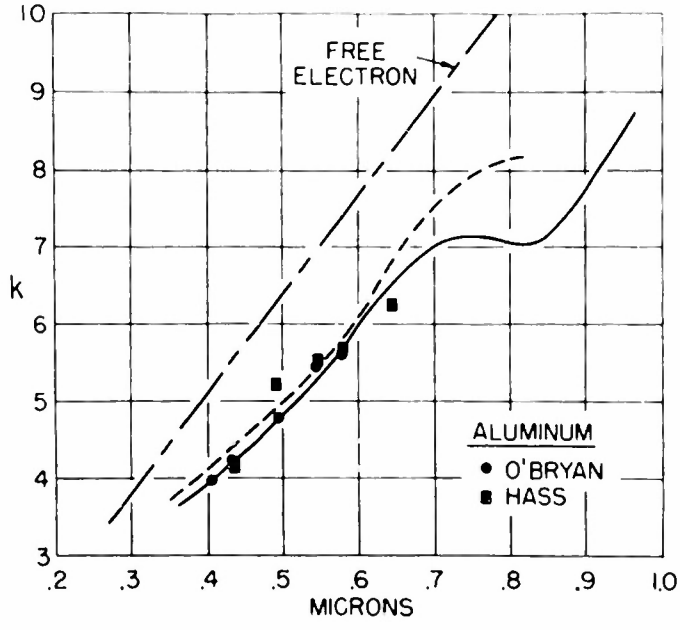

Fig. 7. Values of the absorption coefficient k as a function of wavelength for Al.

older Drude procedure. The variation among the results for the determination of k is much smaller, however, than the variation of n as will be shown in Part II. As the techniques used for sample preparation have improved, the k values obtained have increased. The new values in Figs. 4 to 7 tend to be as high, or slightly higher, than older values. In the comparisons of Figs. 4 to 7, the much quoted results of Försterling and Fréederickszˢ[20] have not been included, since they were most concerned with the region beyond 1μ . Although their measurements extend down to the visible, their method was not at its best here; therefore, a comparison would be unfair to them.

In most of the earlier papers in this field almost fantastic accuracy was claimed. Apparently no consideration was given to errors resulting from sample defects. On the whole, the results in Table II are probably accurate to no better than $\pm$ 2 per cent, which by older standards is a very large uncertainty. This figure, however, includes errors due to sample defects as well as instrumental errors.

Although transmission filters were employed in these experiments, the method used is based on reflectivity measurements. This is clearly shown by the fact that Eq. (5), which was used to calculate k, is concerned with reflectivity. The information given by any reflection experiment is limited to that part of the surface layer to which the incident energy penetrates. Recent theoretical work[21,22,23] has shown that when the mean free path of the conduction electrons in the metal is much longer than the skin depth, anomalous skin effects can be expected. In particular, the value of k determined by a reflection measurement will be lower than the bulk value. It was found that transmission experiments[24] gave higher values of k than did reflection experiments but only in the region where absorption is due primarily to free electron damping. Included on the graphs in Figs. 4 to 7 are the k values calculated from the Drude free electron theory.[6] For Ag at the longest wavelengths, the experimental values approach the calculated ones; for Au the deviation is more pronounced; and for Cu a big difference remains even at 1μ . The case of Al is exceptional in that effects other than those due to free electrons are appreciable even at longer wavelengths.

This research was supported in part by Air Force Contract Number AF33(038)-6534.

References

1. L. G. Schulz, J. Opt. Soc. Am. 41, 1047 (1951).
2. L. G. Schulz and E. J. Scheibner, J. Opt. Soc. Am. 40, 761 (1950).
3. L. G. Schulz, J. Opt. Soc. Am. 41, 261 (1951).
4. L. G. Schulz and F. R. Tangherlini, J. Opt. Soc. Am. 44, (1954).
5. Handbuch der Physik (Verlag. Julius Springer, Berlin, 1928) Vol. 20, Chapter 6.
6. F. Seitz, Modern Theory of Solids (McGraw-Hill Book Company, Inc., New York, 1941), Chapter 17.
7. A. H. Wilson, Theory of Metals (The University Press, Cambridge, England, 1936), Chapter 3.
8. N. F. Mott and H. Jones, The Theory of the Properties of Metals and Alloys, Oxford University Press, New York, 1936) p. 105.
9. L. N. Hadley and D. M. Dennison, J. Opt. Soc. Am. 38, 492 (1948).
10. Mica is double refracting; therefore the transmission bands are always in pairs with components about 15A apart. The larger wavelength of each pair was arbitrarily selected for use in these experiments.
11. E. Einsporn, Physik. Z. 37, 83 (1936).

12. See Reference #1. Fig. 2 presents the results in the form of k/λ vs λ but without an explicit statement of the k values.
13. R. Minor, Ann. Physik 10, 581 (1903).
14. G. Hass, Optik 1, 2 (1946).
15. R. Kretzman, Ann. Physik 37, 303 (1940).
16. W. Meier, Ann. Physik 31, 1017 (1910).
17. A. Tool, Phys. Rev. 31, 1 (1910).
18. J. B. Nathanson, J. Opt. Soc. Am. 28, 300 (1938).
19. H. O'Bryan, J. Opt. Soc. Am. 26, 122 (1936).
20. K. Försterling and V. Fréedericksz, Ann. Physik 40, 200 (1913).
21. G. E. H. Reuter and E. H. Sondheimer, Proc. Royal Soc. 195A, 336 (1948).
22. T. Holstein, Phys. Rev. 88, 1427 (1952).
23. R. B. Dingle, Physica 19, 311 (1953).
24. To be given later.

V

THE OPTICAL CONSTANTS OF Ag, Au, Cu, AND Al
II. THE INDEX OF REFRACTION n

L. G. Schulz and F. R. Tangherlini
(Submitted to The Journal of the Optical Society of America)

Abstract

The reflectivities of Ag, Au, Cu, and Al were measured at an angle of incidence of 45° in the wavelength range of 0.40μ to 0.95μ at glass-metal and air-metal interfaces. These reflectivities, together with previously determined values of the absorption coefficient k, were used to calculate the index of refraction n. Samples were prepared by evaporation and deposition from the vapor. The important experimental results are: (1) The ratios of the reflectivities in the s-plane to those in the p-plane agreed with the theoretical values. This result indicates that the boundary conditions required for the application of the equations of electromagnetic theory have been satisfied. (2) Ageing and annealing resulted in increased reflectivity at both air-metal and glass-metal interfaces. (3) The values of n obtained from aged or annealed samples were in many cases considerably lower than previously published values. A discussion is given of the significance of the results for the study of surfaces and for the theory of metals.

Introduction

The experiments wnich will be described were undertaken for three reasons: First, to develop methods for the accurate measurement of reflectivity; second, to use the method to obtain more accurate values for the index of refraction of metals; and third, to explore the possibility of using oblique illumination for studying the structure of metal surfaces. Although it was not the purpose to develop alternatives to the usual polarimetric method[1] for determining optical constants, it was found that new methods are capable of giving results comparable to, or superior, in accuracy to those found with older methods. The value of the absorption coefficient k determined earlier,[2] together with the index of refraction n obtained here, makes available a complete set of optical constants. In addition to their interest in the field of optics, accurate determinations of optical constants of metals are of importance in the theory of metals.[3-6] Much of the experimental work involved a study of the effect of annealing and ageing on evaporated metal films.

Preparation and Annealing of the Samples

The metals were deposited from the vapor in a vacuum of about 10^{-5} mm of Hg onto part of each of the hypotenuse faces of right-angle prisms (see Fig. 1B). Ag, Au, and Cu were evaporated from shallow v-shaped troughs of sheet molybdenum and Al from 40-mil tungsten wire. The deposits were usually about 1500A to 2000A in thickness, i.e., considerably more than opaque.

Since the part of the metal deposit in immediate contact with the glass substrate is of great importance, every effort was made to keep the glass-

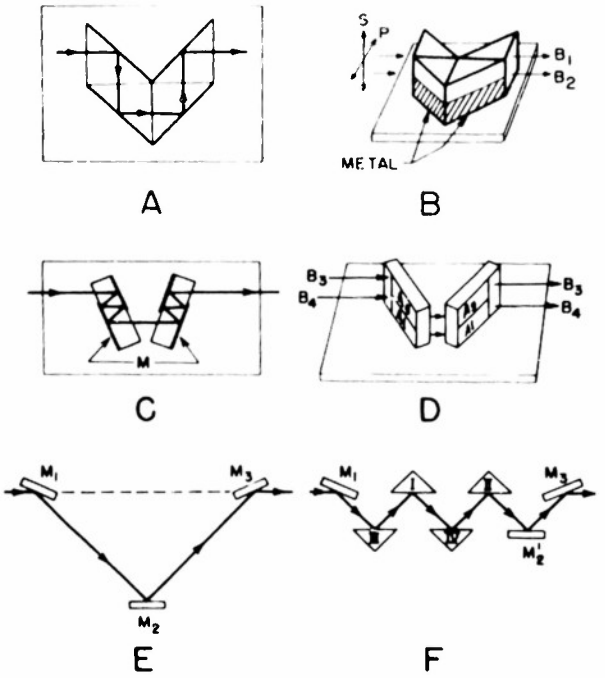

Fig. 1. Drawings showing the optical path through the samples. The prisms of A and B were placed close to one another but not in optical contact. The glass blocks of C and D are shown with four internal reflections in each, but they could also be turned to give two or six reflections in each. These blocks were 4" x 1" x 7/8". The sample of F labelled I-II-III-IV was formed from the four prisms used in A and B. The square face of each prism was 1.25" on an edge.

metal interface free from contamination. The metal charge was prefused in an initial evacuation of the evaporation equipment; and in the second evacuation, during which deposition took place, a movable barrier placed over the glass surfaces intercepted the initial metal vapor. To minimize roughness[7] at the air-metal interface the metals were deposited as rapidly as the equipment permitted, which was about 1000A in 30 seconds. A suitable jig was used to support a unit of four prisms.

Annealing was carried out in a metallurgical type furnace which could be evacuated to about 10^{-6} mm of Hg. The usual treatment was to heat a sample for periods of 30 hours, the temperature for each period being 20°C higher than the preceding one. Reflectivity measurements were made between each annealing period. It was found that the maximum temperature before deterioration of the films began was about 130°C. Above this temperature the reflectivities in the s and p planes no longer had the proper ratio. While not being tested the samples were kept in a desiccator; the longest ageing period was two years.

Experimental Arrangements for Measuring Reflectivity

The drawings of Fig. 1A and B show the arrangement of a sample formed from four right-angle prisms. In passing through the prisms the Beam B_1 experienced four total reflections at glass-air interfaces; beam B_2, on the other hand, was reflected four times at glass-metal interfaces.

By raising and lowering the four prisms as a unit either B_1 or B_2 could be directed into a Pulfrich photometer[8] (see Fig. 2). The quotient of B_2/B_1 is very nearly equal to the fourth power of the glass-metal-glass reflectivity (a small correction must be made for multiple reflections). For the case of high reflectivity the four-prism sample was used, but for lower reflectivities one to three of the sample prisms were replaced by blanks (no metal on the hypotenuse face). For comparing the reflectivities of two metals the arrangement of drawing C and D was employed.

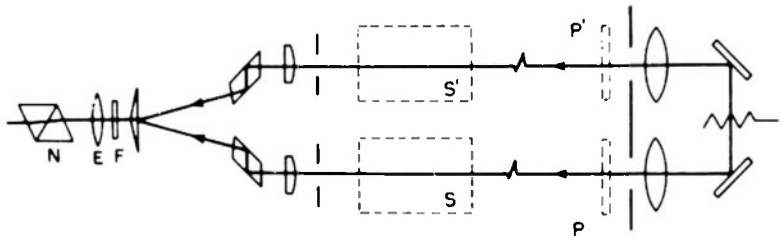

Fig. 2. Drawing showing how the sample, S or S', was inserted into the Pulfrich photometer. A Nicol prism N mounted beyond the eyepiece E made it possible to measure separately the reflectivity in the s and p planes. The polaroid, P or P', was inserted only when testing the sample or the photometer for stray polarization effects. F indicates the position at which the various filters could be placed.

Reflection at air-metal interfaces was measured with the arrangement of Fig. 1E and F. The mirrors M_1, M_2, and M_3 of drawing E were aligned so that the center ray of the beam leaving M_3 was continuous with that incident on M_1. After measuring the light intensity through the mirror system in both the s and p planes, the mirror M_2 was shifted to the position M_2' of drawing F and the sample (I, II, III, and IV) was added. The principle of the procedure is the same as that used by Strong[9] except that 45° incidence is employed here.

The photometer, shown in Fig. 2, was equipped with filters which had pass-bands about 70A in width at half-maximum. (The wavelengths at which measurements were made are indicated in Figs. 6 and 7.) A Nicol prism was added to the eye-piece to polarize the beam in the s or p planes. Experience showed that individual settings of the photometer were accurate to about $\pm$ 2 per cent, and the average of several readings reduced the probable error to $\pm$ 1 per cent. A careful test was made for stray polarization in the photometer and in the samples. With a polaroid placed in one beam (as shown in Fig. 2) and set with its transmission plane vertical (or horizontal) the Nicol, when turned to a crossed position, transmitted less than 0.1 per cent. When a sample of four glass prisms was added, the transmitted light increased to about 0.1 per cent, which is still less than the experimental error in the actual reflectivity measurements. The strain in the right-angle prisms, although too small to be found with the ordinary crossed polaroid method, was easily detectable when a knife edge was used in conjunction with the polaroids. A further check of the prisms was made by comparing the transmission in the s and p planes for glass-air-glass reflectivities; they were always found to be equal. Parts could be interchanged, such as the sample shifted from one beam to the other, without any change in the results. By securing a sample to a metal base it could be turned so that its plane was either horizontal or vertical.

The chief advantage of a visual type photometer for exploratory work is

its extreme flexibility. For example, by a suitable arrangement of lenses a very fine beam could be used thereby making possible a study of variations over a sample surface. For accuracy and convenience, however, the Beckman spectrophotometer[10] was found to be far superior. (A suitable mechanism had been constructed for moving the samples.) Also the wavelength range was extended beyond the visible.

Calculations Using the Equations of Electromagnetic Theory

The equations required to describe the reflection of light at a dielectric-metal interface were selected from the complete list given by König.[1] The reflectivity is indicated by R with s and p designating the two planes of polarization:

$$R_s = \frac{a^2 + b^2 - 2a \cos i + \cos^2 i}{a^2 + b^2 + 2a \cos i + \cos^2 i} \tag{1}$$

$$R_p = R_s \frac{a^2 + b^2 - 2a \sin i \tan i + \sin^2 i \tan^2 i}{a^2 + b^2 + 2a \sin i \tan i + \sin^2 i \tan^2 i} \tag{2}$$

The angle i is the angle of incidence. The two variables a and b are defined by the following equations:

$$a^2 = \frac{1}{2n_o^2}\left[\sqrt{[n^2 - k^2 - n_o^2 \sin^2 i]^2 + 4n^2k^2} + n^2 - k^2 - n_o^2 \sin^2 i\right] \tag{3}$$

$$b^2 = \frac{1}{2n_o^2}\left[\sqrt{[n^2 - k^2 - n_o^2 \sin^2 i]^2 + 4n^2k^2} - n^2 + k^2 + n_o^2 \sin^2 i\right] \tag{4}$$

Here k and n are the optical constants of the metal and n_o is the index of refraction of the dielectric (glass or air). For normal incidence ($i = 0^o$) both R_s and R_p reduce to R_o which is given by

$$R_o = \frac{k^2 + (n_o - n)^2}{k^2 + (n_o + n)^2} \; . \tag{5}$$

When n^2 and n_o^2 are small relative to k^2, a further simplification is possible:

$$R_o = 1 - 4n_o n/k^2 \tag{6}$$

Since it is inconvenient to solve Eq. (1) or (2) explicitly for n in terms of R_s (or R_p), k, n_o, and i, the experimental data, R_s and R_p, were combined in a manner which made it possible to use the much simpler Eq. (5). A preliminary step was to define a new reflectivity, $\overline{R} = 1/2(R_s + R_p)$. Since the difference $R = R_o - \overline{R}$ is relatively small, $\overline{R}$ was used in Eq. (5) to get a provisional value of n. This n was in turn used to obtain ΔR from the graph of Fig. 3. Figure 4 has been included to show the manner in which the various R's depend on the angle of incidence.

The method of calculating just described makes use of the average of

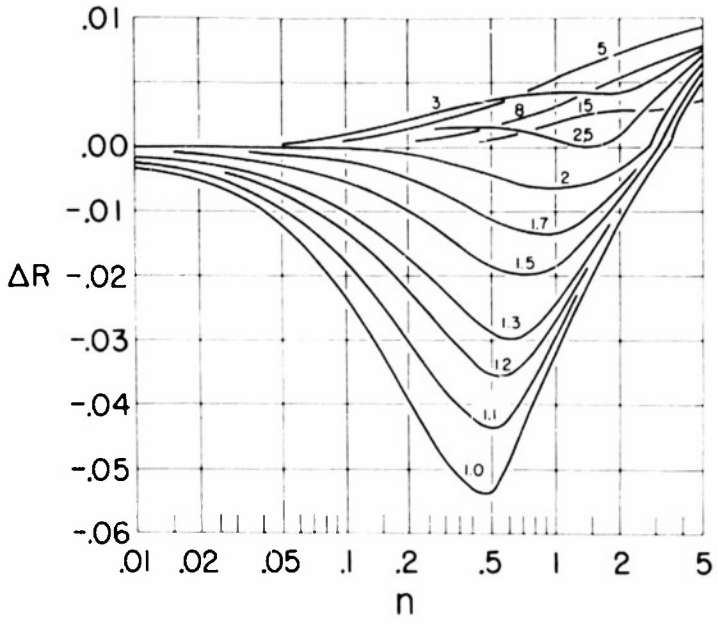

Fig. 3. Graph showing the values of ΔR as a function of n and k. The numbers on the curves indicate the k values. Note that the vertical scale for the positive ΔR region is different from that for the negative region. The calculations are for a vacuum-metal interface. To use the graph for the case of a dielectric other than vacuum, n and k must be normalized, that is, divided by the index of refraction of the dielectric.

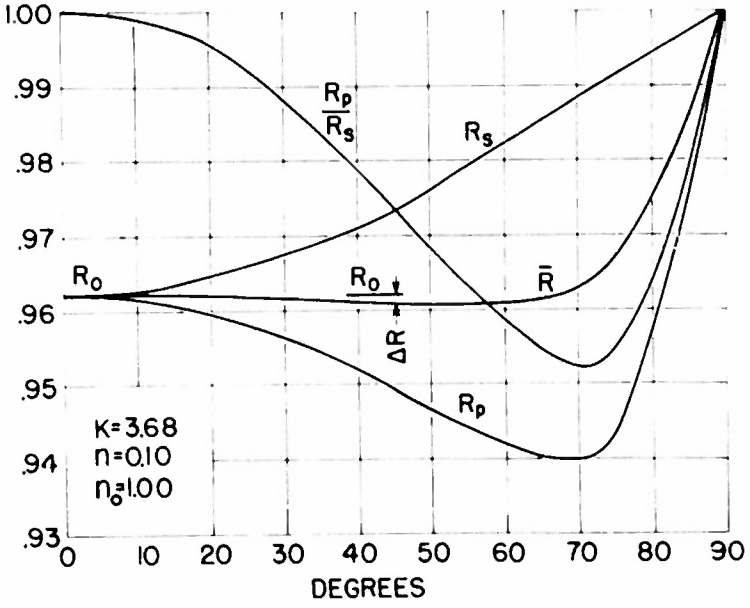

Fig. 4. Graph showing the variation in reflectivities with changing angle of incidence for a particular set of values for k, n, and n_0. Note that at 45° the value of R_s^2 is equal to R_p.

R_s and R_p; a second method of combining them is to take their ratio. It is evident from Eq. (1) and (2) that R_s^2/R_p is equal to unity when i is equal to 45^o. Accordingly, the value of R_s^2/R_p was used as a test to determine whether or not the reflection interfaces satisfied the boundary conditions assumed when Eq. (1) and (2) were derived. The assumptions of particular interest are that the interface be plane (not rough) and that at the interface the optical properties change discontinuously (no gradients). These conditions are satisfied in a practical way when the roughness amplitude and the thickness of the transition region are very small relative to the wavelength of the radiation.

When using Eqs. (5) or (6) it is advantageous to keep in mind the relative magnitude of the quantities involved. Since for the metals being studied here k^2 was usually large relative to n^2, the discussion will be based on Eq. (6). It might appear from this equation that the calculated n value would be very sensitive to k because k appears to the second power. This is indeed true, but k is known to a few per cent whereas 1-R is only crudely known. It follows that in regions of high reflectivity any reasonable k value is sufficient but that it is highly important to measure R accurately. Since this is difficult, the per cent error for n will usually be many times that for k.

Because of multiple reflections between the four prisms composing a sample, it was necessary to add a correction to $\bar{R}$ and R_s^2/R_p. This correction was computed on the basis of intensity addition. The results are shown in Fig. 5 for the case of all four prisms metallized. Similar graphs were constructed for the cases of less than four prisms metallized.

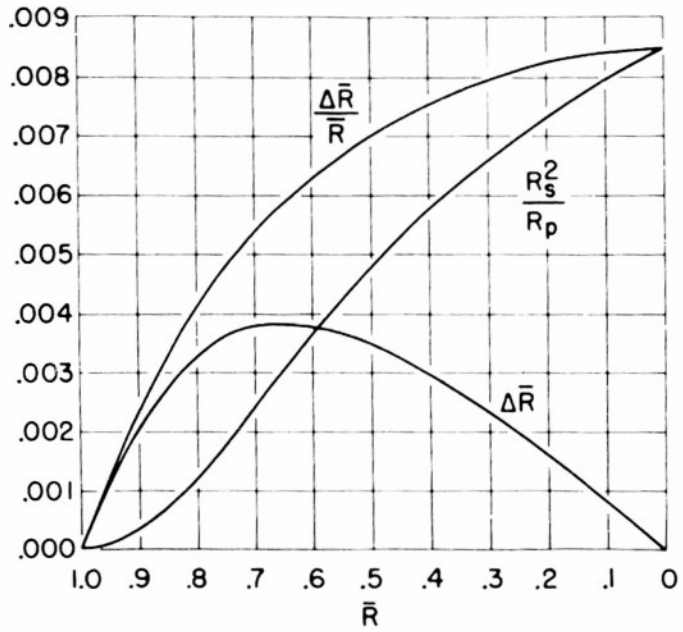

Fig. 5. Graph showing the corrections for the errors due to multiple reflections between the prisms. $\Delta \bar{R}$ and $\Delta(R_p^2/R_s)$ are to be added to the experimental values of $\bar{R}$ and R_s^2/R_p respectively. Included on the graph is the fractional error in $\bar{R}$. (This graph is for the case of a 4-prism sample with ali prisms metallized.)

Discussion of Results

Because there is no particular use for reflectivities at glass-metal interfaces measured at an angle of incidence equal to 45°, the discussion will be concerned only with the n values calculated from these measurements. Before considering actual cases, several general features of the results will be discussed.

If the experimental values of R_s^2/R_p did not agree with the theoretical (unity for i equal to 45°) to within the accuracy of the measurements, the sample was considered unsatisfactory. Usually the deviations of R_s^2/R_p and R were in the same direction; both were either too high or too low. Annealing at temperatures higher than 150°C produced the highest values of $\overline{R}$, but such values were not used to calculate n because the associated values of R_s^2/R_p were above unity by more than the experimental error. The exact nature of the sample defect in these cases was not discovered. On the other hand, when a sample was defective because of surface roughness, both R_s^2/R_p and $\overline{R}$ were low.

It was assumed that evaporated films formed on substrates at room temperature would be strained and would contain crystal defects.[11-13] The effect of annealing or ageing was to remove these strains and defects thereby producing a higher reflectivity and therefore a lower value of n. For a given metal there was always some variation in the $\overline{R}$ measured on freshly prepared samples both for the air-metal and the glass-metal interfaces. The effect of ageing or annealing was to make all such samples identical to within the experimental accuracy. Whereas the n values of preannealed samples tended to be lower for the air-metal than for the glass-metal interfaces, the order was reversed after annealing. This suggested that the strain was initially greatest at the glass-metal interface. The best values of n (the lowest) were obtained from glass-metal measurements on aged samples; these values are given in Table I and Fig. 8.

Figure 6A for Ag illustrates some of the general effects just mentioned and also for comparison gives results of two older investigations.[14,15] Measurements on the air-metal interface after annealing are not shown since it was assumed that exposure would alter the unprotected metal surface.

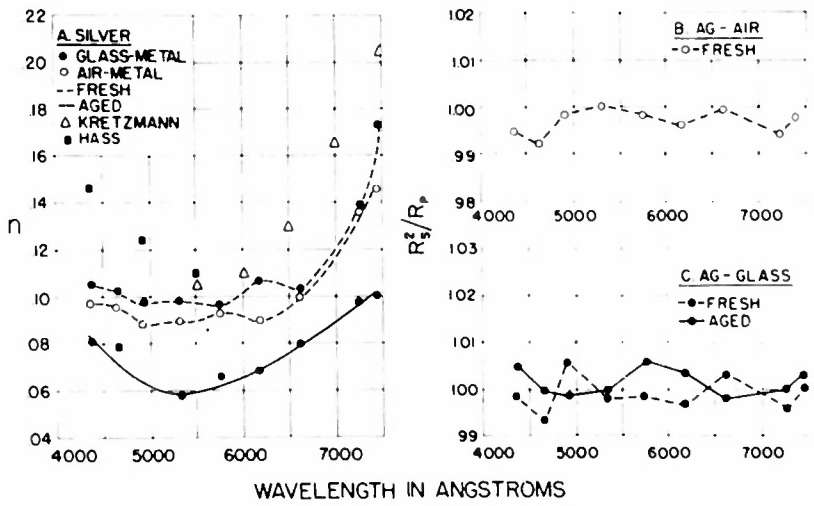

Fig. 6. Graph A shows various n values for a Ag sample together with the results of two older measurements. Graphs B and C show R_s^2/R_p values for the same sample.

TABLE I

Values of the Index of Refraction, n, for Ag, Au, Cu, and Al. These values are based on glass-metal reflectivities measured with a Beckman spectrophotometer on samples which had been annealed or aged and which satisfied the condition $R_s^2 = R_p$. The number of samples (a sample consists of 4 metallized prisms) for each metal was as follows: For Ag, 4; for Au, 2; for Cu, 2; and for Al, 4.

$\lambda(\mu)$	Ag	Au	Cu	Al
0.40	0.075	1.45	0.85	0.40
0.45	0.055	1.40	0.87	0.49
0.50	0.050	0.84	0.88	0.62
0.55	0.055	0.34	0.72	0.76
0.60	0.060	0.23	0.17	0.97
0.65	0.070	0.19	0.13	1.24
0.70	0.075	0.17	0.12	1.55
0.75	0.080	0.16	0.12	1.80
0.80	0.090	0.16	0.12	1.99
0.85	0.100	0.17	0.12	2.08
0.90	0.105	0.18	0.13	1.96
0.95	0.11	0.19	0.13	1.75

It is evident that when the value of n is small (reflectivity high), ageing causes reductions of n of nearly 50 per cent. Graphs B and C show that the ratio R_s^2/R_p on the average was near unity even for fresh samples but with rather pronounced deviations at certain wavelengths. After treatment these deviations were no longer observed. It was found that both ageing and annealing produced increased reflectivity, but ageing gave the most consistent results. The initial change with time was approximately linear, but there was a leveling off after about six months.

Although the k values of Kretzmann[14] and of Hass[15] are in good agreement with the new values reported in Part I, their n values are considerably higher than those in Fig. 6A. This is understandable since k is dependent on the density of free electrons in the metal[4] which is probably independent of the structure defects. On the other hand, n depends on the conductivity of the sample which is highly sensitive to the presence of strains and defects in general.

Figure 7A for Cu shows, in addition to general trends, the effect of annealing on regions both of high and low values of n (low and high values of $\overline{R}$ respectively). For comparison purposes the values of Lowery[16] are included as they are among the lowest found in the literature; the values of Tool[17] and Meier[18] (Part I) are rather high.

In all essential aspects the results for Au (Table I and Fig. 8) are similar to those of Cu. It was observed that annealing changed the color of a film slightly: A fresh deposit was slightly orange in appearance, but after

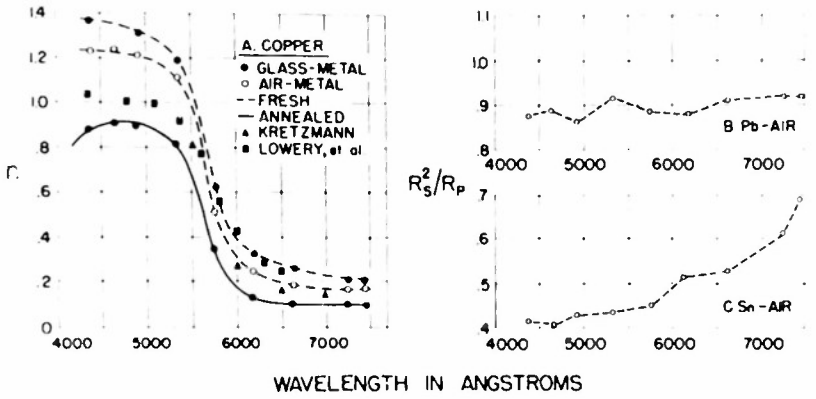

Fig. 7. Graph A shows various n values for one of the Cu samples. Graphs B and C show the R_s^2/R_p values for the air-metal interfaces of samples of Pb and Sn respectively.

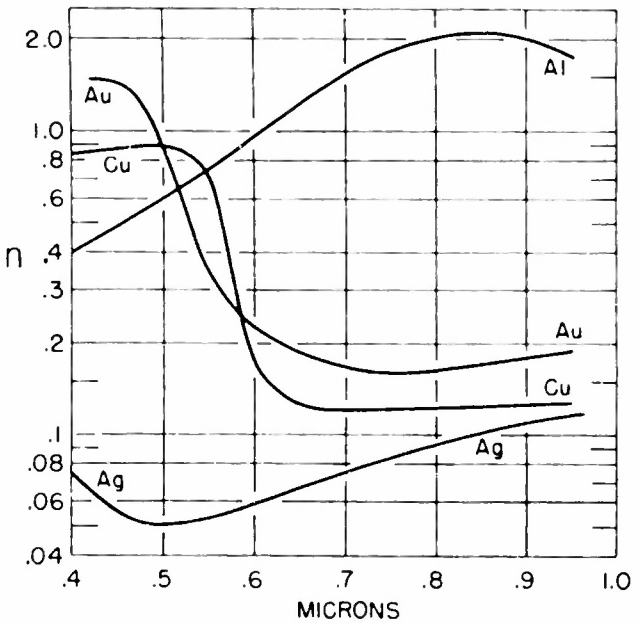

Fig. 8. Values of n for Ag, Au, Cu, and Al. It is interesting to compare the dispersion shown here in the n values with that of the k values shown in Figs. 4-7 of Part I.

an annealing treatment this changed to the typical yellow of pure Au.

For Al comparison data exist only for the visible region. The new results (see Table I and Fig. 8) are lower than those of O'Bryan[19] but somewhat higher than those reported by Hass.[15] Although the reflectivities of glass-metal interfaces of Al samples increased somewhat with ageing and annealing, the change was less than for the other three metals. Using the data of Table I and Table II of Part I the calculated reflectivity at normal incidence for a vacuum-Al interface in the wavelength region of 0.40μ to 0.45μ was 0.905 which is higher than the experimental result of Strong[9] (0.900) but lower than that of Hass[15] (0.915).

Discussion of Errors

Auxiliary experiments were performed to obtain general information on several types of surface defects. To test the effect of surface roughness, measurements were made on films of Pb and Sn (one 4-prism sample of each). The air-metal surfaces of Pb films are grossly rough relative to those of Ag, Au, Cu, and Al, but still not so rough as to impair image formation severely. Figure 7B shows that the R_s^2/R_p values for the air-Pb reflection averaged about 0.90. This result suggests that in the group Ag, Au, Cu, and Al the error attributable to surface roughness must be extremely small, even for air-metal interfaces.

Measurements on milky white Sn films which had extremely rough surfaces led to the results given in Fig. 7C. This graph shows that for long wavelengths there is less diffuse scattering than for shorter ones. For both Pb and Sn measurements on glass-metal interfaces, the R_s^2/R_p values were essentially unity. It was impossible to carry through the calculations for n because reliable k measurements were not available. It was found that annealing had no apparent effect on the Pb sample but that ageing produced a noticeable increase of the reflectivity of the glass-metal interface. One would expect a Pb film to be free from strain but not from lattice defects.

To obtain a practical estimate of the experimental error in the measurements made with arrangement A and B of Fig. 1, the results for Ag and Al were compared with those given by the arrangement shown in drawings C and D. It was found that the ratio of reflectivities $\overline{R}_{Ag}/\overline{R}_{Al}$ as determined by each method differed by about 0.2 per cent.

When all possible sources of error were considered, the probable error, Δn, in n was found to depend on the value of n in the following manner: when $n > 1.0$, the value of Δn was ± 0.03; for n values in the range of 1.0 to 0.4 the value of Δn was ± 0.02; and for $n < 0.4$ the value of Δn was ± 0.01. Although these may seem to be small absolute uncertainties, the equivalent percentage is very great. For Ag, for example, the uncertainty is ± 20 per cent.

Conclusions and General Remarks

1. The present paper and the preceding one describe accurate procedures for determining the optical constants of metals. With these procedures a new set of values has been given for the wavelength region of 0.45μ to 0.90μ.

2. It has been shown that the values of n obtained by a reflection method are very sensitive to the presence of strains and crystal defects occurring in freshly prepared samples made with an evaporation technique. These defects can be removed, however, by annealing or by ageing to obtain the more nearly correct values of n. The absorption coefficient k, on the other hand, appears to be independent of these defects (see Part I).

3. The ratio of reflectivities, R_s^2/R_p, at 45° angle of incidence can be used to judge the suitability of a dielectric-metal interface for reflectivity measurements. The samples used to prepare Table I satisfied this condition to within the experimental error of ± 0.005 in R_s^2/R_p.

4. As was emphasized in Part I, it is not possible in general to determine directly the bulk properties of a metal from surface measurements. Accordingly the n values of Table I based on reflectivity measurements apply only to surface properties and are different from those associated with the interior. The k and n values of this paper and Part I can be used for any real physical problem but cannot be used to check a solid state theory

of metals. The extent of the difference in the optical constants measured at the surface and in the interior is the subject of a subsequent paper.

This research was supported in part by U. S. Air Force Contract No. AF 33(038)-6534.

References

1. W. König, Handbuch der Physik (Verlag. Julius Springer, Berlin, 1928), Vol. 20, Ch. 6.
2. L. G. Schulz, J. Opt. Soc. Am. 44, 000 (1954).
3. C. F. E. Simons, Physica 10, 141 (1943).
4. F. Seitz, Modern Theory of Solids (McGraw-Hill Book Company, Inc., New York, 1941), Ch. 17.
5. N. F. Mott and H. Jones, The Theory of the Properties of Metals and Alloys (Oxford University Press, New York, 1936), Ch. 3.
6. A. H. Wilson, Theory of Metals (The University Press, Cambridge, England, 1946), Ch. 4.
7. R. S. Sennett and G. D. Scott, J. Opt. Soc. Am. 40, 203 (1950).
8. W. West, Physical Methods of Organic Chemistry (Interscience Publishers, Inc., New York, 1946), edited by Arnold Weissberger, p. 852.
9. John Strong, Procedures in Experimental Physics (Prentice-Hall, Inc., New York, 1938), Ch. 9.
10. H. H. Carey and A. O. Beckman, J. Opt, Soc. Am. 31, 682 (1941).
11. P. G. Wilkenson and L. S. Birks, J. Appl. Phys. 20, 1168 (1949).
12. Eber Halteman, J. Appl. Phys. 23, 150 (1952).
13. R. Suhrman and G. Barth, Z. Physik 103, 157 (1936).
14. R. Kretzmann, Ann. Physik 37, 303 (1940).
15. George Hass, Optik 1, 2 (1946).
16. Lowery, Wilkinson, and Smare, Phil. Mag. 22, 769 (1936).
17. A. Q. Tool, Phys. Rev. 31, 1 (1910).
18. W. Meier, Ann. Physik 31, 1017 (1910).
19. H. O'Bryan, J. Opt. Soc. Am. 26, 122 (1936).

VI

THE THICKNESS OF THE HELIUM FILM

Lothar Meyer
(Submitted to The Physical Review)

It is suggested that the change in thickness of the helium film at the λ-point is not caused by any essential change in the thermodynamic relation between film thickness, pressure, and temperature. It can be due to the onset of superfluidity below the λ-point which causes a great change in the rate of approach to equilibrium and consequently of the average of the film thickness during the experimental fluctuation of pressure and temperature.

The thickness of the helium film in contact with bulk liquid has usually been measured by using a vertically oriented specimen hanging in the vapor space and touching the liquid at its lower end.[1] It has been found that the thickness of the film is markedly different above and below the λ-point, changing from a thickness of 10-15 layers above the λ-point to values an order of magnitude higher at temperatures below the λ-point, this change occurring within a temperature region of a few thousandths of a degree, as the λ-point is crossed.

This abrupt change of thickness under saturation conditions means that at constant thickness the equilibrium pressure of the vapor in contact with the film must change sharply at the λ-point. However, thermodynamics puts rather sharp limitations on this change.[2] The equilibrium pressure of this one-component system is a measure of the free energy, which cannot change in this manner; therefore, some other explanation must be sought.

It is the purpose of this note to point out a mechanism to resolve this apparent paradox.

The adsorption isotherm of helium and of other simple gases goes asymptotically to infinity—at least mathematically—as the equilibrium pressure P over the film approaches P_o, the vapor pressure of the bulk liquid. Theoretical considerations by Frenkel,[3] Halsey,[4] Hill,[5] and McMillan and Teller,[6] have shown that at high saturations the isotherms should have the form:

$$n^3 = \frac{k}{\ln P/P_o} \qquad (1)$$

where n is the number of adsorbed layers and k is a constant. Bowers[7] has shown that Eq. (1) represents his data quite well for the adsorption of N_2, A, O_2, and He at high saturations ($P/P_o \sim 0.70$ to 0.99). For a given adsorption system the constant k is a function of temperature, and for helium is found to lie between 15 and 25 in the neighborhood of the λ-point.

In Table I is given for helium the number of adsorbed layers in films at four values of the saturation P/P_o between 0.9900 and 1.0000, as calculated from Eq. (1), with a chosen value of k = 20. Table I represents, therefore, an extrapolation of the direct measurements of Bowers, using Eq. (1) for the extrapolation.

TABLE I

P/P_o	n
0.9900	12.6
0.9990	27.2
0.9999	58.4
1.0000	∞

Even under the most carefully controlled conditions P and T will fluctuate during an experiment, with the result that P/P_o changes by at least 0.1 per cent, and in many cases even by as much as 1 per cent, i.e., over the whole range given in Table I.

In such a case the experimentally determined value of the film thickness will correspond to the average of P/P_o only if the changes in thickness occur rapidly enough to follow the fluctuations in P/P_o without appreciable delay. If, after a disturbance, the approach to equilibrium is slow compared to the period of the fluctuations, the observed film thickness can deviate considerably from the value which corresponds to the average P/P_o during the experiment.

Equilibrium between a condensed phase and its vapor is usually established extremely fast by evaporation and condensation. In the case of helium, the kinetic flux vapor-film is $\sim$ 1 gm/cm^2/sec (Ref. 1), whereas less than 10^{-8} gm/cm^2 are sufficient to change the thickness by one layer. However, Picus[8] has pointed out that for helium films this mechanism is inhibited, due to the relatively high heat of vaporization. The heat capacity of the film and substrate system is so small that any change of film thickness by condensation or evaporation would lead to such strong local heating or cooling, respectively, that the process is stopped immediately. It can proceed only at a rate such that the heat of vaporization is dissipated (or provided). Above the λ-point, this is a very slow process indeed.*

It may safely be assumed that above the λ-point the approach to equilibrium between film and vapor is sufficiently slow to allow a considerably lag between the fluctuations in P/P_o and the resulting changes in film thickness, e.g., if P/P_o was initially low, and is increasing, the number of adsorbed layers will increase only with considerably delay. If, however, P/P_o drops from a temporarily high value to a lower saturation, the film can rid itself of the excess fluid comparatively fast. Bulk liquid is formed which simply runs off the vertical walls, eventually forming drops. This drop formation has been observed by Burge and Jackson[9] and by Ham and Jackson[10] even below the λ-point.

Since, according to these arguments, the film thickness can decrease more rapidly than it can increase, the average observed thickness will therefore be smaller than that which corresponds to the average of P/P_o during the experiment, and may even be expected to be rather near to that

* Bowers (Ref. 1) observed that even below the λ-point the approach to equilibrium between film thickness and pressure, after a change of pressure, required minutes in his geometry, and was roughly proportional to the film flow rate; this is consistent with the argument, since below the λ-point the heat transport which governs the rate of condensation or evaporation is determined by the superfluid motion of the film.

corresponding to the lowest value of P/P_0 reached during the fluctuations. The observed values of 10-25 layers are consistent with this interpretation.

The situation is radically changed as soon as the temperature is lowered below the λ-point. In this region the well-known superfluidity of the film provides a new and fast mechanism for changing the film thickness, which can now increase about as fast as it can decrease, because superfluid film can run up from the reservoir of bulk liquid. The approach to equilibirum by evaporation and condensation is enhanced to the same degree as heat transport in the film is provided by superfluid flow.*

The asymmetry in the speed with which the film thickness can follow fluctuations in P/P_0 is therefore removed below the λ-point; consequently, the average thickness must move from the low values found above the λ-point to values which more nearly correspond to the equilibrium case of $P/P_0 = 1$, somewhere between 50- ∞ layers, according to Table I. (The average film thickness will then be determined by other factors, such as gravity, geometry, etc., not subject to the fluctuation arguments presented here.) In this way the observed film thickness can change by a considerable factor at the λ-point, although the thermodynamic relationship between n and P/P_0 remains the same.

The comparatively great differences in the results of different investigators (compare Ref. 1) may be due, at least in part, to the effects described above. The average observed film thickness should depend on the amplitude and period of the fluctuations in temperature and pressure during a given experiment. Since these fluctuations are not easily measured, and actually were never recorded, it seems impossible for the time being to try a quantitative analysis of the discrepancies between the results of different investigators.

Thanks are due to E. A. Long and M. H. Cohen for criticism and advice.

References

1. For experimental details and a review of the data, see R. Bowers, Phil. Mag. 44 (in press) (1953).
2. Compare: Earl Long and Lothar Meyer, Advances in Physics 2, 1, 1953; Phil. Mag. 44, 788 (1953).
3. J. Frenkel, Kinetic Theory of Liquids (Oxford Univ. Press) (1946), p. 332.
4. G. D. Halsey, J. Chem. Phys. 16, 931 (1948).
5. T. L. Hill, J. Chem. Phys. 14, 263, 441 (1946); 15, 767 (1947); 17, 580, 668 (1949); Advances in Catalysis (Academic Press, New York, 1952) Vol. IV, p. 225.
6. W. G. McMillan and E. Teller, J. Chem. Phys. 19, 25 (1951).
7. R. Bowers, Phil. Mag. 44, 467, 485 (1953).
8. G. S. Picus, Thesis, University of Chicago, 1953.
9. E. J. Burge and L. C. Jackson, Proc. Roy. Soc. A205, 270 (1951).
10. A. C. Ham and L. C. Jackson, Phil. Mag. 44, 214 (1953).

* Even below the λ-point the thickness of the film is smaller by a factor of about 2.5 when the specimen is not touching the bulk liquid (Compare Ref. 1). This evidence is quite consistent with the picture that the flow of film from the reservoir of bulk liquid is necessary to shift the average observed thickness to the high values observed in the He II region.

VII

GAUSSIAN FUNCTIONS IN MOLECULAR INTEGRALS

Ryoichi Kikuchi
(Submitted to The Journal of Chemical Physics)

The usual procedure of evaluating many-center integrals appearing in molecular problems is to expand functions around one common center. On the other hand, Boys[1] has shown that if one uses functions of the Gaussian type instead of the ordinary exponential ones, the many-center integrals can be evaluated in closed forms. This note is to show a method, which might be worth being exploited, to transform integrals including exponential functions into ones including Gaussian functions.

The following relation holds for a non-negative r:

$$e^{-r} = \frac{2}{\sqrt{\pi}} \int_0^\infty \exp\left[-(r/2t)^2 - t^2\right] dt. \tag{1}$$

By putting $r = \sqrt{s}$ and $4t^2 = 1/z$, one sees that this is a modification of the Laplace transformation. In order to prove Eq. (1) straightforwardly, the following integral is shown to be independent of r ($\geqq 0$) by differentiation with respect to r:

$$\int_0^\infty \exp\left[-\left(\frac{r}{2t} - t\right)^2\right] dt.$$

The procedure of transforming into Gaussian functions becomes helpful particularly when dealing with two-electron wave functions which depend on the relative distance. As an illustration, a case of four-center integrals is shown below to be reduced to a quadruple integral.

$$\int d\mathbf{r}_1 \int d\mathbf{r}_2 \, (1/r_{12}) \exp\left(-ar_{1A} - br_{1B} - cr_{2C} - dr_{2D} - 4\alpha r_{12}^2\right)$$

$$= \frac{abcd\sqrt{\pi}}{64} \int_0^\infty \rho^8 \, d\rho \int_0^{\pi/2} d\theta \, \cos^4\theta \, \sin^4\theta$$

$$\times \exp\left\{-\frac{1}{\rho^2}\left[\frac{\overline{AB}^2}{\cos^2\theta} + \frac{\overline{CD}^2}{\sin^2\theta}\right] - \frac{\rho^2}{8}\left[(a^2+b^2)\cos^2\theta + (c^2+d^2)\sin^2\theta\right]\right\} \tag{2}$$

$$\times \int_{-1}^{1} du \, (1-u^2) \exp\left\{-\frac{\rho^2}{8}(a^2-b^2) \, u \cos^2\theta\right\}$$

$$\times \int_{-1}^{1} d v\,(1-v^2)\ \exp\left\{-\frac{\rho^2}{8}(c^2-d^2)\ v \sin^2\theta\right\}$$

$$\times (1+\alpha\,\rho^2 K)^{-1}\ K^{-1/2}\ F(4\,\overline{PQ}^2\left\{1+\alpha\,\rho^2 K\right\}^{-1}\ \rho^{-2}\ K^{-1})$$

where

$$K = 1 - u^2 \cos^2\theta - v^2 \sin^2\theta$$

$$F(z) = \frac{1}{\sqrt{z}} \int_0^{\sqrt{z}} e^{-t^2}\, dt$$

and

$$4\overline{PQ}^2 = [\,\mathbf{r}_A + \mathbf{r}_B - \mathbf{r}_C - \mathbf{r}_D - (\mathbf{r}_A - \mathbf{r}_B)\,u - (\mathbf{r}_C - \mathbf{r}_D)\,v]^2 .$$

When one puts $\alpha = 0$, Eq. (2) reduces to an ordinary four-center integral. As the integrand of Eq. (2) is a fairly well-behaved function of the variables, except for the values near the upper and the lower limits, it may not be impracticable to carry out the numerical quadrature.

References

1. S. F. Boys, Proc. Roy. Soc. (London) 200, 542 (1950).

XII

EFFECT OF PRESSURE ON F-CENTER ABSORPTION IN ALKALI HALIDES

I. S. Jacobs
(Submitted to The Physical Review)

Abstract

Measurements are reported for the effect of hydrostatic pressure to 5000 atmospheres on the F-center absorption of seven alkali halides. An interpretation is made of the shift of the absorption band maximum with pressure, and of the difference between the shift with pressure and that with temperature. The shift with pressure depends almost entirely on the local interionic distance at the F-center. The shift with temperature is largely governed by this same factor, but it must be supplemented by a contribution from the interaction of the F-center electron with the optical vibrations of the lattice. Effects of the pressure-induced structure transformation in RbCl are described for both photochemically and additively colored crystals.

I. Introduction

The properties of the alkali halide crystals have merited particular attention in the field of solids partly because of the hope that their inherent simplicity will lead to an understanding which may be extended to the whole field. The problems and phenomena associated with the externally induced colored absorption bands in alkali halides have commanded considerable attention since Pohl[1] and his co-workers subjected them to many careful experiments, starting in the 1920's.

Both experimental and theoretical investigations of recent years on the colored absorption bands in ionic crystals seem to confirm the defect model of the centers responsible for the absorption. This model assumes the presence of electrons in quasi-atomic or molecular states trapped in the vicinity of lattice imperfections in ionic crystals, and attributes the bands to electronic transitions between these states. Excellent reviews of these problems may be found in the work of Mott and Gurney[2] and of Seitz.[3]

Among these colored bands, the so-called F-bands of the alkali halides play a very fundamental role. Their absorption spectra, in or near the visible range, are bell-shaped. The peak wave number and width may be made to vary with temperature and pressure. Over the range of alkali halide crystals with the NaCl lattice structure, Mollwo[4] has indicated that, at a given temperature, the peak wavelength of the F-band is approximately proportional to the square of the interionic distance. More recently, Ivey[5] has made a better representation in this form using the exponent 1.84 instead of 2. This relation is an empirical one. Its successful prediction from theory is bound up with the problem of calculating the wave functions and energy levels of electrons trapped at lattice defects.

Most of the theoretical calculations for F-centers have treated the crystal as a homogeneous dielectric continuum, with the electron moving

in the central field of the halogen ion vacancy which serves as the trapping site. Among the contributors to this approach are Tibbs,[6] Kubo,[7] Simpson,[8] Inui and Uemura,[9] Pincherle,[10] and Krumhansl and Schwartz.[11] An alternative approach employs a molecular orbital model of an F-center, wherein the wave function of the electron is taken as the linear combination of atomic orbitals, each representing the extra electron in an atomic state on one of the atoms adjacent to the halogen ion vacancy. The first calculations of this type are due to Muto[12] and to Inui and Uemura.[9] The molecular orbital model has received significant support from the electron spin resonance absorption experiment on colored KCl, performed by Hutchison and Noble.[13] Kahn and Kittel[14] have made an interpretation of this work, and additional experiments of this type have been done by Kip, Kittel, Levy and Portis.[15] At the present time, the work of Inui and Uemura, confined to the lithium salts, is the only quantitative calculation of energy levels with this model.

In recent years considerable attention has been directed toward the explanation of the shift of the absorption peak toward longer wavelengths, and of the increase in the absorption band width, with increasing temperature. The importance of the interaction of the electron with optical vibrations of the lattice, to account for both the shift and the broadening, has been emphasized in the work of Muto,[12] Huang and Rhys,[16] Lax,[17] and O'Rourke.[18] On the other hand, the temperature shift has been ascribed mainly to the thermal expansion of the lattice by Inui and Uemura[9] and Nagamiya.[19] The last two investigators and Burstein and Oberly[20] have employed an adiabatic approximation to determine the effect of neighboring ion position on the F-center energy, and accordingly the effect of thermal agitation on the width.

Muto has pointed out that, in reality, we have to consider simultaneously not only effects arising from thermal expansion but also those connected with the excitation of lattice vibrations in order to obtain a full knowledge of the phenomena concerned. In an attempt to separate and clarify these effects, an investigation was undertaken to study the dependence on hydrostatic pressure of the F-band parameters. One limited experiment of this type has been reported briefly by Burstein, Oberly, and Davisson.[21] Measurements are reported below on the F-absorption band of seven alkali halides at room temperature up to pressures of 5000 atmospheres. The compounds studied were NaCl, NaBr, KCl, KBr, KI, RbCl, and CsCl. Other compounds were not studied owing to difficulties in procurement or preparation of suitable samples, experimental difficulties in the optical transmission of the pressure chamber, or the instability of their F-band at room temperature.

The results of the experiments on the shift of the band peak with pressure are compared with the existing data in the literature on the shift with temperature, in an effort to interpret how the effects mentioned above have to be taken into account to form a consistent picture. For most of the compounds studied, the shift of the peak with pressure is less than that with temperature. In the analysis of the data for these compounds, it is shown that a small part (up to 5 percent) of the pressure shift is due to the interaction of the electron with the optical lattice vibrations. The remainder of the shift is due to the explicit dependence of the F-center energy on local interatomic distance. The additional increment for the temperature shift above the pressure shift is attributed to a further interaction with optical lattice vibrations. An expression is obtained for the band width which combines the two existing theories and is consistent with the analysis of the shift of the band peak with pressure and temperature. The negligible effect

of pressure on the band width is in agreement with these considerations.

A subordinate purpose of the present investigation is a study of the effects on the F-band of the structure transformation in the rubidium halides. Excepting the fluoride, these salts show a polymorphic transition at room temperature and about 5000 atmospheres pressure, which was first observed by Slater[22] and was measured by Bridgman.[23] R. B. Jacobs[24] has shown that the crystal structure changes from the NaCl structure to the CsCl structure in the high pressure form. Although various difficulties prevented the detection of a new F-band in the transformed state, a number of interesting observations are described and discussed.

II. Experimental Method

A. Apparatus

A high pressure system to allow for spectrophotometric measurements was constructed for this investigation. It was used in conjunction with a Beckman Model DU Quartz Spectrophotometer, employing the usual tungsten lamp and phototubes for the visible range. The system is capable of subjecting the sample to 8000 atmospheres pressure, although problems with failure of the windows restricted most of the work to a range of 5000 atmospheres.

The need for compactness and portability gave rise to several special features in this apparatus. The whole system is self-contained, with the pump for generating pressures made in the form of a plug screwing into the high pressure bomb. To minimize the optical path through the bomb, a search was made for a more compact method of sealing the synthetic sapphire windows[25] than the Poulter[26] packing usually employed. Our experiments have shown that it is feasible to use ordinary synthetic rubber O-rings to seal pressures to at least 8000 atmospheres. With this technique only one O-ring is used to seal both the window and its supporting plug.

The high pressure apparatus consists of the pump, the bomb, a mounting carriage with wheels, and a baseboard arrangement for positioning the Beckman spectrophotometer. This baseboard provides a track on which the carriage can be rolled so that either the observation hole or the blank reference hole is in position in the light path. A black cloth is fastened over the bomb and photocell units to keep out stray light during measurements. The pump is capable of producing a pressure of 2000 atmospheres. The pump liquid is 20 centistoke DC-200 silicone fluid (Dow-Corning). Figure 1 shows a diagram of the high pressure bomb. The bomb contains a piston intensifier to magnify the 2000 atmosphere pressure delivered by the pump to a maximum pressure of 8000 atmospheres at the sample. Pressure is determined by measurement of the change in resistance of a manganin resistance gage which is immersed in the pressure fluid. The gage calibration procedure has been described previously.[27] The hydraulic medium around the sample is 3 centistoke DC-200 silicone fluid, which is sufficiently transparent over the visible range. The sample holder is a split cylinder, with a $\frac{1}{4}$-inch hole transverse to the cylinder axis to permit passage of light. One of the cylinder halves has a recess 3/8" x 5/16" x 1/16" for the crystal samples which are cleaved to that size. A coil spring around the cylinder keeps the halves together and provides the necessary friction with the walls to maintain the holder in a fixed position in the bomb.

The Beckman spectrophotometer needs no modification for use with the high pressure system except for the separation of the photocell housing

from the main unit by about 4 inches to accommodate the bomb.

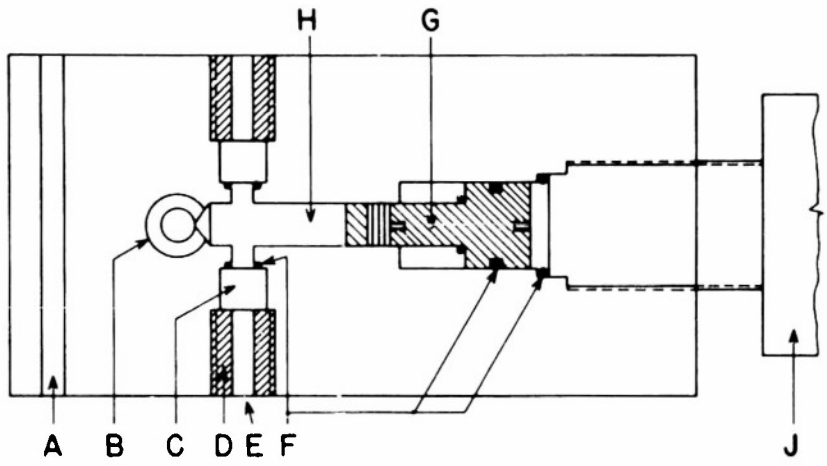

Fig. 1. Diagram of the high pressure bomb. A, reference hole; B, gage plug hole; C, synthetic sapphire window; D, window plug; E, sample observation hole; F, O-rings; G, piston intensifier; H, sample region; J, portion of pump.

B. Preparation of Samples

The specimens of NaCl, KCl, and KBr used in this work were cleaved from single crystal blocks obtained from the Harshaw Chemical Company. No analysis of these samples was made, but the work of Duerig and Markham[28] includes a representative analysis of this type of commercial sample. Single crystal specimens of the other four compounds were grown in the laboratory. The NaBr salt was Mallinkrodt, Analytical Reagent, and the KI salt was Baker and Adamson, Reagent. The CsCl salt used was 99+ percent, 0.5 percent K, 0.02 percent Pb, the two listed impurities having been added for a prior experiment. The RbCl samples were grown from two sources of the salt. One grade was Fairmount, c.p., for which spectroscopic analysis showed 5 percent K, 0.5 percent Ba, 0.4 percent Na, 0.1 percent Cs, and lesser quantities of Li, the other alkaline earths and Pb. A purer source was Mackay "99.99%" for which spectroscopic analysis showed 0.3 percent K, 0.03 percent Na, and smaller quantities of Cs, and the alkaline earths.

The NaBr, KI, and RbCl crystals were grown in air from a platinum crucible by the Czochralski[29] method, with crystallization occurring on a platinum wire that was slowly withdrawn from the melt surface. The divalent impurities in these salts were reduced in concentration by a factor of two to ten in crystals grown in this manner. The CsCl specimen was grown by slowly lowering through a gradient furnace an evacuated and sealed Vycor tube containing the salt in a small spun platinum crucible with a conical bottom. All samples were annealed after growth for a 12-hour period. The air-grown crystals were readily cleaved to desired sizes. The CsCl specimen, however, did not cleave, and was sanded to shape on emery paper and finished with polishing powders and jeweler's rouge. This handling was done under silicone fluid due to the deliquescent nature of CsCl. Similar handling precautions were taken with those of the

other samples whose surfaces tended to fog easily.

The F-band was produced in the crystals by irradiating them with x-rays from a Machlett type A-2 molybdenum target tube with a beryllium window. The irradiations varied from 5 minutes to 90 minutes (40-50 k.v., 20 m.a.) with the sample about one inch from the tube window. The ranges of time correspond to the varying darkenability of the different compounds. X-irradiation was performed in the dark, during which all samples showed a faint green or blue-green flourescence. This effect has also been observed by Molnar[30] and attributed to impurities because the flourescence differs in natural and synthetic NaCl. Subsequent handling of colored samples was done in the near-dark or with appropriate filters over the light source to remove F-band light.

Samples of KCl and RbCl were also additively colored with excess K or Na metal. A crystal somewhat larger than sample size was sealed in an evacuated Vycor tube with the metal. The metal was previously melted in a rough vacuum to draw off trapped gas. The tube, crystal, and metal were so arranged in the furnace that the crystal was kept at 660°C, while the metal was at about 300°C. After about 20 hours the tube was quenched in a brine solution. Samples suitable for measurement were cleaved from inner regions of the colored crystal.

C. Measurement Procedure

The absorption coefficients of the crystals were measured at each desired pressure, as a function of wave number, over a range embracing the whole F-band. Readings were taken on a linear wave number scale, 250 cm^{-1} apart. To minimize the bleaching effect of the measuring light, the sensitivity adjustment on the spectrophotometer was set so that minimum slit widths were required. In this way the entire range of pressures could be explored with one x-irradiation of a sample. Such readings measured the transmission of the crystal and associated liquid and windows with respect to the reference hole which presented the same geometrical aperture. To obtain the true color center absorption curve, a correction had to be applied for the effect of the blank crystal and associated apparatus. This could be measured by assembling the system with an uncolored crystal or by bleaching the x-ray colored crystal still in the bomb at the end of a pressure run. No significant differences were detected between these alternatives, if the bleaching with an ordinary incandescent lamp were sufficiently long. The latter procedure was usually adopted for the x-rayed specimens, while the former procedure was necessary for the additively colored samples. It was found that these blank absorption curves changed with pressure only by a linear displacement of the ordinate of the curve. This effect arose in part from changes in the interface reflections with the variation of the index of refraction with pressure and in part from irreversible changes in interfacial conditions induced by pressure. From this it follows that one blank absorption curve taken at one pressure was sufficient to make the necessary correction. This curve was merely linearly displaced to fit the colored absorption curves at one point where the F-band absorption was negligible. Figure 2 shows an uncorrected F-band curve and a correction curve taken on the same sample.

A very slow contamination of the bomb fluid took place at the violet end of the spectral range due to a dissolution of binding agents from the O-rings and piston washer. This resulted in some uncertainty in the height of the F-band and gave rise to an uncertainty in the width at half-maximum, γ, of $\pm\ 0.004 \cdot 10^4\ cm^{-1}$.

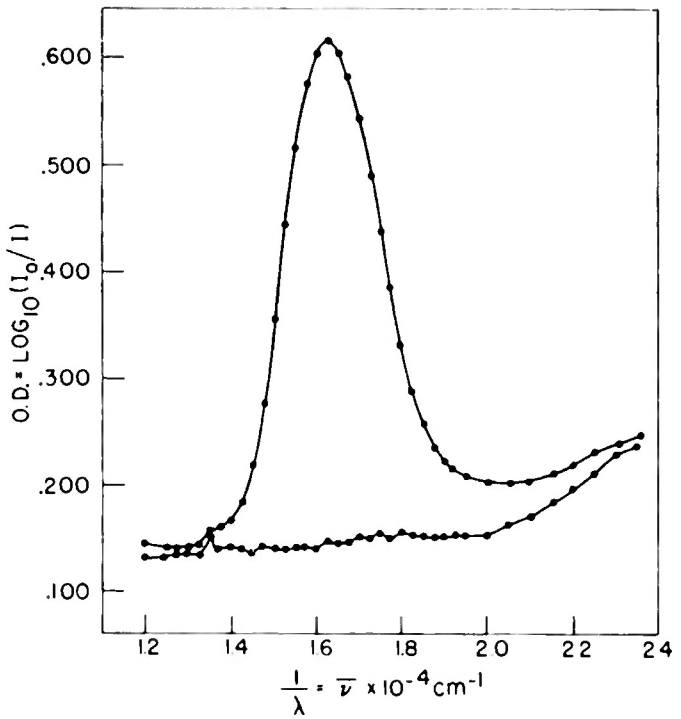

Fig. 2. Typical uncorrected F-band curve and a correction curve for the same sample.

To avoid the distortion in the position of the band maximum due to the optical bleaching during the measurements, absorption curves were taken with both increasing and decreasing wavelengths in separate runs on each compound except NaBr and KI. The corrected absorption curves were plotted with optical density (O.D. = $\log_{10} I_o/I$) as ordinate and wave number ($\tilde{\nu} = 1/\lambda$) as abscissa. For each curve the band parameters were measured, that is, the peak wave number, $\tilde{\nu}_m$, and the width at half-maximum, γ. The peak wave number was determined by extrapolation on the curve formed by the midpoints of the bell-shaped band at four O.D. values, starting up from half the maximum height of the band. With this method the uncertainty in $\tilde{\nu}_m$ was usually $\pm 0.002 \cdot 10^4$ cm^{-1}.

III. Results

A. Pressure Dependence of F-Band Parameters

The data from the measurement of the F-band peak wave number at intervals of about 1000 atmospheres are presented in Table I and in terms of wavelength in Table II. These data represent the average of two or more runs, except in the cases of NaBr and KI for which only one run was made. The experiments were conducted at room temperature, which was constant within 1°C during any single run but which varied during separate runs from 20° to 28°C. The agreement of the atmospheric pressure values in Table II with those listed by Ivey[5] is reasonably satisfactory in most cases. The agreement is even better with the recent values of Gnaedinger[31] for the compounds which he studied. The largest discrepancy from Ivey's tabulation is in the case of CsCl, but a re-examination of the source[1] of this value suggests that our value in Table II is reliable. The values based on

Table I

Pressure Dependence of F-band Peak Wave Number

Pressure bars[a]	Peak wave number[b] 10^4 cm^{-1}						
	NaCl	NaBr[c]	KCl	KBr	KI[d]	RbCl	CsCl
1	2.147	1.865	1.787	1.593	1.446	1.578	1.656
1000	2.161	1.876	1.798	1.604	1.460	1.591	1.666
2000	2.175	1.886	1.810	1.616	1.474	1.604	1.676
3000	2.190	1.897	1.821	1.628	1.489	1.615	1.685
4000	2.203	1.909	1.832	1.640	1.503	1.624	1.693
5000	2.215	...	1.842	1.652	1.517	1.634	1.701
6000	2.226	...	...	...	...	...	...
7000	2.238	...	...	...	...	...	...
8000	2.250	...	...	...	...	...	...

a 1 bar = 10^6 dynes/cm^2 = 1.01971 kg/cm^2 = 0.98692 atmos.
b $\pm$ 0.002 · 10^4 cm^{-1}.
c Measured with increasing wavelength only.
d Measured with decreasing wavelength only.

Table II

F-band Wavelength and Shift with Pressure

Crystal	λ_{max}(1 bar) A	$\lambda_{max}(1) - \lambda_{max}(5000)$ A
NaCl	4658 ± 5	143 ± 7
NaBr[a]	5362 ± 6	154 ± 8[c]
KCl	5596 ± 6	167 ± 9
KBr	6277 ± 8	224 ± 11
KI[b]	6916 ± 10	324 ± 14
RbCl	6337 ± 8	217 ± 11
CsCl	6039 ± 7	160 ± 10

a See footnote c, Table I.
b See footnote d, Table I.
c Extrapolated value.

a single run are distorted in the direction anticipated from the optical bleaching. It should be pointed out that the reported location of the peak may be affected by the method chosen to fix its location, due to the considerable width of the room temperature bands.

In order to make a more significant physical correlation, the results are considered as a function of the crystallographic unit cell distance, a.

This is calculated from the compressibility at 30°C determined by Slater and Bridgman, as tabulated by Birch,[32] with regard for recent corrections in the value of the compressibility of iron. For the complete data on the compressibility of RbCl, the original article by Bridgman[33] must be consulted. The effect on the elastic constants due to the presence of F-centers is negligible for color-center concentrations encountered in usual practice. A calculation of this type has been presented by MacKenzie,[34] in which the correction term is proportional to the relative decrease in density of the material due to the presence of small cavities or vacancies. This density change has been measured in two investigations,[35,36] but it is insignificant in the case at hand. A simple correlation of the pressure data is found by plotting $\log_{10}\tilde{\nu}_m$ against $\log_{10}a$ for each individual compound. The points lie along a straight line whose slope can be measured with an uncertainty of about 5 percent. Figure 3 presents typical curves from individual runs on each of the seven compounds, plotted on reduced scales. The straight lines become more clearly defined when data from several runs are considered, but these are omitted from the figure for the sake of clarity.

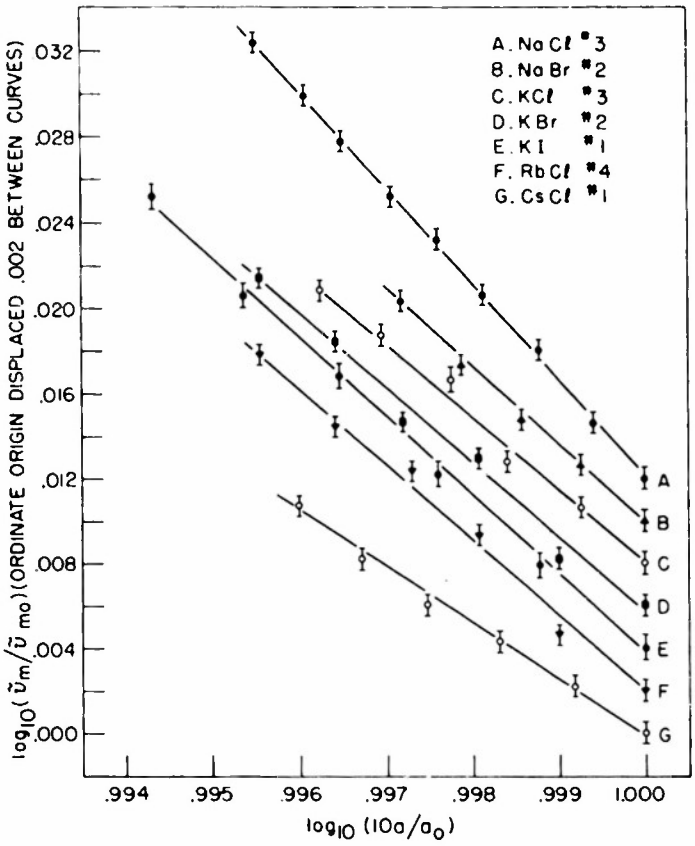

Fig. 3. Experimental curves showing dependence of peak wave number on lattice parameter. The reduced ordinates are referred to their values at atmospheric pressure.

The quantity of interest in this method of considering the results is the parameter $n_T(P)$, which is the negative of the slope of the line, i.e., $n_T(P) = -(\partial \ln \tilde{\nu}_m/\partial \ln a)_T$. From the figure it is seen that most of the lines

have nearly the same $n_T(P)$, i.e., 3.5, with the exception of NaCl which is high (4.4), and of CsCl which is low (2.8). The specific values are recorded in column 2 of Table III. The slopes did not vary outside the limits of uncertainty on different samples of the same compound, or on samples of different purity obtained from separate sources as in the case of RbCl, or on samples colored by different methods, additively or photochemically (x-ray) as in the cases of KCl and RbCl.

The widths of half maximum at atmospheric pressure are in good agreement with previously published values, subject to the experimental uncertainties mentioned above. For five of the seven compounds studied, the width of the band does not change with pressure, within fluctuations of 2 or 3 percent. For NaBr there appeared to be a decrease in band width amounting to about 10 percent in 4000 atmospheres. The experiment on NaBr left much to be desired because of a tendency of the sample to become fogged, impairing the optical measurements. In view of behavior of the five other compounds of the same structure and similar properties, the validity of this result for NaBr remains in considerable doubt. CsCl also shows a dependence of width on pressure, but in the opposite direction. The amount of the increase is about 5 percent and appeared in each of two runs on the same sample, despite a 5 percent difference in the zero pressure value of the width of the band between the two runs. The average value of this zero pressure width at room temperature is found to be $\gamma = 0.295 \pm 0.009 \cdot 10^4$ cm^{-1}. A value for comparison does not appear to be available in the literature. The validity of this width increase with pressure for CsCl is in doubt, as the argument employed above need not apply to a compound of different structure. Further experiments are required to confirm the results.

B. Effects of Structure Transformation

Experiments were performed on colored and uncolored crystals of RbCl at pressures in excess of that required to induce the structure transformation mentioned in Section I. The equilibrium transition pressure is about 5000 atmospheres and the associated relative decrease in volume is about 15 percent.[23] We shall consider first some observations on uncolored crystals, made visually rather than volumetrically due to the nature of the apparatus. The indication of the transition occurs at about 6500 atmospheres, at which point the ordinarily transparent crystal abruptly becomes almost opaque as though shattered into a large number of tiny crystals. The light transmission in this state is less by a factor of 50 to 100 than that of the normal crystal. The opacity is retained at high pressure but gradually decreases as the pressure is released. At atmospheric pressure the crystal is nearly as transparent as before the transformation and is often indistinguishable from ordinary crystals in normal light. Under crossed Nicols at moderate magnification (20x), such crystals show a highly developed strain pattern of many short lines covering the whole sample. (In some cases the region near the surfaces was free of strain.) The lines lie predominantly in the {110} planes, corresponding to the slip planes and directions of alkali halides.[37] Thus the transformation is accompanied by considerable plastic flow on a local scale.

The higher transition pressure observed in this work is in agreement with previous experience with salts of less than "atomic weight" purity.[24] Thus no difference not noted when the relatively purer RbCl salt was introduced in the present experiment.

The phenomenon of opaque or shattered crystals which regain their transparency is visually similar to that observed by Kraus and Nutting[38] for the low temperature transition in ammonium chrome sulfate and

selenate alums.

The crystallographic aspects of this type of structure transformation have been discussed by Buerger.[39] A contraction along a body diagonal of the face-centered cubic cell with an expansion perpendicular to that axis will transform the structure to simple cubic. Since there is no observable macroscopic distortion of the RbCl sample in the high pressure modification, the transformation must proceed from a large number of nucleation centers, at each of which there is a choice of four possible trigonal axes along which to propagate. Thus there may be some degree of mismatch between adjoining regions characterized by different transformation axes. Associated with this mismatch, or with that between regions which have transformed and those which have not, there should be variations in the index of refraction which give rise to light scattering and to the observation of opacity.

Laue back-reflection x-ray pictures of uncolored RbCl samples which had been through the transformation generally produced patterns of smeared ring segments, if the strain extended throughout the crystal. Annealing at 300°C for one day brought about recrystallization. These results differ somewhat from findings in a recent single-crystal study[40] of the CsCl transformation to the NaCl structure at 469°C.

Observations were made on x-ray colored crystals with the hope, initially, of detecting an F-band in the high pressure form of RbCl. A rough estimate of the expected spectral location of the band can be made by assuming the approximate validity of a Mollwo-like relation for salts of the CsCl structure. The position of the F-band at room temperature in CsCl is given in Table II, while the value of λ_{max} for CsBr at room temperature is 6750A, from measurements of Pringsheim.[41] If the peak wavelength is assumed to be proportional to some power of the interionic distance, calculation with these data yields the result that the power is about 2.6. Then, using Bridgman's data for the density of the high pressure form of RbCl, it is estimated that the F-band should be near 5200A.

The features described above for uncolored crystals remain valid for x-ray colored crystals. The optical density of the transformed crystals is about 1.5 to 2.0, which is a very insensitive region for the spectrophotometer. To reduce the light intensity passing through the reference hole, fine mesh screems were used. This reduced the apparent optical density of the crystals, but the measurements obtained were frequently erratic. Frequent development of window cracks around 7000 atmospheres also interfered with the work.

High pressure absorption measurements taken just after the transformation revealed the F-band located in its pre-transition position but decreased in height by 40 percent. Returning to one atmosphere, the band retained about 50 percent of its original height. Subsequent experiments of a "before and after" type demonstrated that 85-95 percent of the band could be destroyed by subjecting the colored crystal to the two-way transformation. For these experiments, the crystals were taken to 8000 atmospheres between the two absorption curve measurements.

The explanation of this effect is readily found in the experiments of Smekal[42] and of Schröder,[43] interpreted by Seitz,[44] which show that x-ray darkened crystals are bleached by cold work. As noted above, considerable plastic deformation accompanies the structure transformation. Schröder reduced the F-band height by 20 percent with uniaxial stresses of 40-400 g/mm^2. A separate experiment in this study confirmed his result by reducing the band height by at least 25 percent after the application

of a load of 500 g/mm^2 on an x-rayed KCl sample in a bath at 0°C. This result makes allowance for the natural thermal bleaching during the period between measurements.

Experiments were also undertaken on additively colored RbCl crystals to study the effect of the structure transformation. For conventional work this type of coloration is relatively stable. In absorption measurements above the transition pressure, no new band was observed, but there was evidence of a considerably reduced pre-transition F-band. "Before and after" experiments on samples colored with excess K metal produced complete destruction of the F-band and recrystallization of the sample upon returning to atmospheric pressure. An uncolored but quenched sample did not recrystallize during such an experiment. Its behavior was identical to that of an annealed uncolored specimen.

The effect of plastic flow on additively colored crystals was investigated in an auxiliary experiment. Such work does not appear to have been undertaken in the past. KCl crystals containing excess K metal were subjected to uniaxial loads of from 200 to 500 g/mm^2, while the samples were kept at 0°C. The decrease in the height of the F-band is negligible and there is no detectable growth of subsidiary long-wavelength bands. Compared with the effects in x-ray colored crystals, this result is a bit surprising. In analyzing this we take note of the suggestion of Tyler,[45] based on the experiments of Gyulai and Boros,[46] that electronic processes may contribute to the enhanced conductivity due to plastic flow.[47] The latter workers, using low stresses of 100 g/mm^2, observed short decay times (10^{-3} sec) for the enhanced conductivity in alkali halide crystals. The magnitude of the effect was doubled when photochemically or additively colored crystals were studied, but the decay time was unaffected. For the present experiments, the work of Gyulai and Boros implies that the plastic flow causes the evaporation of electrons from the F-centers. The conclusion to be drawn from the null effect observed is that the necessary rearrangements of vacancy aggregates to form M- or other centers cannot take place in the few seconds during which the dislocations are moving rapidly. Thus the electrons are mostly retrapped in the isolated negative ion vacancies from which they were ejected.

In discussing the effect of plastic flow on x-ray colored crystals, Seitz[44] offered three tentative explanations. Only the first of these is consistent with the observations of Gyulai and Boros and with the null effect of plastic flow on additively colored crystals. This is the suggestion that the region about the vacancies associated with the color centers becomes heated when a dislocation passes very close, and that the electrons and holes evaporate and have an opportunity to recombine. The vacancies involved probably lie close to dislocations,[48] and should be in an ideal position to experience the thermal effects which accompany the motion of dislocations. Variations of the other two suggested explanations would allow a bleaching effect due to cold work in additively colored crystals, contrary to our observations.

IV. Theory

The theoretical interpretation of the shift of the absorption peak with pressure or temperature must include the effect of the variation of interatomic distance and also the effect of the interaction of the F-center electron with the lattice vibrations. These effects have been considered separately by various investigators, as mentioned in Section I, in attempts to

account for the temperature shift. There does not appear to have been any attempt to combine both parts into a consistent picture. The reason for this probably lies in the difficulty in making a theoretical estimate of the relative magnitudes of the separate contributions of each effect and in the lack, up to this time, of sufficient experimental data from which to evaluate these relative contributions. The results of the present experiment provide the additional data with which to overcome this obstacle and to make empirical estimates of the magnitudes of the individual effects.

We characterize the results of the pressure experiment in terms of the parameter $n_T(P)$ listed in column 2 of Table III. Along with it we require for comparison the corresponding parameter for the temperature shift, $n_P(T) = -(\partial \ln \tilde{\nu}_m / \partial \ln a)_P$. It is listed in column 3 of the same table and is evaluated for a range around room temperature except as otherwise noted. The data for the dependence of $\tilde{\nu}_{max}$ on temperature is mainly due to Mallwo,[4] supplemented in various cases by data from Gnaedinger,[31] Molnar,[30] and Pringsheim.[41] Room temperature thermal expansion data is employed in most cases, because considerable discrepancies often appear in the values from different workers as they depart from room temperature. The values used are listed in column 4. It is seen that for most compounds the "pressure slope," $n_T(P)$, is smaller than the "temperature slope," $n_P(T)$.

Table III

Experimental and Theoretical Parameters Describing the Dependence of the F-band Maximum on Pressure and Temperature

1	2	3	4	5	6	7	8	9
Compound[a]	$n_T(P)$	$n_P(T)$	α_P	b/θ	n_Q[b]	f[c]	n_M[d]	f[e]
			10^{-6} deg^{-1}	(cm deg)$^{-1}$				
NaCl	4.4 ± 0.1	4.0 ± 0.2	40 ± 1	~0	1.5	2.9	1.94	2.3
NaCl[f]		4.4 ± 0.2	44 ± 1	~0				
NaBr	3.6 ± 0.2	3.8 ± 0.2	41 ± 1	0.2 ± 0.2	(1.5)	2.4	1.83	2.0
KCl	3.5 ± 0.1	5.0 ± 0.2	35 ± 1	0.9 ± 0.1	1.6	2.1	1.74	2.0
KBr	3.5 ± 0.1	4.5 ± 0.2	41 ± 1	0.7 ± 0.1	(1.6)	2.1	1.66	2.1
KI	3.7 ± 0.1	4.4 ± 0.2	41 ± 1	0.4 ± 0.1	(1.6)	2.3	1.55	2.4
RbCl	3.4 ± 0.1	5.2 ± 0.2	35 ± 1	1.0 ± 0.1	(1.6)	2.1	1.66	2.0
CsCl	2.8 ± 0.2	4.9 ± 0.2[g]	46 ± 1	1.6 ± 0.2	1.76	1.5	2.65[h]	1.0

a At room temperature, unless otherwise noted.
b Calculated from square well model; values in parentheses estimated.
c Using values from column 6.
d Derived from plot of $\log_{10}E$ vs a^{-1}.
e Using values from column 8.
f At 200°C.
g Calculated for CsBr; λ_m(-190°C) = 6450A, reference 41.
h Obtained by plotting data from CsCl and CsBr.

We use a high temperature representation for the F-center energy at the peak of the absorption curve, E, in the form

$$E = E_o\,[R(a)] - b\,T/\theta(a). \qquad (1)$$

A suitable modification may be made for the low temperature region. E_o is the energy at absolute zero and is a function of the distance parameter, R, which in turn depends on the interionic distance, a, in the bulk crystal. The distance R is the significant parameter in determining the energy E_o, and its interpretation depends on the model employed to calculate the F-center energy levels. It may be the radius of the potential well of the vacancy in a continuum model, or it may be the actual interionic distance of the ions immediately surrounding the vacancy after relaxation has taken place in a molecular orbital model. The form of the second term in Eq.(1) has its basis in the work of Huang and Rhys[16] and of Muto.[12] Huang and Rhys assume that the predominant coupling between electron and lattice is produced by the long-range Coulomb interaction between the F-center electron and the electric polarization associated with the single-frequency longitudinal optical vibrations of the lattice. They use this coupling to account for the temperature broadening of the band. They find, however, as has been confirmed in the more general treatments of Lax[17] and of O'Rourke,[18] that this idea does not give rise to any shift of the absorption peak with temperature. To rectify this, they use an idea (previously put forth by Muto) that when an F-center changes its state the lattice frequency is altered by a small amount. This small frequency change, proportional to b in Eq. (1), does not appear in the harmonic forces approximation usually used to describe the lattice. Thus the parameter $\theta(a)$, in our expression for the energy, is the characteristic temperature related to the longitudinal optical vibration frequency of the lattice. This temperature is sufficiently close to the usual Debye temperature that we need not distinguish them.

For the shift of the absorption band peak with pressure we must form the derivative $(\partial \ln E/\partial \ln a)_T$ from Eq. (1). Thus we have

$$\left(\frac{\partial \ln E}{\partial \ln a}\right)_T = -\,n_T(P) = \left(\frac{\partial \ln E}{\partial \ln \theta}\right)_{T,R} \frac{d \ln \theta}{d \ln a} + \left(\frac{\partial \ln E}{\partial \ln R}\right)_{T,\theta} \left(\frac{\partial \ln R}{\partial \ln a}\right)_T. \qquad (2)$$

From the Grüneisen relation we obtain

$$d \ln \theta / d \ln a = -\,3\,\gamma_G, \qquad (3)$$

where γ_G is the Grüneisen constant. The term $(\partial \ln R/\partial \ln a)_T$, the ratio of the relative change in R to the relative change in a at constant temperature, is equal to the ratio of the effective isothermal compressibility around the F-center to the isothermal compressibility of the bulk material. There are several ways of estimating this, but we shall consider it as unknown and designate it by the symbol f_T. The derivative $(\partial \ln E/\partial \ln R)_{T,\theta} = (d \ln E_o/d \ln R)$ may also be estimated in a number of ways. A particular model may be assumed for the F-center, from which the energy levels may be calculated in terms of their dependence on R, and thus the value of the derivative may be calculated. We designate the negative of this derivative by the symbol n_Q. As an alternative the slope of a plot of the experimental values of $\log_{10}E$ vs $\log_{10}a$ may be employed, if it is assumed that the factor which relates the equilibrium values of R and a does not vary rapidly from one

compound to another. Such a plot should be made using the values of E and a at absolute zero or as an intermediate compromise, using values which correspond to the characteristic temperature, θ. The negative of the slope of this plot we call n_M, to distinguish it as a different way of estimating n_Q.

This matter will be discussed further in the following section. For the present, we shall use values calculated from an exceedingly simple continuum model, namely that which represents the F-center as an electron trapped in a spherically symmetric square potential well. The radius of the well R is chosen equal to the interionic distance a. The depth of the well is chosen so that the energy difference between the ground s-state and the excited p-state is equal to the observed F-center energy. To evaluate the variation of E_o with R, it is assumed that the well depth is inversely proportional to its radius R. The results of such a calculation are that the values of n_Q are 1.5, 1.6, and 1.76 for NaCl, KCl, and CsCl respectively. Thus we obtain for the pressure shift

$$n_T(P) = 3\,\gamma_G\, b\, T / E\,\theta + n_Q\, f_T \,. \qquad (4)$$

The shift of the absorption band peak with temperature is derived in an analogous fashion, by forming $(\partial \ln E / \partial \ln a)_P$. From Eq. (1) we obtain

$$\left(\frac{\partial \ln E}{\partial \ln a}\right)_P = -\,n_P(T) = \left(\frac{\partial \ln E}{\partial T}\right)_{\theta,R} \left(\frac{\partial T}{\partial \ln a}\right)_P + \left(\frac{\partial \ln E}{\partial \ln \theta}\right)_{T,R} \frac{d \ln \theta}{d \ln a} +$$

$$\left(\frac{\partial \ln E}{\partial \ln R}\right)_{T,\theta} \left(\frac{\partial \ln R}{\partial \ln a}\right)_P \,. \qquad (5)$$

The term $(\partial T/\partial \ln a)_P$ which appears here is the reciprocal of the isobaric linear thermal expansion coefficient, α_P. Similar to its counterpart in the pressure shift, the term $(\partial \ln R/\partial \ln a)_P$ is equal to the ratio of the effective thermal expansion coefficient around the F-center to the bulk value of the thermal expansion coefficient. We designate this factor by the symbol f_P. The expression for the temperature shift is then given by

$$n_P(T) = b/E\,\theta\,\alpha_P + 3\,\gamma_G\, b\, T/E\,\theta + n_Q\, f_P \,. \qquad (6)$$

We may consider that the thermal expansion of a solid arises from the effect of an outward thermal pressure set up by the anharmonicity of the vibrations of the atoms of the solid. This thermal pressure acts against the same forces as does the external pressure considered with respect to the compressibility of a solid. Since the thermal expansion is particularly dependent on the non-linearities in these forces, we may expect that the effective thermal expansion factor, f_P, is at least as large as the effective compressibility factor, f_T, in the neighborhood of the F-center. We lack, however, a method of evaluating this difference in detail. Consequently, we may not make too great an error if we assume that the two factors are approximately the same. If we then drop the subscripts from these two factors in Eqs. (4) and (6), we may combine these two expressions to obtain the result

$$b/E\,\theta\,\alpha_P = n_P(T) - n_T(P) \,. \qquad (7)$$

In this way the quantity b/θ may be calculated from the experimental data

on the pressure and temperature shifts of the F-band absorption maximum. These values are listed in column 5 of Table III. Making a substitution back into Eq. (4), the value of the factor f may be obtained. The magnitude of this factor will depend directly on the value used for the term n_Q. Using the calculations from the square well continuum model, the values of f listed in column 7 of Table III are obtained. If values of n_Q obtained from a different method are used, a new set of values for f will result.

In the preceding analysis we have presented a simple approach in which the temperature and pressure dependence of the F-band absorption peak are treated in a unified manner. The conclusion is reached that the shift of band with pressure is due mainly to the dependence of the energy on interatomic distance, with a small contribution, amounting to 5 percent at most, arising from the interaction with optical lattice vibrations. The temperature shift is governed by the same factors as the pressure shift, plus an additional term, as large as 40 percent, arising from a further contribution from this same electron-lattice interaction.

We turn now to a consideration of the width of the F-band. This problem is rather unsettled. As pointed out in Section I, two explanations have been offered by separate groups of investigators. We have mentioned the long range electron-optical lattice vibration interaction used by Huang and Rhys. This coupling gives rise to a broadening of the absorption band. Lax and O'Rourke have shown that a simple formula describes this width, in the approximation in which all lattice modes have the same frequency (that of the longitudinal optical vibrations). If we call γ_1 the width at half-maximum due to this mechanism, we have from O'Rourke[18]

$$\gamma_1 = 2(2\ln 2)^{\frac{1}{2}} \hbar\omega [S \coth(\hbar\omega/2kT)]^{\frac{1}{2}}, \qquad (8)$$

where ω is the frequency just mentioned, S is the net number of vibrational quanta involved at the absorption maximum, and the numerical factor in front converts the root-mean-square value of the distribution to the width at half-maximum, on the assumption that the distribution is approximately Gaussian. The width γ_1 is independent of the parameter b introduced in Eq. (1).

The second contribution to the broadening arises when we consider that the local deformation of the lattice causes variations in the gap between the electronic energy levels. In an adiabatic approximation, we may say that absorption takes place when the wavelength of light coincides with the energy gap determined as a function of the displacement of the surrounding ions. Several versions of this approach have appeared.[9,19,20] Their principal achievement has been the demonstration that the finite width of the F-band at low temperatures may be accounted for by the zero-point vibrations of the neighboring ions. The idea which is common to all is that the mean square fluctuation in the F-center energy is determined by the mean square fluctuation in a suitable radius for the vacancy.

A factor which has been overlooked in these versions is the role of shear waves in causing a broadening. When the region of the vacancy is distorted from its spherical shape, it is reasonable to expect a change in the F-center energy, at least through an interaction with the angular momentum of the excited p-state. The continuous variation of the non-spherical distortion would then contribute to the band width. Since we lack a detailed calculation of this effect, we may account in a rough way for the two shear modes by multiplying the contribution to the width from the radial distortions by the factor $(3)^{\frac{1}{2}}$.

Both explanations of the band width seem to be valid. Consequently, we would like to combine their separate contributions to obtain the total band width. Since they appear to be independent, and assuming, for simplicity, that each gives rise to a Gaussian shape, we must add them as the square root of the sum of the squares of the individual widths.

To be specific, we consider a very simple calculation for the local deformation width. The coupling in this case is to the acoustical modes of the lattice. From the Einstein formula for fluctuations, we may write for the mean square fluctuation in the volume around the F-center

$$\langle (V-V_o)^2 \rangle = V_o \chi_{eff} kT , \qquad (9)$$

where V_o is the equilibrium value of this volume, χ_{eff} is the effective compressibility around the F-center, and kT is the Boltzmann constant times the absolute temperature. This expression assumes that the temperature is sufficiently high that equipartition of energy has occurred. This formula gives values differing by only a few percent from a more rigorous formula containing a Debye function and the zero point energy explicitly. The corresponding fluctuation in the F-center energy is obtained from a Taylor expansion about its mean value. We next consider that the volume is a sphere of radius R, that the effective compressibility χ_{eff} is greater than the bulk compressibility χ_o by the factor f, that the shear modes are accounted for by the simple factor $(3)^{\frac{1}{2}}$, and that the conversion factor from root-mean-square to width at half-maximum is that for a Gaussian shape. Thus we obtain for γ_2, the deformation width,

$$\gamma_2 = n_Q E [(2 \ln 2) f \chi_o kT/\pi R^3]^{\frac{1}{2}} . \qquad (10)$$

For KCl at room temperature, using $n_Q = 1.6$, a calculation from Eq. (10) gives $\gamma_2 = .20 (f)^{\frac{1}{2}}$ ev.

We are now able to combine γ_1 and γ_2. For KCl under the same conditions, Eq. (8) gives $\gamma_1 = 0.088 (S)^{\frac{1}{2}}$ e.v., where S is still undetermined. One possible procedure is to fit these results to the observed total band width, γ, after choosing a suitable value of f, say 2. This produces an estimate of S such that S = 5.4. If we had ascribed the full width to the interaction with optical lattice vibrations, with Huang and Rhys, the value of S required would be 16 for KCl. On the other hand, Huang and Rhys estimate from Simpson's wave functions for NaCl that S should be about 4. Thus our simple model for the deformation width, using a value for f consistent with the pressure shift data, enables us to make a reasonable estimate of the parameter S in the Huang-Rhys contribution to the width.

The preceding discussion of the theories of the width of the F-band serves principally to illustrate that there is considerable room for a careful theoretical analysis of the problem.

Of particular interest in the present research is the fact that the observed F-band width did not change with pressure for most of the compounds studied. Using the various expressions for the width, either separately or in suitable combination, it may be predicted that the width should increase about 1 or 2 percent in 5000 atmospheres. In view of the uncertainties described in measuring the width, such an increase could not be detected.

V. Discussion

Several points in the preceding section require further consideration.

The first to which we turn our attention is the term $f_T = (\partial \ln R/\partial \ln a)_T$, appearing in Eq. (2). It is easy to understand why this term may be greater than unity. R represents a measure of the radius of a spherical cavity from which matter has been removed, i.e., a halogen ion, while a is the normal interionic distance in the crystal at a great distance from the cavity. The ion which previously occupied this region exerted a repulsive force on the surrounding material. The electron which replaces the negative ion does not exert this repulsion in a first approximation. Thus when the crystal is subjected to an external pressure, it is natural to expect that the cavity will contract more when it is empty than when it is occupied by matter. This line of reasoning suggests that it may be fruitful to consider the crystal as a continuous elastic medium. From this point of view the problem at hand reduces to the simple calculation of the radial strain in a shell bounded by concentric spherical surfaces. The solution of this problem provides an independent estimate of $f_T \simeq f$. The details may be obtained from any standard text-book on elasticity, e.g., Love.[49] The radius of the internal sphere is R and the internal pressure is taken to be zero. We let the radius of the external sphere become infinite and equate the pressure on its surface to the pressure applied externally to the crystal. Thus we obtain

$$(\Delta R/R)/(\Delta a/a) = (\partial \ln R/\partial \ln a)_T = 1 + (3K/4\mu), \quad (11)$$

where the crystal is treated as an isotropic body describable by two elastic constants: K, the bulk modulus and μ, the shear modulus. The ratio (K/μ) may be calculated from the experimental data,[32] using an average of the two shear moduli C_{44} and $\frac{1}{2}(C_{11} - C_{12})$ for μ. An alternate way to obtain this ratio is to assume that Poisson's ratio is $\frac{1}{4}$ for these crystals, from which we can readily find $(K/\mu) = (5/3)$. In this approximation the result is $f = 2.25$, while the values obtained from the experimental data range from about 2.13 to 2.25. The results of this independent estimate of f are in approximate agreement with those obtained from the pressure-temperature shift theory in the preceding section.

From another point of view we may expect that f should be smaller for CsCl since it has a more closely packed structure than the other compounds. The ions may be treated as hard spheres and the distance that the nearest neighbors can move toward the center of the vacancy without coming into contact may be calculated for the two structures involved. Thus for Cs and Cl ions it is found that they may move nearly twice as far when arrayed in the NaCl structure as when in the CsCl structure. This is a very crude approach, but it does serve to indicate why the f values for CsCl may be lower, as found in Table III.

We now consider in further detail the various ways of estimating the quantity n_Q which appears throughout the theory of the pressure and temperature shift. It was emphasized earlier that the values calculated for f from the theory depend on the values used for this quantity. If some model for the F-center is assumed for which the energy levels can be calculated, then n_Q may be computed readily. The various continuum models that have been used lend themselves to an easy calculation of this term. Before adopting the square well model described in the preceding section, calculations were made with Simpson's[8] model using the revised potential well depth suggested by Krumhansl and Schwartz,[11] and with Pincherle's[10] model which simplifies the calculations of the Simpson model. In the Pincherle calculation the potential well has a flat bottom out to a radius R and has a

simple or slightly modified coulomb dependence at large distance. In our calculation with this model the well depth was chosen so as to reproduce the experimentally observed energy difference between the two states, as was done in the square well model. In obtaining n_Q, the well depth was assumed to vary inversely with the radius R, again as in the square well model. This assumption is certainly a reasonable one, for the principal contribution to the depth is the Madelung energy which is controlled mainly by the distance to the nearest neighbors, and the secondary contribution is the energy of polarization of the surroundings, which is inversely proportional to the well radius. The result of this calculation for NaCl is n_Q = + 1.53 when the static and high frequency dielectric constants are held fixed, and + 1.50 when they are allowed to vary with pressure. An earlier calculation with Simpson's model with more restricted conditions gave a result of about + 1.3. The similarity of these results led to the adoption of the square well model which is the easiest to handle numerically. Recent evidence, noted in Section I, has pointed to the importance of the molecular orbital model of the F-center. This model has found its greatest success in explaining hyperfine interactions in electron spin resonance experiments. For the present experiment, involving a relatively large scale effect, it is felt that the continuum model represents a suitable approximation with which to treat the problem. Also, the only quantitative calculation[9] of F-center energy levels with this model is not presented in a way which may be readily adapted to the type of calculation just described.

The alternative to calculating n_Q from a specific model is to obtain it from some sort of plot of the experimental data, as mentioned in Section IV. We then replace n_Q by n_M in Eqs. (4) and (6). Assuming that a straight line may be drawn through the points on a $\log_{10}E$ vs $\log_{10}a$ plot, we might be tempted to adopt Ivey's value for its slope, namely $n_M = 1.84$. If the data is plotted corresponding to the Debye temperature for each compound, we find that a better straight line may be drawn for which $n_M = 1.6$. Actually, the notion of a straight line on such a plot is more fiction than fact. Plotting the data for the chloride, bromide, and iodide of sodium, potassium, and rubidium, with $\log_{10}E$ and $\log_{10}a$ as ordinates, we find that curves (not straight lines!) having approximately the same shapes may be drawn through the points with a common cation. Without knowing the exact shape of these curves, defined by only three points, some sort of compromise must be adopted to estimate the values of n_M, which change from compound to compound. It would be desirable to find a suitable choice of ordinates on which a straight line could be drawn with some reliability. In attempting to do this, it was found that a plot of $\log_{10}E$ vs a^{-1} produces a line which is at least as good as the $\log_{10}E$ vs $\log_{10}a$ "straight line." Evaluating the n_M parameters from this plot gives a variation from compound to compound in the same direction as found with the curves above. Considering all these alternatives, it is important to note that they do not differ significantly from one another in the results that they give. Also, these results are not particularly different from those found with the various models. To show approximately how these alternatives vary, we have tabulated values of n_M and f in columns 8 and 9 of Table III as obtained from the plot of $\log_{10}E$ vs a^{-1}.

An additional observation may be made in connection with the graphical way of estimating $n_M \approx n_Q$. We may plot the results of the molecular orbital calculation of Inui and Uemura on a $\log_{10}E$ vs $\log_{10}a$ graph. Using their model IV with a potential due to 26 neighboring ions, the data for LiCl, LiBr, and LiI fall on a rather good straight line with $n_M = 1.43$. This bit of

evidence, in general agreement with what has gone before, may be taken as support for our contention that no startling deviation is to be expected from the molecular orbital model, and that the continuum model is a useful approximation for this experiment.

By introducing the factor f, and making use of the lattice interaction constant b, we are able to develop a reasonably consistent account of the behavior of F-center absorption as a function of pressure and temperature. The factor f, as derived in the theory, is in satisfactory agreement with an estimate of its value from elasticity theory. Also, it is used in a simple theory of the band width, which combines the two proposed mechanisms of broadening, in such a way as to give a reasonable value for the number of vibrational quanta involved in broadening by interaction with optical lattice vibrations. The coupling constant b/θ does not vary too greatly, if we exclude the sodium salts and CsCl. As used by Huang and Rhys and others, it would appear that negative values for b/θ are inadmissable. For this reason we say $b/\theta \sim 0$ for NaCl, when small negative values would appear from the calculation. Perhaps some experimental uncertainty, unknown to us, may account for the discrepancy. Another possibility is that the theory has not included some term which, although it may be small, may be sufficient to account for the different behavior of NaCl and NaBr in contrast to the other compounds. The term in b appears to be the only satisfactory suggestion, thus far offered, which is capable of treating the difference in the pressure and temperature shifts. A better understanding of its behavior must await a better theoretical elucidation of the mechanism involved in the electron-optical lattice vibration coupling which brings about the small change in lattice frequencies.

VI. Acknowledgments

The author wishes to express his gratitude to his sponsor, Professor A. W. Lawson, for his advice and encouragement throughout the course of this investigation. Much appreciation is expressed to the members of the Institute for the Study of Metals for many suggestions and discussions, and to the members of the Laboratory of Molecular Structure and Spectra for their cooperation and for making available their experimental facilities. Acknowledgment is also made to Messrs. K. Lindholm and N. D. Nachtrieb for assistance in the design, construction, and maintenance of the high pressure apparatus. The author is indebted to the Shell Oil Company for the grant of a fellowship during this work. The experiment was supported in part by the Office of Naval Research.

References

1. R. W. Pohl, Proc. Phys. Soc. (London) 49 (extra part), 3 (1937).
2. N. F. Mott and R. W. Gurney, Electronic Processes in Ionic Crystals (Oxford University Press, London, 1940).
3. F. Seitz, Revs. Modern Phys. 18, 384 (1946).
4. E. Mollwo, Z. Physik 85, 56 (1933).
5. H. F. Ivey, Phys. Rev. 72, 341 (1947).
6. S. R. Tibbs, Trans. Faraday Soc. 35, 1471 (1939).
7. R. Kubo, J. Phys. Soc. Japan 3, 254 (1948); 4, 322, 326 (1949).
8. J. H. Simpson, Proc. Roy. Soc. (London) A197, 269 (1949).
9. T. Inui and Y. Uemura, Progr. Theoret. Phys. 5, 252, 395 (1950).
10. L. Pincherle, Proc. Phys. Soc (London) A64, 648 (1951).

11. J. A. Krumhansl and N. Schwartz, Phys. Rev. 89, 1154 (1953).
12. T. Muto, Progr. Theoret. Phys. 4, 181, 243 (1949).
13. C. A. Hutchison, Jr. and G. A. Noble, Phys. Rev. 87, 1125 (1952).
14. A. H. Kahn and C. Kittel, Phys. Rev. 89, 315 (1953).
15. A. F. Kip, C. Kittel, R. A. Levy, and A. M. Portis, Phys. Rev. 91, 1066 (1953).
16. K. Huang and A. Rhys, Proc. Roy. Soc. (London) A204, 406 (1950).
17. M. Lax, J. Chem. Phys. 20, 1752 (1952).
18. R. C. O'Rourke, Phys. Rev. 91, 265 (1953).
19. T. Nagamiya, J. Phys. Soc. Japan 7, 354 (1952).
20. E. Burstein and J. J. Oberly, Natl. Bur. Standards Circular No. 519, 285 (1952).
21. E. Burstein, J. J. Oberly, and J. W. Davisson, Phys. Rev. 85, 729 (1952).
22. J. C. Slater, Phys. Rev. 23, 488 (1924).
23. P. W. Bridgman, Z. Krist. 67, 363 (1928).
24. R. B. Jacobs, Phys. Rev. 54, 468 (1938).
25. Purchased from The Linde Air Products Co., Synthetic Gem Division, Chicago, Ill.
26. T. C. Poulter, Phys. Rev. 35, 297 (1930); see also P. W. Bridgman, The Physics of High Pressure (G. Bell and Sons, Ltd., London, 1949), p. 58.
27. D. Lazarus, Phys. Rev. 76, 545 (1949).
28. W. H. Duerig and J. J. Markham, Phys. Rev. 88, 1043 (1952).
29. See H. E. Buckley, Crystal Growth (John Wiley and Sons, Inc., New York, 1951).
30. J. P. Molnar, Thesis, Massachusetts Institute of Technology, 1940 (unpublished).
31. R. J. Gnaedinger, Jr., J. Chem. Phys. 21, 323 (1953).
32. F. Birch, et al., Handbook of Physical Constants (Geological Society of America, Special Papers, No. 36, 1942), p. 52. See also reference 27.
33. P. W. Bridgman, Proc. Am. Acad. Arts Sci. 67, 345 (1932).
34. J. K. MacKenzie, Proc. Phys. Soc. (London) 63B, 2 (1950).
35. Estermann, Leivo, and Stern, Phys. Rev. 75, 627 (1949).
36. H. Witt, Nachr. Akad. Wiss. Göttingen, Math-physik Kl. No. 4, 17 (1952).
37. E. Schmid and W. Boas, Plasticity of Crystals (F. A. Hughes Company, London, 1950), pp. 228, 233.
38. D. L. Kraus and G. C. Nutting, J. Chem. Phys. 9, 133 (1941); see also J. Eisenstein, Revs. Modern Phys. 24, 74 (1952).
39. M. J. Buerger, "Crystallographic Aspects of Phase Transformations," Chapter in Phase Transformations in Solids (John Wiley and Sons, Inc. New York, 1951).
40. Menary, Ubbelohde, and Woodward, Proc. Roy. Soc. (London) A208, 158 (1951).
41. P. Pringsheim (private communication). The author is indebted to Dr. Pringsheim for providing this information.
42. A. Smekal, Z. Ver. deut. Ing. 72, 667 (1928).
43. H. J. Schröder, Z. Physik 76, 608 (1932).
44. F. Seitz, Phys. Rev. 80, 239 (1950).
45. W. W. Tyler, Phys. Rev. 86, 801 (1952).
46. Z. Gyulai and J. Boros, Math. naturw. Anz. ungar. Akad. Wiss. 59, 115 (1940).
47. See reference 44 for a discussion of the earlier experiments of Gyulai and Hartly on the influence of plastic flow on conductivity.
48. See the recent work of J. J. Markham, Phys. Rev. 88, 500 (1952) and F. Seitz, Phys. Rev. 89, 1299 (1953) for development of the idea that F-

centers are located near dislocations, as a consequence of their formation at incipient vacancies associated with jogs in Taylor dislocations.
49. A. E. H. Love, The Mathematical Theory of Elasticity (Cambridge University Press, Cambridge, 1927), p. 142.

IX

THE SUPERCONDUCTIVITY OF SOME TRANSITION METAL COMPOUNDS*

George F. Hardy** and John K. Hulm
(Submitted to The Physical Review)

Abstract

About eighty transition metal compounds comprising borides, carbides, nitrides, oxides, silicides, and germanides of Groups 4A, 5A, and 6A metals were tested for superconductivity down to 1.20°K, using a magnetic method. Among the specimens were most of the known compounds of the above type not examined magnetically for superconducting behavior by previous workers, and in all cases their structures were checked by x-ray diffraction analysis. The eleven new superconductors W_2B (3.10°), Nb_2C (9.18°), Ta_2C (3.26°), Nb_4N_3 (7.2°), V_3Si (17.1°), V_3Ge (6.01°), Mo_3Si (1.30°), Mo_3Ge (1.43°), α-$ThSi_2$ (3.16°), β-$ThSi_2$ (2.41°), and W_3Si_2 (2.84°) were discovered, with the transition temperatures (°K) shown in parenthesis. These compounds include the first superconducting germanides, V_3Ge and Mo_3Ge, which, together with V_3Si and Mo_3Si, crystallize in the cubic β-tungsten structure. The transition temperature of V_3Si is apparently the highest known for any binary superconducting compound.

I. Introduction

It is well known that there exists a group of compounds of transition metals with non-metals, typified by the borides, carbides, and nitrides of "A group" transition metals, which possess most of the properties of metals or alloys. These compounds show metallic luster and have thermal and electrical resistivities of the same order of magnitude as those for pure metals, together with a positive temperature coefficient of electrical resistivity. In many cases they are known to have high hardness values, high moduli of elasticity, high melting points, and relatively high strengths at elevated temperatures, properties which cause them to be of considerable technological importance.[1] At the time of the first extensive crystal structure determinations for these substances, carried out by Hägg,[2] it seemed appropriate to call them "interstitial" compounds, implying that the non-metal atoms merely fit into interstices in the metallic lattice, thereby slightly modifying the properties of the pure metal. More recent investigations have shown that for borides the interstitial picture is inadequate owing to the tendency of the boron to form chains, nets, and three-dimensional networks,[3] while even for carbides and nitrides it is the exception rather than the rule for the lattice of metal atoms in the compound to be identical with the lattice of the pure metal.[4]

* Based on a dissertation submitted by G. F. Hardy in partial fulfillment of the requirements for the degree of Doctor of Philosophy at the University of Chicago.

** Now at the Research and Development Laboratories, The Barrett Division, Allied Chemical and Dye Corporation, Glenolden, Pa.

Among the typically metallic properties of transition metal compounds one may include the fact that many become superconducting at temperatures of a few degrees absolute. This behavior was first discovered during the extensive investigations of Meissner and his co-workers over twenty years ago.[5-7] Unfortunately, Meissner's results were obtained using electrical resistance measurements, which have since been shown to yield unreliable results with impure specimens. The problem has recently been taken up by several other investigators[8-10] using more decisive magnetic methods; these experiments have revealed a number of new superconducting compounds, and have corrected several errors in the earlier work.

In spite of the increased interest in this field, the results reported to date have been confined mainly to the borides, carbides, and nitrides of the "A group" transition metals and even here have not covered all of the known compounds. Since these data are important for the light which they may throw on the fundamental chemical and crystallographical conditions favoring the occurrence of superconductivity, we have felt that it would be of value to complete and extend them as far as possible. Using a magnetic method for the detection of superconductivity, we have studied a number of borides, carbides, nitrides, and oxides which have not previously been tested for superconducting behavior, and have reinvestigated several compounds of this type already tested by previous workers. We have also systematically surveyed the occurrence of superconductivity among the silicides and germanides of the "A group" transition metals, since these compounds have been largely neglected in previous superconducting work, although they have received much study from the metallurgical standpoint. While many of our data on the latter compounds have already been briefly reported,[11] the present paper describes the experimental techniques used and the detailed structural and superconducting results so far obtained.

II. Experimental Details

A. Method

Superconductivity is most simply detected by measuring either the electrical resistance or the magnetic permeability of a given specimen. The ideal specimen for both these tests is a long solid rod of pure, homogeneous, strain-free material; for such a specimen the electrical resistivity and magnetic permeability in a small field may both be expected to drop to zero rather sharply as the temperature is lowered through the superconducting transition point.[12] Unfortunately, since most of the compounds with which the present work is concerned exhibit such properties as high melting points, brittleness, and ease of contamination, the fabrication of an ideal specimen of the above type is, with present techniques, a very tedious and difficult task. Thus, in preliminary experiments it is necessary to work with more readily prepared specimens, which, for the refractory compounds, include arc-melted pellets, porous sintered rods, or even fine powders. For these specimens the onset of superconductivity is often smeared out over a range of temperature, but a large drop in resistance or permeability usually gives unmistakable evidence of superconducting behavior.

Some caution is necessary in interpreting the results on inhomogeneous specimens, for the following reasons. It is not infrequent for such specimens, even when carefully prepared, to contain small amounts of superconducting impurities, often as one or more separate phases. Small quantities of the latter will sometimes form a continuous path through the specimen, for example at the grain boundaries, and cause the apparent resistance of the entire specimen to disappear at the transition point of the impurity.[13]

Alternatively, the impurity may be deposited in a thin skin around the individual grains or particles of the specimen; if the thickness of this skin exceeds the penetration depth ($\sim 10^{-5}$ cm), the onset of superconductivity in the impurity is accompanied by the exclusion of magnetic flux from the grain or particle as a whole, so that the impurity produces a much greater magnetic effect than one might expect from its actual volume. Thus, in both electrical and magnetic tests for superconductivity it is essential to take account of impurities, even trace amounts, in the specimens. Failure to observe this point in early work led to a number of ambiguities, some of which crop up in the present investigation. However, the difficulties resulted mainly from resistance tests, which are apparently more sensitive to impurities than magnetic tests, presumably because continuous filaments are formed more readily than closed skins. For this reason, and also because of the unsuitability of the resistance method for powdered samples, the magnetic method is preferred in the present work.

B. Apparatus

The magnetic test arrangement used in earlier work[9] was supplemented by a new gas thermometer cryostat in which specimens could be studied not only in the liquid hydrogen and liquid helium ranges, but also at accurately known temperatures in the intervening region. The essential low temperature parts of this apparatus are shown in cross-section in Fig. 1. For simplicity, the surrounding liquid nitrogen dewar flask and the head of the cryostat with its associated electrical connections and pumping lines are omitted from the diagram.

The six specimens which could be tested during a single experiment were mounted in radial positions just inside the rim of a hollow copper spool, which also served as a gas thermometer bulb, D. The top and bottom plates of the spool were slotted radially to minimize magnetic disturbance due to eddy currents. Fragmented or powdered specimens and sintered rods were contained in lucite tubes A, each having a thin-walled section upon which a detector coil B, consisting of about 250 turns of 40-gauge formex insulated copper wire, was tightly wound. Melted pellets were held in position in the spool by micarta supports and had detector coils wound directly upon them. Leads from the six coils passed out of the cryostat via the terminals E and were connected through a selector switch to an almost critically damped ballistic galvanometer. Uniform magnetic fields up to about 700 oersteds could be applied to the specimens by a liquid-nitrogen-cooled solenoid which was suspended outside the liquid helium dewar flask S, but inside the liquid nitrogen flask. The pyrex helium dewar was itself attached to the cryostat head by a copper-to-glass seal and an easily disconnected Rose's metal joint T, while the interspace could be evacuated through the tube U and an external needle valve.

C. Temperature Measurement

For measurements below 4.2°K, the specimen holder was completely submerged in liquid helium; temperatures down to just below 1.2°K could be attained by suitably varying the pumping rate on the liquid helium bath. In this range the specimen temperatures were obtained by measuring the vapor pressure of the bath, using for conversion the 1949 International Scale.[14] A similar procedure was used in the liquid hydrogen range.

For measurements between 4.2°K and 13.9°K, the triple point of liquid hydrogen, the helium bath level was allowed to fall below the specimen holder. The temperature of the specimen holder was then raised above that of the bath by means of a heater coil C of 30-gauge manganin wire wound noninductively upon the outside of the gas thermometer bulb. Heat from this

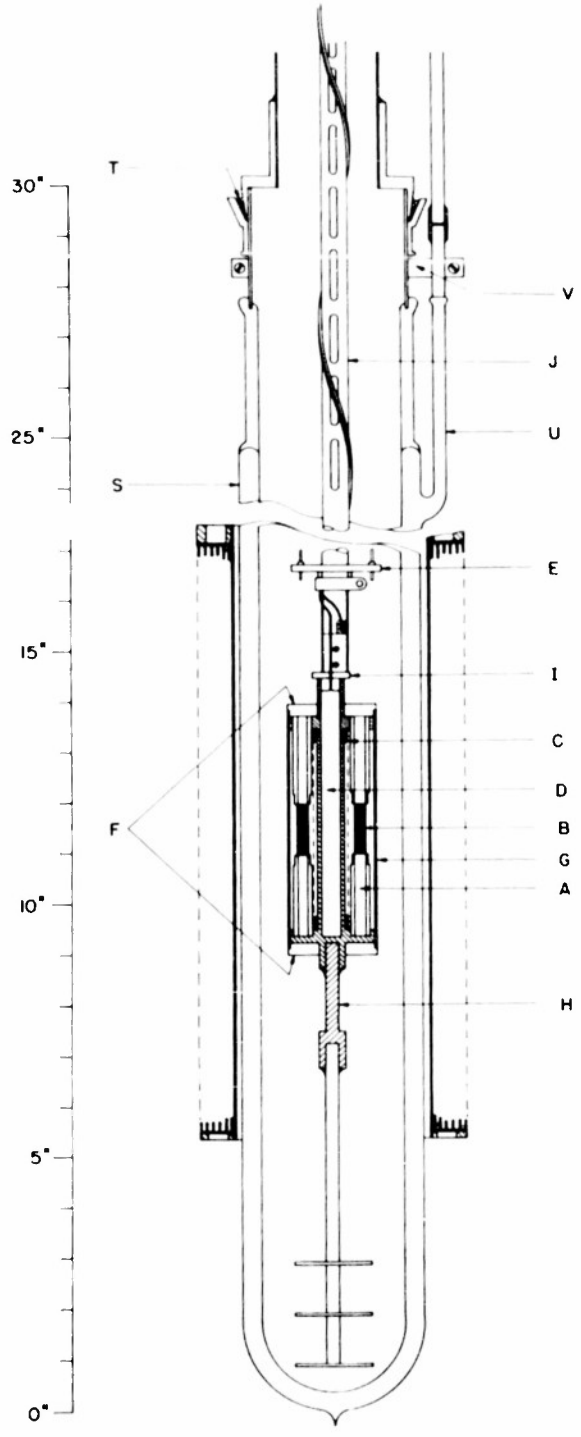

Fig. 1. Gas thermometer cryostat (lower half), liquid nitrogen dewar flask removed.

coil flowed down a brass rod H and was dissipated in the helium bath via a copper fin system which extended to the bottom of the dewar. Owing to the high thermal conductivity of copper relative to that of brass, almost the entire temperature drop occurred in the brass rod and the gradient in the specimen holder was negligible. In addition, the slotted support tube J of super-nickel ensured that the heat input from the cryostat head was negligible compared to that generated in the heater coil, while a thin brass envelope G and Lucite endplates F prevented convection in the helium vapor from disturbing the temperature equilibrium of the specimens.

Specimen temperatures above 4.2°K were measured with the constant volume helium gas thermometer (bulb D) which had previously been calibrated when immersed in liquid helium. After corrections for dead-space volume, gas imperfections, and thermo-molecular pressure gradient in the capillary tube, specimen temperatures between 4.2° and 13.9°K were known to better than 0.01°K. This accuracy was checked in two ways, first by using the gas thermometer to investigate certain superconducting transition curves which lay above 13.9°K and which had previously been studied by immersing the specimens directly in liquid hydrogen, and second by comparing our results for a single crystal of lead with those of previous workers.[15] In both cases the specimen temperatures agreed to within one hundredth of a degree, while temperature inequalities within the specimens could be presumed to be even smaller than this value.

D. Magnetic Measurements

Prior to each experiment the magnetic system was calibrated at room temperature by observing the galvanometer throw from each detector coil due to switching off an accurately known solenoid field of a few oersteds. This procedure was carried out first with the coils empty and second with the specimens in place, in order to show up ferromagnetic or other anomalous magnetic properties. In most cases, however, there was no noticeable difference between the "full" and "empty" readings, indicating a specimen permeability close to unity. Moreover, the galvanometer throw was quite accurately proportional to the applied field for fields up to a few hundred oersteds.

On cooling to liquid hydrogen or liquid helium temperatures, there was always a small, reproducible increase in deflection per unit change of field, presumably due to small changes in the detector coil dimensions and circuit resistance. When the specimen become superconducting, however, a large decrease in deflection was observed such as shown in Fig. 2. In this diagram the effective permeability, μ, is the ratio of the actual deflection due to switching off a given field, H', to the deflection obtained in the normal region by switching off the same field. Initial tests showed that the deflection given by each coil was unaffected by the presence of superconductors in any of the five remaining coils within the specimen holder.

The onset of superconductivity usually took place over an appreciable range of temperature, as shown in Fig. 2; such transition broadening is thought to be mainly due to inhomogeneities in composition and strain which produce variations of transition temperature from one region of the specimen to another. Thus, as will be seen later, very wide transitions, spread over a degree or more, were observed for certain carbides and nitrides in which quite large variations of carbon and nitrogen content are known to be possible. On the other hand, much sharper transitions were found for most of the silicides and germanides in which far smaller deviations from stoichiometric composition are permitted. Assuming that the variations of composition throughout a specimen are mainly random deviations from an ideal,

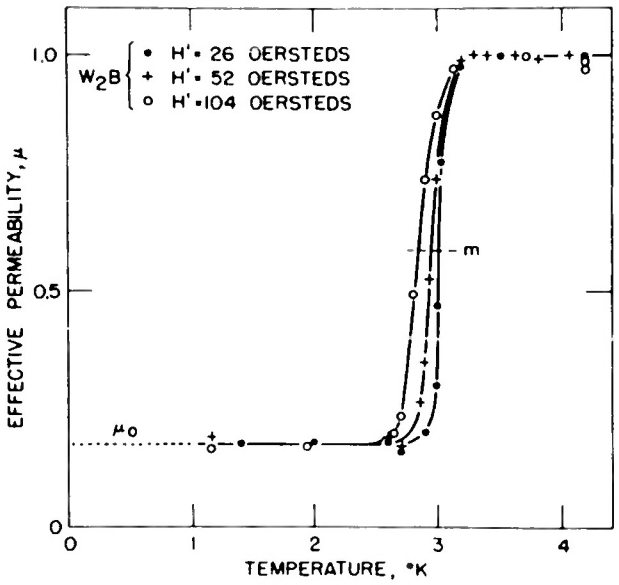

Fig. 2. Temperature variation of effective permeability at various values of measuring field, H', arc-melted W_2B specimen.

stoichiometric formula, it seems reasonable to obtain the transition temperature from the midpoint of the transition curve, corresponding to an effective permeability $(\mu_o + 1)/2$, where $\mu \rightarrow \mu_o$ as $T \rightarrow 0$. Most of our data were treated in this fashion, but in a few cases, for example certain nitrides, where most of the spreading was attributable to a specific dissolved impurity which displaced T_c in one direction, the transition temperature was estimated from the point of onset of superconductivity in the purest sample.

A slight broadening of the transition occurs for purely geometrical reasons when the specimen does not have the ideal long, cylindrical shape. Thus, for an ellipsoid of demagnetizing coefficient $4\pi n$ in a measuring field H' small compared to the critical field at absolute zero, H_{co}, it may be shown that the midpoint of the transition T_m and its total breadth ΔT are given by

$$T_m/T_c = 1 - 1/4[(2 - n)/(1 - n)][H'/H_{co}] \qquad (1)$$

and

$$\Delta T/T_c = 1/2[n/(1 - n)][H'/H_{co}] \qquad (2)$$

respectively. The first equation indicates that T_m always depends upon H', even for an ideal, cylindrical specimen with zero n; a linear dependence of this type was in fact observed for all our specimens (e.g., Fig. 2), and each transition temperature was determined from the value of T_m obtained at several different field strengths by extrapolating to zero field. Since our estimated n values rarely exceeded one-third (the value for a sphere) and H'/H_{co} could usually be assumed to be less than 0.1, the geometrical transition width was less than $T_c/40$ which was in most cases negligible compared to the broadening due to inhomogeneity. Owing to the non-ideal nature of the specimens, no accurate values of H_{co} were obtained in the

present work.

The effective permeability of our specimens in the limit $T \rightarrow 0$, μ_0, was never actually zero, for several reasons. First, there was flux leakage between the windings of the detector coil and the specimen and also through the specimen itself in the case of powders or sintered rods. Second, it was often necessary to work with specimens containing substantial amounts of other phases besides the compound of chief interest. Where these impurity phases were known to be normal down to 1.20°K, they merely served to further dilute the specimens and to increase μ_0. For superconducting impurities, however, the situation was less clear owing to the possibility of an anomalous decrease in μ_0 due to magnetic shielding of the type discussed in IIA. Fortunately, it was almost always possible to exclude such impurities in our work, and there were only three cases[16] in which a large magnetic effect could perhaps be attributed to a minor superconducting phase.

E. Specimen Preparation

The borides, carbides, and monoxides tested were, in most cases, prepared by the fusion of compressed pellets consisting of appropriate mixtures of the pure powdered metals with boron, carbon, or higher metallic oxide powders in an arc-melting furnace. Melting was carried out in an atmosphere of specially purified argon. The pellets were melted repeatedly, using a tungsten electrode, in a water-cooled copper crucible; spectrographic analyses of representative specimens showed that the copper and tungsten pickup of the arc-melts was considerably less than 0.1 per cent in all cases. When phases that formed only at very high temperatures were not under investigation, the specimens were then annealed at about 1500°C for between 20 and 50 hours in an atmosphere of purified helium.

Most of the silicides were prepared by heating compressed pellets of the powdered metals and silicon for several hours at about 1500°C in a furnace heated by "Globar" resistance elements. The pellets were supported by "Alundum" boats placed in the center of the "Sillimanite" furnace tube in which a slight overpressure of pure helium was maintained during heating. Many duplicate silicide specimens were prepared by arc-melting, and gave in most cases superconducting results practically identical with those obtained for sintered specimens of the same composition.

Germanide specimens were also prepared by the sintering technique, compressed pellets of germanium and metal powders being heated at about 1000°C in pure helium gas. Arc-melting preparations were tried for many of these compounds, but were usually unsuccessful due to extensive volatilization of germanium. In particular, we were unable to obtain suitable specimens of the lower niobium and tantalum germanides for this reason; these specimens could not be prepared by sintering even after very extended periods, since the inertness of the metals caused spongy, extremely inhomogeneous specimens to be produced.

Nitride preparations were usually carried out in a second "Globar" furnace in which metal powders could be heated to about 1450°C in carefully purified nitrogen. In one case, vanadium nitride, the compound was obtained by decomposing ammonium metavanadate in a stream of dry ammonia.

The composition of all specimens was checked by x-ray powder diffraction analysis and lattice parameter determinations were carried out wherever feasible. The results were for the most part in good agreement with those of earlier workers,[17] and need not be discussed in great detail. Our structural data will be mentioned explicitly only in cases of appreciable

deviation from earlier work or where new phases were observed. When the exact composition of the very existence of a phase is in doubt, the formula appears in quotation marks.

Spectrographic analyses showed that most of the specimens contained less than 0.1 per cent of dissolved metallic impurities, and here again the exceptions are discussed later. Finally, vacuum fusion analyses were performed in an iron bath at about 2100°C for most of the nitrides and proved essential in relating the oxygen and nitrogen contents of these specimens to their superconducting behavior.

III. Results and Discussion

A. Borides

Of eighteen transition metal borides tested magnetically by Matthias and Hulm,[9] only two, NbB and Mo_2B, were superconducting above 1.28°K. Ziegler and Young[10] reported normal behavior in seven borides down to 1.8°K. Among the remaining borides we have tested the nine compounds TiB, "ThB", "V_2B" (two forms), VB, Ta_2B, Cr_2B, W_2B, and Ru_2B down to a temperature slightly below 1.20°K. The results for these compounds are summarized in Table I (superconducting) and Table II (normal), together with our data for carbides, nitrides, and oxides of the transition metals discussed in later sections. These tables also show the borides, carbides, and nitrides tested by earlier workers, classified according to the best available evidence.

Of the compounds tested by us, only Ta_2B and W_2B showed superconducting behavior, the latter exhibiting a fairly sharp transition (Fig. 2)

TABLE I

Superconducting Nitrides, Carbides, and Borides of the Groups 4, 5, and 6 Transition Metals.

TiN (5.6°)[a]	VN (8.2°)[a]	None reported for chromium
ZrN (8.9°)[a]	Nb_4N_3 (7.2°)[a]	Mo_2N (5.0°)[b]
["ZrB" (3.3°)][d]	NbN (14.7°)[c]	MoN (12.0°)[b]
	Nb_2C (9.18°)[a]	Mo_2C (2.78°)[b]
None reported for hafnium or the lanthanide and actinide series of metals	NbC (6.0°)[a]	MoC (9.26°)[b]
	NbB (8.25°)[b]	Mo_2B (4.74°)[b]
	Ta_2C (3.26°)[a]	W_2C (2.74°)[b]
	[Ta_2B (3.12°)][a,e]	W_2B (3.10°)[a]

a Transition temperature from present work, magnetic data.
b Transition temperature from reference 9, magnetic data.
c Transition temperature from reference 8, magnetic data.
d Transition temperature from reference 7, electrical data only.
e Superconductivity doubtful owing to free tantalum (see text).

TABLE II

Nonsuperconducting Borides, Carbides, Nitrides, and Oxides of the Groups 4, 5, and 6 Transition Metals

TiB[a]	"V_2B" (2)[a]	Cr_2B[a]
TiB_2[b,c]	VB[a]	CrB[b]
TiC[a,c,e]	V_2C[a]	CrB_2[b]
TiO[a]	VC[a,c,e]	Cr_4C[a]
	"V_5N_2"[a]	Cr_7C_3[a]
	VO[a]	Cr_3C_2[a,b]
		CrN[b]
ZrB_2[c]	Nb_3B_4[b]	
ZrC[a,c,e]	NbB_2[b,c]	MoB (2)[b,c]
	Nb_2N[a]	Mo_2B_5[b]
	NbO[a,e]	
HfB[e]		WB[b,c]
HfC[e]	TaB[b]	W_2B_5[b]
	Ta_3B_4[b]	WC[b,c]
"ThB"[a]	TaB_2[b,c]	W_2N[b]
ThB_2[c]	TaC[a,c]	
ThC[a]	Ta_2N[a,d]	UC[a]
Th_3N_4[a]	TaN[a,d]	UN[a]

a Tested magnetically down to 1.20°K, present work.
b Tested magnetically down to 1.28°K, reference 9.
c Tested magnetically down to 1.8°K, reference 10.
d Tested magnetically down to 1.88°K, reference 8.
e Tested electrically down to about 1.2°K, references 5-7.

centered on 3.10°K. Unfortunately, in common with previous investigators,[3,18] we were unable to prepare a specimen of Ta_2B which did not contain substantial amounts (about 30 per cent of each) of free tantalum and TaB, even though a number of different annealing procedures were tried. These specimens all showed superconductivity at about 3.12°K. In spite of the very high flux expulsion from the detector coil (about 80 per cent), it

was felt, for the reasons discussed in Section II, that the magnetic effect could be due to the free tantalum in the specimens. This view was supported by the data for an arc-melted specimen of tantalum saturated with boron, which had a transition temperature of 3.32°K. Thus, although Ta_2B itself may become superconducting close to 3°K, this result is not definitely established.

The normal compounds include the recently reported phase VB;[19] and two new phases which were observed in several specimens of the overall composition V_2B prepared by arc-melting, followed by prolonged annealing, in some cases, at temperatures of 1500° and 1700°C. These specimens were shown by x-ray diffraction analysis to contain two new compounds of unknown crystal structure. Only one of these phases was present in the unannealed arc-melts; all of the annealed specimens contained both phases in roughly equal amounts.

The specimen of Ru_2B[20] was prepared by melting together the elements under pure helium at 1450°C, followed by twelve hours' annealing at 1100°C. The complex x-ray diffraction pattern of this compound has not been interpreted; the x-ray data showed, however, that our specimen contained no RuB or free ruthenium.

Several attempts were made to prepare the monoboride of zirconium, which has recently been investigated by Post and Glaser.[21-23] This compound is of special interest in view of Meissner, Franz, and Westerhoff's earlier result[7] that the electrical resistance of "ZrB" drops to zero between 3.8° and 2.8°K. Since "ZrB" is reported as forming only between 1000° and 1200°C, our preparations were carried out in a vacuum induction furnace or in the annealing furnace. All of the resulting specimens proved to contain only Zr, ZrB_2, and traces of ZrO_2, so that the superconductivity of zirconium monoboride could not be checked.

Magnetic data are now available for four hemiborides which crystallize in the tetragonal $CuAl_2$ [D_{4h}^{18}] type of lattice, namely, Mo_2B and W_2B (superconducting), Ta_2B (doubtful), and Cr_2B (normal to 1.2°K). Including, as it does, two of the three known superconducting borides, this lattice evidently favors superconductivity, perhaps because the individual boron atoms are isolated. One might expect the higher borides to be somewhat less "metallic" in character owing to the progressive increase in the number of covalent linkages between boron atoms with increasing boron content,[24] although it must be admitted that this change does not seem to be accompanied by a systematic increase in electrical resistivity.[1,22] Another interesting feature is that the known superconducting borides are clustered in a single region of the periodic system in which two of the parent metals, molybdenum and tungsten, remain normal down to very low temperatures. This situation will shortly be seen to be repeated, with some variations in several other classes of compounds.

B. Carbides

Meissner and his co-workers[5,7] observed that the electrical resistance of monocarbide specimens of ZrC, NbC, TaC, MoC, and WC dropped steeply, in some cases to zero, in the temperature intervals 4.07° - 3.35°, 10.5° - 10.1°, 9.5° - 9.3°, 7.8° - 7.6°, and 4.2° - 2.5°K, respectively. However, in magnetic measurements Ziegler and Young[10] found no evidence of superconducting behavior in TiC, ZrC, VC, TaC, and WC down to 1.8°K, while Matthias and Hulm[9] reported WC to be normal down to 1.28°K, but MoC as superconducting at about 9.26°K, which is somewhat higher than Meissner and Franz's value.

To check and extend these results we studied the seven monocarbides

TiC, ZrC, ThC, VC, NbC, TaC, and UC down to 1.20°K. Most of these compounds were prepared by arc-melting, but the specimen of UC was obtained in a vacuum induction furnace by the reaction at 1800°C of an intimate mixture of U_3O_8 and graphite powder, contained in a graphite crucible.[25,26] This method of preparation might be expected to yield a product containing appreciable amounts of oxygen in solution; unfortunately, the previously reported values[25,26] of the lattice constant of "pure" UC differ by 0.004A, with the result that the lattice parameter for our specimen (4.952A), while it lay between the two published values, did not provide a very precise indication of the specimen purity. The specimens of ThC and UC, both of which are unstable in air, were handled in a dry-box under argon, and were tested while sealed in thin-walled glass tubes under pure helium.

No evidence of superconducting behavior was found in the monocarbides of titanium, zirconium, thorium, vanadium, tantalum, and uranium, so that we must conclude, in agreement with Ziegler and Young,[10] that the disappearance of electrical resistance found by Meissner and Franz in ZrC and TaC was due to traces of superconducting impurity, possibly the nitride in the former case and free tantalum in the latter. Our NbC specimen showed a rather broad superconducting transition over a range of about 3°K with its midpoint at 6°K (Fig. 3). Since the x-ray diffraction pattern of this specimen contained only monocarbide lines, we presume that the electrical transition which Meissner and Franz[5] found between 10.5° and 10.1°K for "NbC" may have been due to impurities, perhaps Nb_2C (see below) or free niobium.

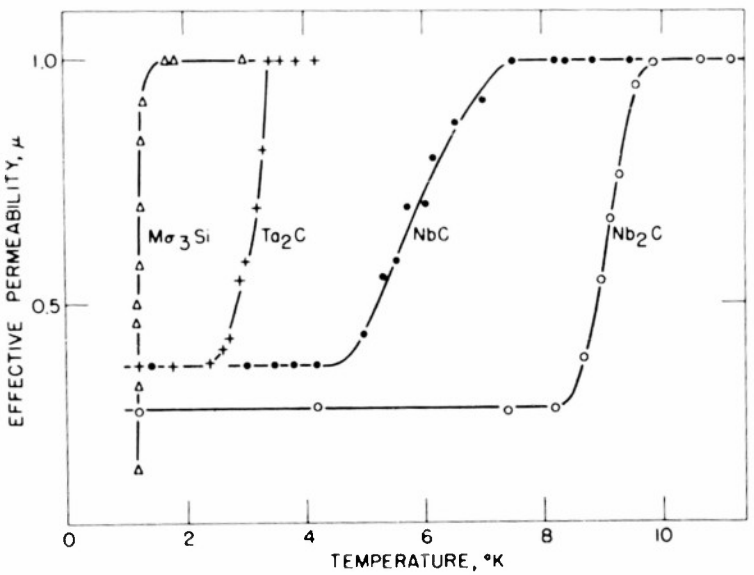

Fig. 3. Temperature variation of effective permeability for arc-melted Nb_2C, NbC, Ta_2C, and sintered Mo_3Si specimens, measuring field 26 oersteds.

In addition to the monocarbides, we investigated the lower compounds V_2C, Nb_2C, Ta_2C, Cr_4C, Cr_7C_3, and Cr_3C_2 down to 1.20°K. Since Cr_4C was reported[27] to be unstable above 1530°C, this specimen was annealed at about 1450°C for 50 hours, after arc-melting. Nb_2C and Ta_2C were also subjected to a similar, especially long annealing treatment and their x-ray diffraction patterns contained no lines due to other compounds or to

the free metals. It should be mentioned that although the hemicarbides of vanadium and niobium have been reported by several workers,[28-31] some doubt has been expressed regarding their actual existence.[32] However, our x-ray data for these compounds indicated a hexagonal structure, similar to that of Ta_2C, Mo_2C, and W_2C, with the lattice parameters 2.944, 4.508A (V_2C) and 3.105, 4.970A (Nb_2C).

Of the six lower carbides tested, only Nb_2C and Ta_2C became superconducting above 1.20°K; both these compounds exhibited quite sharp transitions centered upon 9.18°K (Nb_2C) and 3.26°K (Ta_2C) [Fig. 3]. Neither compound has been investigated for superconductivity in previous work.

C. Nitrides

Electrical resistance transitions similar to those found by Meissner and his co-workers in the monocarbides were also reported by these investigators for the mononitrides TiN (two drops in resistance, at 5.5° and 1.2°K), ZrN (9.6° - 9.3°K), and VN (3.2° - 1.5°K). More recently, Justi and his co-workers[33] and Horn and Ziegler[8] independently found magnetic evidence of superconductivity in NbN at about 15°K, while the latter workers reported TaN as normal down to 1.88°K. Matthias and Hulm[9] observed a superconducting transition in MoN at about 12°K.

Since the electrical data for several monocarbides were not confirmed by later magnetic tests, it was felt necessary to check the above electrical results for the mononitrides. While our magnetic studies have shown that all three compounds, TiN, ZrN, and VN, are indeed superconducting, the behavior of our specimens of TiN and VN was found to be quite sensitive to variations in the small quantities of oxygen which entered the specimens during preparation.

By heating various samples of titanium for about 8 hours at 1450°C in nitrogen gas subjected to different degrees of purification, we prepared three specimens of TiN (A, B, and C) containing slightly different amounts of oxygen. The oxygen contents determined by vacuum fusion analysis are shown in Table III and the superconducting results in Fig. 4. X-ray evidence

TABLE III

Influence of Oxygen Contamination on the Super-conductivity of TiN.

Specimen	Oxygen content (weight %)	Lattice Parameter (A)	T_c* (°K)
A	0.4	4.240	5.58
B	0.8	4.240	5.58
C	1.5	4.240	4.86
D	1.6	4.230	2.90

* Onset temperature, extrapolated to zero field.

("tailing" off of diffraction peaks at high angles) and slight changes of color from the surface to the interior of these specimens suggested that the oxygen content was somewhat higher in the surface region than at the center. This was also supported by the very wide range of the superconducting transition; the sharp drop in permeability at about 5.5°K for specimen A is attributed to a pure central core in which the oxygen content was even less than the 0.4 per cent average value for the specimen as a whole. It should

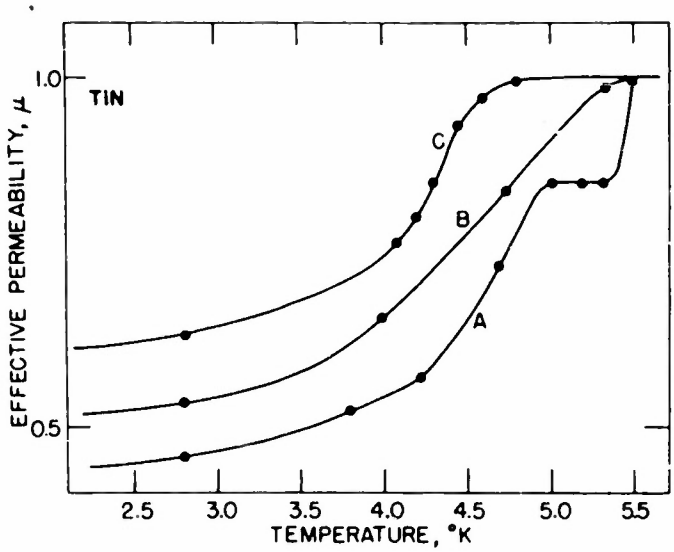

Fig. 4. Temperature variation of effective permeability for sintered TiN samples containing different amounts of oxygen (Table III), measuring field 26 oersteds.

be noted that the same lattice parameter was obtained for A, B, and C, 4.240A, which lies between the values 4.242A and 4.235A reported previously for pure TiN.[34,35]

As a further check on the above results, a fourth TiN specimen, D (Table III) was prepared by annealing part of specimen C under purified helium for twenty hours at 1500°C. The total oxygen content was hardly changed, but, presumably owing to diffusion of oxygen into the purer parts of the specimen, the lattice parameter decreased appreciably and the temperature of onset of superconductivity (not shown in Fig. 4) was depressed to 2.9°K. Replacement of nitrogen by oxygen in the TiN lattice evidently decreases the superconducting transition temperature, which is not unreasonable in view of the fact that the isostructural monoxide, TiO, is itself normal down to 1.20°K (Section III D).

From the temperature of the sudden onset of superconductivity in specimen A, extrapolated to zero field, we obtain a value 5.6°K for the transition point of pure TiN. This compares quite favorably with the upper electrical transition observed by Meissner and Franz; their second transition at 1.2°K may have been due to oxygen contamination or perhaps to the presence of impure titanium metal.[36]

Samples of ZrN prepared by the same method as TiN gave quite broad superconducting transitions of the type shown in Fig. 5, with midpoints in all cases close to 8.9°K, in good agreement with Meissner and Franz's electrical data. Oxygen contamination does not seem seriously to affect the superconductivity of this compound, perhaps because the formation of ZrO_2 is preferred to the replacement of nitrogen by oxygen in the nitride lattice; no evidence has been found for the existence of ZrO.[37]

In preparing VN by heating NH_4VO_3 in ammonia, previous investigators[38,39] found that at temperatures high enough to ensure complete reduction of the vanadium oxides (about 1200°C), the VN itself loses appreciable amounts of nitrogen. To see how this affected the superconductivity, we prepared three VN specimens of about the same shape at three different temperatures, with the results shown in Table IV and Fig. 6. Even though

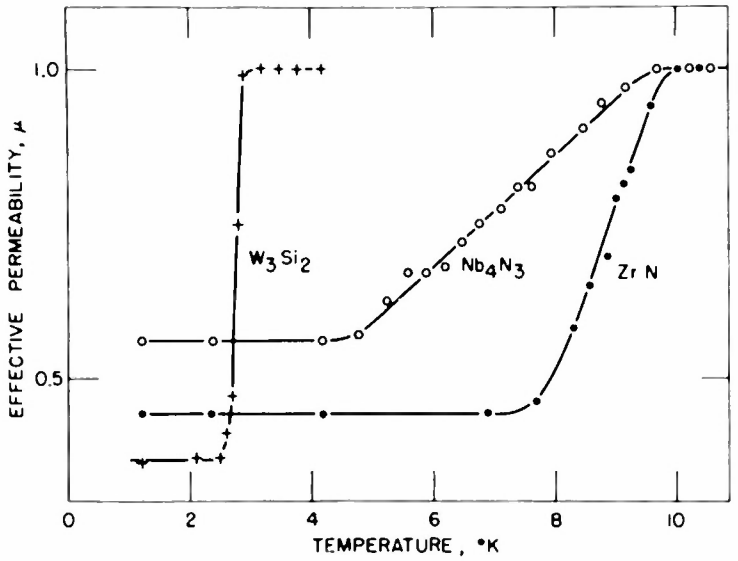

Fig. 5. Temperature variation of effective permeability for sintered ZrN, Nb_4N_3, and W_3Si_2 specimens, measuring field 26 oersteds.

specimen A contained the most oxygen, it exhibits the sharpest superconducting transition and the lowest effective permeability, probably owing to the fact that the oxygen occurs as residual oxides (VO_2 or V_2O_5) which are not superconducting. As the preparation temperature is raised, more oxygen is driven off but at the same time more apparently goes into solution in the VN lattice and depresses the superconducting transition point. This may have been responsible for the low transition temperature observed by Meissner and Franz; in view of the fact that our specimen A was the most completely superconducting and gave a lattice parameter closest to the values reported by previous workers[39-41] for pure VN (4.134A and 4.137A), we regard the temperature of onset of superconductivity in this specimen (8.2°K) as the most reliable transition temperature at present available.

In addition to the above mononitrides we tested the seven compounds Th_3N_4, "V_5N_2", Nb_2N, Nb_4N_3, Ta_2N, TaN, and UN down to 1.20°K. Normal behavior was observed in all cases except that of Nb_4N_3, which became superconducting over a range of 5°K with its midpoint at 7.2°K (Fig. 5); according to Brauer and Jander[42] this compound has a crystal structure based upon a tetragonally deformed NbN (NaCl type) lattice. In view of the high

TABLE IV

Influence of Preparation Temperature on the Superconductivity of VN.

Specimen	Prepn. temp. (°C)	Oxygen content (wt.%)	Nitrogen content (wt.%)	Latt. par. (A)	T_c* (°K)
A	1000	7.6	13.7	4.135	8.2
B	1200	2.3	18.6	4.132	6.7
C	1350	2.4	11.8	4.130	5.8

* Onset temperature, extrapolated to zero field.

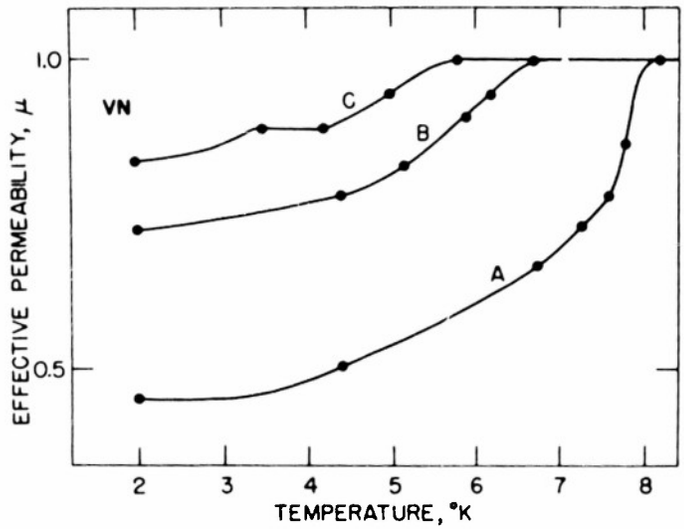

Fig. 6. Temperature variation of effective permeability for "VN" samples containing different amounts of oxygen and nitrogen (Table IV), measuring field 26 oersteds.

transition points of the vanadium and niobium mononitrides, and of the metals themselves, it is interesting that the hexagonal lower nitrides "V_5N_2" and Nb_2N remain normal down to 1.20°K. Both these compounds involve a close-packed hexagonal metal lattice with nitrogen atoms in the interstices,[30,39] however, as Hahn has pointed out, since the holes in the vanadium lattice are too small for the nitrogen atoms, the compound is formed in the range $VN_{0.37}$ to $VN_{0.43}$ instead of at the ideal composition $VN_{0.50}$.

The absence of superconductivity in Th_3N_4 is perhaps to be expected, since this compound is usually regarded as a typical "ionic" and non-metallic nitride.[43] While our particular specimen of TaN showed no trace of superconductivity, its x-ray diffraction pattern did not resemble that reported by Horn and Ziegler[8] for a sample which remained normal down to 1.88°K, and neither of these patterns agree with that given by Becker and Ebert[44] for TaN. On the other hand, our Ta_2N, which was made by heating an intimate mixture of TaN and tantalum at 1450°C, gave a hexagonal pattern similar to that of Nb_2N and identical with the data of van Arkel[45] for a specimen which he called "TaN." Chiotti[46] has shown convincingly that this hexagonal close-packed phase is actually the heminitride of tantalum, but the structures existing around the composition "TaN" remain obscure.

D. Oxides

Arc-melted pellets of the monoxides TiO, VO, and NbO showed no trace of superconductivity down to 1.20°K. The TiO and VO specimens were found to have a sodium chloride structure, with lattice parameter in good agreement with values obtained by earlier workers.[47,48] NbO also gave an x-ray diffraction pattern in good agreement with that previously reported,[49] which apparently corresponds to a structure derived from the NaCl type by the orderly removal of niobium and oxygen atoms from one-fourth of the lattice positions. These oxides all had a metallic appearance; VO and NbO were silvery and TiO was a dull golden color. Rough tests showed that the electrical resistivity of the latter was about 300 micro-ohm cm at room temperature and rose by a few per cent on cooling to 78°K, which suggests semi-

conducting behavior. It should be remarked that Meissner, Franz, and Westerhoff[6] found a gradual drop in electrical resistance for NbO between about 4.2° and 1.4°K, which, in view of the present results, was probably due to impurities.

E. Silicides

Although the radius of silicon is too large for the extensive formation of interstitial compounds, many of the transition metal silicides have metallic character and their structures have been extensively studied.[50] In the present work all the known silicides of the Groups 4, 5, and 6 transition metals, with the exception of hafnium and uranium, were tested for superconductivity down to 1.20°K. The results of these studies, together with those for similar tests on the corresponding germanides, are summarized in Table V (superconducting) and Table VI (normal).

TABLE V

Superconducting Silicides and Germanides of Groups 4, 5, and 6 Transition Metals (present work).

None found for titanium or	V_3Si (17.1°) V_3Ge (6.01°)	None found for chromium
None tested for hafnium	["Nb_2Ge" (1.9°)]*	Mo_3Si (1.30°) Mo_3Ge (1.43°)
α -$ThSi_2$ (3.16°)	["Ta_2Ge" (1.6°)]*	W_3Si_2 (2.84°)
β -$ThSi_2$ (2.41°)		

* Doubtful owing to presence of free metal.

Superconducting behavior was observed in the five silicides V_3Si (17.1°K, Fig. 7), Mo_3Si (1.30°K, Fig. 3), α -$ThSi_2$ (3.16°K, Fig. 8), β -$ThSi_2$ (2.41°K, Fig. 8), and W_3Si_2 (2.84°K, Fig. 5), representing four structure types in which the phenomenon has not previously been reported. The most striking feature of these results is the transition temperature of V_3Si, which is the highest known for any binary compound. Since both V_3Si and Mo_3Si crystallize in a cubic structure of the β-tungsten type [O_h^3], it is interesting that a third silicide of the same structure, Cr_3Si, remains normal down to 1.20°K. According to Zener[51] these compounds might be expected to possess an antiferromagnetic spin arrangement, but this point does not seem to have been checked with neutron diffraction; there is at present no known case in which superconductivity and antiferromagnetism coexist.

At an early stage in the investigation of V_3Si it was found that certain impurities often present in commercial vanadium metal, in particular iron, tend to depress the superconducting transition temperature. The transition curves for three specimens prepared from vanadium obtained from three different sources are shown in Fig. 7; Table VII gives the main impurity content of these specimens and indicates that as little as 0.1 per cent of iron lowers the transition temperature by nearly one degree. Since all our specimens contained about the same amount of manganese, it was not possible to decide how much effect this impurity had upon the transition temperature.

TABLE VI

Silicides and Germanides of Groups 4, 5, and 6 Transition Metals Nonsuperconducting down to 1.20°K (present work).

Ti_5Si_3, Ti_5Ge_3	"V_3Si_2", V-Ge	Cr_3Si, Cr_3Ge
TiSi	VSi_2	Cr_3Si_2, Cr_3Ge_2
$TiSi_2$, $TiGe_2$		CrSi, CrGe
	Nb_3Si_2	$CrSi_2$
Zr_4Si, Zr_2Si	"Nb_2Si"	
Zr_3Si_2, Zr_4Si_3	$NbSi_2$, $NbGe_2$	Mo_3Si_2, Mo_3Ge_2
Zr_6Si_5		$MoSi_2$
ZrSi, Zr-Ge	Ta_5Si, Ta_5Si_2	α - $MoGe_2$
$ZrSi_2$, $ZrGe_2$	Ta_3Si_2	β - $MoGe_2$
	$TaSi_2$, $TaGe_2$	
Th_3Si_2, Th-Ge		WSi_2

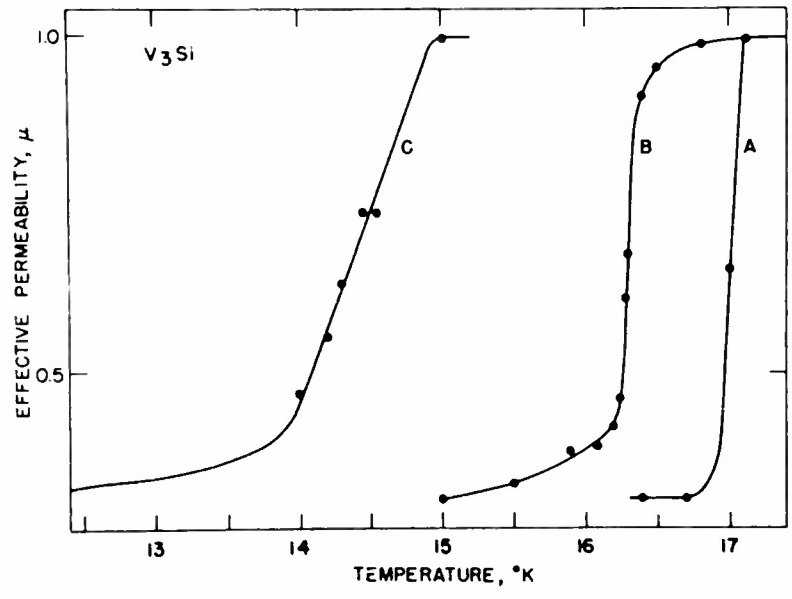

Fig. 7. Temperature variation of effective permeability for arc-melted V_3Si samples containing different amounts of impurity (Table VII), measuring field 8 oersted.

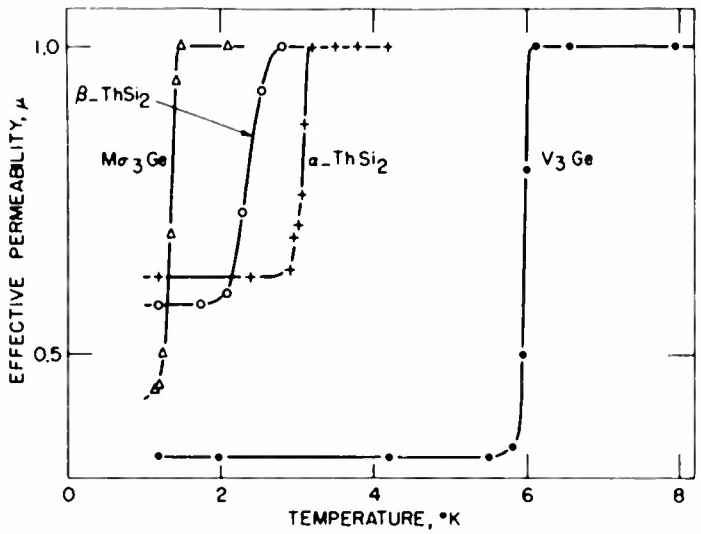

Fig. 8. Temperature variation of effective permeability for arc-melted V_3Ge, Mo_3Ge, and sintered α-$ThSi_2$, β-$ThSi_2$ specimens, measuring field 26 oersteds.

TABLE VII

Influence of Impurities on the Superconductivity of V_3Si.

Specimen	Impurities % Fe	% Mn	Latt. par. (A)	Midpoint* (°K)
A	0.05	0.2	4.722	17.0
B	0.1	0.3	4.723	16.3
C	1.0	0.3	4.720	14.4

* Applied field 8 oersteds.

However, since the neighboring elements iron and chromium (see Table VIII) tend to depress the transition, manganese probably has the same effect and we presume that the transition temperature of extremely pure V_3Si lies somewhat above 17°K.

In an attempt to raise the transition temperature of V_3Si specimens, we investigated the effect of varying the silicon content and also of replacing part of the vanadium or silicon by other elements. Changes up to ± 20 atomic per cent of silicon produced hardly any change of T_c, probably because the single phase region for V_3Si is rather narrow. The introduction of other elements caused the changes listed in Table VIII; although many of the added elements did not dissolve completely in the V_3Si phase, in spite of melting in the arc furnace, the results show that the transition temperature was lowered in all cases.

Of the remaining new superconductors, the tetragonal compound α-$ThSi_2$ [D_{4h}^{19}] is well known;[52] we tested the isomorphous compounds[53-55] $CeSi_2$, $LaSi_2$, and YSi_2 (distorted), but all three remained normal down to 1.20°K. A series of Th-Si specimens of different silicon contents also yielded, in addition to α-$ThSi_2$, two previously unreported phases,[56]

TABLE VIII

Effect of Added Elements on the Superconductivity of V_3Si.

Composition	Latt. par. (A)	Trans. range* (^oK)	Midpoint* (^oK)
V_3Si	4.722	16.4 - 17.1	16.8
$V_3Si_{0.9}C_{0.1}$	4.723	15.5 - 16.7	16.4
$V_3Si_{0.9}Ge_{0.1}$	4.731	13.0 - 14.4	14.0
$V_3Si_{0.9}B_{0.1}$	4.720	15.0 - 16.3	15.8
$V_3Si_{0.9}Al_{0.1}$	4.727	13.1 - 14.9	14.05
$(V_{0.9}Ti_{0.1})_3Si$	4.736	10.0 - 12.0	10.9
$(V_{0.9}Zr_{0.1})_3Si$	4.724	11.0 - 15.3	13.2
$(V_{0.9}Nb_{0.1})_3Si$	4.756	12.0 - 13.5	12.8
$(V_{0.9}Mo_{0.1})_3Si$	4.732	11.5 - 12.5	11.7
$(V_{0.9}Cr_{0.1})_3Si$	4.697	11.0 - 11.9	11.3
$(V_{0.9}Ru_{0.1})_3Si$	4.707	2.0 - 3.8	2.9

* Applied field 26 oersteds.

β-$ThSi_2$ (hexagonal $[D_{6h}^1]$ superconducting at 2.41°K) and Th_3Si_2 (tetragonal $[D_{4h}^5]$ normal). These specimens also contained a good deal of ThO_2, which, however, merely served to increase the effective permeability in the superconducting range.

In a previous paper[11] superconductivity was reported in Mo_3Si_2, which is apparently isomorphous with the superconductor W_3Si_2, both structures being unidentified. This result was an erroneous one due to the presence of Mo_3Si impurities in the original "Mo_3Si_2" specimen. Since the x-ray diffraction pattern of pure Mo_3Si_2 contains all the lines of Mo_3Si, the presence of these impurities remained undetected for some time. However, prolonged annealing of the specimen caused the superconductivity to disappear, presumably owing to the removal of Mo_3Si.

It is of interest to mention some normal phases found by us in silicide systems which have hitherto been incompletely explored. For the vanadium-silicon system a new phase of unknown structure was observed at the approximate composition V_3Si_2. In addition to $NbSi_2$, two lower niobium silicides have been previously mentioned without x-ray diffraction data.[57] Our specimens sintered at 1450°C contained a phase of approximate composition Nb_5Si_3; we found the x-ray diffraction pattern to be identical with that reported[58] for Ta_5Si_3. Arc-melted specimens gave an additional phase of composition Nb_2Si which is apparently formed only at very high temperatures.

Finally, we note that four tantalum silicides[58,59] remained normal

down to 1.20°K, which strongly suggests that the disappearance of electrical resistance observed by Meissner, Franz, and Westerhoff[7] in a "TaSi" specimen was due to impurities, probably free tantalum.

F. Germanides

Structural interest in the transition metal germanides is quite recent, and far less information is available than for the silicides. However, the data so far obtained seem to indicate that the silicides and germanides of a given transition metal are much more closely related to each other than to the carbides or nitrides of that metal. Whereas the carbides and nitrides tend to have "interstitial" structures, the silicides and germanides have structures based, to some extent, on bonding of non-metal atoms to each other,[53] and on equivalence between the roles of metal and non-metal atoms in the structure, in analogy with the borides.[24]

We tested the known germanides of the Groups 4, 5, and 6 metals down to 1.20°K, with the results given in Tables V (superconducting) and VI (normal). Only two new superconductors were observed, V_3Ge (6.01°K, Fig. 8) and Mo_3Ge (1.43°K, Fig. 8), both of which are isomorphous with V_3Si.[60,61]

In view of our incomplete knowledge of the phase diagrams, it was usual to prepare for each transition metal about eight sintered specimens of different germanium contents in the range M_4Ge to MGe_2, where M is the metal. X-ray studies for the systems Zr-Ge, Th-Ge, and V-Ge indicated the presence of several new phases in addition to the known compounds[60] $ZrGe_2$ and V_3Ge, but since none of these were superconducting above 1.20°K, they were not investigated further. In both arc-melted and sintered specimens of Nb-Ge and Ta-Ge, evidence was found for existence of the previously reported[60] digermanides, which remained normal down to 1.20°K, and two lower compounds of approximate composition "Nb_2Ge" and "Ta_2Ge" which showed superconducting behavior at about 1.9° and 1.6°K respectively. However, since free metal was present in all specimens of these hemigermanides, their superconductivity remains in doubt.

In the Ti-Ge, Cr-Ge, and Mo-Ge specimens, only known compounds were present,[60-62] the normal compounds including Mo_3Ge_2 and two forms of $MoGe_2$ upon which x-ray data has recently been published.[63] Just as for Mo_3Si_2, discussed in III E, the superconducting behavior previously reported[11] for Mo_3Ge_2 disappeared after prolonged annealing and was therefore presumed to have been due to Mo_3Ge impurities. No compounds were found in the W-Ge system.

G. Other Compounds

Since superconductivity was observed in four compounds, V_3Si, V_3Ge, Mo_3Si, and Mo_3Ge, which crystallize in a structure of the β-tungsten type, it was thought worthwhile to test several intermetallic compounds of this structure. However, four such compounds, Ti_3Pt,[64] Ti_3Au,[64] V_3Co,[65] and Mo_3Zr,[66] remained normal down to 1.20°K.

The lowest known sulphide of niobium, NbS,[67] was prepared by heating the powdered metal and sulphur in a sealed, evacuated "Vycor" tube at about 1000°C until equilibrium was attained. No trace of superconductivity was observed in this compound down to 1.28°K.

IV. Conclusion

Excluding the bismuthides,[9] about thirty compounds of metals with nonmetallic elements have now been shown to be superconducting on the basis of quite reliable magnetic evidence. Most of these are listed in Tables I and V, including the eleven new superconductors found in the present work;

the others comprise CuS[68] and several compounds of Group 8 metals recently reported superconducting by Matthias.[69] Errors in early work due to reliance upon electrical measurements or due to inadequate knowledge of the specimen composition have now been largely corrected. Most of the compounds of Groups 4, 5, and 6 transition metals with boron, carbon, nitrogen, oxygen, silicon, and germanium have been tested for superconductivity down to about 1°K, but even here, as the detailed phase diagrams (which are lacking in most cases) become available, a few new compounds will probably remain to be tested. Attention should be drawn to the fact that the fraction of superconducting compounds in our tables is roughly the same as the fraction of known superconducting elements, that is, about one-fourth of the total.

The superconducting compounds now outnumber the superconducting elements (21), and offer a greater diversity of structures than heretofore. The most common structure for such compounds is still the cubic NaCl type (5 normal, NbC, NbN, TiN, ZrN, VN, and 3 distorted, Nb_4N_3, Mo_2N, W_2N), but the cubic β -tungsten type (V_3Si, V_3Ge, Mo_3Si, and Mo_3Ge) and the hexagonal structure based upon a close-packed array of metal atoms with non-metal atoms in the interstices (Nb_2C, Ta_2C, Mo_2C, W_2C, and very distorted NbB) have recently come into prominence. There are also at least ten other important superconducting structure types, ranging in symmetry from the cubic fluorite type[70] ($CoSi_2$) through the tetragonal $CuAl_2$ type (the hemiborides), the tetragonal α -$ThSi_2$ type, the hexagonal NiAs type[69] to the orthorhombic MnP and monoclinic PdBi types.[69] There are several unknown structures, including for example W_3Si_2; this compound is probably closely related to its cubic neighbor Mo_3Si.

It was remarked in a previous paper[9] that superconducting transition temperatures of both cubic elements and compounds tend to be higher than those for hexagonal elements and compounds. This tendency seems to have been confirmed in the present work, in view of the rather high transition points of the β -tungsten structure vanadium compounds and the cubic mononitrides, in contrast to the absence of superconductivity in the hexagonal heminitrides and the low transition points of the hexagonal hemicarbides. It must be admitted, however, that the normal behavior of most of the cubic monocarbides forms an exception to the above hypothesis.

As regards the positions of the superconducting compounds in the periodic system, if one excludes the thorium disilicides, Tables I and V seem to indicate a diagonal character in the arrangement, that is, a displacement to the right (higher Group number) as one proceeds down a column of the table. This is due to the persistent failure of either hafnium or chromium to form superconducting compounds; the fact that fourteen chromium compounds remain normal down to 1.28°K may be partly due to the magnetic influence of the incomplete chromium d-shell. One may contrast with this the extensive formation of superconducting compounds by the other Group 6A metals, molybdenum and tungsten, which apparently come close to possessing the requisite electronic structure for superconductivity.

Recently certain theoretical relationships have been established[71,72] between the occurrence of superconductivity in a metal and the normal properties of the metal, in particular the "ideal" electrical resistivity at room temperature. While in their present form these relations seem to be mainly applicable to metals of rather simple outer electronic structure, nevertheless it would be interesting to test their validity for a few of the approximately one hundred compounds listed in our tables. In particular, the added complication of differences of crystal structure, which are not taken into account in the above free-electron theories, might be removed by work-

ing with an isostructural group such as the NaCl structure monocarbides, mononitrides, and monoxides with many superconducting and normal members. Unfortunately, however, little accurate information is available on the normal properties of most of these compounds, chiefly owing to the difficulty of preparing them in stoichiometric, homogeneous, solid form. Various estimates[1] of the room-temperature electrical resistivities of the carbides and nitrides, for example, differ by more than an order of magnitude in some cases, and since hardly any low temperature data are available, it is impossible to derive accurate values of the "ideal" resistivity. If the most recently obtained resistivity values are assumed to be correct, the nitrides, which include most of the superconductors of NaCl structure, seem to have resistivities predominantly lower than those of the carbides and monoxides, but beyond this little can be said.

A more systematic investigation of the normal electronic properties of transition metal compounds is clearly desirable, not only for the light which may be thrown on their superconducting behavior, but also for the intrinsic interest of the chemical binding in these compounds. Whereas many are known to have metallic character, a few semiconductors, such as titanium monoxide, have also been reported; thus, solid solutions of TiC or TiN with TiO may provide a continuous transition from metallic to semiconducting properties in the same, relatively simple lattice. A similar, but less smooth, transition may occur with increasing non-metal content in the borides and silicides, since during this increase each boron or silicon atom tends to form step by step a greater number of linkages with its boron or silicon neighbors. Experiments to check these hypotheses through the detailed study of electrical properties are now in progress.

We are grateful to Professors E. A. Long and W. H. Zachariasen for helpful discussions; to Dr. W. Rostoker (Illinois Institute of Technology) for the loan of TiO specimens; to Mr. A. Moskowitz and Mrs. A. R. Tompkins for carrying out vacuum fusion and spectrographic analyses, respectively; to Mr. E. Selmanoff for metallurgical assistance; and to Mr. R. Szara for liquefying helium. Part of the work was carried out during tenure by one of us (G.F.H.) of a U. S. Rubber Company Fellowship at the University of Chicago.

References

1. The term "hard metals" is often applied to this whole group of materials. See P. Schwarzkopf and R. Kieffer, Refractory Hard Metals (Macmillan Company, New York, 1953).
2. G. Hägg, Z. physik. Chem. B6, 221 (1930); B12, 33 (1931).
3. R. Kiessling, Acta Chem. Scand. 1, 893 (1947); 3, 90 and 595 (1949); 4, 146 and 209 (1950).
4. R. E. Rundle, Acta Cryst. 1, 180 (1948).
5. W. Meissner and H. Franz, Z. Physik 65, 30 (1930).
6. Meissner, Franz, and Westerhoff, Ann. Physik (5) 13, 505 (1932), and 17, 593 (1933).
7. Meissner, Franz, and Westerhoff, Z. Physik 75, 521 (1932).
8. F. H. Horn and W. T. Ziegler, J. Am. Chem. Soc. 69, 2762 (1947).
9. B. T. Matthias and J. K. Hulm, Phys. Rev. 87, 799 (1952).
10. W. T. Ziegler and R. A. Young, Phys. Rev. 90, 115 (1953).
11. G. Hardy and J. K. Hulm, Phys. Rev. 89, 884 (1953).
12. See D. Shoenberg, Superconductivity (Cambridge University Press, 1952), 2nd edition.
13. D. Shoenberg, Nature 159, 303 (1947).

14. H. Van Dijk and D. Shoenberg, Nature 164, 151 (1949).
15. J. G. Daunt and K. Mendelssohn, Proc. Roy. Soc. (London) A160, 127 (1937).
16. Ta_2B, "Nb_2Ge" and "Ta_2Ge" specimens all contained traces of free metal (see later discussion).
17. The literature on the crystal structure and phase diagram constitution of the transition metal borides, carbides, nitrides, and silicides is very extensive, but, fortunately a comprehensive survey of this field has recently been published (Reference 1). The present paper does not, therefore, include an exhaustive list of all the references consulted in connection with our chemical and structural studies, and specific mention is made only of very recent publications or those articles having close bearing on the superconductive investigation.
18. Brewer, Sawyer, Templeton, and Dauben, J. Am. Ceram. Soc. 34, 173 (1951).
19. H. Blumenthal, J. Am. Chem. Soc. 74, 2942 (1952), reported VB as isomorphous with CrB (Orthorhombic D_{2h}^{17}), lattice parameters 3.10, 8.17, and 2.98A. We had independently reached the same conclusion and found the lattice parameters 3.058, 8.026, and 2.971A.
20. J. H. Buddery and A. J. Welch, Nature 167, 362 (1951).
21. B. Post and F. W. Glaser, J. Chem. Phys. 20, 1050 (1952).
22. F. W. Glaser, J. Metals 4, 391 (1952).
23. F. W. Glaser and B. Post, J. Metals 5, 1117 (1953).
24. R. Kiessling, J. Electrochem. Soc. 98, 166 (1951).
25. Rundle, Baenziger, Wilson, and McDonald, J. Am. Chem. Soc. 70, 99 (1948).
26. Litz, Garrett, and Croxton, J. Am. Chem. Soc. 70, 1718 (1948).
27. See M. Hansen, Der Aufbau der Zweistofflegierungen (J. Springer, Berlin, 1936) p. 354.
28. A. Westgren, Metallwirtschaft 9, 921 (1930).
29. M. Oya and A. Osawa, Sci. Rep. Tokohu Univ. 19, 95 (1930).
30. G. Brauer, Z. Elektrochem. 46, 397 (1940).
31. J. S. Umanski, Zhur. Fiz. Khim. (U.S.S.R.) 14, 332 (1950).
32. See Reference 1, pages 104, 110.
33. Aschermann, Friederich, Justi, and Kramer, Physik. Z. 42, 349 (1941).
34. P. Ehrlich, Z. anorg. u. allgem. Chem. 259, 1 (1949).
35. A. K. Brager, Acta Physicochimica U.R.S.S. 11, 617 (1939).
36. Although the present accepted transition temperature of titanium is 0.53°K, early specimens had transitions at 1.2° and 1.8°K, presumably owing to impurities. See reference 12, p. 223.
37. D. D. Cubicciotti, J. Am. Chem. Soc. 73, 2032 (1951).
38. V. A. Epelbaum and B. F. Ormont, Acta Physicochimica U.R.S.S. 22, 319 (1947).
39. H. Hahn, Z. anorg. u. allgem. Chem. 258, 58 (1949).
40. A. K. Brager and V. A. Epelbaum, Acta Physicochimica U.R.S.S. 13, 595 and 600 (1940).
41. V. A. Epelbaum and B. F. Ormont, Zhur. Fiz. Khim. (U.S.S.R.) 21, 3 (1947).
42. G. Brauer and J. Jander, Z. anorg. u. allgem. Chem. 270, 160 (1952).
43. A. F. Wells, Structural Inorganic Chemistry (Oxford Univ. Press, 1950) 2nd ed., p. 477.
44. K. Becker and F. Ebert, Z. Physik 31, 268 (1925).
45. A. E. van Arkel, Physica 4, 286 (1924).
46. P. Chiotti, J. Am. Ceram. Soc. 35, 123 (1952).
47. W. Rostoker, J. Metals 4, 981 (1952). (Our TiO specimen was obtained

from Dr. W. Rostoker.)
48. W. Klemm and L. Grimm, Z. anorg. u. allgem. Chem. 250, 42 (1942).
49. G. Brauer, Z. anorg. u. allgem. Chem. 248, 1 (1941).
50. For a detailed list of papers, see Reference 1.
51. C. Zener, Phys. Rev. 81, 440 (1951).
52. G. Brauer and A. Mitius, Z. anorg. u. allgem. Chem. 249, 325 (1942).
53. W. H. Zachariasen, Acta Cryst. 2, 94 (1949).
54. F. Bertaut and P. Blum, Acta Cryst. 3, 319 (1950).
55. G. Brauer and H. Haag, Z. anorg. u. allgem. Chem. 267, 198 (1952).
56. We are indebted to Professor W. H. Zachariasen for informing us of his unpublished structural results for these two phases (to be published shortly) and for identifying the phases in our specimens.
57. W. Klemm, FIAT Rev. Germ. Sci. 1939-1946, Inorg. Chem. II, p. 105, G. Brauer (1948).
58. Brewer, Searcy, Templeton, and Dauben, J. Am. Ceram. Soc. 33, 291 (1950).
59. Nowotny, Schachner, Kieffer, and Benesovsky, Monatshefte für Chemie (Vienna) 84, 1 (1953).
60. H. J. Wallbaum, Naturwiss. 32, 76 (1944).
61. Searcy, Peavler, and Ycarian, J. Am. Chem. Soc. 74, 566 (1952).
62. P. Pietrowsky and P. Duwez, J. Metals 3, 772 (1951).
63. A. W. Searcy and R. J. Peavler, Abstracts of papers presented at the 124th annual meeting of the American Chemical Society, Chicago, September 1953.
64. P. Duwez and C. B. Jordan, Acta Cryst. 5, 213 (1952).
65. P. Duwez, J. Metals 3, 564 (1951).
66. W. Klemm, FIAT Rev. German Sci. 1939-1946, Inorg. Chem. IV, p. 81, H. Nowotny (1948).
67. W. Biltz and A. Köcher, Z. anorg. u. allgem. Chem. 237, 369 (1938).
68. See reference 12, p. 229.
69. B. T. Matthias, Phys. Rev. 87, 380 (1952); 90, 487; 91, 413 (1953).
70. B. T. Matthias and J. K. Hulm, Phys. Rev. 89, 439 (1953).
71. H. Fröhlich, Phys. Rev. 79, 845 (1950).
72. J. Bardeen, Phys. Rev. 80, 567 (1950).

X

POLARIZATION EFFECTS IN THE IONIC CONDUCTIVITY OF SILVER BROMIDE

Robert J. Friauf
(Submitted to The Journal of Chemical Physics)

I. Introduction

The purpose of the experiments to be described has been to study the ionic defects which occur in AgBr. In order to facilitate the description of the experiments and the accompanying theory, it will be convenient to summarize the current state of information about the defects in AgBr.

It is well known that AgBr has an appreciable ionic conductivity at elevated temperatures.[1,2] Recent investigations of the conductivity of pure AgBr and of AgBr to which small amounts of divalent impurities such as cadmium have been added indicate that the conductivity can be adequately described, at least for temperatures below 300° C, by assuming that Frenkel defects exist for the silver ions.[3,4] An analysis of the measurements yields values for the equilibrium concentration of defects and for the mobilities of each of the two types of charge carriers—interstitial silver ions and silver ion vacancies.

A number of other properties of AgBr, however, have led many investigators to suggest that at least some Schottky defects—bromide as well as silver ion vacancies—must also exist. There is an anomalous increase in the conductivity at temperatures near the melting point (422°C), and Kurnick has tentatively ascribed this behavior to the presence of an appreciable number of Schottky defects.[4] The explanation is reasonably consistent with observed anomalous increases in thermal expansion[5] and specific heat,[6,7] but it must be realized that the evidence is not very conclusive in any of these cases because of the necessity of extrapolating "normal" quantities to high temperatures. There is also a contention that the thermal expansion can be related to the lattice expansion as determined by high temperature X-ray measurements,[8] but the interpretation of the X-ray measurements may be incorrect.[9] Several writers have concluded from studies of the absorption spectrum of AgBr with small amounts of Ag_2S that Schottky defects must be present to a lesser or greater extent,[10,11] but the interpretation of these experiments is rather modelistic in nature. Finally there are scattered reports of diffusion of bromine in AgBr, but the high temperature experiments were conducted at only one temperature,[12] and the interpretation of the results obtained at room temperature[13,14] has been disputed because of the small size of the particles involved.[15] In conclusion it may be said that the presence of some Schottky defects is suggested by many experiments but has not been definitely proved by any.

In view of this situation it was thought that a study of the polarization effects associated with the ionic conductivity might lead to further information about the possible presence of some Schottky defects. The polarization effects appear experimentally in the following way. When an alternating voltage is applied to a sample of AgBr with silver electrodes, the electrical behavior of the sample is not equivalent to that of an ideal resistance. Rather there is a capacitive component in the current flowing through the sample,

and the resistance also varies with the frequency of the applied voltage. It is these deviations from the behavior as an ideal resistance that form the object of interest for these investigations.

A qualitative explanation of these anomalies may be given as follows. Imagine the ionic defects to be mobile charge carriers moving in a continuous medium. When an a.c. voltage is applied to the sample, the charge carriers in the interior will move back and forth in phase with the applied voltage and thus contribute to the ordinary bulk conductivity of the sample. When the charge carriers arrive at the electrodes, however, some of them may not be able to carry their charge out of the sample. In this case the charge carriers will pile up at the electrodes and thus produce a capacitive effect. The electric field produced by the piled-up charges will also hinder the approach of additional charge carriers and hence tend to increase the resistance. On the basis of this picture it is to be expected that the anomalous effects will be larger at low frequencies, and this behavior is observed.

Since it seems probable that bromine ion vacancies, if any are present in AgBr, would be more likely to pile up at silver electrodes than either silver ion vacancies or interstitial silver ions, it was originally hoped that the anomalous impedance effects observed in AgBr with silver electrodes could be ascribed to bromine ion vacancies. In this case a study of the anomalous effects would provide information about the Schottky defects in AgBr. An analysis of the theory corresponding to the picture above, however, indicates that the Frenkel defects are principally responsible for these effects, as they are for the ionic conductivity itself.

In Sections II and III the experimental procedure and results are described. In Section IV a theory is developed on the basis of the qualitative picture presented above, and in Section V the results of the theory are compared to the experimental results.

II. Experimental Procedure

For some of the early work powdered AgBr prepared by Goldsmith Bros. Smelting and Refining Co., Chicago, was used. When later batches of this material appeared to contain an excessive amount of impurity, AgBr was prepared by precipitation from $AgNO_3$ and HBr (48%) obtained from Mallinckrodt Chemical Works. From all indications the material so prepared contains no more than one part in 10^5 of harmful impurities. A spectroscopic analysis shows traces of this order of magnitude of several divalent metal impurities, and visual inspection shows no signs of sulfur. (As little as 0.0002 mole per cent of Ag_2S can be detected.) The HBr is specified to contain no more than 0.05% chloride and 0.003% iodide, but these impurities do not cause any serious effect. The primary effect of impurities for the purposes of this experiment is to cause the equilibrium number of defects to be different from that for the pure substance; it is to be expected and has been verified that the polyvalent impurities produce a much larger effect in this respect than the monovalent impurities.[3,16] Since the equilibrium concentration of defects is of the order of one part in 10^5 at room temperature, a larger concentration of divalent impurities would cause a noticeable effect in the room temperature conductivity; a comparison of the observed conductivity to the value extrapolated from the data of Kurnick[4] indicates that the polyvalent impurities do not exceed the amount detected by the spectroscopic analysis.

Single crystals were grown by withdrawing from the melt at a rate of two inches per hour (Czochralski method). These were machined in a lathe to cylinders about 3/8 in. in diameter and 1/4 in. long; several thousandths

of an inch was then removed by etching in a sodium thiosulfate solution, and the samples were annealed at 390° C for about 20 hours. Since AgBr is cubic and therefore electrically isotropic, no special attention was paid to the orientation of the crystals. For some samples several small grains were visible on each end; these were not considered serious because in no case did a grain extend the entire length of the sample. The samples darkened somewhat during handling because of the photolytic action of the light, but most of the darkening could be annealed out, and at no time were any effects detected that could be ascribed to a variable amount of darkening.

Polycrystalline samples were employed for the earlier work. These were produced by pouring molten AgBr into a pellet die and then subjecting the AgBr to a pressure of 10,000 atm.; the average grain size was of the order of 1 mm. There is some difference, but no tremendous amount, between the measurements on the polycrystalline and single crystal samples.

Electrodes of silver and of gold were applied to the samples by evaporation of the metals in a vacuum. For the silver electrodes DuPont silver paint was applied on top of the evaporated silver film, and this coating was backed up by solid silver. For the gold electrodes no gold paint was available, and consequently gold foil was held directly against the evaporated gold film during measurements. In some cases the samples were re-annealed after the electrodes had been applied; this treatment affects the magnitude of the polarization effects somewhat.

The furnace is rather massive in order to reduce temperature gradients and temperature fluctuations in time. The temperature gradient at the position of the samples is less than 0.5° C/in. up to 340° C, and the ordinary drift of temperature at a fixed control temperature is of the order of 0.4° C in a cycle of about a one hour period. A larger drift cannot be tolerated because a change of 0.005° C is quite noticeable in the resistive part of the bridge balance. Temperature is controlled with a proportioning temperature controller. Thermocouples are made from standard Chromel P and Alumel thermocouple wire, and although they have not been calibrated, it is believed that the temperature measurements are correct within 0.5° C. Whenever a direct comparison has been made between two such thermocouples, the agreement is within 0.1° C, and the measured conductivity agrees with that reported by Kurnick[4] within 1.5%, which corresponds to about 0.5° C.

The samples are mounted with solid pieces of silver or gold held against them by a light spring pressure of about 5 gm/mm^2. Four samples can be mounted simultaneously with a separate thermocouple placed about 1 mm from each. The sample holder is especially designed so that the lead wires contain no screw contacts in the high temperature region; in this way any possible copper oxide rectifying effects are avoided. A few measurements have been made at high pressure using the arrangement described by Kurnick.[4] In this case the electrical leads from the sample do contain some screw contacts at high temperature, but there does not seem to be any especially noticeable effect because of this.

The a.c. impedance measurements are made with a General Radio Type 716-C capacitance bridge as shown in Figs. 1 and 2. The frequency of the Hewlett-Packard Model 200 D audio oscillator has been checked frequently against the 60 cycle line frequency and is constant within 1.5%. The tuned amplifier has both positive and negative feedback through RC coupling and is tuned by means of a variable condenser. It is necessary to have good frequency selectivity in the detecting device in order to remove 60 cycle pick-up and to discriminate against a small amount of second harmonic which is present because the sample is a non-linear circuit element. The

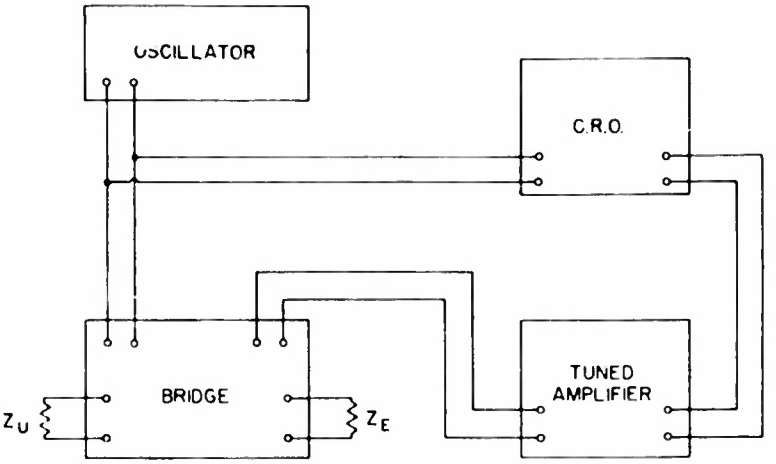

Fig. 1. Schematic diagram of the measuring circuit.

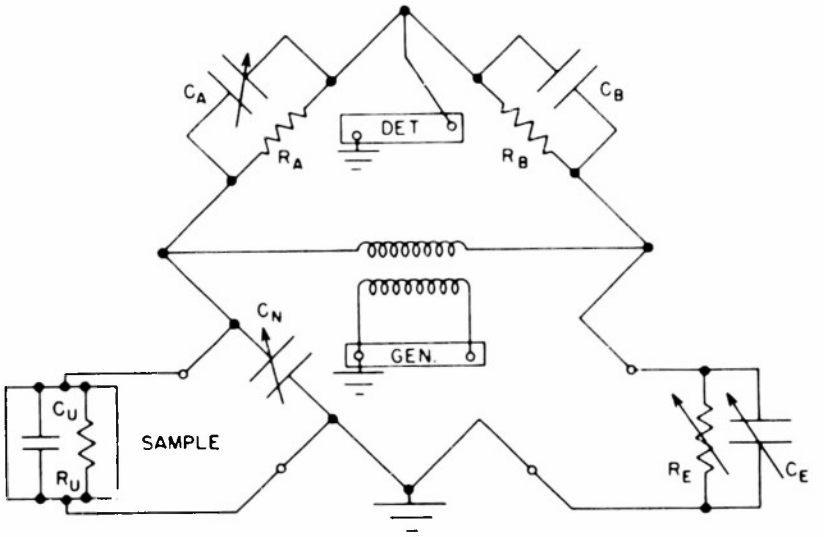

Fig. 2. Circuit diagram of the bridge.

output of the amplifier is applied to the vertical plates of the oscilloscope, and the bridge is balanced by reducing the ellipsoidal Lissajous figure which appears on the screen to a horizontal straight line.

The capacitance bridge is especially suitable for the measurements since the generator, detector, and sample can all be grounded and since the wiring capacities are carefully balanced out in the two fixed arms. The bridge is used as an equal arm bridge with $R_A = R_B = 200$ ohms and $C_A = C_B = 205$ $\mu\mu$f; then $R_U = R_E$, and $C_U + C_N = C_E$. The values chosen for the fixed arms give the smallest values of $R_AC_A = R_BC_B$ obtainable with the settings available on the bridge; the effect of a small difference between C_A and C_B on the accuracy of the measurement of C_U is minimized by this choice. The final adjustment to assure that $R_AC_A = R_BC_B$ is made by balancing the bridge with combinations of known resistances and capacitances. Any difference in the parallel capacity present in the two resistance boxes can be eliminated by interchanging the resistance boxes and rebalancing. It is convenient, both in making the electrical measurements and in presenting the results of the theory, to represent the impedance of

the sample at any given frequency by an equivalent parallel resistance and capacity as is indicated in Fig. 2. In general both parameters of this equivalent circuit will depend on frequency.

Unfortunately for the study of polarization effects the ionic conductivity of AgBr is rather large. This means that in most circumstances the polarization effects are fairly small compared to the normal bulk conductivity; from the viewpoint of the electrical measurements the phase angles encountered range from 1 to 10^{-5} radians compared to a pure resistance. The measurement of such small phase angles in the presence of a low resistance is a rather unusual situation in the use of an a.c. impedance bridge, and considerable care must be taken to avoid spurious effects. For one thing the resistance standard R_E, which is a General Radio Type 602-M resistance box, contains a small parallel capacity of the order of 10 to 40 $\mu\mu$f according to the General Radio specifications. Corrections have been made for this according to the average values given in the specifications.

A more serious effect occurs at low resistances because of small inductances in the resistance box and in the lead wires to the sample. The specifications for the resistance box give an inductance of approximately .3 μh for R = 100 ohms, and a simple calculation for two No. 20 gauge wires 100 cm long and 1 cm apart gives an inductance of approximately 1 μh. In both cases the primary effect of the residual inductance is to introduce a negative effective capacity $\Delta C = - L/R^2$. For R = 100 ohms and L = 1 μh, $\Delta C = 100 \mu\mu f$; for R = 10 ohms, $\Delta C = .01$ μf. Effects of this order of magnitude have been observed during checks of the bridge with known R and C combinations. Because of this effect it is not possible to obtain reliable capacity measurements when the resistance is less than 100 ohms.

There is a certain amount of leakage resistance and capacity between the high leads and ground, especially in the sample holder; this is usually about 10 megohms and 50 $\mu\mu$f in parallel at room temperature. The leakage resistance is unimportant because the resistance of the samples at elevated temperatures is always less than 2000 ohms. The zero capacity has been measured at room temperature and subtracted from the observed results; a check at 230° C shows that at the higher frequencies where the correction is important (1000 and 5000 cps) the zero capacity is not changed by more than 10 $\mu\mu$f. The capacity between the different high leads when more than one sample is mounted can be shown by an experimental check to be less than 1 $\mu\mu$f.

The dimensions of the samples have been chosen so as to avoid as far as possible the difficulties described above. Because of the uncertain ties in the zero capacity of the sample holder and in the capacity of the resistance box, values of capacity below 100 $\mu\mu$f are unrealiable; and because of the effect of the residual inductance, the resistance of the sample cannot be much less than 100 ohms. The size chosen makes the capacity at 210° and 1000 cps about 100 $\mu\mu$f and the resistance at 280° about 100 ohms. Within these limits the error of the capacity measurements is less than 1.5% or 10 $\mu\mu$f, whichever is larger; the resistance measurements are much more accurate. All in all the accuracy of the electrical measurements is sufficiently good so that other effects to be described later contribute the principle uncertainty in the experimental results.

For making d.c. measurements of the resistance the voltage drop over a standard 1 ohm resistor connected in series with the sample is measured with a Leeds and Northrup Type K potentiometer. The voltage applied to the sample and standard resistor is checked frequently by substituting a resistance box for the sample.

III. Experimental Results

General

Alternating current impedance measurements have been made on single crystals of pure AgBr with silver and with gold electrodes at frequencies from 50 to 5000 cps and at temperatures between 200° and 280° C. There has been some investigation of the effect of varying the applied voltage, and several measurements have been made of the d.c. resistance. A few measurements have been made with high pressure applied to polycrystalline samples, and measurements have also been made on samples of AgBr containing a small amount of $CdBr_2$.

A summary of the results obtained for a number of samples is presented in Table I. The values of T = 253° C and f = 200 cps have been chosen as reference points because they represent convenient middle points in the temperature and frequency ranges. When log C is plotted against log f, approximate straight lines are obtained (Figs. 5 and 6). Hence the frequency dependence of C can be represented by a formula of the type C = const/f^n; the magnitude of n is given as the frequency slope. Figures enclosed in parentheses are considered to be less reliable because of scatter in the experimental points for the particular curve or, especially for the temperature slopes, because of the changes in the condition of the electrodes with time which are described below.

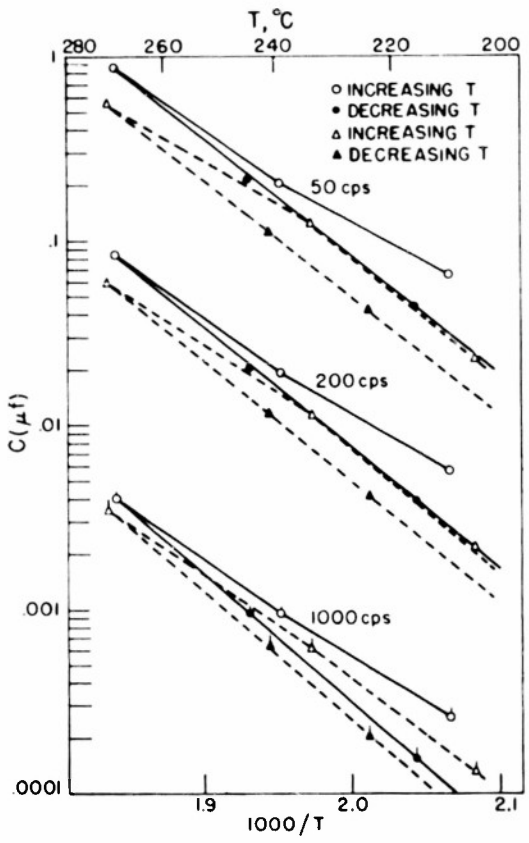

Fig. 3. Capacity as a function of temperature for No. 6a (silver electrodes).

TABLE I

Summary of Results

Sample	Material (a)	Structure (b)	Electrodes	Anneal (c)	l (cm)	A (cm^2)	σ (ohm-cm)$^{-1}$ T=253°C	W(σ) (k cal /mole)
5b	M	S	Ag	WO	.592	.709	.00465	17.7
6a	M	S	Ag	WO	.570	.711	.00446	18.0
5b	M	S	Ag	W	.592	.709	.00462	17.9
6a	M	S	Ag	W	.570	.711	.00451	17.9
5b	M	S	Ag	W	.592	.709	.00462	17.9
6a	M	S	Ag	W	.570	.711	.00451	17.9
3a	M	S	Ag	WO	.585	.710	.00459	17.9
3b	M	S	Ag	WO	.597	.650	.00460	17.6
3a	M	S	Ag	W	.585	.710	.00454	17.9
3b	M	S	Ag	W	.597	.650	.00465	17.8
5a	M	S	Au	WO	.661	.709	.00452	17.9
6b	M	S	Au	WO	.674	.705	.00443	17.7
20	G	P	Ag	W	1.224	.696	.00419	17.6
21	G	P	Ag	W	1.277	.697	.00435	17.6
22	G	p	Ag	W	1.243	.691	.00418	17.8
23	G	P	Ag	W	.632	.701	.00442	17.6
26	G	P	Ag	W	.634	.695	.00419	17.6
27	G	P	Ag	W	.624	.693	.00395	17.6
28	D	P	Ag	W	.696	.696	.00378	18.0
29	D	P	Ag	W	.688	.697	.00340	17.6
14	G	P	Ag	W	1.245	.712	.00526	18.7
15	G	P	Ag	W	.506	.706	.00520	18.6

(a) Material
- M AgBr precipitated from Mallinckrodt chemicals
- G AgBr obtained from Goldsmith Bros.
- D AgBr from Goldsmith with 0.1% (molar) $CdBr_2$ added

(b) Structure
- S Single crystal
- P Polycrystalline

(c) Anneal
- W With electrodes
- WO Without electrodes

TABLE I (Continued)

Sample	C_S (μ f/cm^2) T=253°C f=200 cps	W (C) (k cal/mole)			f slope (T as shown)		
		50 cps	200 cps	1000 cps			
						241°	267°
5b	.02-.003	(29.5)	(31.5)			(1.55)	(1.40)
6a	.03-.005	(25.6)	(26.0)			(1.62)	(1.33)
					211°		270°
5b	.038	29.3	29.8	31.7	1.76	. . .	1.72
6a	.048	29.5	30.5	32.0	1.79	. . .	1.71
					223°	241°	271°
5b	.02-.006	(d)	(d)	(d)	(1.46)	(1.50)	(1.40)
6a	.031	29.1	30.0	32.0	1.70	1.67	1.61
					223°	241°	271°
3a	.02-.008	(26.7)	(27.0)	(25.5)	1.46	1.40	1.46
3b	.01-.006	(24.0)	(25.2)	(26.7)	1.50	1.46	1.42
					219°	244°	266°
3a	.023	(28.2)	(27.5)	(25.4)	1.50	1.48	1.60
3b	.017	(29.3)	(27.8)	(27.2)	1.61	1.64	1.70
					219°	244°	266°
5a	.21	30.0	29.8	29.6	1.62	1.68	1.66
6b	.17	29.4	29.8	29.4	1.60	1.63	1.60
					210°		267°
20	.042	20.0	20.9	21.8	1.35		1.38
21	.033	(21.9)	(23.6)	(26.1)	1.49		1.37
22	.036	(15.8)	(16.9)	(20.4)	1.52		1.28
					210°		267°
23	.040	(19.6)	21.4	23.3	1.33		1.29
26	.072	16.5	17.8	20.6	1.43		1.36
27	.091	17.8	20.0	20.1	1.36		1.33
					210°		267°
28	.12	20.6	24.9	26.1	1.48		1.37
29	.17	15.5	19.9	21.2	1.36		1.29
					210°	245°	292°
14	.0024	20.4	18.0	20.3	1.60	1.61	1.51
15	.028	19.5	20.6	21.8	1.50	1.42	1.37

(d) A d.c. voltage was applied to this sample a number of times.

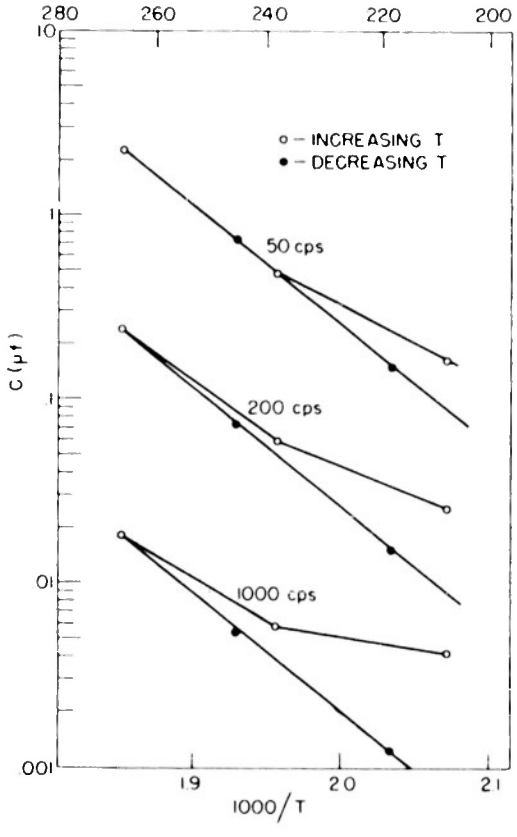

Fig. 4. Capacity as a function of temperature for No. 6b (gold electrodes).

Temperature Dependence

When the resistance is measured at sufficiently high frequencies so that the small influence of the polarization effects on the resistance is negligible (see below), the resistance is a single valued function of the temperature. The conductivity values for the single crystal samples in Table I agree quite well with the values obtained from a plot of Kurnick's results, $\sigma = .00460\ (\text{ohm} - \text{cm})^{-1}$ at T = 253° C and W = 18.2 k cal/mole. The larger discrepancies for the polycrystalline samples are due to errors in the geometrical factors, especially the area, in $\sigma = L/RA$.

Figs. 3 and 4 show the measured capacity for two typical samples; this is the equivalent parallel capacity as in Fig. 2. The vertical lines extending upwards from the capacity points at 1000 and 5000 cps in these and other capacity graphs represent the possible correction necessitated because of the previously described effects of residual inductances in the wiring. For each measurement the voltage applied to the sample is set at 0.1 ± 0.002 volts rms. For each sample a sequence of measurements at different temperatures is obtained by heating the sample from room temperature to about 200° C, increasing the temperature in steps of about 40° C to 280° C, and finally decreasing the temperature by similar steps back to 200° C. Because of the necessity of waiting for good temperature equilibrium at least two hours elapses between the measurements at two successive temperatures.

The most striking feature of the curves is that the actual value of the capacity is not a unique function of the temperature, but rather, for a given temperature and frequency, tends to decrease in the course of time. This

behavior, along with a similar variation in magnitude of capacity between different samples with supposedly identical electrodes, appears to be characteristic of the system under observation, namely, AgBr with evaporated metal electrodes; it is believed that the change of capacity is related to changes in the precise conditions of the electrodes. A change of capacity, usually a decrease, of the same order of magnitude as those shown in Figs. 3 and 4 is also often observed after a small direct current (causing a total charge flow of about one coulomb) has passed through the sample.

It should also be mentioned that the treatment of the samples after the electrodes have been applied has some influence on the magnitude of the observed capacity. The sample with silver electrodes shown in Fig. 3 (No. 6a) was annealed at 390° C after the electrodes were applied; for all samples treated in this way the magnitudes of the capacity agree within about a factor of two (see Table I). For samples which are not annealed after the electrodes are applied, however, the magnitudes of the capacity are less by as much as a factor ten, and the changes in time are considerably larger than those in Fig. 3. Again it appears as if there is a change in the condition of the electrodes, and observation of the electrodes after annealing shows two noticeable effects: (a) Since there is no spring pressure acting on the electrodes during annealing, the silver paint has a tendency to pull together creating ridges and thin spots. (b) There is also a reddish coloration of the AgBr to a distance of about 1 mm from the electrodes.

A certain amount of non-reproducibility of results is not unusual in connection with polarization effects.[17] The encouraging feature of the results presented here is that the dependence of the capacity on the temperature and frequency is much more reproducible than the actual magnitude is, both for different observations on the same sample and for different samples. The broken curves in Fig. 3 show a second set of measurements on the same sample after the furnace had cooled to room temperature and remained there for several days. It is seen that the capacity curves fall on the decreasing temperature curves of the preceding set of measurements at the lower temperatures, that there is some additional decrease in capacity at the highest temperature, and that the slopes of the decreasing temperature curves are very nearly the same as before. It appears reasonable to assume, therefore, that the temperature slopes obtained while temperature is being decreased result from changes in the density and mobilities of the ionic charge carriers in AgBr rather than from changes in the boundary conditions. The temperature slopes in Table I are obtained from the decreasing temperature curves, and it is seen that there is good agreement of both the temperature and frequency slopes for groups of similarly prepared samples.

Frequency Dependence

The frequency dependence of the observed capacity is shown in Figs. 5 and 6. A complete set of frequencies is covered at a fixed temperature, starting at 200 cps, then proceeding from 50 to 5000 cps, and finally checking at 200 cps. The possibility of a change in the boundary conditions between readings at different frequencies is not very large because only about fifteen minutes is required to cover the frequency range compared to the two hours required to proceed from one temperature to the next. Also the values of the first and last readings of each frequency sequence (at 200 cps) usually agree within a few per cent.

In addition to the parallel capacity there is also an additional resistance, which is largest at low frequencies. A rough picture of the frequency dependence of this excess resistance is shown in Figs. 7 and 8. ΔR has been determined as $\Delta R(f) = R(f) - R_o$, where R_o is the normal bulk resistance which is observed at large enough frequencies—5000 cps for silver electrodes and

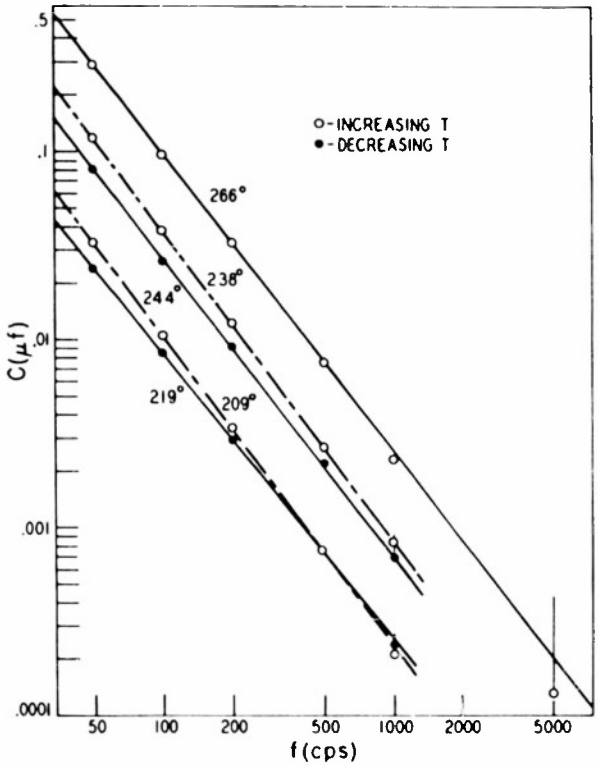

Fig. 5. Capacity as a function of frequency for No. 3a (silver electrodes).

Fig. 6. Capacity as a function of frequency for No. 6b (gold electrodes).

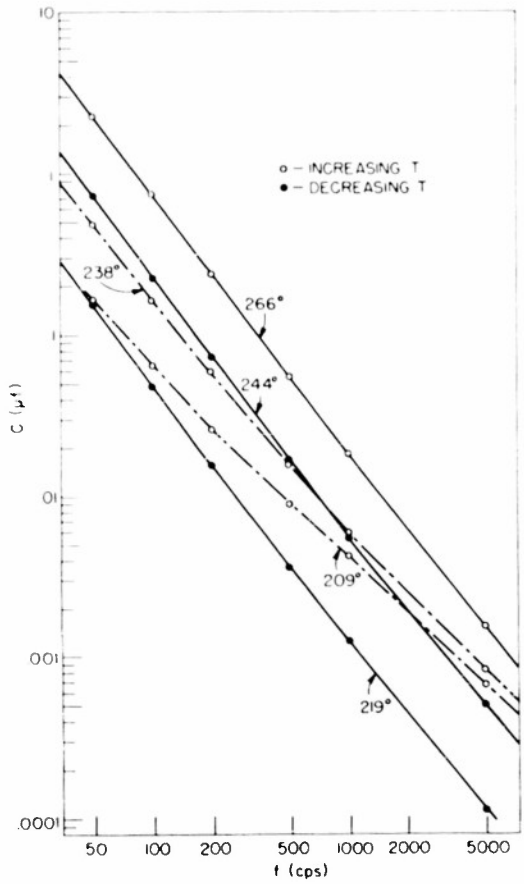

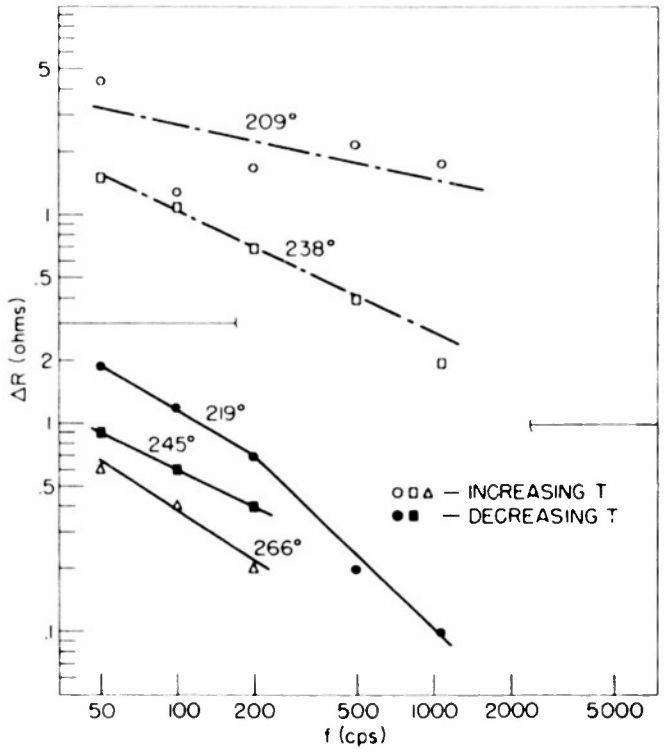

Fig. 7. Excess resistance as a function of frequency for No. 3a (silver electrodes).

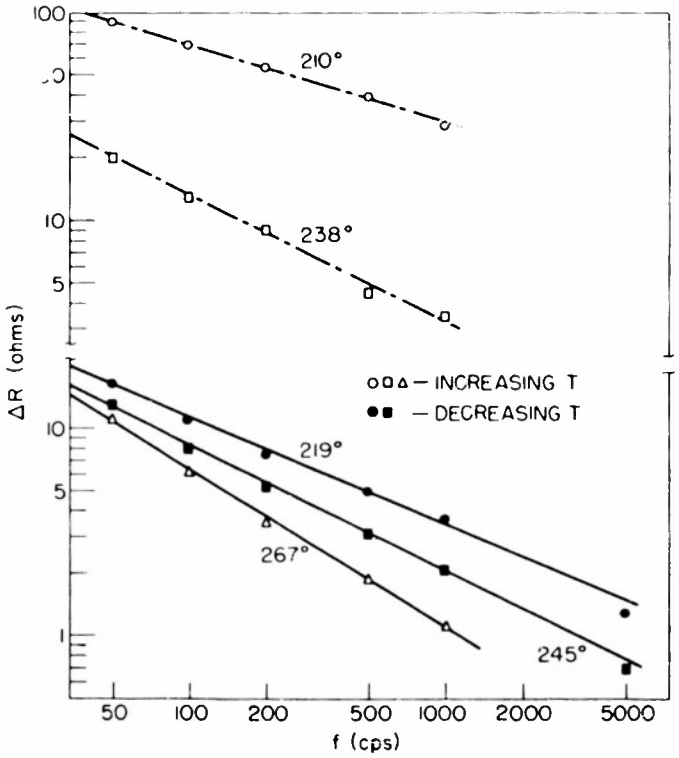

Fig. 8. Excess resistance as a function of frequency for No. 6b (gold electrodes).

20,000 cps for gold electrodes. The individual points, especially for the sample with silver electrodes, are quite inaccurate for two reasons. In the first place the resistance can be measured only to 0.1 ohm. Secondly the small temperature changes which inevitably occur during a frequency sequence cause changes in the total resistance amounting at times to several ohms. The individual resistance measurements are corrected for these changes according to the temperature indicated by the thermocouple near each sample; usually the indicated corrections appear to explain all of the variation of resistance with time at a given frequency, but sometimes there are additional unexplainable small changes of resistance. Nonetheless the results in Figs. 7 and 8 do seem to indicate the general behavior.

Dependence on Voltage, Impurity Content, and Pressure

The theory to be developed shows that in general the sample is a non-linear circuit element. Solutions of the equations are obtained only by introducing the approximation that the electric field is weak; the approximation is good if $eV/2kT \ll 1$, where V is the amplitude of the a.c. voltage applied to the sample. Experimentally it has been observed that the capacity values do approach a limiting value as the applied voltage approaches zero and that the value measured at 0.1 volt rms is within 2% of the limiting value (Fig. 9). Since 0.1 volt is the smallest voltage which permits a fairly

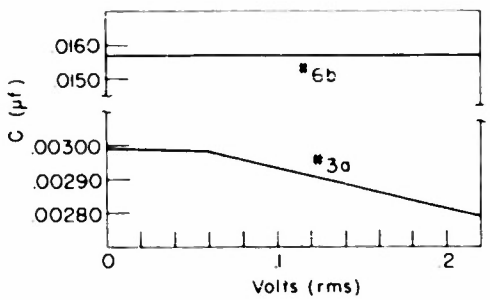

Fig. 9. Variation of capacity with applied voltage for No. 3a (silver electrodes) and No. 6b (gold electrodes) at T = 218°C and f = 200 cps.

sensitive bridge balance, this voltage is used for all measurements as previously mentioned. It is interesting to note that for T = 300° K and V = 0.1 volt $eV/2kT \approx 1$ and that it is at this value of the voltage that the non-linearity appears for sample No. 3a.

Two polycrystalline samples were prepared with 0.1 mole per cent $CdBr_2$ added to the melt. The results in Table I show that the general behavior is not greatly altered although the magnitude of the capacity is somewhat larger. Since there is only about 0.001 mole per cent of impurity in the pure AgBr, these results indicate that the effects observed for the pure AgBr are characteristic of the ideally pure substance.

Measurements have been made on two polycrystalline samples (No. 14 and No. 15) subjected to hydrostatic pressures up to 7500 atmospheres. Considerable trouble was experienced with the electrodes of these samples, but nonetheless the observed temperature and frequency slopes at atmospheric pressure are in approximate agreement with the slopes for the other polycrystalline samples (Table I). When log R and log C are plotted against pressure P, the experimental curves are approximately straight lines. The slopes of such curves have the dimensions of a volume per mole and are expressed in terms of cm^3/mole (Table II). The resistance slopes agree moderately well with the value of 11.0 cm^3/mole obtained from a plot of the

results of Kurnick[4] at 251° C. The capacity slopes are, just as is the case with the temperature slopes, slightly larger than the resistance slopes. The frequency dependence of the capacity is not affected much by pressure; in some cases the frequency slope is smaller by up to 10% at the higher pressures.

TABLE II

Variation of Resistance and Capacity with Pressure
(Slopes of log R and log C vs. P are expressed in cm^3/mole.)

Sample	T, °C	V(R)	V (C)		
			50 cps	200 cps	1000 cps
14	210	10.6	11.7	11.0	. . .
	245	10.9	13.3	13.4	. . .
	292	11.1	14.6	13.8	. . .
15	210	10.6	11.7	12.7	12.1
	245	11.3	12.7	12.3	11.0
	292	11.4	11.2	10.2	8.5

Direct Current Resistance Measurements

The direct current resistance of several samples has been measured with 0.1 volts d.c. applied. For samples with silver electrodes the d.c. resistance is about 5% larger than the high frequency a.c. resistance on the average, with variations of up to 5% about the average. These variations occur in times of the order of minutes; usually the resistance increases after the initial reading, about 15 seconds after the voltage has been applied. In a few instances the resistance decreases with time, and occasionally there are erratic jumps in resistance. For samples with gold electrodes the d.c. resistance is much larger than the high frequency a.c. resistance; at 15 seconds the d.c. resistance is 20 times larger and increases to 100 times larger within 3 minutes without showing any signs of attaining a limiting value.

IV. Theory

Fundamental Equations

In Section I a qualitative explanation of the polarization effects has been presented in terms of the motion of mobile charge carriers in a continuous medium. This qualitative picture can be developed into a macroscopic mathematical theory. The substance—AgBr in this case—is regarded as a continuous medium with a certain dielectric constant and with various types of charge carriers of specified concentrations and mobilities. If formation and recombination of the different types of charge carriers are important, the rate constants for these processes are also supposed to be specified. The various parameters of the charge carriers will depend on the temperature of the medium; for each temperature the appropriate values of the parameters are to be used in the macroscopic theory. Finally the conditions of current flow at the boundaries of the medium must be specified for each type of charge carrier.

The charge carrying medium is placed between two parallel, plane electrodes, which are normal to the x-axis. It is assumed that the conductivity of the medium is large enough so that fringing effects are unimportant; then the space part of the problem is one dimensional. Since only symmetrical combinations of electrodes are considered, it is convenient to place the origin

at the middle of the sample of length 2L. The equations are developed and solved for the case of two types of charge carriers, positive and negative, with equal equilibrium concentrations but with different mobilities. In AgBr the positive charge carriers are interstitial silver ions, and the negative charge carriers are silver ion vacancies.

One of the fundamental equations is Poisson's equation. (See Appendix A for a list of symbols.)

$$\frac{\partial E}{\partial x} = \frac{4\pi e}{K}(p - n). \tag{1}$$

The other equations give the changes of p and n with time.[18]

$$\begin{aligned}\frac{\partial p}{\partial t} &= -\mu_p \frac{\partial (pE)}{\partial x} + D_p \frac{\partial^2 p}{\partial x^2} + k_1 (N - n) - k_2 pn;\\ \frac{\partial n}{\partial t} &= \mu_n \frac{\partial (nE)}{\partial x} + D_n \frac{\partial^2 n}{\partial x^2} + k_1 (N - n) - k_2 pn,\end{aligned} \tag{2}$$

where k_1 and k_2 are the rate constants for formation and recombination, respectively. Since the value of c_o/N is less than .001 for the situations to be considered in AgBr, the term $k_1 n$ can be neglected in comparison to $k_1 N$ in the equations above. Then a detailed balance argument shows that $k_1/k_2 = c_o^2/N$, and with k_2 replaced by γ Eqs. (2) become

$$\begin{aligned}\frac{\partial p}{\partial t} &= -\mu_p \frac{\partial (pE)}{\partial x} + D_p \frac{\partial^2 p}{\partial x^2} + \gamma(c_o^2 - pn);\\ \frac{\partial n}{\partial t} &= \mu_n \frac{\partial (nE)}{\partial x} + D_n \frac{\partial^2 n}{\partial x^2} + \gamma(c_o^2 - pn).\end{aligned} \tag{3}$$

Eqs. (1) and (3) are the three fundamental equations for the three dependent variables p, n, and E.

Two rather generally accepted assumptions have been made in deducing the fundamental equations. The first is the treatment of the crystal as a continuous medium; since some of the characteristic lengths involved are of the order of ten lattice spacings, there may be some doubt as to the validity of this assumption. The second is the treatment of the electrodes as perfectly plane surfaces. The actual conditions at the interface between the medium and the electrodes, especially on a microscopic scale, must be far less ideal than this treatment supposes. It is quite reasonable to assume that the electric field is normal to the actual surface at nearly all points since the metal electrodes have a much larger conductivity than the medium, but the effective area of contact may be several times larger than the nominal area, and it is certainly conceivable that different boundary conditions may apply for different parts of the surface.

Deduction of Approximate Equations

There are non-linear terms in each of Eqs. (3). Physically this means that harmonics of the applied a.c. voltage are generated in the sample and that the impedance of the sample depends on the magnitude of the applied voltage. Mathematically it is extremely unlikely that an exact solution of the differential equations exists in a closed form. Therefore a method of approximation has been developed which does not take the two non-linear effects into account but which does succeed in linearizing the equations.

First suppose that the applied voltage has the form $V(t) = V_0 + V_1 e^{j\omega t}$.

It is then assumed that the dependent variables can be represented by[19]

$$p(x,t) = p_o(x) + p_1(x)\, e^{j\omega t}, \tag{4}$$

with similar equations for n(x,t) and E(x,t). When these expressions are substituted into Eqs. (1) and (3), the following sets of equations are obtained.

$$\text{d.c.:}\quad 0 = -\mu_p \frac{d(p_o E_o)}{dx} + D_p \frac{d^2 p_o}{dx^2} + \gamma(c_o^2 - p_o n_o)$$

$$0 = \mu_n \frac{d(n_o E_o)}{dx} + D_n \frac{d^2 n_o}{dx^2} + \gamma(c_o^2 - p_o n_o) \tag{5}$$

$$\frac{dE_o}{dx} = \frac{4\pi e}{K}(p_o - n_o)$$

$$\text{a.c.:}\quad j\omega p_1 = -\mu_p \frac{d(p_o E_1 + E_o p_1)}{dx} + D_p \frac{d^2 p_1}{dx^2} - \gamma(p_o n_1 + n_o p_1)$$

$$j\omega n_1 = \mu_n \frac{d(n_o E_1 + E_o n_1)}{dx} + D_n \frac{d^2 n_1}{dx^2} - \gamma(p_o n_1 + n_o p_1) \tag{6}$$

$$\frac{dE_1}{dx} = \frac{4\pi e}{K}(p_1 - n_1)$$

The terms depending on time as $e^{2j\omega t}$ are not considered further because experimentally only the terms in $e^{j\omega t}$ are observed. In general the series of Eq. (4) should be extended to include in $e^{sj\omega t}$ with $s = 0,1,2, \ldots \infty$; there would then be an infinite number of sets of equations like those above.

The general procedure for solving Eqs. (5) and (6) would be as follows. First solve Eqs. (5) for the d.c. terms; these equations are still non-linear but have only one independent variable. Next put the d.c. solution into Eqs. (6); these now become linear equations with variable coefficients and in principle can be solved for the a.c. terms. Actually none of these steps is feasible in practice, and a further approximation must be made.

Notice that a consistent solution of the d.c. equations when no external d.c. voltage is applied to the sample is given by

$$p_o(x) = c_o, \quad n_o(x) = c_o, \quad \text{and} \quad E_o(x) = 0. \tag{7}$$

If this solution is substituted in Eqs. (6), a set of linear, homogeneous equations is obtained and can be solved in a straightforward manner.[20]

$$j\omega p_1 = -\mu_p c_o \frac{dE_1}{dx} + D_p \frac{d^2 p_1}{dx^2} - \gamma c_o (p_1 + n_1)$$

$$j\omega n_1 = \mu_n c_o \frac{dE_1}{dx} + D_n \frac{d^2 n_1}{dx^2} - \gamma c_o (p_1 + n_1) \tag{8}$$

$$\frac{dE_1}{dx} = \frac{4\pi e}{K}(p_1 - n_1)$$

The same set of a.c. equations is obtained if the a.c. current densities are written from the beginning as

$$i_p = e\mu_p c_o E_1 - eD_p(dp_1/dx);$$
$$i_n = e\mu_n c_o E_1 + eD_n(dn_1/dx). \tag{9}$$

This is a reasonable approximation so long as p_1 and n_1 are small compared to c_o; otherwise extra terms appear in the conduction current. The actual solutions show that this condition is equivalent to having $eV_1/2kT \ll 1$. Now in a qualitative sense eV_1 represents the electric forces acting on the charge carriers, whereas kT represents the random temperature forces tending to cause diffusion of the charge carriers. Thus the equivalence of the two conditions above is expressed qualitatively by saying that so long as the electric forces are weak compared to the diffusive forces the equilibrium distribution of charge carriers is not seriously affected.

Discussion of the Approximations

Because it has been necessary to make several approximations in order to obtain solutions for the fundamental equations, there are two major shortcomings in the theory as presented above. The first of these is that Eq. (4) does not represent the most general time variation; terms in $e^{-sj\omega t}$ as well as terms in $e^{sj\omega t}$ should be included to give a general Fourier expansion. This omission becomes evident in the form of Eqs. (6), for since these equations are linear in the a.c. terms, the solutions for p_1, n_1, and E_1 will vary linearly with V_1. Thus any non-linear variation with V_1 has already been excluded, and for large enough V_1 equations like Eq. (4) can give a negative value for the concentration of charge carriers, an obviously incorrect result. If all terms were included in Eq. (4), however, every set of equations like Eqs. (5) and (6) would contain a jumble of all coefficients in the Fourier time expansion and would be quite impossible to solve.

The second difficulty is that Eqs. (7) do not represent a good solution for the d.c. equations in the vicinity of the electrodes, even when no external field is applied. Descriptions have been given of the situation in ionic crystals near a free surface[21] and in the contact between AgBr and metallic silver.[22] In both cases there are strong electric fields and large deviations from the equilibrium number of defects in the vicinity of the surface —all in contrast to Eqs. (7). The dependence of p_o, n_o, and E_o on x is sufficiently complicated, however, so that if these functions were introduced into Eqs. (6) the resulting equations would be impossible to solve analytically.

Despite these difficulties the approximation procedure leading to Eqs. (8) has several important advantages. In the first place it is easy to see the physical significance of the approximations as described above. Because of this it is possible to obtain an idea from physical considerations whether or not the approximations are reasonable for a particular physical situation. Secondly none of the terms in the fundamental equations have been discarded in the process of arriving at Eqs. (8). Consequently the solutions of these equations can be expected to show all of the interesting effects arising from the interaction of the different types of processes which are involved—the interplay of the conduction and diffusion currents; the influence of one type of charge carrier on the motion of the other type, which arises because the concentrations of both types appear in Poisson's equation; and the effect of the formation and recombination of pairs of the charge carriers. Thus it seems that the results obtained from the solutions of Eqs. (8) should contain

at least a correct qualitative description of the polarization effects.

A rather different approach to the problem of solving the fundamental equations has been given by Jaffé[19] and Chang and Jaffé.[23] They use the abbreviated Fourier time expansion of Eq. (4) and then proceed to make further approximations in such a way as to make the motion of each type of charge carrier independent of all other types. They are forced to choose zero order solutions somewhat arbitrarily and also introduce an additional length in a completely arbitrary and incorrect fashion. Thus their method contains all of the disadvantages described above and none of the advantages of the present theory.

Boundary Conditions

The normalising condition is always that the potential drop within the sample be equal to the applied potential drop.

$$\int_{-L}^{L} E \, dx = V. \tag{10}$$

There are two extreme types of boundary conditions which can be applied to the passage of charge carriers through the boundary between the sample and the electrode. One of these is that the charge carriers of a particular type are completely blocked at the electrodes: The charge carriers cannot pass through themselves and cannot pass their charges through either, e.g., by transfer of an electron.

$$i_p(\pm L,t) = 0, \quad \text{or} \quad i_n(\pm L,t) = 0. \tag{11}$$

The other extreme is that the charge carriers can pass through the boundary freely. Then if Δp and Δn represent the change in concentration from that existing when no external voltage is applied and hence when no current is flowing, the condition for this case is

$$\Delta p(\pm L,t) = 0, \quad \text{or} \quad \Delta n(\pm L,t) = 0 \tag{12}$$

It is interesting to consider intermediate possibilities for the boundary conditions, and one way of doing this is to say that the current flowing across the boundary is proportional to the excess concentration at the boundary.[23]

$$\begin{aligned} i_p(\pm L,t) &= \pm (e D_p r_p/L) \ \Delta p(\pm L,t), \\ \text{or} \qquad i_n(\pm L,t) &= \mp (e D_n r_n/L) \ \Delta n(\pm L,t). \end{aligned} \tag{13}$$

The signs are adjusted so that particle current flows out of the sample when there is an excess concentration of particles at the boundary. The introduction of the factors $e D_p/L$ and $e D_n/L$ makes the rate constants r_p and r_n dimensionless and simplifies the later calculations. It is possible for r_p and r_n to have values between 0 and ∞: when $r_p = 0$, $i_p = 0$, and the electrode is blocking for positive charge carriers; when $r_p = \infty$, $\Delta p = 0$, and the electrode is open for positive charge carriers.

A possible physical significance for the blocking parameters r_p and r_n may be seen in the following way. Suppose there is a symmetrical potential barrier of height E at the interface between the medium and the electrode, and suppose there are an excess number of particles in the layer of ions next to the electrode (thickness a). The current flowing across a unit area

is then

$$i_p(L) = (\Delta p)\, ea\, \nu_o \exp(-E/kT).$$

By comparison to Eq. (13) it is seen that

$$r_p = (a\, L\, \nu_o / D_p) \exp(-E/kT).$$

Using approximate values for AgBr of $a = 5 \times 10^{-8}$ cm, $\nu_o = 10^{13}$ sec^{-1}, $D_p = 10^{-4}$ cm^2/sec, L = .3 cm, and T = 253° C, the following values are found for r_p.

E(eV)	.5	1.0	1.4
r_p	20,000	.3	5×10^{-5}

This range of values is sufficiently large to give either complete blocking or complete passage for the experimental conditions considered. It seems reasonable to suppose that the barrier has a height somewhere in the neighborhood of 1 eV., especially since Grimley and Mott[22] calculate the contact potential between AgBr and metallic silver to be 1.4 eV. Even though this model gives reasonable values for the blocking parameters, however, the actual significance of the barrier is still unspecified.

One disadvantage of these intermediate boundary conditions is that the same rate constant is used for the flow of charge carriers out of the substance into the electrode as for the flow in the opposite direction. In so far as a physical picture can be obtained of the actual situation at the electrodes for the AgBr—Ag metal system, it seems as if this would not be the case but rather that there should be some rectifying features at a single electrode. Unfortunately there would be considerable mathematical difficulties involved in trying to apply any sort of rectifying boundary conditions in the theory.

Calculation of the External Current

The bridge measurements described in Section II measure the total current passing through the sample. In terms of the elements of the equivalent circuit in Fig. 2 the external current is

$$i_{ex} = (1/R + j\omega C)\ (V_1/A). \qquad (14)$$

When the solutions of the differential equations have been found and the arbitrary constants have been determined by appiying the boundary conditions to these solutions, the remaining step in the calculations is to determine the current which flows in the external circuit and compare the result to Eq. (14) to identify the equivalent resistance and capacity.

There are two ways of calculating the external current. In one the actual current flowing up to one of the metal electrodes is considered.

$$i_{ex}(t) = \frac{K}{4\pi} \frac{\partial E(L,t)}{\partial t} + i_p(L,t) + i_n(L,t).$$

In the other the average conduction and displacement currents are calculated.

$$i_{ex}(t) = \frac{1}{2L} \int_{-L}^{L} [\, i_p(x,t) + i_n(x,t)]\, dx + \frac{1}{2L} \frac{K}{4\pi} \frac{dV(t)}{dt}\ .$$

It can be shown using only the most general fundamental equations, Eqs. (1)

and (2), that these two forms for i_{ex} are equivalent. It is convenient to use the second form in the actual calculations because both terms of i_p and i_n in Eqs. (9) can be integrated immediately.

$$\text{Let} \quad i_{ex} = \frac{e\mu_p c_o}{2L} V_1 + \Delta i_{exp} + \frac{e\mu_n c_o}{2L} V_1 + \Delta i_{exn} + j\omega \frac{K}{4\pi} \frac{V_1}{2L} .$$

$$\text{Then} \quad \Delta i_{exp} = - e D_p [p_1(L) - p_1(-L)] ;$$

$$\Delta i_{exn} = + e D_n [n_1(L) - n_1(-L)] . \tag{15}$$

Notice that when both charge carriers are completely free at the electrodes, i.e., $p_1(\pm L) = 0$ and $n_1(\pm L) = 0$, there are no polarization effects. Only the bulk conductivity of the sample and the displacement current remain, as would be expected.

V. Comparison of Theoretical and Experimental Results

Calculation of Theoretical Curves

Typical curves calculated from the results of the theory of Section IV (see Appendix B) are shown in Figs. 10-13. The frequency dependence of C and ΔR is shown at 253° C and the temperature dependence at 200 cps, all for a number of different boundary conditions. For most of the curves the effect of formation and recombination is not included, but for one curve this effect is included. For the numerical calculations the values of c_o, μ_p, and μ_n reported by Kurnick[4] are used (D_p and D_n are calculated by means of the Einstein relation.), and the dimensions of the sample have been taken as $2L = .61$ cm and $A = .71$ cm^2.

First the capacity curves will be discussed. Notice that a decrease of T is qualitatively equivalent to an increase of ω; this occurs because ω enters into the formulas only in the combination ω/D. Since there are other temperature dependent quantities in the formulas, however, there is not a complete correspondence between the two plots.

The solid curves represent the extreme boundary conditions; the curves have been calculated from the simpler formulas in which terms of the order of ν/α^2 or less are neglected—Eq. (B5) for the (0,0) curve and Eq. (B9) for the (∞,0) and (0,∞) curves. The dielectric capacity $(K/4\pi)(A/2L) = 1.16$ $\mu\mu$f should be added to the curves and would be noticeable for the (∞,0) curve at high frequencies. Since the observed capacity is always much larger than the dielectric capacity, however, and since there is some reason to believe that the curves should be multiplied by a factor of two or more before adding on the dielectric capacity, this capacity has not been included in the curves of Figs. 10 and 11. For purposes of comparison to the experimental slopes in Table I the slopes of the theoretical curves are given in Table III. For the completely blocked case (0,0) the slopes are taken from the straighter portion of the curves.

For the intermediate boundary conditions the values for the blocking parameter $r_p = 20$ and $r_p = 3$ have been chosen so as to make the curves calculated from Eq. (B11) fall approximately midway between the curves for the extreme boundary conditions for the temperatures and frequencies considered. Rough calculations for the cases (3,3) and (0,20) show that both these curves lie fairly close to the curve (3,0) and have the same general shape. If r_p is interpreted according to the discussion following Eq. (13), there should also be a temperature dependence of r_p, whereas r_p has been

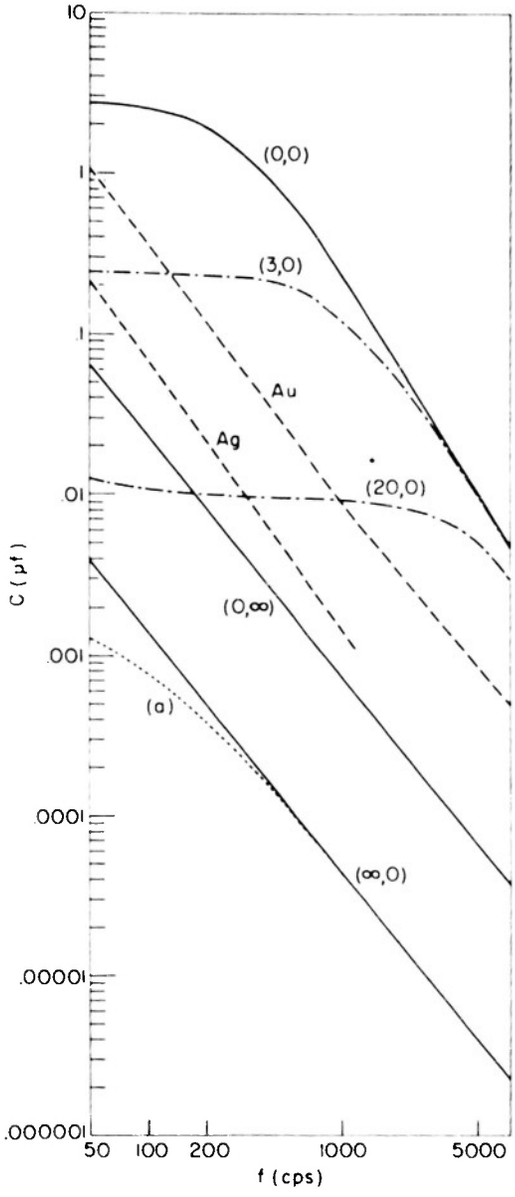

Fig. 10

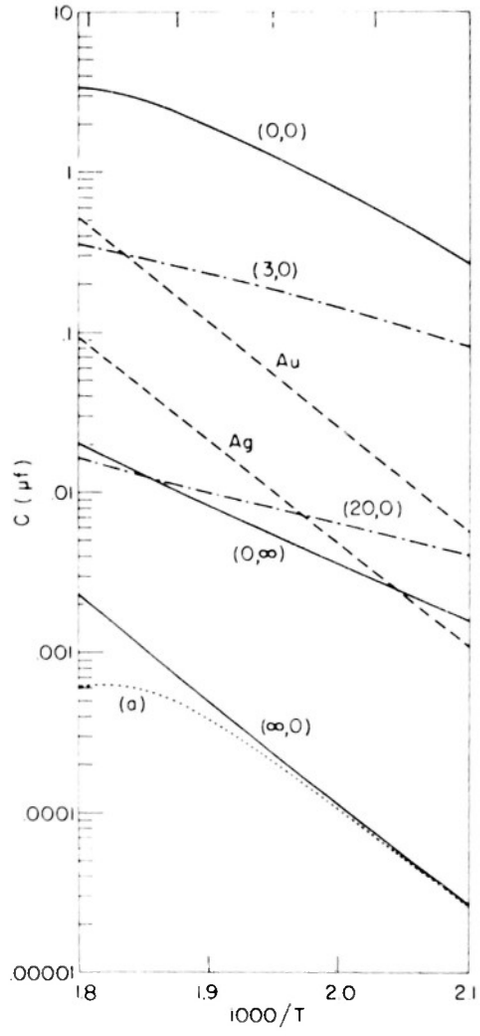

Fig. 11

Fig. 10. Theoretical curves of C vs. f at 253°C. The parentheses enclose the values of the blocking parameters. The various labels mean the following.

(0,0)	Both charge carriers blocked.
(∞,0)	Positive carriers free, negative carriers blocked.
(0,∞)	Positive carriers blocked, negative carriers free.
(3,0)	Positive carriers partially blocked, negative carriers
(20,0)	blocked.
(a)	The effect of formation and recombination on the (∞,0) curve is shown.
Ag	Experimental results for a sample with silver electrodes.
Au	Experimental results for a sample with gold electrodes.

Fig. 11. Theoretical curves of C vs. T at 200 cps. Notation as in Fig. 10.

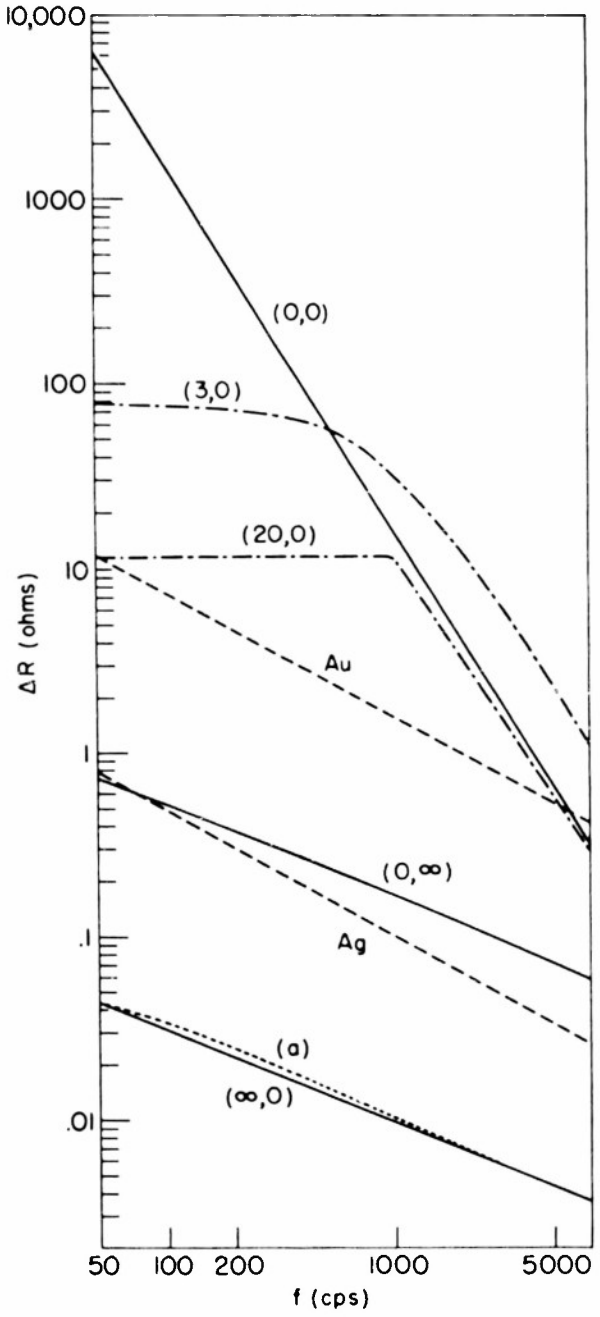

Fig. 12. Theoretical curves of ΔR vs. f at 253°C. Notation as in Fig. 10.

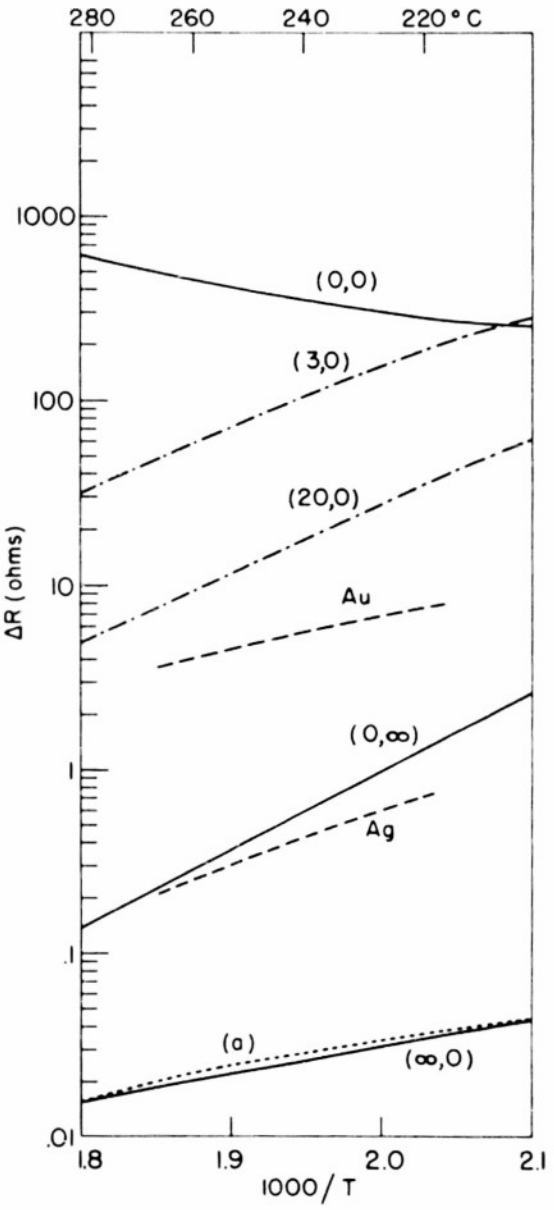

Fig. 13. Theoretical curves of ΔR vs. T at 200 cps. Notation as in Fig. 10.

assumed to be independent of both temperature and frequency. The principle reason that no calculations have been performed with r_p depending on T is that the frequency curves for the intermediate boundary conditions would still show the transitional character displayed in Fig. 10. Thus it does not appear as if this change would be of particular use in bringing the curves for intermediate boundary conditions into better overall agreement with the experimental curves.

TABLE III

Temperature and Frequency Slopes of Theoretical Curves

r_p	r_n	C f/cm^2 T=253°C f=200cps	Temperature slope (k cal/mole)			Frequency slope		
			50 cps	200 cps	1000 cps	227°	253°	283°
0	0	2.7	8.7	21.4	28.5	1.97	1.95	1.82
0	∞	0.012	16.9	16.9	16.8	1.50	1.50	1.50
∞	0	0.00071	29.4	29.4	29.4	1.50	1.50	1.50

The dotted curves (a) show the change produced in the (∞,0) curves by a moderately large value of the rate constant for formation and recombination and have been calculated from Eq. (B9). The values of γc_o used in the calculation were determined by taking the minimum value consistent with Pochapsky's experiment, $\gamma c_o = 4000\ sec^{-1}$ at 350°C (see Appendix C), and scaling this down to the lower temperatures by means of Eq. (C1) with $1/2E_F + U_i = 18.5$ k cal/mole; this gives $\gamma c_o = 230\ sec^{-1}$ at 253°C. The values calculated in this manner are somewhat larger than would be found from Eq. (C2) with $E_F^* + U_i - 1/2E_F = 27.0$ k cal/mole as found in Appendix C; this procedure gives $\gamma c_o = 70\ sec^{-1}$ at 253°C. It is seen that even with the somewhat larger value for γc_o the change is not tremendous. The effect of these values of γc_o on the (0,∞) curves would be about the same; there would be no noticeable effect on the (0,0) curves.

The curves for the excess resistance ΔR are shown in Figs. 12 and 13. ΔR has been calculated from $\Delta(1/R)$ by

$$\Delta R = - \frac{R_o^2 \, \Delta(1/R)}{1 + R_o \, \Delta(1/R)} ; \qquad (16)$$

since $\Delta(1/R)$ is negative, ΔR is positive. When Eq. (B6) for the completely blocked case is used in Eq. (16), it turns out that $\Delta R = R_o/(\omega\tau)^2$, and this is the frequency dependence shown by the (0,0) curve. The curves (∞,0) and (0,∞) have a frequency dependence $1/\omega^{1/2}$ as indicated by Eq. (B10). The analogy between a decrease of T and an increase of ω is not valid here because of the extra temperature dependent terms in Eq. (16).

Comparison of Experimental Results to Calculated Results

The dashed curves in Figs. 10-13 show representative experimental results. On the capacity plots the sample with silver electrodes is No. 6a, and the one with gold electrodes is No. 6b. On the excess resistance plots the sample with silver electrodes is No. 3a, and the one with gold electrodes is No. 6b.

In comparing the experimental curves to the theoretical ones, it is seen that the best agreement for the slopes is obtained with the (∞,0) curves for positive carriers free and negative carriers blocked; this is evident from the figures and from a comparison of Tables I and III. Unfortunately the magnitude of the calculated curves is too small; for the sample with silver electrodes the calculated curves are too small by a factor 40 for capacity and a factor 15 for excess resistance. Now if the results of Eq. (B9) multiplied by some constant were to be in complete agreement with the experimental results, the ratios given above should be equal to each other; the discrepancy of a factor three from this condition is not tremendously large,

especially in view of the inaccuracy of the excess resistance measurements. For the sample with gold electrodes the ratios between observed and calculated values are 240 for capacity and 160 for excess resistance; there is thus an even better agreement of the two ratios.

The magnitudes of the polarization effects calculated for the opposite case $(0,\infty)$ are in better accord with the observed magnitudes. In this case, however, there is quite a difference in the calculated and observed temperature dependence of the capacity. Since the slopes are more reproducible experimentally than the actual magnitudes, this seems to be quite a serious fault.

The calculations with both carriers blocked (0,0) give larger magnitudes than are observed. The turn over of the capacity at low frequencies should have been observed, however, if it were present to this amount experimentally. Furthermore the calculated excess resistance is extremely large at low frequencies and has a frequency dependence that is quite different from the observed frequency dependence. In addition the d.c. resistance measurements indicate that there is by no means complete blocking with silver electrodes, and not quite complete blocking with gold electrodes.

The theoretical curves for intermediate boundary conditions have far too much curvature to afford much hope of a good comparison to the experimental curves.

The writer would like to propose that the most nearly correct explanation of the experimental results is contained in the $(\infty,0)$ curves. The only major discrepancy here is the small magnitude of the calculated curves, but there are several reasons that this may not be too serious. From the experimental viewpoint the magnitudes are not especially reproducible anyway, and the magnitudes observed when the samples are not annealed after the electrodes have been applied are less by a factor of ten. It is also encouraging that the ratios of observed to calculated magnitudes for capacity and excess resistance are equal within a factor three. From the theoretical viewpoint there are two possible reasons for expecting larger results than those given by the theory. The first is that the effective area of the electrodes is doubtlessly larger than the nominal area of the sample. Since the characteristic length in this case is of the order of 10^{-4} cm and since the finishing cut in the lathe leaves the surface fairly rough on this scale, there is probably a difference of at least a factor two and perhaps a factor as large as five. The other reason is that in the situation with no field applied there are a large number of vacancies near the electrodes. According to Grimley and Mott[22] there are about one hundred times as many vacancies in the layer one Debye length thick next to the electrodes as there are in the interior of the sample. Although it is by no means certain that the results of Eq. (B9) multiplied by one hundred are appropriate for this situation, it does seem likely that there will be some enhancement of the polarization effects, and since the motion of the charge carriers in the alternating field is determined by the mobility of the carriers, it is possible that the temperature and frequency dependence of the effects may not be drastically changed.

It is not surprising that there is not exact agreement with any of the calculated curves since it is very likely that the actual boundary conditions are not so ideal as the boundary conditions described in Eqs. (11), (12), and (13). This certainly seems to be the conclusion if a detailed picture on an atomic scale is imagined of the situation at the electrodes. For one thing the possible effect of the dependence of the boundary conditions on temperature is rather difficult to estimate without knowing much about the boundary conditions; hence the results of the $(0,\infty)$ curves cannot be completely ruled out on the basis of the temperature dependence alone. It seems reasonable to

suppose, however, that it is more difficult for vacancies to move through the interface than for interstitials, especially when vacancies are trying to move into the AgBr. Furthermore, as mentioned previously, it seems likely that some sort of rectifying boundary conditions would be more appropriate for describing the actual situation than the symmetrical conditions used. It is also probable that the boundary conditions vary from place to place on the surface so that some sort of composite effect is observed.

It seems quite unlikely that the polarization effects could be produced only by the motion of bromine ion vacancies, with both silver ion vacancies and interstitial silver ions being free at the electrodes. Since the d.c. resistance measurements show that a fairly large portion of the current passes through the silver electrodes, the situation if bromine vacancies were present in appreciable numbers and were blocked at the electrodes would be similar to the $(0,\infty)$ case rather than the $(0,0)$ case. Now in the first place the activation energies for both the formation and mobility of bromine vacancies are presumably somewhat larger than the corresponding energies for the silver vacancies; Kurnick suggests 35-50 k cal/mole for the formation of Schottky defects.[4] These larger values would lead to considerably larger values for the theoretical temperature slopes, whereas the slopes calculated with the activation energies for silver vacancies are in quite good agreement with the observed slopes. Secondly since the contribution to the conductivity of the bromine vacancies is less than one-hundredth of the contribution of the silver vacancies in the temperature range considered,[4] the calculated magnitudes of the polarization effects would be even smaller than those calculated for the silver vacancies. Thus even if the bromine vacancies do make a small contribution, their presence is completely masked by the silver vacancies and interstitials.

On the basis of the d.c. resistance measurements it would seem as if the samples with gold electrodes should show a behavior closer to the completely blocked case. It is gratifying in this respect that the observed polarization effects are larger by about a factor ten with gold electrodes. On the other hand the character of the curves is nearly the same as for the samples with silver electrodes; it might be expected that some of the characteristics of the completely blocked case would appear.

Since the experimental curves do not show any of the curvature exhibited by the curves (a), it must be concluded, if the $(\infty,0)$ or $(0,\infty)$ curves are appropriate for describing the experimental results, that the formation and recombination rate is somewhat smaller than the value 230 sec^{-1} at 253°C used to calculate the curves (a). A value smaller by about a factor ten would scarcely affect the calculated curves, and would not be especially inconsistent with the lower limit suggested by Pochapsky's experiment.

Discussion of Other Aspects of the Experimental Results

The peculiar dependence of the magnitude of the capacity on the treatment of the electrodes described in Section III can now be qualitatively explained. It will be seen from Figs. 10 and 11 that for the range of temperatures and frequencies employed in the experiments a decrease in the amount of blocking at the electrodes causes a decrease of the capacity and vice versa. When the samples are annealed after the electrodes have been applied, the electrodes seem to deteriorate somewhat, as described; this treatment then must increase the blocking at the electrodes and hence cause the larger values of capacity which are observed after this treatment. While the samples are held in the sample holder, on the other hand, there is a moderate spring pressure acting on the electrodes. Since silver bromide shows a relatively large amount of plastic flow at elevated temperatures, it is believed that the contact between the silver metal and the silver bromide is

improved during this time. Also the passage of a direct current would seem to improve the contact at the electrodes. Thus the slow decrease of capacity in these situations, especially the larger decrease at the higher temperatures in the first situation, is explained.

For the completely blocked case at high frequencies and for the case with one carrier blocked and the other free at all frequencies, the capacity should vary as $1/L^2$. Because of the problems involved in making the electrical measurements, it is not possible to vary the length very much, but some samples have been used with about twice the length of the others. As can be seen from Table I the capacity is somewhat less for these samples than for the shorter samples. The factor looks more like two than four, which would be expected, but as usual there is some uncertainty in the measurement of magnitudes, and the change is in the proper direction.

In order to obtain a basis for comparison to the results for the variation of the capacity with pressure the approximate formulas of Eqs. (B6) and (B10) are used. Using the values of Kurnick[4] for the free volumes, which are proportional to the slope of log σ vs P, etc. ($\Delta V = 16$ cm^3/mole for formation; $\Delta V_i = 2.6$ cm^3/mole and $\Delta V_v = 7.4$ cm^3/mole for mobility), the values of the pressure slopes given in Table IV are found. For purposes of comparison the temperature slopes have been calculated by the same method. The slopes for the completely blocked case (0,0) are appropriate only at high frequencies ($\omega\tau \gg 1$). It will be seen by comparison to Table II that the calculated pressure slopes for the (0,0) and (∞,0) cases are somewhat too large, whereas the pressure slope for the (0,∞) case is slightly too small. This is the same situation that exists for the temperature slopes of the polycrystalline samples, and the numbers are even approximately proportional for the two cases. Hence the pressure dependence appears to be in substantial agreement with the temperature dependence.

TABLE IV

Pressure Slopes of Theoretical Curves

r_p	r_n	P slope (cm^3/mole)	T slope (k cal/mole)
0	0	18.0	29.7
∞	0	19.1	29.0
0	∞	9.5	16.2

Conclusions

Considering the approximations made in solving the differential equations, the uncertainties about the boundary conditions, and the somewhat peculiar behavior of the experimental results, it is considered that the theory gives a reasonably good qualitative picture of the experimental results. It seems certain that the observed polarization effects in AgBr are caused by the motion of the Frenkel defects in the crystal with some amount of blocking at the electrodes, rather than the motion of any bromine vacancies which may be present.

Since there is no indication in the experimental results of the effects which would be caused by a fast formation and recombination rate, it is probable that the rate constant for these processes is somewhat smaller than might be expected on the basis of a simple picture. The proposed upper

limit for the rate constant is not especially inconsistent with other experimental evidence, however, and does not appear to be unreasonable on the basis of a slightly more refined picture of the formation process.

From the viewpoint of studying polarization effects as such the experimental situation is far from ideal. The greatest difficulty is caused by the large bulk conductivity of silver bromide. Also the uncertainty about the boundary conditions makes the comparison of experimental and theoretical results less definite than might be desired. A considerable advantage, on the other hand, is that both the concentrations and mobilities of the Frenkel defects in silver bromide are known from other experiments.

Although some approximations are necessary in the theory, a number of interesting polarization effects are predicted, and many of these have been observed, at least qualitatively, in this experiment. Since polarization effects have been known experimentally for many years, especially in connection with electrolytic solutions, it is interesting to have even a semi-quantitative explanation starting from the fundamental laws of physics.

Acknowledgments

The author would like to express his appreciation for the constant encouragement of his sponsor, Professor A. W. Lawson. The Atomic Energy Commission granted a fellowship for one and one-half years. Part of this work was supported by funds from the Office of Naval Research.

Appendix A. List of Symbols

Properties of the entire sample:

- L = half the length
- A = area
- K = dielectric constant
- R = equivalent parallel resistance
- C = equivalent parallel capacity
- R_o = limiting value of R at high frequency
- C_o = limiting value of C at low frequency
- V_o = magnitude of d.c. voltage drop
- V_1 = magnitude of a.c. voltage drop
- i_{ex} = current per unit area flowing in external circuit

Electrical quantities:

- E = electric field
- p,n = concentration of positive and negative charge carriers, respectively
- i_p,i_n = current densities
- e = magnitude of the charge on the electron
- ω = angular frequency
- j = $\sqrt{-1}$

Parameters of the charge carriers:

- c_o = equilibrium concentration
- N = number of ion pairs per unit volume in the crystal
- μ_p, μ_n = mobilities
- ϕ = μ_p/μ_n = ratio of mobilities
- D_p,D_n = microscopic diffusion coefficients
- σ = conductivity
- r_p,r_n = blocking parameters

γ = rate constant for formation and recombination
ν_o = vibrational frequency of an ion in the lattice
a = interionic distance

Quantities which appear in the solutions of the differential equations:

a_1, a_2 = reciprocals of characteristic lengths
A_1, A_2, A_3 = arbitrary constants of integration

$$\alpha^2 = \frac{4\pi e}{K}\frac{e}{kT}c_o, \qquad \begin{aligned} \nu_p &= j\omega/D_p, & \lambda_p &= \gamma c_o/D_p \\ \nu_n &= j\omega/D_n, & \lambda_n &= \gamma c_o/D_n \end{aligned} \tag{A1}$$

$$\alpha_p^2 = \alpha^2 - \lambda_p, \qquad \nu_p^1 = \nu_p + 2\lambda_p \tag{A2}$$

$$\alpha_n^2 = \alpha^2 - \lambda_n, \qquad \nu_n^1 = \nu_n + 2\lambda_n$$

Appendix B. Detailed Formulas

Solutions of the Differential Equations

Eqs. (8) are solved by eliminating first E_1 and then n_1 to obtain a fourth order equation in p_1, which gives

$$p_1(x) = A_1 \sinh a_1 x + A_2 \sinh a_2 x. \tag{B1}$$

The terms in $\cosh a_1 x$ and $\cosh a_2 x$ which should also be present in the general form of p_1 are not needed here because only symmetrical boundary conditions are considered and the origin is placed at the center of the sample. The expressions for $n_1(x)$ and $E_1(x)$ can now be found by direct substitution; E_1 contains an additional integration constant A_3. The quantities a_1 and a_2 are given by

$$\left\{\begin{matrix} 2\,a_1^2 \\ 2\,a_2^2 \end{matrix}\right\} = (\alpha_p^2 + \alpha_n^2) + (\nu_p^1 + \nu_n^1) \tag{B2}$$

$$\mp\left[(\alpha_p^2 + \alpha_n^2)^2 + (\nu_p^1 - \nu_n^1)^2 + 2(\alpha_p^2 - \alpha_n^2)(\nu_p^1 - \nu_n^1)\right]^{1/2},$$

using the definitions of Eqs. (A1) and (A2). In the definition of α in Eq. (A1) the Einstein relation $\mu/D = e/kT$ for both types of charge carriers has been used; with Frenkel defects in AgBr there appears to be no mechanism which can contribute to diffusion but not conduction.

It is easier to see the physical meaning of the solutions if the simpler formulas which are appropriate for equal mobilities of the charge carriers are used; for the experimental conditions in AgBr the mobilities do not differ by more than a factor of ten, and all of the features of the theory appear in a qualitatively correct fashion in the results for equal mobilities. Then with $\mu_p = \mu_n$ and consequently $D_p = D_n$, and also neglecting formation and recombination for the moment ($\gamma c_o = 0$), Eqs. (B2) become

$$a_1^2 = \nu = j\omega/D; \quad a_2^2 = 2\alpha^2 + \nu . \tag{B3}$$

One of the characteristic lengths in Eq. (B1) is $1/a_2$, which is essentially equal to $1/2\alpha$ except at extremely high frequencies. The length $(2\alpha^2)^{-1/2} = (\frac{4\pi e}{K}\ \frac{e}{kT}\ 2c_o)^{-1/2}$ is the Debye length which appears in the Debye-Hückel theory of strong electrolytes; it is a measure of the distance over which an appreciable accumulation of charge can occur when a steady electric field is applied. The other characteristic length is $1/a_1 = (D/j\omega)^{1/2}$ and is related to the distance the charge carriers can diffuse during one cycle: in the time $1/f$ the mean square displacement by diffusion is $(2D/f)^{1/2}$, which is equal to the magnitude of $1/a_1$ except for small numerical factors. For the conditions in AgBr the Debye length is of the order of 5×10^{-7} cm and the diffusion length is of the order of 10^{-4} cm.

It is interesting to note that the solutions in the case of equal mobilities can be written

$$p_1 - n_1 = 2A_2 \sinh a_2 x;$$

$$p_1 + n_1 = 2A_1 \sinh a_1 x.$$

Thus only the net space charge, $e(p_1 - n_1)$, is associated with the Debye length, whereas only the excess number of charge carriers, $p_1 + n_1$, is related to the diffusion length. If formation and recombination are considered, the only change required is to replace a_1 in Eqs. (B3) by

$$a_1^2 = \nu + 2\lambda = (j\omega + 2\gamma c_o)/D.$$

Since it can be seen in Eqs. (8) that formation and recombination act only when the excess number of charge carriers, $p_1 + n_1$, is different from zero, it is not surprising that a_1 should be modified whereas a_2 is unchanged.

Results for Both Charge Carriers Blocked

When the arbitrary integration constants of the solutions of Eqs. (8) are determined by the application of the boundary conditions of Eq. (11) to both types of charge carriers, along with the condition of Eq. (10), the general expression for the external current is (see Eq. [15])

$$\Delta i_{ex\,p} = -\frac{e\mu_p c_o}{2L} V_1 (1 - F) S; \tag{B4}$$

$$\Delta i_{ex\,n} = -\frac{e\mu_n c_o}{2L} V_1 \left(-\frac{\alpha_p^2 + \nu_p^1 - a_2^2}{\alpha_p^2} + \frac{\alpha_p^2 + \nu_p^1 - a_1^2}{\alpha_p^2} F\right) S,$$

where

$$F = \frac{a_1^2 - \nu_n^1 + \alpha_p^2 - \alpha_n^2}{a_2^2 - \nu_n^1 + \alpha_p^2 - \alpha_n^2}\ \frac{a_2}{a_1}\ \frac{\coth a_2 L}{\coth a_1 L};$$

$$\frac{1}{S} = \frac{\alpha^2}{\alpha_p^2}\left(-\frac{a_1^2 - \nu_p^1}{a_1^2} F + \frac{a_2^2 - \nu_p^1}{a_2^2}\right)$$

$$+\left[\left(1-\frac{\alpha^2}{\alpha_p^2}\,\frac{a_2^2-\nu_p^1}{a_2^2}\right)\right.$$

$$\left.-\left(1-\frac{\alpha^2}{\alpha_p^2}\,\frac{a_1^2-\nu_p^1}{a_1^2}\right)\frac{a_1^2-\nu_n^1+\alpha_p^2-\alpha_n^2}{a_2^2-\nu_n^1+\alpha_p^2-\alpha_n^2}\right] a_2 L \coth a_2 L.$$

For the situations encountered in AgBr a considerable simplification is possible if terms of the order of $\nu/2\alpha^2$ and $\lambda/2\alpha^2$ or smaller are neglected (These terms are smaller than .001 in all cases.). Then

$$\Delta i_{ex\,p} = -\frac{e\mu_p c_o}{2L} V_1 \frac{1-F}{1+j\omega\tau}\;;$$

$$\Delta i_{ex\,n} = -\frac{e\mu_n c_o}{2L} V_1 \frac{1+F}{1+j\omega\tau}\;, \qquad \text{(B5)}$$

with $$\tau = \frac{L}{\sqrt{2}\,\alpha}\,\frac{2}{D_p+D_n}\;.$$

If F, which is never larger than .01, is also neglected, the parameters of the equivalent circuit can be expressed as

$$-\Delta\frac{1}{R} = \frac{1}{R_o}\frac{1}{1+(\omega\tau)^2}\;; \qquad C = \frac{1}{R_o}\frac{\tau}{1+(\omega\tau)^2}\;. \qquad \text{(B6)}$$

$R_o = 2L/A\, e(\mu_p+\mu_n)\, c_o$ is the bulk resistance of the sample; it is the measured resistance at frequencies so large that $\Delta(1/R)$ is negligibly small.

As ω decreases from a value for which $\omega\tau$ is comparable to unity, C approaches a limiting value

$$C_o = \tau/R_o = (KA/4\pi)\,(\alpha/\sqrt{2}), \qquad \text{(B7)}$$

and $-\Delta(1/R)$ becomes nearly equal to $1/R_o$, causing R to increase toward infinity. The second form for C_o above shows that the sample has become a condenser with an effective thickness comparable to the Debye length rather than the length of the sample. Since the Debye length is very short in AgBr at elevated temperatures, the value of C_o can be quite large: at 253° C the value of C_o is 3.9 μf/cm^2, and $\omega\tau = 1$ for f = 300 cps. For $\omega\tau \gg 1$ both C and $\Delta(1/R)$ vary as $1/\omega^2$. The dependence on frequency of the parallel quantities given by Eq. (B6) is the same as that obtained from an equivalent series combination of R_o and C_o with $R_oC_o = \tau$. This approximation is not valid for $f > 10^9$ cps, but at this frequency the polarization effects are completely negligible.

The effect of formation and recombination in this case is scarcely noticeable in the calculations. In Eqs. (B5) only F is modified if γc_o is different from zero, and the magnitude of F decreases as γc_o increases. For the case with equal mobilities there is actually no effect at all because the

boundary conditions require A_1 in Eq. (B1) to be zero.

Results for One Type of Charge Carrier Blocked, the Other Free

The results will be given for the case in which the negative carriers are blocked, the positive carriers free. The results for the opposite case can be obtained by interchanging the subscripts p and n throughout (also replacing $\phi = \mu_p/\mu_n$ by $1/\phi$). The integration constants are now determined by using Eq. (12) for the positive carriers, Eq. (11) for the negative carriers, and Eq. (10). Then

$$\Delta i_{ex\,p} = 0; \quad \Delta i_{exn} = -\frac{e\mu_n c_o}{2L} V_1 \frac{a_2^2 - a_1^2}{\alpha_p^2} S, \tag{B8}$$

where

$$\frac{1}{S} = \left(\frac{a_2^2 - \nu_n^1}{\alpha_p^2} - \frac{\alpha^2}{\alpha_p^2} \frac{\nu_p^1}{a_1^2} + \frac{\alpha^2 - \alpha_n^2}{\alpha_p^2} \right) a_1 L \coth a_1 L$$

$$+ \frac{\alpha^2}{\alpha_p^2} \frac{\nu_p^1 (a_2^2 - a_1^2)}{a_1^2 \; a_2^2}$$

$$- \left(\frac{a_1^2 - \nu_n^1}{\alpha_p^2} - \frac{\alpha^2}{\alpha_p^2} \frac{\nu_p^1}{a_2^2} + \frac{\alpha^2 - \alpha_n^2}{\alpha_p^2} \right) a_2 L \coth a_2 L.$$

Again if terms of the order of ν/α^2 and λ/α^2 or smaller are neglected, simplified formulas are obtained.

$$\Delta i_{ex\,n} = -\frac{e\mu_n c_o}{2L} V_1 \, 2S;$$

$$\frac{1}{S} = \left(\frac{2\phi}{1+\phi}\right)^{1/2} (\nu_n + 2\lambda_n)^{1/2} L + \frac{\nu_n}{\alpha} \frac{L}{\sqrt{2}}. \tag{B9}$$

These are valid between 10^{-3} and 10^9 cps. The second term in $1/S$ is of the order of one-hundredth of the first term; if this is neglected and it is supposed that formation and recombination are unimportant ($\gamma c_o = 0$), the equivalent parallel quantities can be expressed as

$$-\Delta(1/R) = \omega C = \frac{e\mu_n c_o A}{\sqrt{2}\, L^2} \left(\frac{D_n}{\omega}\right)^{1/2} \left(\frac{1+\phi}{2\phi}\right)^{1/2}. \tag{B10}$$

C now varies as $1/\omega^{3/2}$ and $\Delta(1/R)$ as $1/\omega^{1/2}$ in contrast to the $1/\omega^2$ dependence of both quantities at high frequency in the previous case. The effect of formation and recombination appears in Eq. (B9) in the expression $\nu_n + 2\lambda_n = (j\omega + 2\gamma c_o)/D_n$; when γc_o is comparable to or larger than ω, there is an appreciable effect. It is interesting to note that to the ap-

proximation of Eq. (B9)

$$\frac{i_{ex\ p}\ (\text{positive carriers blocked})}{i_{ex\ n}\ (\text{negative carriers blocked})} = \phi^2 .$$

The reason that the behavior of the polarization effects for this combination of boundary conditions is considerably different from that for the previous combination is that the physical situation is considerably different for the two cases. First consider the case in which both charge carriers are blocked. If a steady d.c. voltage is applied to the sample, a certain amount of charge builds up near the electrodes, and this induces a charge on the metal electrodes which gives the capacity C_o of Eq. (B7). If the applied voltage is made to alternate slowly, the induced charge alternates accordingly and gives rise to an a.c. capacity of the same magnitude. If a steady d.c. voltage is applied in the second case, however, in which the positive carriers are free and the negative carriers blocked, only the negative carriers pile up near the electrodes and induce half the charge of the previous case; there is a steady current of the positive carriers which corresponds to their bulk conductivity. If the applied voltage is made to alternate slowly, there are now two effects: one is the wobbling of the induced charge on the electrodes as before; the other is a phase change in the large steady current which flows even for $\omega = 0$ in this case. The second effect occurs because the pile-up of the negative carriers modifies the electric field through Poisson's equation. At very low frequencies the second effect is dominant, and the limiting value of the capacity for frequencies less than 10^{-7} cps is $(K/4\pi)(\alpha^2 L/12)$ which is of the order of 1 farad/cm^2 in AgBr at 253° C. For the frequencies used in the experiments the predicted capacity is smaller for this case than for the previous case because C has been decreasing from the large initial value of C_o for many more decades of frequency than in the previous case.

Results for Intermediate Boundary Conditions

The calculations with intermediate boundary conditions have been performed only with $\gamma c_o = 0$; in Section V it appears that neither the use of intermediate boundary conditions nor inclusion of the effects of formation and recombination gives much assistance to the explanation of the experimental results, and the algebra would be quite complicated. If the boundary conditions of Eq. (13) are applied to both types of charge carriers, then, with $\gamma c_o = 0$, the external current is

$$\Delta i_{ex\ p} = -\frac{e\mu_p c_o}{2L} V_1 (1 - F)\, S; \qquad \text{(B11)}$$

$$i_{ex\ n} = -\frac{2\mu_n c_o}{2L} V_1 \left(-\frac{\alpha^2 + \nu_p - a_2^2}{\alpha^2} + \frac{\alpha^2 + \nu_p - a_1^2}{\alpha^2} F\right) S,$$

where

$$F = \frac{(a_1^2 - \nu_n)\, a_2 L \coth a_2 L + \alpha^2\, r_p + (\alpha^2 + \nu_p - a_2^2)\, r_n}{(a_2^2 - \nu_n)\, a_1 L \coth a_1 L + \alpha^2\, r_p + (\alpha^2 + \nu_p - a_1^2)\, r_n};$$

$$\frac{1}{S} = -F\left(\frac{\nu_p L}{a_1}\coth a_1 L + r_p + \frac{a_1^2 - \nu_p}{a_1^2}\right)$$

$$+\left(\frac{\nu_p L}{a_2}\coth a_2 L + r_p + \frac{a_2^2 - \nu_p}{a_2}\right) .$$

The usual effect of these formulas is to give results somewhat in between the results of the extreme cases previously described. For a given value of r_p, for instance, the positive carriers appear almost completely blocked at high frequencies and almost completely free at low frequencies; if $r_p < 5$, however, the blocking is apparent even for $\omega = 0$.

Appendix C. Estimates of the Formation and Recombination Rates

In order to determine the effect of formation and recombination on the calculated results, it is necessary to obtain at least an estimate of the rate constant involved. Since γc_o has the dimensions of a reciprocal time and is compared to ω in Eq. (B9), this quantity will be referred to as the rate constant.

Theoretical Estimates

A direct estimate of the formation rate may be obtained as follows.[24] The process involves the jumping of a silver ion from a normal lattice site to an interstitial position, leaving a vacancy; the energy required is the energy to form a pair of Frenkel defects, $E_F = E_v + E_i$, plus an energy something like the energy U_i for the mobility of an interstitial ion to allow the interstitial ion to move away from the vacancy (which has a smaller mobility). The number of formation processes per unit time per unit volume is $N\ \nu_o \exp[-(E_F + U_i)/kT]$, and when this is identified with γc_o^2 in Eq. (3),

$$\gamma c_o = \nu_o \exp[-(\tfrac{1}{2} E_F + U_1)/kT], \qquad (C1)$$

using $c_o = N \exp(-\frac{1}{2} E_F/kT)$. Approximately the same formula can also be obtained by considering the collision of interstitials and vacancies if the cross section for recombination is taken to be comparable to πa^2. If the values of E_F and U_i determined from conductivity measurements, E_F = 27.5 k cal/mole and U_i = 4.7 k cal/mole[4], are substituted in Eq. (C1), with $\nu_o \sim 10^{13}$ sec^{-1}, γc_o is found to have a value 2×10^5 sec^{-1} at T = 253° C. Although this value does not seem especially unreasonable,[25] it is large enough to produce a major change in the theoretical result for the case with one carrier free and the other blocked. Since the experimental results do not indicate any such effect, it is interesting to consider whether there is any reason for a slower formation or recombination rate.

In the previous calculation the energy E_F determined for the equilibrium condition is used; actually a somewhat different value should be used for the calculation of the formation rate. Part of the energy required to form a silver ion vacancy or to insert an interstitial silver ion is compensated by the subsequent relaxation of the ions in the neighborhood of the defect. Since it seems very likely that the jumping ion must practically complete its jump before all of the relaxation of the surrounding ions can occur, the activation energy which determines the formation rate should be larger than $E_F + U_i$.

According to the calculations of Mott and Littleton for several alkali halides, the change in repulsive energy during relaxation is only about three-tenths of the change in polarization energy of the lattice;[26] hence a rough estimate of the amount of energy released during the relaxation process can be obtained by considering only the polarization energy. Using the model of Jost,[27] the change in polarization energy is $(e^2/2R)(1/K_o - 1/K)$, where K_o is the high frequency dielectric constant. The detailed calculations of Mott and Littleton for the alkali halides indicate that R/a is 0.6 for positive ion vacancies and 0.5 for positive interstitial ions. Using these values for AgBr and introducing a factor of 0.7 to correct for the neglect of the change in the repulsive energy, the relaxation energy for a pair of Frenkel defects is found to be 20 k cal/mole, with about equal amounts coming from the creation of each type of defect. Now in place of Eq. (C1) for calculating γc_o it is necessary to use

$$\gamma c_o = \nu_o \exp\left[-(E_F^* + U_1 - \tfrac{1}{2} E_F)/kT\right], \qquad (C2)$$

where E_F^* is larger than E_F by at least some of the relaxation energy. If the entire relaxation energy is inserted into Eq. (C2), $\gamma c_o = 10^{-3}$ sec.$^{-1}$ at 253°C; this is evidently a rather exaggerated lower limit.

Experimental Information About Recombination Rates

Rapid specific heat measurements on AgBr have recently been performed by Pochapsky.[28] At temperatures above 350° C there is an anomalous increase in specific heat, which is supposed to represent the extra energy that is required to form lattice defects. It is not clear whether these are Schottky or Frenkel defects, but if it is assumed that they are Frankel defects, a lower limit can be obtained for the rate constant. Since there is no evidence in these measurements that the establishment of equilibrium of the defects is not complete within 5×10^{-4} secs., a lower limit for γc_o is estimated to be 4×10^{13} sec.$^{-1}$ at 350° C. If this value is used in Eq. (C2) to determine E_F^*, it is found that E_F^* is greater than E_F by 9.5 k cal/mole, which is not unreasonable in view of the estimate of this quantity made above, namely, a maximum of 20 k cal/mole. It is then calculated that $\gamma c_o = 70$ sec.$^{-1}$ at 253° C.

Experiments on the room temperature conductivity of AgBr subjected to plastic deformation also give information about the recombination rate of interstitial ions.[29] The value of γc_o is found to be 4×10^{-7} sec.$^{-1}$, which agrees remarkably well with the value extrapolated to room temperature by Eq. (C2) from the results of the specific heat measurements, 3×10^{-7} sec^{-1}.

References

1. W. Lehfeldt, Z. Phys. 85, 717 (1933).
2. C. Tubandt, Hand. der Exp. Physik XII, Part 3 (1932).
3. J. Teltow, Ann. Phys. 5, 63, 71 (1949).
4. S. Kurnick, J. Chem. Phys. 20, 218 (1952).
5. A. Lawson, Phys. Rev. 78, 185 (1950).
6. R. Christy and A. Lawson, J. Chem. Phys. 19, 517 (1951).
7. H. Kanzaki, Phys. Rev. 81, 884 (1951).
8. C. R. Berry, Phys. Rev. 82, 422 (1951).
9. P. H. Miller, Jr. and B. R. Russell, J. Appl. Phys. 23, 1163 (1952).
10. O. Stasiw, Ann. Phys. 5, 151 (1949); Z. Phys. 127, 522 (1950); 130, 39 (1951).
11. J. W. Mitchell, Phil. Mag. 40, 249, 669 (1949).

12. A. Murin and Yu. Taush, Dokl. Akad. Nauk, SSSR 80, 579 (1951).
13. A. Langer, J. Chem. Phys. 11, 11 (1943).
14. T. B. Grimley, Fundamental Mechanisms of Photographic Sensitivity, Ed. by J. W. Mitchell (Butterworths Scientific Publications, London, 1951), p. 46.
15. K. E. Zimen, reference 14, p. 53.
16. J. Teltow, Z. phys. Chem. 195, 197, 213 (1950).
17. G. Jaffé and J. A. Rider, J. Chem. Phys. 20, 1077 (1952).
18. G. Jaffé, Ann. Phys. 16, 217, 249 (1933).
19. G. Jaffé, Phys. Rev. 85, 354 (1952).
20. After most of the work in this paper had been completed, the writer learned that J. R. MacDonald at Argonne National Laboratory had developed a similar procedure for solving the same differential equations. His method of approximation is identical to the one described here, as are his results for the boundary conditions that he considers (both carriers blocked). His work is to be published in the Physical Review.
21. J. Frenkel, Kinetic Theory of Liquids (Oxford University Press, London, 1946), pp. 36-40.
22. T. B. Grimley and N. F. Mott, Disc. Faraday Soc. 1, 3 (1947).
23. H. C. Chang and G. Jaffé, J. Chem. Phys. 20, 1071 (1952).
24. J. Frenkel, reference 21, pp. 17-27.
25. A roughly similar value of $\gamma c_0 = 10\ \text{sec}^{-1}$ at room temperature (the calculations here give $\gamma c_0 = 1\ \text{sec}^{-1}$) is given in F. Seitz, Rev. Mod. Phys. 23, 328 (1951).
26. N. F. Mott and M. J. Littleton, Trans. Faraday Soc. 34, 485 (1938).
27. W. Jost, J. Chem. Phys. 1, 466 (1933).
28. T. E. Pochapsky, J. Chem. Phys. (to be published).
29. W. Johnston, private communication.

VI

THE VELOCITY OF SOUND IN WATER AS A FUNCTION OF TEMPERATURE AND PRESSURE

A. H. Smith* and A. W. Lawson
(Submitted to The Journal of Chemical Physics)

Abstract

The velocity of sound in water has been measured by an ultrasonic echo technique in the temperature range from -12°C to 129°C under hydrostatic pressures varying up to 9600 kg/cm^2. Even at the highest pressures the temperature dependence of the velocity of sound is found to be abnormal. In contradiction to certain previous results, the temperature at which the velocity of sound is a maximum is found to increase with increasing pressure. The behavior of the sound velocity is discussed in the light of recent theories concerning the structure of water. The internal consistency of the data with existing pressure standards is also analyzed.

Introduction

Recently Holton[1] has reported measurements on the velocity of sound in water as a function of pressure at two different temperatures, namely 30°C and 50°C. Holton pointed out the utility of his data in improving the accuracy of our knowledge of the thermodynamical properties of water and, in particular, by correlating his data with that of Bridgman[2] on the isothermal compressibility of water, he computed improved values for the ratio of the specific heat at constant pressure to that at constant volume.

The purpose of the present paper is to report data over a more extended range of pressure and temperature than that investigated by Holton. Although, in a general way, the results reported below agree reasonably well with those obtained by Holton, small discrepancies between the two sets of measurements are found. These discrepancies may have a significant bearing on the various theories about the structure of water. Consequently, it has been deemed desirable to report them in some detail.

The principal discrepancy under review involves the behavior of the maximum in the velocity of sound as a function of temperature as the pressure is increased. Holton concludes from his measurements that this temperature decreases with increasing pressure; the present authors conclude exactly the reverse. Our measurements indicate that the abnormal temperature dependence of the velocity of sound persists even to 10,000 atmospheres. If this be so, Eucken's[3] use of P-V-T data obtained in this pressure range for computing the behavior of "normal" water may be less justifiable than had hitherto been supposed.

Apparatus

The velocity of sound is measured by a pulse echo technique, similar to that employed by other investigators[4,5,6,7] for sound velocity determina-

* Present address: Motorola Research Laboratories, Phoenix, Arizona.

ations as well as the absorption of sound in water. This method is particularly adapted for measurements at high pressures because the experimental chamber is sufficiently small to be readily mounted in a high-pressure vessel of limited capacity. A schematic diagram of the apparatus in Fig. 1 shows the arrangement of the high pressure components together with the control and measuring units.

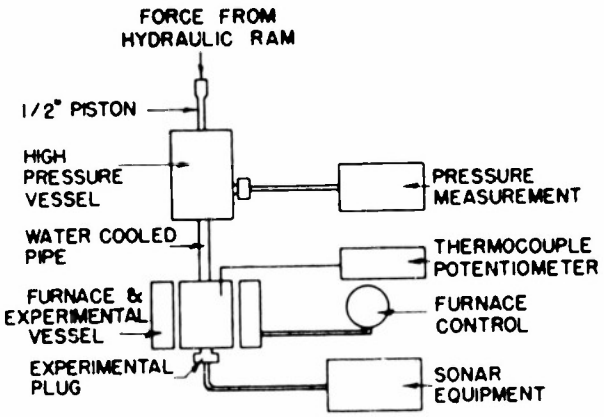

Figure 1. Schematic diagram showing arrangement of high pressure equipment, controls, and apparatus for measuring the velocity of sound.

The pressure system has been described in the literature previously.[8] It will not be described in detail here because the mode of pressure generation is immaterial to this investigation. On the other hand, measurement of the pressure is of the essence. Pressures were determined by means of a manganin resistance gauge. This gauge was calibrated by determining the resistance of the gauge at two pressures established by others as accepted standards by the careful use of free piston techniques. The standare pressures used were the freezing point of mercury as determined by Bridgman[9] (7640 kg/cm^2 at 0°C) and the freezing point of CO_2 as determined by a blocked capillary method by Michels[10] (3439 kg/cm^2 at 0°C). The pressure coefficient of resistance of the gauge was the same at both pressures, indicating a linear dependence of resistance on pressure for this particular gauge. The pressure coefficient of resistance $1/R\ dR/dP$ was found to be $2.43_8 \times 10^{-6}$ cm^2/kg. Because our determination of the CO_2 melting point was also by a blocked capillary technique, it is presumed that a comparison of our determination with that of Michels is to be preferred to a comparison with that of Bridgman, who used a technique involving a change in volume on freezing. Since the latter method gave a freezing point for CO_2 at 0°C about 1 per cent lower than that found by Michels, it is by no means clear whether the most appropriate procedure has been followed. We shall readdress ourselves to this problem below when we consider the internal consistency of the sound velocity data with the pressure calibration.

Depending on the temperature range, the temperature was varied either by a furnace or by a bath surrounding the pressure vessel. The temperature was controlled by a proportioning controlled. In view of the large heat capacity of the system, it is believed that the temperatures are known to be 0.2°C, the limit being set by the technique employed, now to be described. The temperature was measured in the wall of the high pressure

vessel at a point about 1 inch from the interior. A correction was then applied for the temperature gradient between this point and the water under study. This gradient was determined by a separate experiment. All temperatures were measured with a chromel-alumel thermocouple by means of a type K-2 Leeds and Northrup potentiometer.

The ultrasonic pulse was introduced to the water by an X-cut quartz transducer having a natural frequency of 12 megacycles. The oscillator, pulser, receiver, and detector are the same as those previously described by Lazarus,[8] and are indicated in the block diagram Fig. 2. The repetition frequency used was 1000 cycles/sec, the pulse length varied from 1 to 10 microseconds, and the peak voltage of the pulse was about 30 volts.

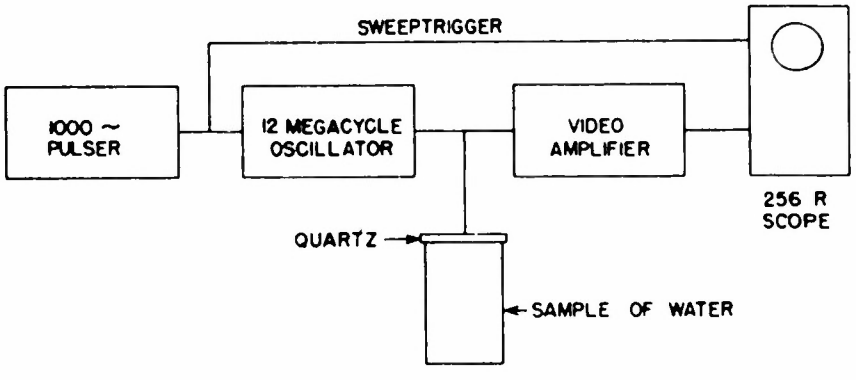

Figure 2. Schematic diagram showing arrangement of components in the apparatus for measuring the velocity of sound.

The echo chamber used is shown in Fig. 3. A principal feature in the design of this chamber is the separation of the water under study from the pressure transmitting fluid, which was silicone oil or hexane, depending on the temperature. This separation is accomplished at one end of the echo chamber by sealing the edge of the quartz transducer C with a neoprene washer. This arrangement not only affords a better acoustical match between the quartz and the water, but also eliminates back reflections from the conical reflecting surface of the space filler behind the quartz. The other end of the chamber is sealed by a sylphon bellows A which provides a reservoir of water to take up the slack arising from the compression of water in the chamber itself. These bellows are screwed on and sealed by a neoprene washer.

All surfaces coming in contact with the water are of stainless steel except for the neoprene washers and the gold-plated quartz crystal. The reflecting surface B is optically ground and polished stainless steel, flat within a wavelength of the mercury green line. Alignment is provided by the accurately machined shoulder in the echo plug against which the transducer is pressed by a spring.

Measurements

The first data obtained in this experiment were isobaric curves in which it was hoped that the shift in the maximum velocity of sound as a function of temperature with increasing pressure could be directly observed. When the temperature of the maximum velocity was observed to

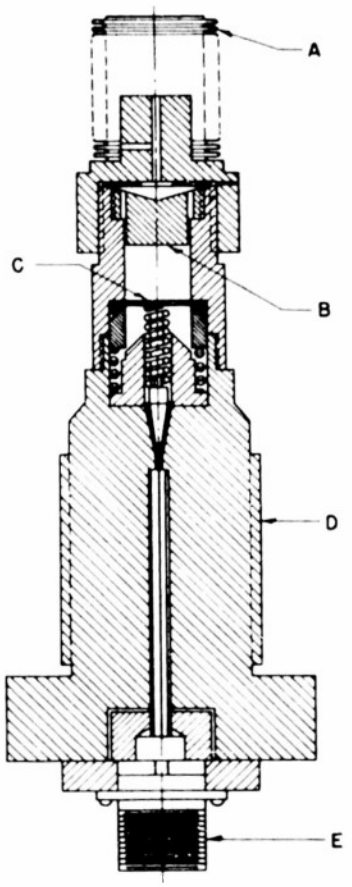

Figure 3. Design of high pressure plug showing (A) the sylphon bellows used as water reservoir; (B) highly polished stainless steel acoustic reflector; (C) the gold-plated 12 mc. quartz transducer; (D) threads for mounting plug in high pressure vessel; (E) connector for cable from oscillator.

increase with pressure and the corresponding discrepancy with Holton's data realized, it was decided to check the 30° and 50° curves isothermally. Further data was taken at other temperatures, some more complete than others, until a complete family of isobaric and isothermal curves was obtained as shown in Figs. 4 and 5. Direct plot of the present data with Holton's data (plotted points) is shown in Fig. 6. The data for these curves is given in Tables I and II with corrections for the effect of the compressibility as a function of temperature and pressure included in the velocity shown, at most a 0.2% correction.

The apparatus as designed is more suitable for making observations of changes in the velocity of sound than in making an absolute determination of this velocity at each temperature and pressure. Therefore the velocity, 1510 m/sec, at 30°C and 1 atmosphere given by Willard[11] and other investigators was used as a reference velocity from which all velocities were calculated. An absolute determination of the velocity of sound in water, using the measured length of the echo chamber (1.583 cm) and an observed time interval gave a velocity at 30°C within 0.1% of the chosen value.

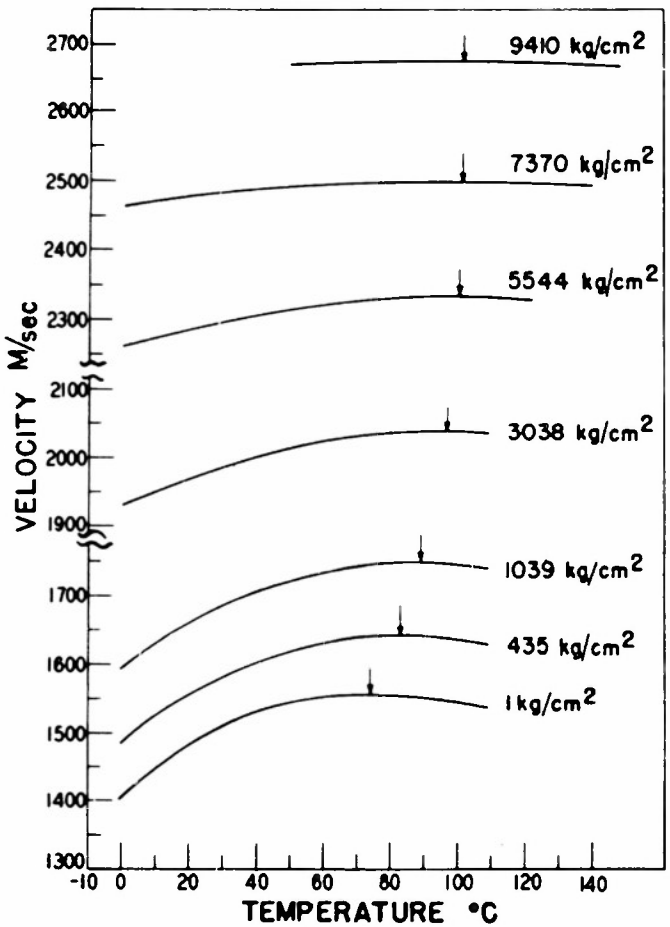

Figure 4. The velocity of sound in water as a function of temperature at different pressures.

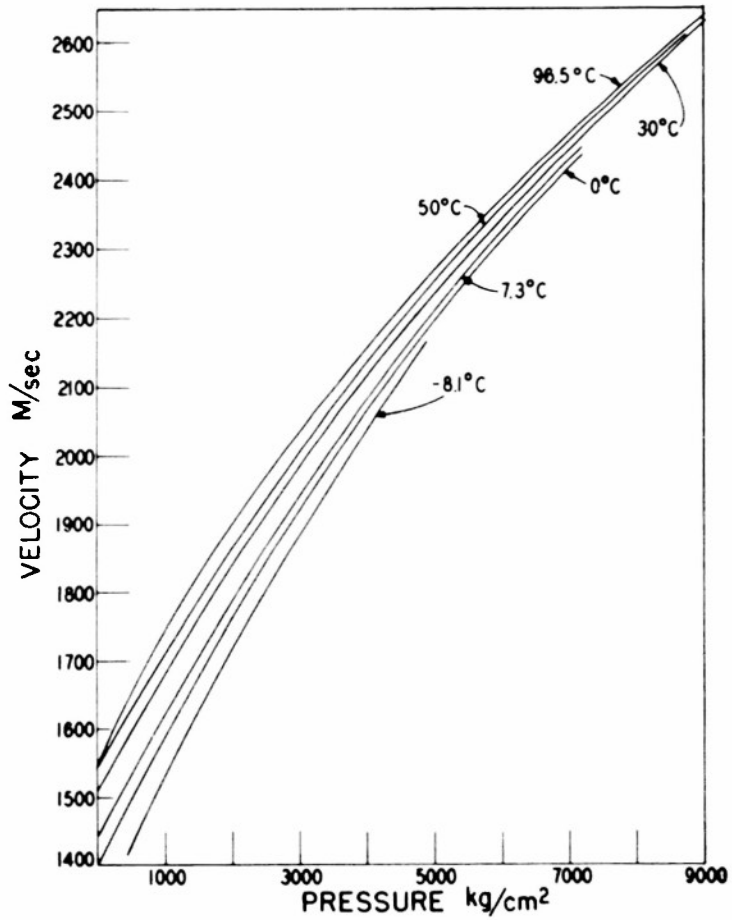

Figure 5. The velocity of sound in water as a function of pressure at different temperatures.

Table I

The Velocity of Sound in Water as a Function of Pressure Determined Isothermally at Various Temperatures

T °C	P kg/cm^2	u m/sec	T °C	P kg/cm^2	u m/sec
-12.0	3467	1954	0.0	4619	2149
-12.0	4118	2065	0.0	5122	2221
-12.0	4311	2085	0.0	5136	2210
- 8.1	1227	1576	0.0	5787	2289
- 8.1	2169	1750	0.0	6447	2363
- 8.1	3000	1889	7.3	11	1444
- 8.1	3932	2023	7.3	1107	1639
- 8.1	4861	2165	7.3	1892	1765
0.0	1	1403	7.3	3447	2006
0.0	1	1403	7.3	4672	2168
0.0	1	1402	7.3	5659	2290
0.0	36	1410	30.0	1	1510
0.0	256	1440	30.0	1989	1334
0.0	315	1468	30.0	3975	2110
0.0	474	1487	30.0	5963	2338
0.0	502	1478	50.0	1	1543
0.0	1011	1576	50.0	860	1684
0.0	1077	1565	50.0	1989	1861
0.0	1470	1666	50.0	2985	1999
0.0	1543	1675	50.0	3038	2011
0.0	1957	1744	50.0	3978	2129
0.0	2006	1761	50.0	5967	2351
0.0	2561	1848	96.5	1	1548
0.0	2562	1855	96.5	435	1638
0.0	3139	1939	96.5	1039	1747
0.0	3582	2014	96.5	5544	2328
0.0	3622	2016	96.5	7370	2506
0.0	4216	2097	96.5	9410	2678

Table II

The Velocity of Sound as a Function of Temperature as Determined Isobarically for Various Pressures

P kg/cm^2	T °C	u m/sec	P kg/cm^2	T °C	u m/sec
1	0.0	1403	1039	104.6	1744
1	22.5	1488	3038	48.8	2008
1	24.2	1494	3038	56.1	2024
1	26.6	1504	5544	0.0	2264
1	27.0	1505	5544	22.6	2290
1	27.6	1504	5544	57.4	2324
1	45.4	1539	5544	66.5	2327
1	55.1	1547	5544	76.3	2331
1	65.5	1555	5544	85.9	2335
1	74.7	1557	5544	96.1	2328
1	83.2	1557	5544	103.3	2334
1	93.8	1549	5544	103.4	2332
435	22.5	1563	7370	19.1	2485
435	57.6	1628	7370	42.8	2492
435	66.9	1637	7370	51.1	2491
435	77.0	1642	7370	63.4	2495
435	86.7	1642	7370	69.7	2495
435	96.5	1638	7370	84.0	2497
1039	26.5	1677	7370	95.6	2506
1039	44.2	1714	9410	56.5	2671
1039	55.4	1729	9410	62.4	2669
1039	63.4	1737	9410	70.2	2672
1039	70.5	1742	9410	82.7	2676
1039	75.5	1745	9410	97.4	2678
1039	80.4	1746	9410	98.4	2676
1039	88.1	1748	9410	128.9	2664
1039	96.4	1747	9410	129.0	2666

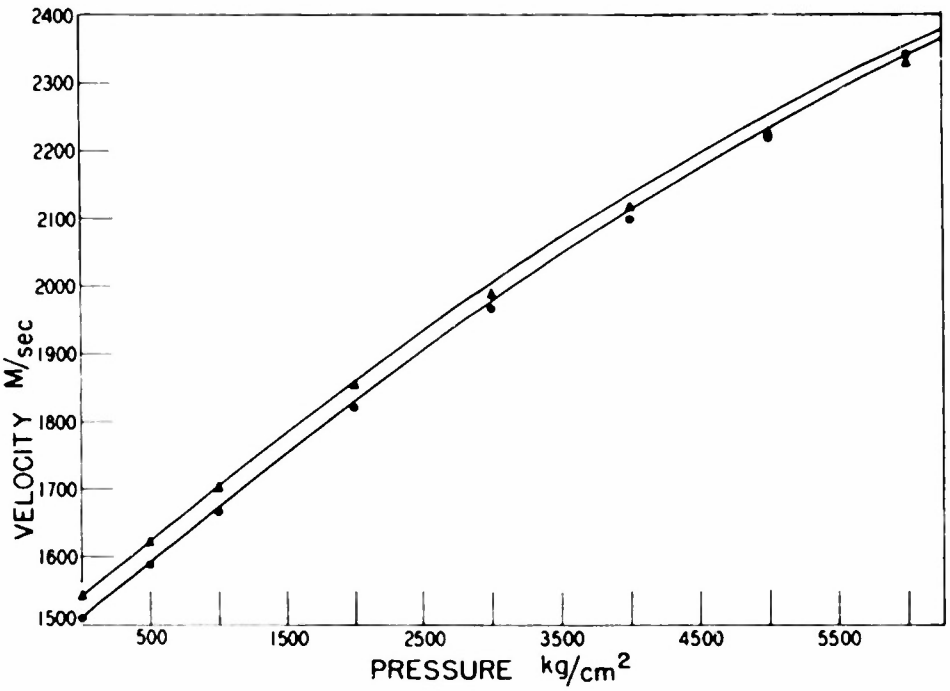

Figure 6. Comparison of Holton's results with those reported here. The solid curves are plotted from the data in Table II; the solid circles and triangles are Holton's observations at 50°C and 30°C respectively.

The water used in this experiment was double distilled water for the most part, although some readings were made with singly distilled water. No difference was observed between the sets of data. No further effort was made to remove gas from the water.

The time interval between echoes was measured by observing the first four echoes and averaging the time interval between them. The input signal was too weak for parts of the temperature-pressure range to use more than four echoes. It is estimated that the time interval could be determined to ± 0.1%. The calibration of the microsecond scale on the delay line of the 256D-A/R oscilloscope was checked against an internal crystal whose natural frequency gave 10μ second markers on the scale. The range markers were calibrated by beating against station WWV, and are accurate to 1 part in 10^5.

Results

From the reference velocity at 30°C and 1 atmosphere, the velocity calculated at 50°C and 0°C is found to be in good agreement with other investigators. Willard gives 1543 m/sec for 50°C, Randall[14] 1403 m/sec for 0°C. The only high pressure work (about 800 kg/cm^2) for comparison is that of Holton and is shown in Fig. 6.

The trend as seen from the curves in Fig. 4 is for the maximum of the velocity of sound vs temperature curve to move to higher temperature rather rapidly with initial rise in pressure, and approach a maximum displacement at about 94°C. In addition to this effect, there is a flattening out of the curve with increasing pressure. Thus the positive temperature coefficient at 30°C and 1 atmosphere (2.5 m/sec per °C) is about twice that

at 30° and 5000 kg/cm^2 (1.2 m/sec per °C). Somewhere above 9500 kg/cm^2 it would appear that the temperature coefficient becomes zero over a range from the freezing temperature to about 100°C. All isothermal curves recorded would apparently cross at this pressure if extrapolated.

Referring to Fig. 6 again, where our results are compared with those of Holton, we observe that, while the two sets of data are in excellent agreement below about 3000 kg/cm^2, above this pressure Holton's two curves begin to converge until, at 5500 kg/cm^2, they have actually crossed. Our corresponding curves on the other hand are still converging very slowly. The implication of Holton's data is that pressure has displaced the maximum in the velocity of sound to lower temperatures. However, none of our more extensive data give any indication that this conclusion is correct but rather the contrary.

Discussion of Experimental Results

It is not difficult to see why the two experiments lead to conflicting conclusions. The numerical discrepancies are small and any slight systematic error could easily account for the difference. A priori, it would be difficult to say which experiment is in error, or, in fact, if the difference did not arise from comparable errors in both experiments.

For this reason the authors have examined the information available from other sources which might indicate in which direction the velocity maximum should be shifted by pressure. Such data is available in the form of isothermal compressibilities as a function of temperature and pressure from the investigations of Bridgman,[2] of Amagat,[12] and of Smith and Keyes.[13]

The following relations are pertinent. The velocity of sound u is related to the adiabatic compressibility K_a and the density ρ by the equation

$$u = (K_a \rho)^{-\frac{1}{2}} \tag{1}$$

Thermodynamics relates the isothermal compressibility K_T to the thermal expansion coefficient α, the specific heat at constant pressure C_p, and K_a by the equation

$$K_T - K_a = \frac{TV\alpha^2}{C_p} \tag{2}$$

Manipulation of Eq. (1) and Eq. (2) in the region of the maximum of the velocity of sound leads to the following conclusions. Corresponding to the maximum in the velocity of sound, both the isothermal and adiabatic compressibilities will exhibit minima as a function of temperature. Near zero pressure it may be shown that the minimum in the isothermal compressibility must occur at a lower temperature than the minimum in the adiabatic compressibility. Furthermore, the minimum in the adiabatic compressibility must occur at a lower temperature than the maximum in the velocity of sound. As an example, using Randall's[14] data for K_T and K_a, we may compute the various temperatures under consideration. At atmospheric pressure, we compute that the minimum in K_T will occur at 45°C, the minimum in K_a at 65°C, while the maximum in the velocity of sound will occur between 70°C and 74°C.

The conclusions of the preceding paragraph should be valid up to pressures of the order of magnitude of 6000 kg/cm^2 where a cross-over occurs between curves of thermal expansion vs pressure for different temperatures. Above this pressure the minimum in K_a vs temperature will occur

for a lower temperature than that for K_T.

If we pursue the reasoning of the preceding paragraphs, it becomes clear that if we can establish that the minimum of K_T vs temperature increases with increasing pressure, then the maximum in the velocity of sound must also increase, as found by our experiments.

Referring now to the behavior of the isothermal compressibility as a function of temperature and pressure, we find unfortunately that neither of Bridgman's experiments[2] on the P-V-T relations in water have been carried out with sufficient accuracy to provide an unambiguous answer to our question.

If, however, we examine the data of Amagat on K_T, we find that his results clearly indicate an increase of the minimum in K_T vs T with increasing pressure. Accordingly, his results lend weight to our conclusion that the maximum of v vs T increases with increasing pressure. To illustrate our point, we have incorporated Amagat's data in Table III. The same conclusion is indicated by the data of Smith and Keyes, whose data are reproduced in part in Table IV.

Table III

Abbreviated Summary of Amagat's Data on the Isothermal Compressibility of Water as a Function of Temperature T and Pressure P

Pressure Range kg/cm^2	30°C	40°C	50°C	60°C	70°C
1 - 100	460	449*	449	455	462
100 - 200	436	429	425*	427	439
200 - 300	422	414	413*	415	425
300 - 400	413	407	402*	406	411
400 - 500	406	404	399	394*	398
500 - 600	392	390	390	388*	391

* Indicates minimum of K_T and illustrates how minimum shifts to higher T with increasing P. The units of K_T are in 10^{-13} dynes/cm^2.

Table IV

Abbreviated Summary of Data of Smith and Keyes on the Isothermal Compressibility of Water as a Function of Temperature and Pressure (Compressibility in Arbitrary Units).

Pressure Range in bars	0°C	20°C	40°C	60°C	80°C
0 - 350	421	415*	418	429	450
350 - 1000	-	-	332	314*	331

* Indicates minimum of K_T and illustrates how minimum shifts to higher T with increasing P. The units of K_T are in 10^{-13} dynes/cm^2.

Self-Consistency of the Sound Velocity and Pressure Measurements

One of the most unsatisfactory aspects in precision investigations at high pressures is the lack of a uniform standard in the measurement of pressure. We have already touched briefly on the discrepancy between the determinations of Bridgman[9] and Michels[10] on the freezing point of CO_2. We do not propose to enter into a discussion of the complex of factors involved in this discrepancy, e.g., difference in observational techniques, purity of sample, etc.

The purpose of this section is to call attention to the fact that the measurement of the velocity of sound in a liquid, the volume of the liquid as a function of pressure, and the pressure itself are not independent. In fact, for an imaginary fluid with no thermal expansion, the following relation between these three quantities must be valid:

$$P - P_o = \int_{V_o}^{V_p} \frac{M}{V^2} u^2 \, dV \qquad (3)$$

For an actual fluid with a finite thermal expansion, it follows from Eq. (2) that the pressure, volume, and velocity of sound in a fluid must obey the relation:

$$P - P_o = \int_{V_o}^{V_p} \frac{M}{V^2} u^2 \left(1 + \frac{MT \alpha^2 u^2}{C_P}\right)^{-1} dV \qquad (4)$$

According to the preceding equation, if the volume of a fluid at some unknown pressure is ascertained, and the velocity of sound at the same pressure is determined, the pressure may then be calculated if rather crude values for the thermal expansion coefficient and the specific heat are available. The latter quantities need not be known very well because they represent a correction of from 3% to 6%. As a result of the integration the effect of an 8% error in α or C_p on P is reduced to about 0.2%.

We are invited, therefore, to calculate the pressure from known P-V-T data and the velocity of sound from Eq. (4) and to compare the result with that determined by the manganin gauge using available pressure standards established by a free piston technique.

In making such a comparison, owing to various discrepancies in the experimental literature, several procedures are possible. The possibilities are denumerated according to whether we use

(1) Bridgman's P-V-T data of 1912;
(2) Bridgman's P-V-T data of 1935;
(3) Holton's data on the velocity of sound;
(4) The present data on the velocity of sound;
(5) Bridman's determination of the freezing point of CO_2;
(6) Michels' determination of the freezing point of CO_2.

Tables V and VI show the results of a number of the possible permuted comparisons. It is difficult to draw a clean-cut conclusion from these calculations, but they may be summarized as follows. On the whole, both Holton's results and ours are in better agreement with Bridgman's P-V-T data of 1935 than those of 1912—this statement being particularly appropriate to the 1912 data at 30°C. Regardless of which set of data on the velocity of sound is employed in the calculation, the deviations between the pressures determined by the free piston technique and that calculated from the velocity of sound seldom exceed 2%—a remarkable result considering the

Table V

Calculation of Pressure from Eq. (4)*

P (kg/cm^2)	V (cc/gm)	T (°K)	u (m/sec) Holton	u (m/sec) Authors	P from Eq. (4) kg/cm^2 Holton	P from Eq. (4) kg/cm^2 Authors
			Based on Bridgman's H_2O Data of 1935			
1	1.0046	303	1510	1510	1	1
500	.9845	"	1588	1593	490	492
1000	.9665	"	1667	1676	989	992
2000	.9368	"	1822	1833	1978	1992
3000	.9127	"	1968	1981	2969	2995
4000	.8925	"	2100	2113	3967	4003
5000	.8754	"	2222	2234	4954	5002
6000	.8603	"	2344	2341	5955	6007
1	1.0120	323	1543	1543	1	1
500	.9916	"	1623	1623	500	500
1000	.9744	"	1703	1704	981	981
2000	.9450	"	1856	1858	1965	1966
3000	.9207	"	1990	2004	2962	2972
4000	.9005	"	2118	2135	3944	3973
5000	.8835	"	2227	2252	4906	4952
6000	.8684	"	2334	2356	5877	5946
			Based on Bridgman's H_2O Data of 1912			
1	1.0041	303	1510	1510	1	1
500	.9837	"	1588	1593	498	500
1000	.9663	"	1667	1676	982	987
2000	.9364	"	1822	1833	1978	1994
3000	.9105	"	1968	1981	3046	3075
4000	.8897	"	2100	2113	4077	4119
5000	.8719	"	2222	2234	5089	5165
6000	.8554	"	2344	2341	6203	6262
1	1.0118	323	1543	1543	1	1
500	.9916	"	1623	1623	496	496
1000	.9743	"	1703	1704	980	980
2000	.9445	"	1856	1858	1978	1980
3000	.9205	"	1990	2004	2965	2973
4000	.8996	"	2118	2135	3987	4008
5000	.8818	"	2227	2252	4998	5037
6000	.8662	"	2334	2356	6007	6065

* Based on calibration of manganin resistance gauge using Bridgman's freezing point of Hg at 0°C and Michels' freezing point of CO_2 at 0°C.

Table VI

Dependence of Calculations in Table V on Gauge Constant† at 30°C.

		Gauge constant* $= 2.410 \times 10^{-6}\ (kg/cm^2)^{-1}$		Gauge constant** $= 2.438 \times 10^{-6}\ (kg/cm^2)^{-1}$	
P (kg/cm^2)	V (cc/gm)	u (m/sec)	Integral	u (m/sec)	Integral
1	1.0046	1510	1	1510	1
500	.9845	1594	492	1593	492
1000	.9665	1678	997	1676	992
2000	.9368	1837	1999	1833	1992
3000	.9127	1986	3007	1981	2995

† Pressure determined assuming gauge resistance varies as $R_p = R_0 (1 + \alpha P)$.

* Based on Bridgman's freezing point of CO_2 3400 kg/cm^2 at 0°C.

** Based on Michels' freezing point of CO_2 3439 kg/cm^2 at 0°C.

lapse of years and the varied sources of the experimental data.

Table VI shows that the rough generalities drawn above are somewhat sensitive to the pressure standards used in the calibration of the resistance gauge. Table V is based on the use of the freezing point of mercury at 0°C as determined by Bridgman, and the freezing point of CO_2 as determined by Michels. If, on the other hand, we confine our comparison to pressures below 3000 atmospheres, we find that the consistency of the pressure data with ours is improved at 30°C by using Bridgman's data on the freezing point of CO_2. The arguments evoked in the selection between the two comparisons are so involved that we do not believe they may be resolved by our data. The suspicion is generated nevertheless that our absolute pressure standards are uncertain to about $\frac{1}{2}$% in the range below 10,000 atmospheres.

Comparison of Theory and Experiment

Although the differences between the results of Holton and ours seem minuscule from an experimental point of view, they have been emphasized because of their apparent importance in discriminating among the various theories of the structure of water. All of these theories incorporate as a basic postulate the concept that a considerable memory of the ice structure is retained in the liquid phase. Perhaps the first significant modern effort to interpret the properties of water was that of Bernal and Fowler,[15] who treated the water as a mixture of two types of H_2O complexes. One type of complex was considered to assume a quartz-like type of arrangement (normal water), while the other type was assumed to have a trydimite type of arrangement as in ice. To explain qualitatively the behavior of water near the ice point, Bernal and Fowler found it necessary to assume that approximately 70% of the molecules were ice-like even near the boiling point. Subsequent investigations of the structure of water using X-ray diffraction patterns indicated that this model was over-simplified and that the molecular rearrangements in the liquid state were more subtle. In par-

ticular, the investigations of Morgan and Warren,[16] and also of Katzhoff,[17] indicated that as the temperature was increased the major change in the structure could be ascribed to an increase in the number of neighbors in the successive shells of molecules surrounding any given molecular center. In an effort to circumvent this objection, Euken[3] in a series of papers addressed himself to a somewhat different approach. He depicted water as composed of a mixture of polymers and considered the equilibrium between a system composed of monomers, dimers, quadrimers, and octomers. He then assumed the P-V-T data at 10,000 atmospheres to reflect the behavior of normal water. By empirically fitting an equation of state to this data, he predicted the behavior of normal water under atmospheric conditions. By differences between the observed and predicted values of the volume of water as a function of pressure, he deduced the number of abnormal molecules (octomers) as a function of temperature and by a rather elaborate structure was able to correlate this dependence with that of the specific heat and other physical properties. For the sake of completeness, we add that recently Gierer and Wirtz[18] have attempted to reconcile Eucken's theory with that of Bernal and Fowler.

If our experimental results be accepted at face value, it would seem that Eucken's assumption that water is behaving normally at 10,000 atmospheres is somewhat dangerous. Although the isothermal compressibility appears to be behaving in a normal fashion, the velocity of sound does not. A re-examination of these early theories, therefore, appears to be in order.

We digress temporarily to discuss a theory by Hall[19] which was developed to explain the anamolous absorption of sound in water. Hall assumes that a water molecule can exist in two states differing in free energy by an amount F. The molal volume V of water is then assumed to be given by

$$V = V_n (1 - x_a) + V_a x_a = V_n + \Delta V x_a \qquad (5)$$

where V_n is the molal volume of normal water, V_a the molal volume of abnormal water, x_n and x_a the corresponding concentrations of the two states assumed to be related by the simplest possible interaction, namely:

$$\frac{x_n}{x_a} = e^{-\Delta F/RT}. \qquad (6)$$

It is now possible conceptually to separate the compressibility K of water into two components: the compressibility at infinite frequency K_∞ plus a structural component K_s, which is easily deduced to be given by the following expression

$$K_s = K - K_\infty = + \frac{(\Delta V)^2}{2RTV\left[1 + \cosh \frac{\Delta F}{RT}\right]} \qquad (7)$$

Estimates of K_∞ may be made from the compressibility of ice and calculations from known intermolecular potential functions. The estimates for K_∞ range between 12 and 24 x 10^{-12} cm^2/dyne. Hall was able to obtain satisfactory agreement with sound absorption measurements by choosing K_∞ to be 18 x 10^{-12} cm^2/dyne, ΔV equal to -8.4 cm^3, and ΔF equal to 500 cal/mole.

We shall now investigate whether Hall's estimates of these quantities also give reasonable values for the compressibility, thermal expansion, and specific heat, and compare the resulting estimates with those obtained by Eucken.

We shall begin our analysis by commenting that the consistent application of thermodynamics to the Hall model leads to the conclusion that in addition to the structural compressibility K_s given by Eq. (7) concomitant structural effects also occur in the thermal expansion coefficient and the specific heat. These quantities are not completely independent, but are related by the following relations, regardless of the validity of Eq. (6):

$$\frac{T(\Delta V)^2 c_s}{V K_s} = (\Delta H)^2 \tag{8}$$

and

$$\alpha_s = c_s \Delta V / V \Delta H \tag{9}$$

where c_s is the structural contribution to the specific heat, α_s is the structural contribution to the thermal expansion coefficient, and ΔH is the difference in enthalpy between normal and abnormal water molecules.

Referring all our calculations for the moment to 0°C, we find from Eq. (7) by assuming ΔF is zero that the minimum value of ΔV is 8.0 cm^3/mole if we use a value for $K_\infty = 12 \times 10^{-12}$ cm^2/dyne. This value for ΔV compares favorably with the value of 8.4 cm^3/mole assumed by Hall and is consistent with the difference between the observed density of water and that which it would acquire if water had the same structure as ice.

If the structure of water were completely ice-like, Pople[20] has estimated that its volume would differ from that of water at 0°C by 0.22 cm^3/gm, a difference which must be accounted for by the transition from abnormal molecules to a normal state. In accordance with this reasoning, assuming Eq. (6) is correct, we deduce that at 0°C the fraction of normal molecules is 50%, a number intermediate to the predictions of Bernal and Fowler on the one hand and Eucken on the other.

Using the value of ΔV equal to 8.0 cm^3/mole deduced above, and Eucken's estimate of 8.5 cal/mole for c_s, we find from Eq. (8) that we must take ΔH equal to 2600 cal/mole to be consistent. This value for ΔH falls within the range of the values assumed by Eucken for the dissociation of the various polymers in his model.

Using the value of ΔH deduced from Eq. (8), we now calculate from Eq. (9) that the consistent value of α_s at 0°C is 14.6 10^{-4}/°C. This value for α_s is eminently reasonable since the average expansion coefficient for methyl alcohol between 0°C and 100°C is about + 12 x 10^{-4}/°C and that for water at 0°C is - 1.0 x 10^{-4}/°C.

Using Eq. (6) again, from the value of x_n at 0°C, we calculate that the value of x_n at 100°C should be 78. Thus, the increase of the normal component between the freezing and boiling points of water is 28%. If we take our value of 2600 cal/mole for ΔH, this implies an excess increase of the enthalpy of water between these two temperatures of 730 cal/mole. The value estimated by Eucken is approximately 785 cal/mole.

It is not difficult to verify from the above data that the minimum in the thermal expansion coefficient must occur in the neighborhood of 0°C. Thus, it must be concluded that the rather crude model used by Hall is in essential agreement with many of the thermodynamic properties of water.

Nevertheless, Hall's theory is subject to the following criticisms. Hall concluded that the difference between the two states assumed in his model was the breaking of a hydrogen bond. If so, the validity of Eq. (6) is open to question. Secondly, the value of ΔH found here is too small to account for the properties of water on this physical model. The heat of evaporation

of ice, for instance, implies that the energy to break a hydrogen bond is at least twice the value of ΔH used here.

This dilemma may be resolved, perhaps, by considering the point of view of Pople[20, 21] and Lennard-Jones.[21] According to their viewpoint the explanation of the anomalies in the behavior of water lies not in the breaking of bonds but in their flexibility. Thus, ΔH should not necessarily be considered as the energy required to break a hydrogen bond but probably as the energy required to bend one. Pople's theory seems to be consistent with the X-ray diffraction data.

Another insufficiency in Hall's model is its failure to describe satisfactorily the molal volume on data at higher pressures. Bridgman's P-V-T data indicate that this quantity goes through a minumum at successively lower temperatures as the pressure is raised and then at even lower temperatures through a maximum. These features are qualitatively described well by the equations given above. Quantitatively, however, the difference in molal volume between the maximum and minimum decreases rapidly with increasing pressure. In the theory this quantity is constant since the variations of ΔV and ΔS with temperature and pressure have been neglected. The theory requires considerable refinement before the fine experimental details can be adequately described.

We revert now to a comparison of the Hall theory with that of Eucken. According to Eq. (7) the structural bulk modulus should decrease somewhat more rapidly than the absolute temperature as the latter is decreased. The behavior of the abnormal adiabatic compressibility, as predicted by Eq. (7), is shown in Fig. 7, where it is compared with that predicted by Eucken. As may be seen, the discrepancy is rather large. Although our measurements seem to support Hall's model, clearly more measurements and analysis are needed to select the preferable theory.

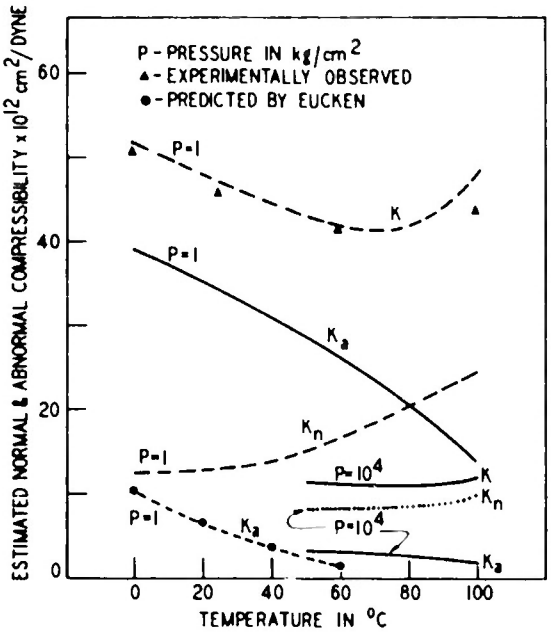

Figure 7. Estimated contributions of the structural and normal components of the adiabatic compressibility of water.

In conclusion, it should be noted that the arguments given above are not particularly sensitive to the form of Eq. (6) because $\Delta F/RT$ is relatively small.

Acknowledgment

It is a pleasure to acknowledge the partial support granted to this investigation by the Office of Naval Research.

References

1. G. Holton, J. Appl. Phys. 22, 1407 (1951).
2. P. W. Bridgman, Proc. Am. Acad. Arts Sci. 48, 309 (1912); J. Chem. Phys. 3, 597 (1935).
3. A. Eucken, Nachr. Wiss. Göttingen 1, 36 (1946); Z. Electrochemie 52, 255 (1948); Z. Electrochemie 53, 102 (1949).
4. R. Pelham and J. Gault, J. Chem. Phys. 14, 608 (1946).
5. A. Weissler and V. del Grosso, J. Acoust. Soc. Am. 23, 221 (1951).
6. J. M. M. Pinkerton, Nature 160, 128 (1947).
7. P. Rosenberg, Radiation Laboratory (M.I.T.) Report #56, 1946.
8. D. Lazarus, Phys. Rev. 76, 545 (1949).
9. P. W. Bridgman, Physics of High Pressures (Bell & Sons, London, 1931).
10. A. Michels, Physica 9, 565 (1942).
11. G. W. Willard, J. Acoust. Soc. Am. 19, 235 (1947).
12. E. Amagat, Ann. Chim. Phys. 29, 68 and 505 (1893).
13. L. Smith and R. Keyes, Proc. Am. Acad. Arts Sci. 69, 285 (1934).
14. C. R. Randall, Bur. Standards J. of Research 8, 94 (1932).
15. J. D. Bernal and R. H. Fowler, J. Chem. Phys 1, 515 (1933).
16. J. Morgan and B. E. Warren, J. Chem. Phys. 6, 666 (1935).
17. S. Katzhoff, J. Chem. Phys. 2, 841 (1934).
18. A. Gierer and K. Wirtz, Z. Naturforschung 5, 577 (1950).
19. L. Hall, Phys. Rev. 73, 775 (1948).
20. J. A. Pople, Proc. Royal Soc. A205, 163 (1951).
21. Sir J. Lennard-Jones and J. A. Pople, Proc. Royal Soc. A205, 155 (1951).

XII

CREEP OF SILVER BROMIDE AT HIGH TEMPERATURE

R. W. Christy
(Submitted to Acta Metallurgica)

Abstract

The transient and steady-state creep rate of single crystal and polycrystalline specimens of AgBr, stressed in compression from 6 to 150 g/mm^2, has been investigated between 300° and 410°C, with the emphasis on the steady-state creep of single crystals. The effects on the creep rate of orientation, of hydrostatic confining pressure, and of impurities were studied. Single crystals deformed by slip, though with rather weak conditions on possible slip systems. The steady-state results were reproducible to within about 15%. At higher stresses, for crystals with axis in the [001] direction, the steady-state creep rate was fit to the empirical formula $\dot{\epsilon} = C \exp\{-Q/RT\} \exp\{B\sigma^{1/2}/RT\}$, with $C = 2.8\times10^{17}$ min^{-1}, $Q = 69.1$ kg-cal/mol, $B = 1.21$ (kg-cal/mol)/$(g/mm^2)^{1/2}$, σ = compressive stress. For [111] crystals, σ can be replaced by $3/4\,\sigma$; for other orientations the rates were intermediate. At lower stresses the rate decreased more sharply with decreasing stress. The steady-state rate was depressed strongly by high pressure, by the factor $\exp\{-p\,\Delta V/RT\}$, with $\Delta V = 38 \pm 3$ cm^3/mol. The effect of impurities in concentrations of about 10^{-3} was in general to decrease the creep rate, S^{--} being more effective than Cd^{++} or Cl^- in this respect. Mott's theory of diffusion-limited creep appears to give a satisfactory interpretation of the temperature, stress, and pressure dependence of the steady-state rate for pure crystals.

I. Introduction

A correlation between the activation energies for steady-state creep of metal crystals and for self-diffusion has often been suggested. Nabarro[1] has shown how plastic deformation can occur without slip by the diffusion of lattice defects. If a surface where vacancies can form is subjected to a compressive force, at this surface the equilibrium vacancy concentration will be decreased. Under the concentration gradient thus established, vacancies will flow to the surface, resulting in a removal of matter from it. Nabarro's formula for the steady-state strain rate is

$$\dot{\epsilon} = (8\sqrt{2}/d^2)(\sigma a^3/kT)\,D, \tag{1}$$

where σ is the compressive stress, a the lattice spacing, D the coefficient of self-diffusion, and d the dimension of the volume in which there are no sources or sinks of vacancies. This mechanism of course cannot account for the crystallographic features of deformation associated with slip.

Mott[2] has suggested low a dislocation mechanism for creep could be diffusion limited. Dislocations, emitted by a course, pile up on their slip plane behind fixed obstacles. At elevated temperatures the dislocations climb out of the slip plane, allowing further emission by the course. The movement of an edge dislocation one atomic distance normal to the slip plane is accomplished by the addition (or removal) of a line of atoms, i.e.

by the diffusion of vacancies from (or to) the dislocation. Mott's formula for the velocity of migration perpendicular to the slip plane for an edge dislocation is

$$(fa^4 F/kT)(j/a)\ \exp\{-W/kT\},$$

where f is the atomic vibrational frequency, F the force per unit length on the dislocation, j/a the number of jogs per unit length in the dislocation, and W the activation energy for self-diffusion.

Since the plastic behavior of ionic crystals at room temperature[3] is similar in many respects to that of metal crystals, measurement of the creep rate of an ionic crystal at elevated temperature should provide an interesting test of these ideas. In ionic crystals, the transport of ion pairs will be limited by the more slowly diffusing ion, and it is with the diffusion coefficient for this ion that a correlation of the creep rate could be expected.

The plasticity of AgBr at room temperature is comparable with that of soft metals, the critical shear stress being about 100 g/mm^2.[4] The lattice defects are predominatly cation Frenkel defects.[5,6] Thus the diffusion of AgBr ion pairs must be limited by the number of Schottky defects and the mobility of the Br^- vacancy, if it is assumed on energetic grounds that the number of interstitial Br^- ions is negligible. The number and mobility of Br^- vacancies is in some doubt. A transport experiment at 406°C shows that any Br^- current is less than 0.3% of the total current.[6] A value of 2.9×10^{-11} cm^2/sec at 300°C has been determined[7] for the self-diffusion coefficient of radioactive Br, compared to 1.02×10^{-7} cm^2/sec for Ag. The activation energy for Br is therefore probably appreciably greater than that for Ag.

In the present experiments, measurements have been made of the transient and steady-state creep rates of single crystal and polycrystalline specimens of AgBr, stressed in compression from 6 to 150 g/mm^2 at temperatures from 300° to 410°C. (The melting point of AgBr is 422°C.) The effects of hydrostatic confining pressure and of impurities on the creep rate were observed.

II. Experimental Apparatus

The apparatus for measuring creep in compression at high temperature and atmospheric pressure is illustrated schematically in Fig. 1. The AgBr sample rests between two polished quartz discs, on a stainless steel plug screwed into the bottom of a stainless steel tube. The quartz discs provide a smooth, inert surface bearing on the sample, reduce heat flow from the sample, and eliminate thermoelectric currents. The load is applied to the sample by a stainless steel ram, whose upper end deflects a dial gauge graduated to 0.0001". The ram is made of a half-inch tube with 1/32" wall, in order to reduce the heat leak up the ram and to permit the application of small loads. It is rigid enough that the creep of the apparatus, with no specimen, is negligible under the conditions of the experiments. The ram assembly weighs 203 g, and it is loaded at the top with B-B's (weight about 0.3 g) so that the load is nearly continuously variable. The load must be corrected for the spring constant and the friction of the dial gauge. The tube is surrounded by a furnace, whose temperature is held constant to within about 0.5°C by a proportioning controller.[8] The temperature is measured by a chromel-alumel thermocouple about 1/16" from the specimen. It is necessary to direct a fan on the upper end of the apparatus in order to overcome spurious gauge deflections caused by the cooling effect

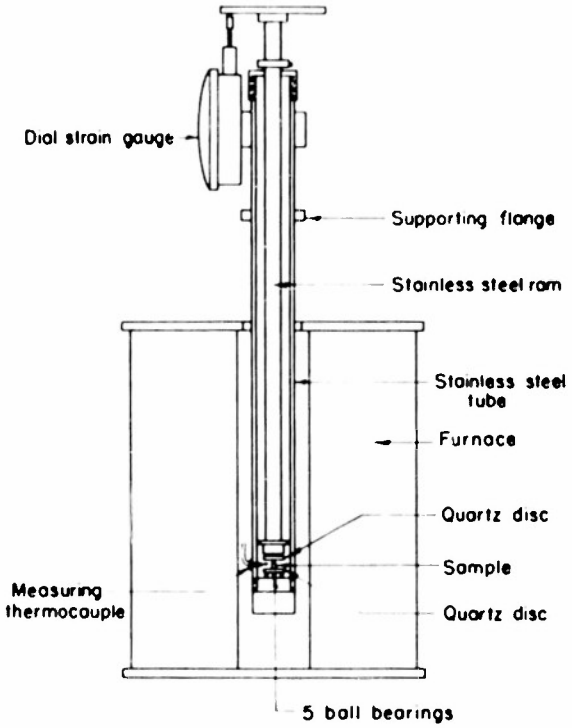

Fig. 1. Apparatus for measuring creep under compression at high temperature.

of random air currents.

Two types of loading were possible. Since the AgBr specimen sticks firmly to the quartz discs at high temperature, if the latter are constrained against lateral motion the specimen axis must remain vertical. This constraint can be removed by setting the lower quartz platen on five freely rolling ball bearings. (These were 'soldered' in place during assembly with naphthalene, which then evaporates when the apparatus is heated.)

The device for measuring creep at high pressure was designed to fit inside the working space of a high pressure bomb.[6] The sample sat on the bottom of a steel can with a tight fitting lid, shown in Fig. 2, with a lead-

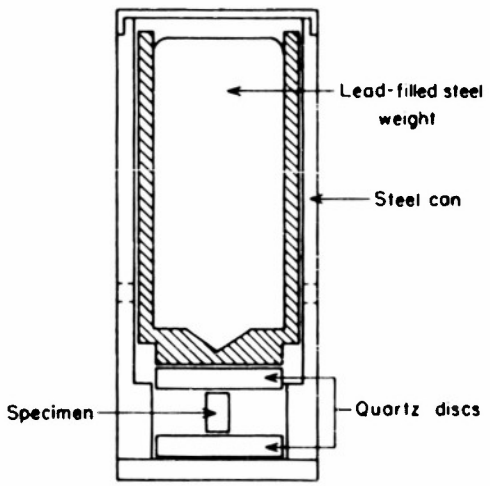

Fig. 2. Device for loading specimen in a high pressure bomb.

filled steel weight resting on it. Holes in the side of the can admitted the pressure fluid (DC 200 3-centistoke silicone oil), so that a surge while pumping on the oil would not smash down the weight on the specimen. Because the arrangement did not permit strain measurements during the experiment (the working space in the bomb is limited), the specimen was measured with micrometer calipers before and after the deformation. Further, the load was applied to the specimen while the bomb was being heated to the temperature of the experiment, but conditions were arranged so as to minimize the contribution to the strain during this period. The weight weighed 243 g in air; although the stresses were calculated for the bouyancy of the pressure fluid at room temperature and pressure, the failure of thermal expansion to compensate for compressibility is a second order correction.

III. Preparation of Specimens

The AgBr used was precipitated in red light from Mallinckrodt HBr and $AgNO_3$. A qualitative spectrographic analysis indicated about 0.001% of Fe, Mg, and Cu, and less than measurable amounts of Cd, Pb, Sr, Ca, Zn, Ba, Ni, Mn, Sn, Be, and Si present as impurities. Less than 0.0002% sulfur is assumed to have been present, since the addition of about this amount caused a noticeable change in color and in the rate of photolytic darkening of the AgBr. Since the crystals were grown in air, they were presumably saturated with oxygen.

Polycrystalline samples were made by pouring molten salt into a steel die and then pressing under about 30 tons. The single crystal specimens were sawed from single crystal rods grown by the Czochralski method, a continuous withdrawal from the melt, at 2 in/hr. The specimens were machined into cylinders, from 5 to 8 mm in height and from 2.3 to 5 mm in diameter, with ratios of height to diameter of 0.9 to 2.6, usually about 2. After machining, about 0.001" was removed from the surface with sodium thiosulfate solution. After this treatment no recrystallization of the single crystal specimens ever occurred. The specimens were measured and washed before the experiment. Orientation determinations of the cylinder axis of the specimen were made to within about 30' by back reflection x-ray photographs. No attempt was made to handle the crystals in the dark, since photolytic darkening was slight and disappeared at the temperature of the experiments.

IV. Experimental Results

1. Single Crystal Specimens

A. Time Dependence of Creep. The strain during the course of a creep experiment at constant stress is commonly divided into three stages: a sudden deformation immediately on application of the load, a transient phase, in which the strain is in many cases proportional to the cube root of the time according to the Andrade law, and finally a steady-state in which the creep rate remains constant. With the present apparatus the sudden compression cannot be measured. After application of the load the strain shows the transient and steady phases. At 300°C the transient state lasts a long time (more than 100 hr), but near 400°C it can be quickly exhausted (about 1/2 hr). The strain during the transient phase is large at high stress and small at low stress. It is less for crystals with axis near the [111] direction than for those near [001]. The transient phase, however, is not always described by the Andrade law. In fact, the slope, and even the shape,

of the strain-time curve during the transient stage is very sensitive to factors beside temperature, stress, and orientation, including previous thermal and mechanical history and purity. The influence of impurities will be described later. In Fig. 3 is shown the effect of 2-1/2% compression at

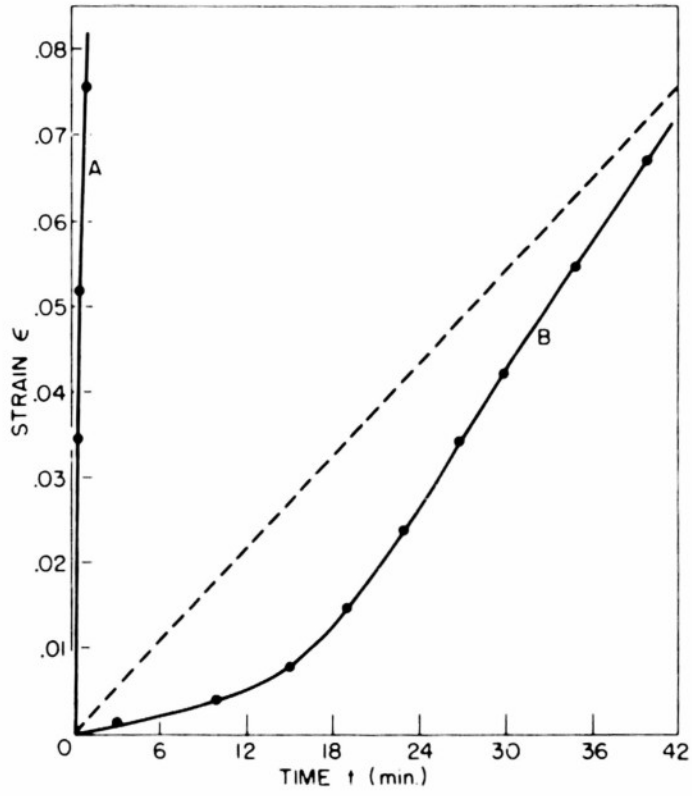

Fig. 3. Transient creep of an annealed (A) and a cold-worked (B) specimen.

room temperature before the run at 370°C (curve B), compared with the behavior of an annealed sample (curve A) and the steady-state rate (dashed line). On the other hand, the steady-state rate is insensitive to these factors, and the emphasis of the experiments has been put on it.

After the steady-state is reached, it continues up to a total strain of 10 to 15%, provided the stress is kept approximately constant by an empirical correction to the load to compensate the increase in the diameter of the sample. (This correction never amounts to more than about 5%.) After about this amount of strain the creep rate usually falls off, probably because of the geometrical distortion of the specimen, since if it is then remachined into a cylinder the original creep rate is restored, without the reappearance of a large transient.

During the steady-state, if the stress is changed suddenly there is then a new transient phase during which the rate is greater or less than the new steady-state rate according as the stress was increased or decreased. If on the other hand the temperature is changed no new transient phase is detectable, provided the change is not so fast as to cause thermal stressing nor so slow as to allow, if the load is removed, annealing. The time required for the creep rate to reach equilibrium after changing the temperature is less than the time required for the apparatus to reach temperature

equilibrium (about an hour) and is therefore not observable.

The steady-state rate is reproducible to about 15% in a single sample after observing the rate at other temperatures and returning to the original temperature, or among different samples if the height to diameter ratio is between 1.3 and 2.6. For smaller ratios the rate was about 30% low, presumably because of inhibition of slip near the platens. There was no dependence on size, within the limits used.

B. Temperature and Stress Dependence. The reproducibility of the steady-state creep rate among different samples is sufficient to permit measurement of its dependence on temperature and stress over rather large ranges. The stress range which could be investigated was limited at the lower end by the design of the apparatus and at the upper end by the large transient strain produced by high stress. In fact, in samples with the axis near the [001] direction at stresses above 60 g/mm^2 the transient strain was often so large that it was necessary to remachine the sample before the steady-state could be observed. The procedure was in general first to get the steady-state value at the highest temperature, at which the transient component was most quickly exhausted, then take the lower temperature points in arbitrary order, and finally repeat the highest temperature. This procedure was adopted, in preference to the alternative of varying the stress at constant temperature, in order to minimize the transient strain during a run. Data will be presented for [001] and [111] samples; for other orientations the creep rates were intermediate.

The logarithm of the creep rate is plotted versus inverse temperature in Figs. 4 and 5, for these two orientations, at different stresses. In these figures an exponential temperature dependence is apparent. In order to exhibit a stress dependence from the same data, the best straight line was drawn by eye through the points of Figs. 4 and 5 for each constant stress, and the ordinates for three fixed temperatures were plotted as a function of stress in Figs. 6 and 7. If the data of Fig. 4 are plotted versus the compressive stress, σ , the points show a tendency which indicates that a linear representation could be improved upon. In Figs. 6 and 7 the data of Figs. 4 and 5 are plotted versus the square root of the stress. In these figures the linear representation appears to be adequate in the region of high stress, with no simple function suggested over the whole range. In fact, the function

$$\dot{\epsilon} = C \exp\left\{-(Q - B\bar{\sigma}^{1/2})/RT\right\}, \tag{3}$$

with

$$C = 2.8\times10^{17}\ \text{min}^{-1}$$

$$Q = 69.1\ \text{kg-cal/mol}$$

$$B = 1.21\ (\text{kg-cal/mol})/(\text{g/mm}^2)^{1/2}$$

$$\bar{\sigma} = \begin{cases} \sigma & \text{for [001] crystals} \\ 3/4\,\sigma & \text{for [111] crystals,} \end{cases}$$

represents, within the experimental reproducibility, all the data in the range $\bar{\sigma}$ greater than about 40 g/mm^2. This function is plotted by the full lines in Figs. 4-7; the dashed lines are added to connect the data at smaller values of $\bar{\sigma}$. In the case of [001] crystals at 30 g/mm^2, two classes of results were obtained, presumably because of small uncontrolled differences in orientation and loading, and with 15 g/mm^2 the results were not very reproducible.

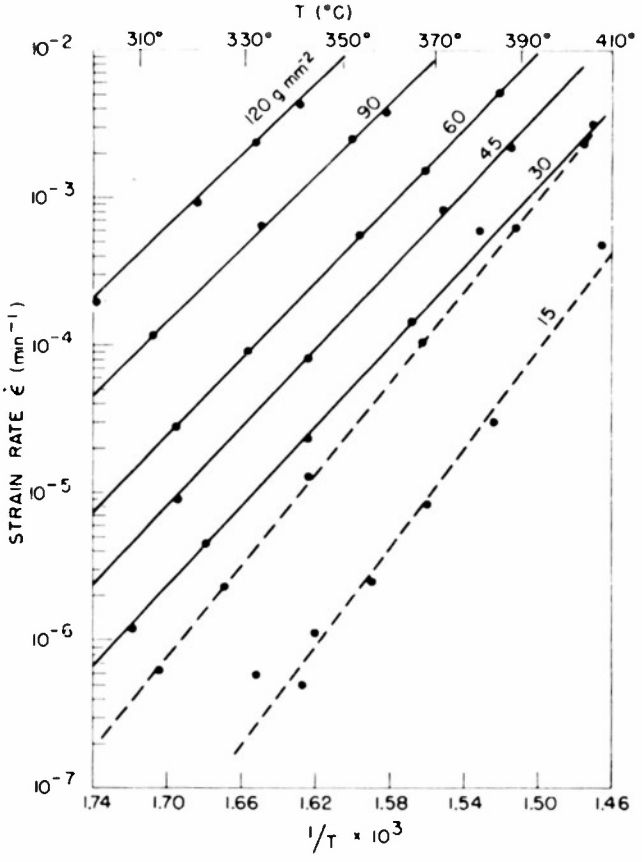

Fig. 4. Steady-state creep rate of [001] specimens.

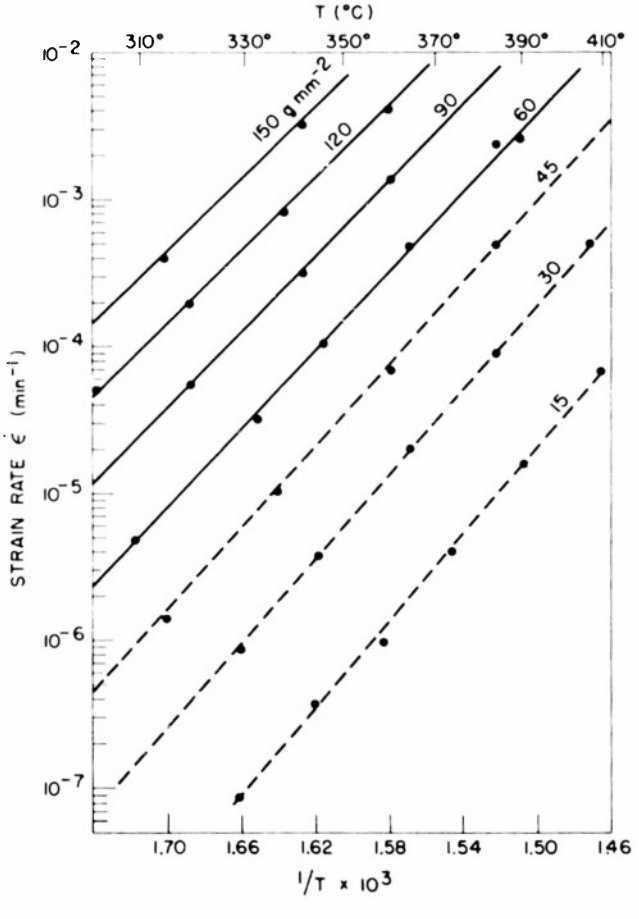

Fig. 5. Steady-state creep rate of [111] specimens.

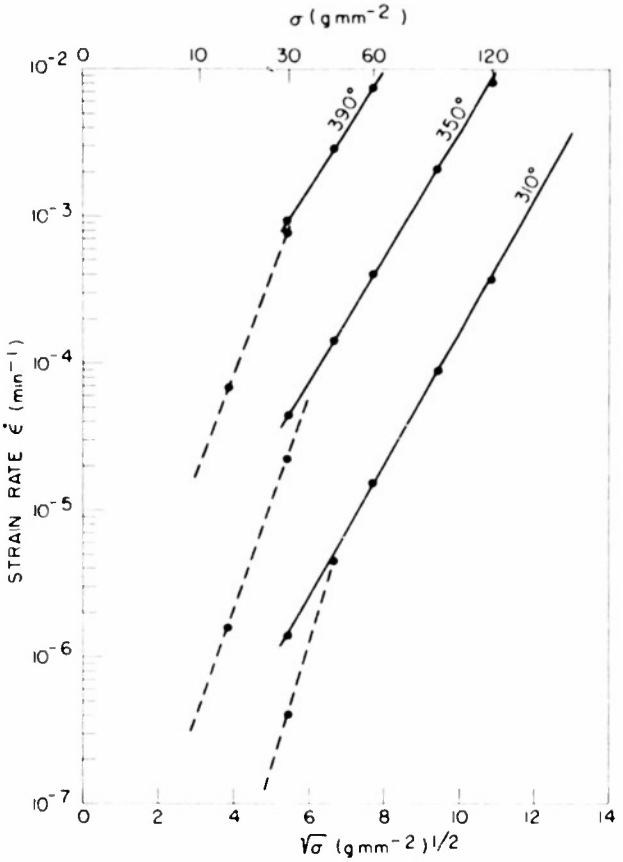

Fig. 6. Steady-state creep rate of [001] specimens.

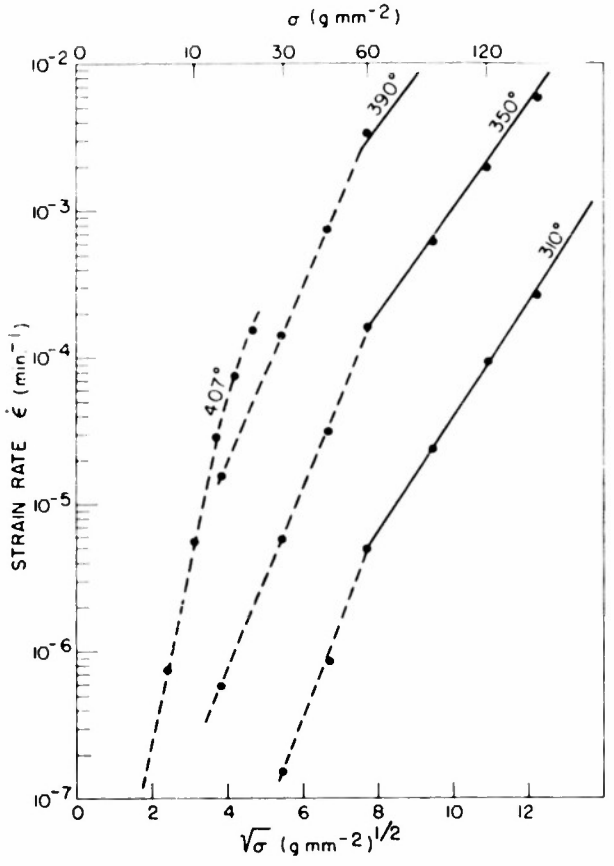

Fig. 7. Steady-state creep rate of [111] specimens.

Because creep by diffusion is expected to vary linearly with stress for small stresses, according to (1), a special attempt was made to investigate the stress dependence of the creep rate of a [111] crystal at the lowest stresses achievable with the apparatus. A [111] crystal with height-to-diameter ratio of 0.9 was measured at 407°C. The results appear in Fig. 7. Down to the lowest attainable stress (6 g/mm^2), the creep rate is still decreasing faster than linearly.

C. Effect of Hydrostatic Pressure. The procedure for the high pressure measurements of steady-state creep was as follows. First the specimen was deformed in the atmospheric pressure apparatus at the stress and temperature to be used in the high pressure experiment, in order to exhaust the transient creep and measure the atmospheric pressure steady-state rate. It was then cooled to room temperature, reheated, and remeasured, to verify that the transient component had not returned and that the steady-state rate was unchanged. The sample was then cooled, measured, transferred to the high pressure apparatus, and brought up to pressure. The temperature was then raised by an external furnace and maintained for a suitable length of time, after which the apparatus was cooled to room temperature and the pressure released. The sample was removed and measured, and the total deformation compared with what it would have been under the same conditions at atmospheric pressure. The procedure for transient creep was the same, except that an unstrained, annealed sample was used.

Five steady-state high pressure runs were made between 3000 and 6000 atmospheres with different applied stresses and using crystals of different orientations. The results are shown in Fig. 9, in which the ratio of the strain rate at high pressures $\dot{\epsilon}$ (p) to the strain rate at atmospheric pressure $\dot{\epsilon}$ (0) is plotted versus p/RT, where p and T are the pressure and temperature of the run. Because the temperature actually was changing at the beginning and end of the runs, the basis of comparison of the high pressure and atmospheric pressure strains is illustrated for one of the runs by Fig. 8, in which the full curve represents $\dot{\epsilon}(T(t))$ for p = 0, $\dot{\epsilon}(T)$ being obtained from the measured atmospheric pressure strain rate and T(t) being the recorded temperature during the high pressure run. The integral of this function is the total strain which would have been observed at atmospheric pressure under the temperature conditions of the high pressure run.

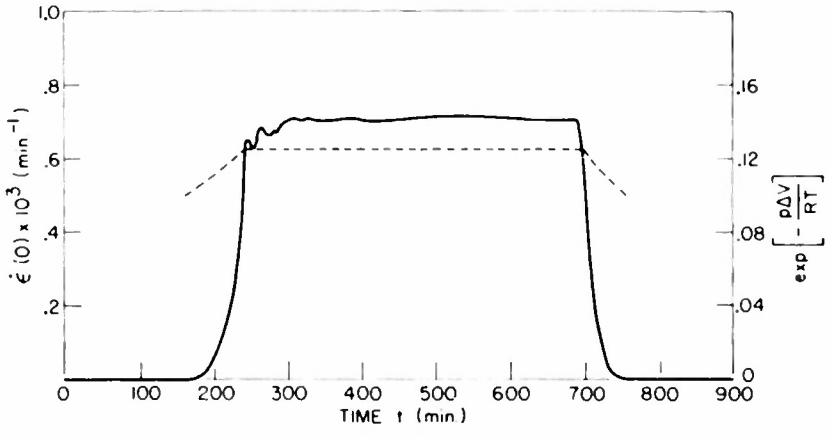

Fig. 8. Atmospheric pressure creep rate corresponding to high pressure run (full line) and pressure factor (dashed line).

The ratio of the actual strain during the high pressure run to this integral is assumed to be equal to the ratio of the strain rate at high pressure to the strain rate at atmospheric pressure, $\dot{\epsilon}(p)/\dot{\epsilon}(0)$. If $\log \dot{\epsilon}(p)/\dot{\epsilon}(0)$ is plotted against p/RT, $\dot{\epsilon}(0)$ being referred to the strain rate before the high pressure run, these data lie approximately on a straight line. The vertical intercept, however, is about 0.5 instead of 1. Furthermore, in all but one case the atmospheric pressure rate was measured also after the high pressure run, and in each case it was about one-half of the rate before it. Therefore in Fig. 9 the data are plotted referred to the rate after the high pressure run; for the point for which the rate was not measured afterward, the rate obtained beforehand was divided by two. Within the precision of the experiment the points lie on a straight line, regardless of orientation or stress, implying a relation of the form

$$\dot{\epsilon}(p)/\dot{\epsilon}(0) = \exp\left\{-p\ \Delta V/RT\right\}.$$

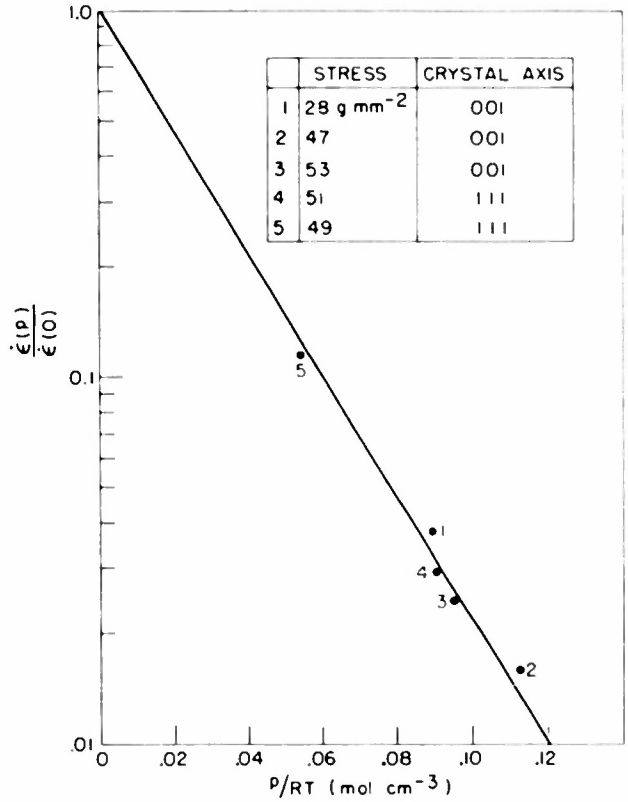

Fig. 9. Relative steady-state creep rates at high pressure.

The slope of the line drawn in the figure is $\Delta V = 38 \pm 3$ cm^3/mol. In Fig. 8 the dashed line shows $\exp\{-p\ \Delta V/RT\}$ during the run, showing that this function is slowly varying where the contribution to the strain is significant, and thus that the analysis of the data is consistent.

The retardation of the creep rate after the high pressure runs was not removed by several hours annealing at high temperature. X-ray diffraction pictures made before and after holding two samples at high pressure and temperature but without loading showed no change in perfection of the crystal

structure. Removal of one or two thousandths of an inch from the surface by etching, however, restored the normal creep rate, and the samples, which were slightly discolored after the high pressure runs, regained their normal color. Therefore it is thought that the cause of the retardation was contamination of the surface by an impurity. Spectrographic analysis of the surface of one sample after the high pressure run showed 0.003% Si, 0.007% Fe, and 0.006% Cu.

An annealed [001] sample was loaded with 53 g/mm^2 for about 260 min at 6000 atmospheres and 378°C. Subtraction of the steady-state strain, computed on the basis of the above results, from the observed strain gave a transient contribution of 1.3%, compared with the usual value of the order of 10 or 20% at atmospheric pressure. Subsequently tested at atmospheric pressure, after removal of the surface, the sample showed a further transient strain of 0.7% and a normal steady-state rate. It thus appears that the transient is also suppressed by pressure, though perhaps less strongly than the steady-state.

D. Effect of Impurities. The effect on the creep rate of additions of a divalent cation, a divalent anion, and a monovalent anion of about the same ionic radius has been observed. Cd^{++}, S^{--}, and Cl^{-} were chosen because the solubility limits were known. For this purpose crystals were grown from melts containing about 0.0006 and 0.25 mol per cent $CdBr_2$, 0.0006 and 0.06 mol per cent Ag_2S, and 0.0017 and 0.17 mol per cent AgCl. The exact impurity content of the resulting single crystals is unknown, although from a crystal grown from a melt containing 0.08% Ag_2S, 0.06% was recovered by chemical analysis.* In the case of sulfur, because of the pronounced color change caused by it, an inhomogeneity associated with the spiral ridges produced on the crystal rods by growth rate, dependent on the temperature gradient in the melt, was seen. Further, in the case of small concentrations of sulfur, richer melts sometimes produced poorer crystals, as evidenced by the rate of photolytic darkening and the effect on the creep rate. Nevertheless, the order of magnitude of the impurity content is believed to be correct, and the following facts emerge.

Sulfur had the greatest effect on the creep rate. The effect on the transient of 0.0006% S^{--}, compared with 'pure' crystals, is shown in Fig. 10. Curve (A) is for an annealed pure crystal which was loaded as soon as temperature equilibrium was attained (about 2 hr after the furnace was turned on); curve (C) is for a sample containing 0.0006% S^{--} under the same conditions. Curves (B) and (D) are, respectively, for a pure crystal annealed 16 hr in situ and a sulfur-doped crystal annealed 12 hr in situ at 397°C before loading. These specimens were sawed from the same single crystal rods as those of curves (A) and (C), respectively, and all were [001] specimens deformed at 370°C with 60 g/mm^2. The inhibitory effect, dependent on holding time at high temperature, was similar for other samples tested. The steady-state rate, however, for the sulfur-doped samples was normal, i.e., the same as for the pure samples. But with a stress of 30 g/mm^2 at 405°C for a sulfur-doped sample, the steady-state rate was 0.7 times normal, and the induction time in the transient stage was an order of magnitude greater. Crystals containing 0.06% S^{--} behaved the same at 30 as at 60 g/mm^2: there was no measurable transient and the steady-state rate was about 0.2 times normal. (See Table I).

Additions of Cd^{++} were similar to additions of Cl^{-} in that the transient

---

* The author is indebted to Dr. Louis Dunicz for performing this difficult analysis.

TABLE I

Effect of Additions of Impurities on Creep Rate

Impurity	Atomic %	Stress (g/mm^2)	Steady-state rate / Normal steady-state rate	Transient
S^{--}	0.0006	60	1.0	induction period
S^{--}	0.0006	30	0.7	induction period
S^{--}	0.06	60	0.2	none
S^{--}	0.06	30	0.2	none
Cl^{-}	0.0015	60	1.0	normal
Cl^{-}	0.15	60	0.6	normal
Cd^{++}	0.0005	60	1.0	normal
Cd^{++}	0.25	60	0.8	normal

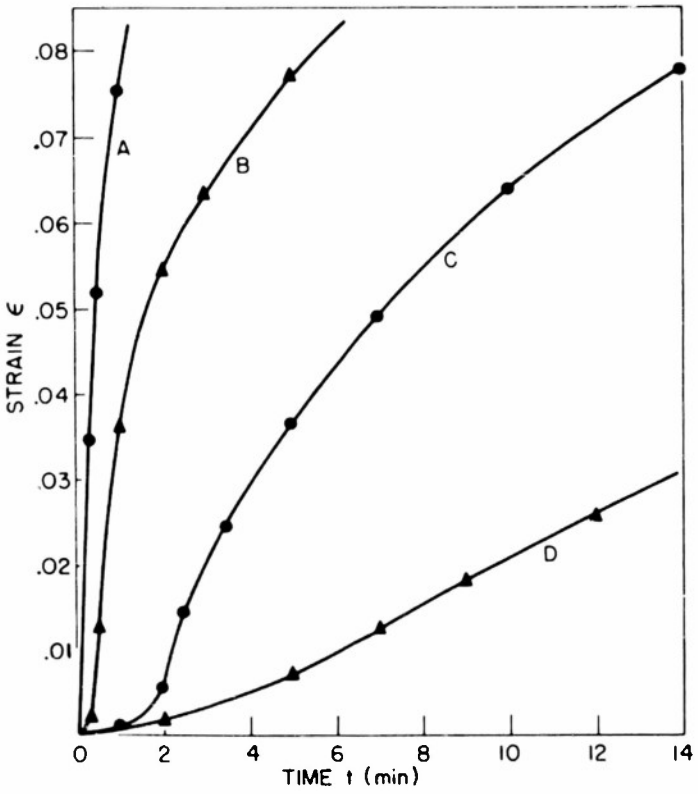

Fig. 10. Transient creep of pure (A,B) and sulfur-doped (C,D) specimens, loaded immediately (A,C) and after annealing in situ (B,D).

behavior was like that of pure crystals, even with the larger concentrations. 0.0017% Cl^{-} had no effect on the steady-state rate with 60 g/mm^2. 0.17% Cl^{-} gave a steady-state rate about 0.6 times normal, and 0.25% Cd^{++} one about 0.8 times normal at 60 g/mm^2.

0.25% Cd precipitated at room temperature in about 8 hr. (In order to

observe the effect in solution the sample was maintained at high temperature before loading.) The precipitate had no effect on the transient, and probably none on the steady-state rate, though the latter conclusion is uncertain because of dissolution during the run.

E. Specimens after Deformation. Slip in AgCl has been studied at room temperature by Nye,[9] who concluded that the slip direction is $[0\bar{1}1]$, while the slip plane is not always a crystallographic plane of low indices, but is always near to the plane in an $[0\bar{1}1]$ zone on which the resolved shear stress in the $[0\bar{1}1]$ direction is maximal. Observations of slip lines on the surface of three AgBr samples similar to those used in the high temperature creep tests, after rapid compression at room temperature, were consistent with Nye's conclusions about AgCl.

After creep at high temperature, slip lines did not always appear on the surface, so that it was difficult to say in all cases what were the active slip systems. This difficulty is the reason for presenting the data in terms of compressive stresses and strains. Nevertheless the occurrence of slip can be inferred from the shape of the specimens after deformation. (See Fig. 11. The very inhomogeneous deformation of the two samples on the

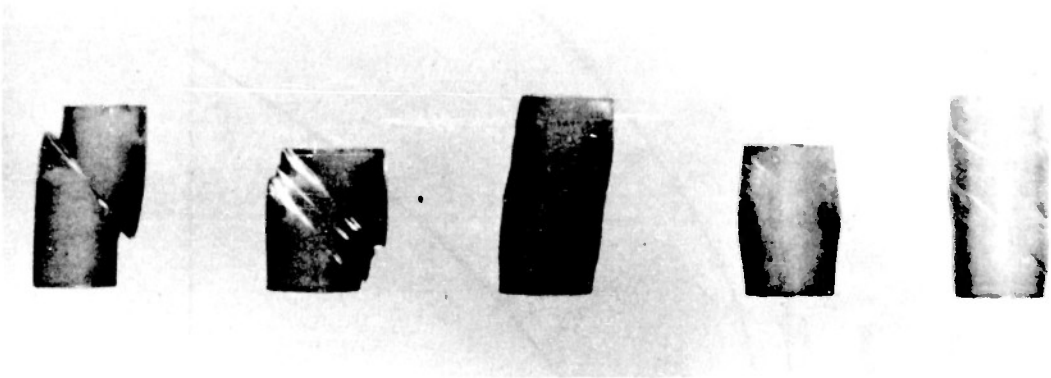

Fig. 11. Single crystals after deformation of about 10%; in the deformation of the three specimens on the left, the ends were free to move laterally.

left was observed only in specimens with the ends free to move laterally slipping on the (011) plane in the $[0\bar{1}1]$ direction. The avoidance of this type of deformation was the reason for determining the stress and temperature dependence of the creep rate with the ends of the specimen laterally constrained, although the results were about the same in either case.) Sometimes planes were traced by not very sharply defined ridges on the surface of the deformed specimen, and occasionally, at high stresses, well defined slip lines could be seen under low magnification. Measurement of the orientation of these features could only be made within an error of about 10°, however, so that the following statements should be understood to have this uncertainty.

These observations indicated first that an (011) plane and an $[0\bar{1}1]$ direction constitute the preferred slip system. For example, a crystal whose axis was [215] was observed to slip in the $[0\bar{1}1]$ direction on the (011) plane, where the resolved shear stress was only 0.79 relative to the maximum resolved shear stress (one-half the compressive stress), in preference to the plane $(1\bar{1}1)$, on which the shear stress resolved in an $[0\bar{1}1]$ direction was greatest, namely 0.95. This conclusion is also supported by the fact that the

creep rate was greatest when the specimen axis was [001], when there are four (011)-[0$\bar{1}$1] systems on which the resolved shear stress is the maximum, and least when the axis was [111], when there are no such systems on which the resolved shear stress is different from zero.

This preference, however, does not appear to be very strong. In every case a slip plane was chosen which was nearly 45° from the specimen axis. In addition, there were cases, particularly when the stress was probably not very homogeneous, when the slip direction apparently cannot have been an [0$\bar{1}$1] direction. For example, a crystal whose axis was [413] and whose ends were laterally free, after considerable slip in the [110] direction (on the (1$\bar{1}$1) plane), appeared to have slipped in the [2$\bar{1}$0] direction (on the (121) plane). In [111] crystals with the ends laterally constrained, traces of (011) planes were seen; since the [0$\bar{1}$1] direction is 90° from the specimen axis, it cannot have been the slip direction. If [100] and [2$\bar{1}$0] are also included as possible slip directions, all the observations can be understood. In view of the multiplicity of possible slip systems, the compressive stresses and strains are probably not too bad a measure of the shear stresses and strains.

X-ray orientation determinations made after the deformation only rarely revealed appreciable net rotation of the lattice with respect to the specimen axis.[10] No correlation could be found between the cases in which it occurred and the conditions of the deformation.

After the deformation, except right at the ends of the specimens, in the back-reflection Laue photographs each individual reflection was split up into a number of discrete spots. The number of distinguishable spots varied from about 10 to 35, and they were spread over an angular region of about 2 to 8°. As the area of the incident x-ray beam at the specimen was about 28×10^{-4} cm^2, the crystals appear to have broken up into regions about 10^{-2} cm on a side with a spread in orientation of about 1 to 4°.

2. Polycrystalline Specimens

Having the single crystal results, the behavior of polycrystalline specimens could be compared with them. Unfortunately, however, it was not possible to produce very small grained specimens. The results for three of them, with average grain size of about 1 mm, are presented in Fig. 12, where the dashed lines represent the results for single crystals of [111] and [001] orientation. The rates do not differ greatly from those for single crystals. It was found after the runs that grain growth had occurred, the samples now consisting essentially of one or two large grains. Also after the runs relative displacements of the original grains of the order of 0.05 mm normal to the surface could be seen.

Two bicrystals with a grain boundary intersecting the plane ends of the specimen were accidentally grown. These were tested, and it was found that slip marks were continuous across the boundary, but with a discontinuous change in direction. The steady-state rate was not greatly lowered by the presence of the boundary, though in both cases there was an initial period of about 90 min, during which the strain was about 3%, in which the strain rate was less than the steady-state rate. This effect was not observed in the polycrystalline samples.

V. Discussion

The most salient features of the experimental results are the large activation energy of the steady-state creep rate, in comparison to soft metals, and the large 'free volume' associated with the high pressure measurements. In this section an attempt will be made to interpret the results in terms of

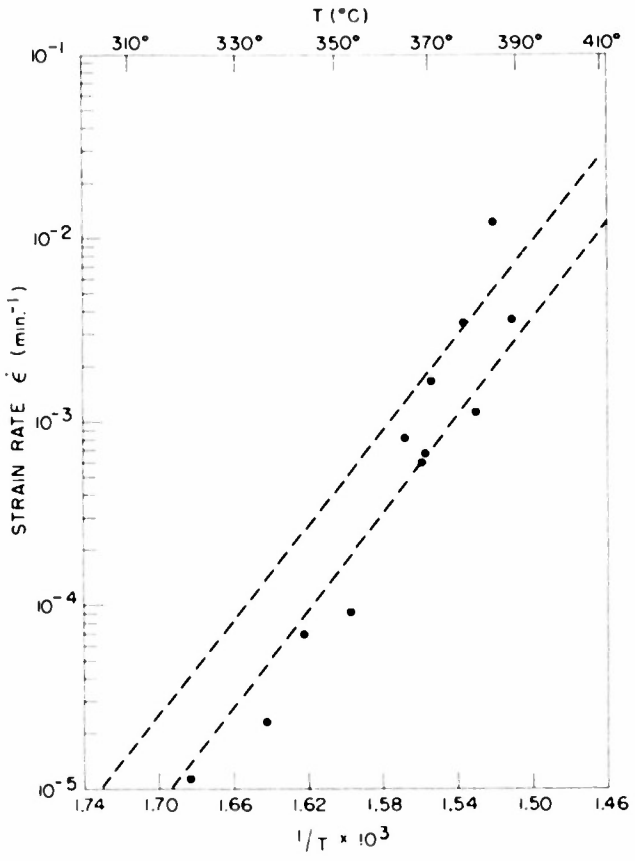

Fig. 12. Steady-state creep rate of polycrystalline specimens at 60 g/mm^2.

current ideas of plastic flow, the emphasis being put on the Mott mechanism, which appears to give a natural explanation of the large activation energy and strong pressure dependence.

In discussing the results obtained with AgBr, it will be interesting to compare them with the measurements by Cottrell and Aytekin[11] of steady-state creep of single crystals of zinc, a metal which, though not cubic, has about the same melting point and critical shear stress as AgBr. Their results are expressed by

$$\dot{\gamma} = C \exp\left\{-(Q_o + B' \tau_o)/RT\right\} \exp\left\{B' \tau /RT\right\},$$

where $\dot{\gamma}$ is the shear strain rate and τ is the shear stress, with

$$C = 10^{10}\text{-}10^{13} \text{ sec}^{-1},$$

$$Q_o = 28\text{-}30 \text{ kg-cal/mol} \quad (\tau_o = 35 \text{ g/mm}^2),$$

$$B' = 0.150\text{-}0.300 \text{ (kg-cal/mol)/(g/mm}^2).$$

If our high stress results are expressed in the same form, assuming $\tau = 1/2\,\sigma$, $\dot{\gamma} = 2\dot{\epsilon}$, we have from (2)

$$C = 10^{16} \text{ sec}^{-1},$$

$$Q_o = 59 \text{ kg-cal/mol},$$

$$B' = 0.145 \text{ (kg-cal/mol)/(g/mm}^2\text{)}.$$

Thus the stress dependence is about the same, whereas the activation energy is twice as large and the pre-exponential factor is several orders of magnitude larger.

This comparison can be understood qualitatively if it is assumed that the behavior of dislocations in the two materials is similar, but that the coefficient of self-diffusion appears as a factor in the creep rate. For Zn the smaller of the two diffusion coefficients (perpendicular to the c-axis) is[12] $90 \exp\{-31{,}000/RT\}$, with an activation energy about 2 kg-cal/mol larger than Q_o. For the coefficient of self-diffusion of Br in AgBr, both the activation energy and the pre-exponential factor would be expected to be considerably larger. (For Cl in NaCl,[13] $D = 3 \times 10^4 \exp\{-62{,}000/RT\}$.) In addition the linear pressure dependence of $\ln \dot{\epsilon}$, independent of stress and orientation, is easily understood in terms of the effect of pressure on the diffusion coefficient. The value of ΔV for the diffusion of Br should be larger than the molar volume of AgBr, 29 cm^3/mol, as is the observed ΔV.

The author[14] has attempted to extend Mott's theory to yield a formula which can be compared with the present experimental results. The resulting expression for the shear strain rate is

$$\dot{\gamma} = N n L \ell^2 j D \exp\{\Delta W/kT\}, \tag{3}$$

where N is the number of dislocation sources (e.g., Frank-Read sources[15]) per unit volume, n is the density of diffusing dislocations per unit area, L is the length of the dislocations, ℓ is the distance on the slip plane in which the dislocations are piled up, j is the proportion of jogs in the dislocations, and D is the coefficient of self-diffusion (for Br, in AgBr). ΔW is the decrease of the energy of formation of a vacancy when the vacancy is formed at a dislocation in a stress field, due to the reduction in strain energy of the dislocation when it climbs. The rate of climb is assumed to be limited by the rate of diffusion of the excess vacancies away from the dislocation. If it is assumed that the driving stress field is primarily that due to the interaction of the accumulated dislocations,* and that the energy of interaction is proportional to the square of the number of dislocations and to a geometrical factor P depending insensitively on their distribution, ΔW is

$$\Delta W = \left[G b a^3 P/4\pi (1 - \nu) \right] n\ell, \tag{4}$$

where G is the shear modulus, ν Poisson's ratio, and b the Burgers vector of the dislocation. The main stress dependence arises through $(n\ell)$.

If the theory is to apply both to AgBr and to Zn, the above comparison suggests that the diffusion coefficient for Br is of the order of magnitude $D = 10^6 \exp\{-61{,}000/RT\}$. According to Mott,[2] the proportion of jogs in the dislocation is $j = \exp\{-U/RT\}$. Then to give the observed activation energy Q = 69 kg-cal/mol, U = 8 kg-cal/mol, giving a proportion of jobs between 10^{-3} and 4×10^{-2} between 300° and 400° C. The x-ray diffraction evidence indicated that discontinuities in orientation occur at separations of the

* This assumption appears reasonable in view of the observation[11] that the process of steady-state creep is related to the process of recovery, after the applied stress is removed.

order of 10^{-2} cm after deformation,# suggesting that the density of dislocation sources should be $N \approx 10^6$ cm^{-3}. Since the surface layer appears to have an appreciable influence on the creep rate,+ ℓ should probably be comparable with the dimension of the crystal, and L should probably be of the order of magnitude of ℓ. Substitution of $N = 10^6$ cm^{-3}, $n = 10^7$ cm^{-2}, $L = \ell = 10^{-1}$ cm, $D = 10^6 \exp\{-61{,}000/RT\}$ into (3) gives the observed value of $C \approx 10^{16}$ sec^{-1}. In addition, using $G = 10^{11}$ dynes/cm^2, $\nu = 0.25$, $b = a = 6 \times 10^{-8}$ cm, formula (4) gives the correct order of magnitude of ΔW if P is about 5. Thus it appears that the formulas can be made to give the correct order of magnitude for the creep rate of AgBr, and, because of the assumption of D for Br, also of Zn. It should be remarked, however, that the diffusion coefficient assumed for Br is not in agreement with that measured by Murin and Taush[7] at 300° C.

It might also be noted that dislocations could be blocked by dislocations emitted from a source on a nearby slip plane.[18] The distance h at which two dislocations can block each other under an applied shear stress τ is

$$h = G\,b/8\pi(1-\nu)\tau.$$

Such interference might be expected if $h \ell L > 1/N$, in which case we would have

$$\ell \cong (\ell L)^{1/2} = [8\pi(1-\nu)/N\,G\,b]^{1/2}\,\tau^{1/2}.$$

Since $h \cong 6 \times 10^{-3}$ cm$/\sigma$ (g/mm^2), this interference might occur within the range of the experiment, and is a possible explanation of a $\sigma^{1/2}$ stress dependence.

For the magnitude of diffusion creep by the Nabarro mechanism, if we again assume that the diffusion coefficient for Br is $D = 10^6 \exp\{-61{,}000/RT\}$, and if we assume that $d = 6 \times 10^{-4}$ cm, we find from (1) $\dot{\epsilon} = 3 \times 10^{-10}$ sec^{-1} at 407° C and 6 g/mm^2. This value is much less than the experimental rate of 10^{-8} sec^{-1} at this temperature and stress, in agreement with the observation made in section IV B that the stress dependence was not characteristic of Nabarro creep.

Except in the case of Cd^{++}, the Mott process does not give the observed dependence of creep rate on impurity concentration by its influence on the equilibrium vacancy concentration. Cd^{++} depresses the number of Br^- vacancies, S^{--} increases it, and Cl^- has no effect.[19] On the other hand, S^{--} depressed the creep rate most, next Cl^-, and finally Cd^{++}. Cd^{++} gave about the effect which would be expected from its influence on vacancy concentration. It is thought that the explanation of the effect of S^{--} and Cl^- is to be sought in an interaction of the impurities with the dislocations, leading to an inhibition of their motion on the slip plane. Particularly in the case of S^{--}, the induction time for transient creep, depending on holding time at high temperature, suggests such an explanation.[20] The nature of the interaction, however, is not entirely clear from the experiments. The radii[21] of S^{--} and Cl^- are about 8% smaller than that of Br^-, while Cd^{++} is a little more than 8% smaller than Ag^+, so that an elastic interaction does not seem to give the observed differences. An electrical interaction between doubly charged impurities and 'incipient vacancies'[22] at jogs in dislocations is conceivable, but also fails to account for the differences. Whatever the nature

---

Hedges and Mitchell[16] have observed optically a polyhedral substructure in AgBr, with dimensions 10^{-3} - 10^{-2} cm.

+ Cf. for example[17].

of the interaction, however, it is believed that accidental impurities account for the sharper decrease of steady-state creep rate at low stress, since the addition of a small amount of S^{--} depressed the rate at 30 but not at 60 g/mm^2.

In alkali halides slip systems are chosen which do not demand the close approach of ions of like sign when a dislocation moves. In contrast to the alkali halides, the large polarizability of the Ag^+ ion may account for the ductility of the silver halides,[4] the monopole repulsion being decreased by dipole interaction.[23] It seems possible to understand qualitatively the comparatively weak conditions on choice of slip system in AgBr on this basis.

Because of the large number of slip systems possible, grain boundaries in polycrystalline AgBr do not appear to inhibit slip in individual grains strongly, in contrast for example to Zn, in which the creep rate of polycrystalline specimens is very much smaller than that of single crystals.[11] On the other hand, grain boundary mobility did not appear to give a large contribution to the strain rate; the contribution would presumably be greater in small grained specimens.

VI. Conclusion

It is concluded that Mott's mechanism for the limitation of steady-state creep at high temperature by self-diffusion is able to give a satisfactory qualitative explanation of the strong temperature and pressure dependence of the steady-state creep rate of single crystals of pure silver bromide. A reasonable choice of parameters appearing in a model derived from it can give also the correct order of magnitude for Cottrell and Aytekin's results on zinc, and, if an assumption of the diffusion coefficient of Br be made, for the present results on AgBr at higher stress levels. Although the results appear to support Mott's theory, a detailed test of the calculation based on it must await measurement of quantities which are at present unknown. The square-root-of-stress activation energy dependence suggests a mechanism involving the interference of Frank-Read sources on different slip planes. The Nabarro mechanism apparently does not make a significant contribution to the creep in the range of the experiments. At low stresses, the creep rate in AgBr is believed to be controlled by the interaction of impurities with dislocations.

VII. Acknowledgments

The writer is grateful to his sponsor, Professor A. W. Lawson, for suggesting the problem and for guidance in its investigation, and to the Shell Oil Company for the grant of a Fellowship. He is also indebted to Messrs. N. D. Nachtrieb and K. Lindholm for the construction of his apparatus and for advice in its design. The work was supported in part by the Office of Naval Research.

References

1. Nabarro, F. R. N. Rep. of a Conference on the Strength of Solids (Phys. Soc. London, 1948), p. 75.
2. Mott, N. F. Proc. Phys. Soc. London, B64 (1951) 729.
3. Schmid, E. and Boas, W. "Plasticity of Crystals" (London, F. A. Hughes and Co., 1950), Ch. VII.
4. Stepanow, A. W. Phys. Z. Sowjet., 8 (1935) 25.
5. Teltow, J. Ann. d. Physik, 5 (1950) 63.
6. Kurnick, S. W. J. Chem. Phys., 20 (1952) 218.

7. Murin, A. and Taush, Yu. Dokl. Akad. Nauk SSSR, 80 (1951) 579.
8. Lazarus, D. and Lawson, A. W. Rev. Sci. Instr., 18 (1947) 730.
9. Nye, J. F. Nature, 162 (1948) 299; Proc. Roy. Soc., 198A (1949) 190, 200A (1949) 47.
10. Taylor, G. I. Proc. Roy. Soc., 116 (1927) 16, 39.
11. Cottrell, A. H. and Aytekin, V. J. Inst. Met., 77 (1950) 389.
12. Banks, F. R. and Miller, P. H., Jr. Phys. Rev., 59 (1941) 943.
13. Chemla, M. C. R. Acad. Sci. (Paris), 234 (1952) 260.
14. Christy, R. W. Unpublished.
15. Frank, F. C. and Read, W. T., Jr. Phys. Rev., 79 (1950) 722.
16. Hedges, J. M. and Mitchell, J. W. Phil. Mag., 44 (1953) 223.
17. Andrade, E. N. da C. and Randall, R. F. Y. Proc. Phys. Soc. London, B65 (1952) 445.
18. Cottrell, A. H. Progress in Metal Physics I (London, Butterworths Sci. Publ., 1949), p. 77.
19. Koch, E. and Wagner, C. Z. f. phys. Chem., 38B (1937) 295.
20. Seitz, F. Phys. Rev., 88 (1952) 722.
21. Mott, N. F. and Gurney, R. W. "Electronic Processes in Ionic Crystals" (2d ed., Oxford, 1948).
22. Seitz, F. Rev. Mod. Phys., 23 (1951) 328.
23. Weyl, W. A. Glastechn. Ber., 23 (1950) 174.

XIII

THE CHANGE OF FERROMAGNETIC CURIE POINTS WITH HYDROSTATIC PRESSURE*

Lyle Patrick**
(Submitted to The Physical Review)

Abstract

The effect of pressure on the Curie temperature has been measured for 13 ferromagnetic materials, comprising 4 elements (Fe, Co. Ni, Gd), 7 metallic alloys, a ferrite and a perovskite. Curie points ranged from 16°C (Gd) to 1120°C (Co), and pressures up to 9000 Atm. The results are in disagreement with two common forms of the interaction curve. The result obtained for Fe is not in agreement with the prediction of Kornetzki, based on volume magnetostriction measurements between 20°C and 100°C.

I. Introduction

Importance of Interatomic Distance

The effect of pressure is considered to be that due to the change produced in interatomic distance, which is known to be an important parameter in the strength of magnetic interaction. Slater[1] first pointed out that ferromagnetism occurs only in those elements in which there is a large ratio of interatomic distance, D, to diameter of unfilled inner shell, d (usually a d shell, but in Gd it is the 4f shell). An accurate calculation of the magnetic interaction is still impossible at the present stage of the theory, but the several theoretical approaches all agree on certain qualitative features of the interaction curve (i.e., the curve showing the strength of the interaction as a function of interatomic distance).

Sommerfeld and Bethe[2] discussed the type of wave function necessary to give a positive exchange integral in the Heisenberg theory, and they drew a curve (Fig. 1) to show qualitatively the features of this positive range. The band theory and Zener's theory both agree that ferromagnetism is not possible for very small or very large values of D, but the width of the ferromagnetic range is still an unsettled question. The salts of ferromagnetic elements, in which D is large, are paramagnetic rather than weakly ferromagnetic. On the other hand, Zener[3] has pointed out the importance of conduction electrons in coupling the d shell spins. The salts may be paramagnetic because of the absence of conduction electrons.

The Forrer Correlation

Forrer[4] has made a correlation of magnetic interaction with interatomic distance, D, for Mn, Cr, Fe, Co, Ni and their compounds in which these elements retain their characteristic moments and in which coupling does not occur through intermediate atoms by the superexchange mechanism. He

* Submitted in partial fulfillment of the requirements for the degree of Ph.D. at the University of Chicago. The work was done at the laboratory of the Institute for the Study of Metals, Chicago, Illinois.

** Now at Westinghouse Research Laboratories, East Pittsburgh, Pennsylvania.

finds that as D increases the interaction changes, for each element, from antiferromagnetic to ferromagnetic and then to paramagnetic. The ferromagnetic range is roughly 10% of D—perhaps as little as 5% in Co. However, one must consider Zener's remarks about conduction electrons. The Forrer correlation overlooks the fact that the range of D in metals is rather limited. Dilution of ferromagnetic elements to increase the average distance does not work in metallic alloys because the conduction electrons of the added metal apparently fill the d band of the ferromagnetic element. The reduction of Curie point in such cases is due to a reduction of average moment rather than to any distance effect. Perhaps the ferromagnetic range would be much greater than 10% if this range could be obtained in metals.

A narrow ferromagnetic range, as suggested by the Forrer correlation, has consequences for the present experiment. A pressure of 10,000 Atm, which is available in the laboratory for an experiment of this type, changes D by only about 0.2%, using an average value for the compressibility of metals. This means that it is impossible to measure any large portion of the interaction curve, but the change of Curie point with pressure does give the slope at a single point. If in Co the Curie temperature rises to 1400°K and falls to zero again within a range of 5% of D, the average rate of rise or fall must be over 10° per 1000 Atm. For Fe this figure is about 4°. This means that changes of this order of magnitude should be expected if the ferromagnetic range is as limited as Forrer suggests.

Interaction Curves

The Forrer correlation is an attempt to define the ferromagnetic range for single elements. The suggestion of Slater that D/d is the significant parameter for ferromagnetic interaction has led to attempts to draw a generalized interaction curve to include all ferromagnetic elements. The assumption is that D and d are the only important parameters in the strength of magnetic interaction; so a correlation is attempted, using a function of D and d as a "reduced" distance. Such attempts must prove futile if other important parameters exist (e.g., conductivity).

Fig. 2 shows one such curve, drawn by Bozorth.[5] In this, Curie temperatures are plotted against D/d. However, the Curie temperature on the

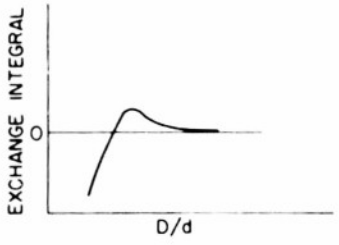

Fig. 1. Bethe Interaction Curve.

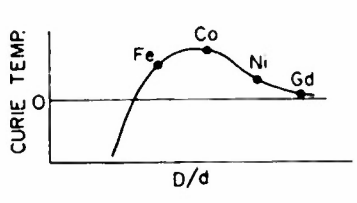

Fig. 2. Bozorth Interaction Curve.

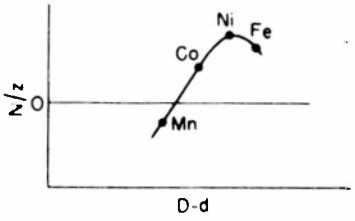

Fig. 3. Neel Interaction Curve.

assumption of a Weiss inner field, is proportional to $\mu^2 N$, in which μ is the atomic moment and N the Weiss field constant; and μ seems to be characteristic of the element, independent of D (the examples given by Forrer show this). Hence it would seem to be more logical to plot N as ordinate instead of the Curie temperature, in which case Ni, having the highest value of N, is at the top of the curve.

Neel[6] has plotted N/z against D-d, as shown in Fig. 3 (z is the number of nearest neighbors). He includes an antiferromagnetic range and has also extended the correlation to include interactions between different atoms in alloys. Iron, however, can be included only by assuming that next nearest neighbors are responsible for the ferromagnetism, the nearest neighbors being near the point where the curve crosses the axis, and therefore ineffective. He has found further evidence to support this curve; and has predicted an increase of Curie point with pressure in Fe of 0.79° per 1000 Atm and decreases in Co and Ni of 4.6° and 0.13° respectively.

Reciprocal Effects

If a change of volume alters the magnetic interaction there should be a reciprocal effect in which the change of intrinsic magnetization by a high field changes the volume of a ferromagnet. This effect has been measured as the volume magnetostriction and more will be said of it later. Also, the loss of magnetization as the temperature is raised has an effect on the volume which shows up as an abnormal thermal expansion. This may be large enough, as in Invar, to compensate the normal thermal expansion over a certain temperature range. Both effects have been used to estimate the volume dependence of the interaction.

II. Previous Results

There have been several unsuccessful or partially successful attempts to measure the change of Curie point with pressure. A short description of each of these will be given. Following this, a summary will be given of estimates of the change to be expected, based on the indications obtained from volume magnetostriction data and from estimates of the anomalous thermal expansion.

Measurements using High Pressure

In 1931 Adams and Green[7] used the method which has been adopted for the present experiment; they used the sample as the core of a transformer and, with a constant small alternating current supplied to the primary, they measured the output of the secondary as a function of temperature. The drop in output at the Curie temperature is very sharp, and although it does not define the Curie point in the conventional way, the method is very satisfactory for finding a change in Curie point. Unfortunately Adams and Green could not obtain a stable temperature in their pressure apparatus. CO_2 was used as a pressure fluid and there were strong convection currents set up in it by the internal furnace. Their results indicate an uncertainty in temperature of about 5°, and this masked all changes.

Steinberger[8] did not attempt to measure the change of Curie temperature, but observed a change from ferromagnetic to paramagnetic for a 30Ni 70 FE alloy under pressure applied at room temperature. The great change was undoubtedly due to a change of Curie point, but Steinberger described it in terms of a change in permeability.

Michels et al.[9] have made measurements on two Monel alloys, using the change of slope of the resistance vs T curve as an indication of the Curie point. The ferromagnetic ordering lowers the resistance of a metal, and results in a change of slope of the curve R vs T at the Curie point. This,

however, is not sharp in practice, and an extrapolation procedure must be set up to define the Curie temperature. The method requires very accurate resistance measurements over large temperature intervals and is complicated by the fact that resistance also changes with pressure.

Ebert and Kussman[10] used large fields to obtain I vs T curves, using special non-magnetic pressure bombs. The purpose was to define the Curie point in the conventional way under pressure, but the great experimental difficulties made accuracy impossible, and small changes could not be detected. In the alloy in which a large change was to be expected (30Ni 70Fe) the I vs T curve drops so slowly that the conventional method of defining the Curie point is not very useful. They decided that no change of Curie point had been observed, but Kornetzki[11] later reinterpreted their data and concluded that there had been a change of Curie point. A criticism of Ebert and Kussman's methods and conclusions has been given by Michels and deGroot.[12]

Predictions based on the Reciprocal Effects

The predicted changes of Curie point with pressure are based on measurements of the thermal expansion anomaly, or on measurements of volume magnetostriction. The latter cannot be carried out at high temperatures, so they actually indicate the volume dependence of the magnetic interaction at the temperature at which they are carried out. This will be discussed under the results on Fe and Fe-Si alloys.

Slater[13] has used the Clapeyron equation as if the transformation from magnetic to non-magnetic state were first order. The equation may be written $d\theta/dp = \Delta V/\Delta S$ in which θ is the Curie temperature. The volume change is estimated from the thermal expansion anomaly, and the disordering entropy may be calculated, assuming dipoles with two orientations. Only order of magnitude is hoped for. For Ni, Slater has estimated an increase of Curie point with pressure of 0.05^{o} per 1000 Atm.

If the transition it treated as second order the corresponding Ehrenfest relation is $d\theta/dp = 3TV\Delta\alpha / \Delta C_p$ in which α is the linear coefficient of expansion and C_p the specific heat. These quantities do not show sharp discontinuities at the Curie point but an extrapolation method must be used. For Ni, Michels and de Groot[12] used average values of several determinations of $\Delta\alpha$ and ΔC_p and estimated the increase of Curie point with pressure to be 0.35^{o} per 1000 Atm which is in agreement with the result obtained in the present experiment. Ni was the only element for which sufficiently accurate experimental data were available.

In order to relate volume magnetostriction and change of Curie point with pressure Kornetzki[14] has used the thermodynamic relation $dV/dH)_p = -dM/dP)_H$ where M is the total moment, and the assumption that the magnetization per gram, σ, is given by a relation of the form $\sigma = f(T/\theta)$. The relation derived from these is

$$\frac{1}{\theta}\frac{\partial\theta}{\partial P} = \frac{1}{T}\frac{\frac{\partial\omega}{\partial H}}{\left(\rho\frac{\partial\sigma}{\partial T} - \frac{3\alpha}{K}\frac{\partial\omega}{\partial H}\right)}$$

in which ω is the fractional change of volume, ρ is the density, α the linear thermal expansion coefficient, and K the compressibility. For Fe, Kornetzki made measurements of volume magnetostriction between $20^{o}C$ and $100^{o}C$ and predicted a decrease of Curie point with pressure of 5 to 10 degrees per 1000 Atm.

III. Experimental Procedure

Transformer Method

The experimental method used is similar to that of Adams and Green,[7] using the magnetic material as the core of a transformer, as shown in Fig. 4, which shows the necessary equipment except for the pressure and furnace systems. The primary and secondary coils are wound on opposite arms of the picture frame sample so as to have very little direct coupling. The linkage is essentially through the sample only, and this fails at the Curie temperature.

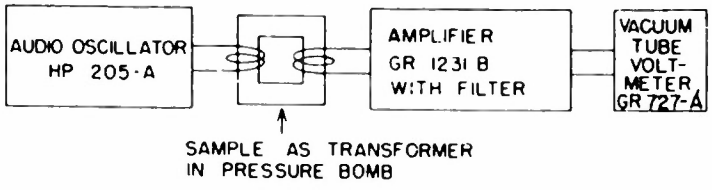

Fig. 4. Schematic diagram of experimental set-up.

A constant 1000 cycle current is supplied to the primary and the signal from the secondary is amplified, then measured as a function of temperature. The primary current was of the order of 0.1 amp, giving a magnetizing field of the order of 1 Oersted; and the secondary volage was amplified to about 10 V, then read on the vacuum-tube voltmeter.

The character of the output curve varies greatly from sample to sample, but usually has the general features of Fig. 5. There is an inflection point between A and B and a very nearly linear portion in most cases from 90% of maximum output to 10%. If the maximum output remains the same under pressure, curves taken at different pressures are simply translated along the temperature axis by the amount of the change of Curie point, and this change is well defined even though the initial permeability curves are not used to define the Curie point itself. If the maximum output should change, a scale adjustment would have to be made before comparing the curves, and the interpretation would not be so simple. Fortunately no change over 10% in the maximum output under pressure ever occurred except in the two cases where it was difficult to get the sample in the usual form and iron was used to complete the magnetic circuit. The initial permeability of Fe at room temperature is depressed by pressure, as was shown by Steinberger;[8] but near the Curie point the initial permeability seems to be unaffected by pressure.

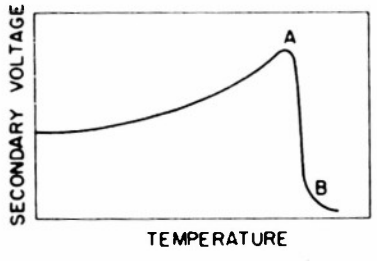

Fig. 5. General form of temperature dependence of voltage in secondary winding.

The temperature range over which the drop from 90% of maximum output to 10% occurs is small in the elements (1.5 for Ni, as can be seen in Fig. 11); and it is small in alloys if the Curie point does not depend much on the composition (as in 68 Permalloy), and it is small if the alloy is very homogeneous (as in Alumel, a fully annealed thermocouple wire). On the other hand Compensator alloy (70 Fe 30Ni) is an example of a sample in which the drop occurs over a wide temperature range; nevertheless, the change under pressure is a simple translation along the temperature axis.

Measurements were made with different primary currents to verify

that changes found were independent of the field. To detect irreversible effects measurements were made with falling and with rising temperatures, and after increases and decreases of pressure. No irreversible changes were found. Measurements were made at several pressures; within experimental error any changes were linear with pressure.

Pressure Equipment

In the application of pressure two separate sets of pressure equipment were used. One is designed to use a liquid as the pressure fluid, and the other is designed to use a gas; these will be referred to as the liquid system and the gas system.

A liquid system has been described by Bridgman.[15] It is used for temperature up to 400°C, and the fact that an external furnace is used to heat the entire pressure bomb means that there is good temperature stability and a large gradient-free experimental region.

The gas system is used for higher temperatures (up to 1120°). No liquid is known which will not decompose or react with other parts of the system at high temperatures, so an inert gas must be used, and argon has been found to be satisfactory. Also the hardened steel of the bombs softens with consequent rupture if it is heated for long periods at high temperatures. Therefore an internal furnace, insulated from the bomb, must be used. A gas system has been described by Yoder.[16]

Furnace Design

For the liquid system the whole bomb is heated externally. With an internal thermocouple it was found to be quite satisfactory to make measurements while allowing the temperature to drift at a rate of several degrees per hour. For Gd the bomb was cooled with dry ice, and measurements were made while it warmed up, which took several hours.

The furnace design for the gas system is much more critical. Three things must be kept in mind—

(1) Insulating material should be of the non-porous type, so as not to be penetrated by the argon under pressure. Lavite was found to be very good. The heat loss is more than doubled if ordinary firebrick is used.

(2) Convection currents in the argon must be cut down to avoid high heat loss, and to achieve stable temperatures. For this purpose, Yoder[16] used a horizontal bomb. With a vertical bomb, the closed top furnace shown in Fig. 6 was found to use only half the power of one which ran the whole length of the lavite cylinder A; and the temperature stability was greatly increased.

(3) All space should be filled. This makes it easier to reach high pressures and also cuts down the convection currents. Lavite was used not only between furnace and bomb (A and D in Fig. 6) but also within the fused quartz cylinder (B and D in Fig. 7) to fill space on both sides of the sample.

The heat capacity of the furnace is small and the heat loss is high under pressure, so it is difficult to hold the temperature constant. Two variacs were used to control the input voltage; the second, in conjunction with a step-down transformer, permitted fine adjustment (7.5 V full scale) and the temperature could be controlled by voltage adjustment so that the rate of drift was about 1° in 3 minutes; this was good enough to permit fairly accurate readings of temperature and secondary output.

Sample Design

In the liquid system the size of sample is limited only by the internal dimensions of the bomb itself, as this region is a uniform temperature. In the gas system, however, the bomb is cool (about 100°C), so only a small

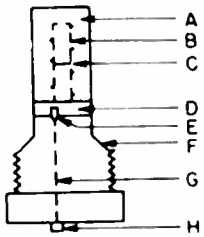

Fig. 6. Plug with furnace and insulation for gas system.
A - Lavite cylinder 3 inches high.
B - Furnace 2-1/2 inches high within lavite insulation.
C - Sample.
D - Lavite plate, insulating furnace from plug.
E - Electrically insulated cone at which a wire enters the high pressure region.
F - Shoulder against which high pressure seal is made.
G - One of seven insulated wires entering bomb.
H - External electrical connection.

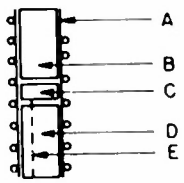

Fig. 7. Furnace with inner parts.
A - Fused quartz tube wound with .015 inch Pt wire.
B - Lavite cylinder above sample.
C - Nickel ring surrounding sample.
D - Lavite cylinder below sample.
E - Electrically insulated wire from sample to cone.

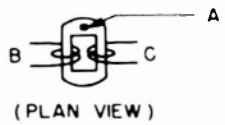

Fig. 8. Sample with windings.
A - Thermocouple junction between two rings.
B and C - Primary and secondary windings.

region at the center of the furnace is gradient-free, and the sample must be quite small. It consisted of two rings of the shape shown in Fig. 8, maximum diameter about 1/2 inch, held together by screws, and with the thermocouple wires between them. Total thickness is about 1/20 inch. Mica rings of the same shape above and below provided insulation for the two windings, which were about 5 turns each of chromel wire. This wire holds its shape well after being bent, and no cement was used. A nickel ring 1/4 inch high (C of Fig. 7) which just fit into the quartz tube, was used to surround the sample in order to smooth out the temperature gradients. This was separated from the sample by mica. When this assmely was placed at the hot spot of the furnace (C of Fig. 6) the sample was free of gradient, as could be verified by the sharp drop of secondary output at the Curie point. When the double ring sample was placed in a temperature gradient the drop accured in two sections, with a plateau at the half-way point. With no gradient in the sample the temperature reading could be considered to be that of the sample, as the thermocouple wires then came out from between the rings for about 1/4 inch in a gradient-free region.

Temperature Measurement

For the liquid system it is convenient to have a thermocouple within the bomb, so that accurate measurements may be made while the temperature is drifting slowly. For the gas system an internal thermocouple is essential because of the large temperature gradients.

Birch[17] has investigated the effect of pressure on thermal emf., and the chromel-alumel couple was found to be independent of pressure within 10 microvolts as far as the calibration was carried (580°C and 4000 Atm). The entire path, including wire in the plug and the insulated cone (G and E in Fig. 6) must be of thermocouple wire. This is especially important in the gas system, as strong temperature gradients exist in just these places. It was

found possible to obtain heavy chromel and alumel wire stock from which the cones were machined. However, there is still the problem that the complete circuit is made up of three different wires (the internal thermocouple, the cone, and the wire in the plug) and a perfect match of thermoelectric powers of these wires is impossible, so that a redistribution of gradients may look like a change of temperature. Such a redistribution does not occur in the liquid system when pressure is applied, but in the gas system the furnace power requirement doubles under pressure, and a redistribution of gradients is certainly to be expected. It was found that nearly all the change in power requirement occurred between 1 and 400 Atm and corresponding to this was an apparent Curie point change of 2 or 3 degrees. Hence measurements below 1000 Atm were not used. Measurements on Ni were made in both systems, and the results checked completely if data above 1000 Atm were used.

It should be emphasized that the precautionary measures are all for the purpose of measuring temperature changes under pressure. The Curie temperature itself does not enter into the experimental results, and need not be known very accurately.

It will be noticed that measurements have been made using the thermocouple beyond its calibrated range; both temperature and pressure exceed the limits of Birch's calibration. The assumption is made that the thermoelectric power continues to be independent of pressure, but it would be desirable to have an extension of the calibration.

Pressure Measurements

Pressure measurements are made by finding the change in resistance of a manganin wire gauge; this is the standard method and has been well calibrated.[18] The uncertainty (of about 0.1%) is insignificant in this experiment.

IV. Results

The results are given in Figs. 9 and 10 and in Table I. Fig. 9 shows the change in Curie point vs pressure for the 8 samples for which the liquid system was used. Consistent results are obtained in each case, although the change is so small for Monel and Alumel that it is about the same order of magnitude as the uncertainty in Birch's pressure calibration of the thermocouple. Fig. 10 shows the results for the 5 samples for which the gas system was used, but plotted in a different way. As explained above, the readings for 1 Atm could not be used. Also the reproducibility was not as good as in the liquid system because of slow changes in the rate of heat loss or because of corrosion of the thermocouple wires. Hence it was thought that the best results were those got by noting the change of Curie point following a change of pressure. For this reason the abscissa zero represents the initial pressure, whatever that might be. For example, if the initial pressure was 4000 Atm, a change to 6000 Atm would be recorded as +2000 Atm and the corresponding Curie point change noted. If the pressure were then reduced from 6000 to 2000 Atm the pressure change would be recorded as -4000 Atm.

It will be noticed that there is considerable scatter of the experimental results for all samples for which the gas system was used. In all cases the change of Curie point is of the same order of magnitude as the experimental error. There is also additional uncertainty in the thermocouple readings because these high temperatures go beyond the range of the thermocouple calibration for the pressure effect. However, the results seem to indicate that the change is very much smaller than that predicted for Fe by Kornetzki

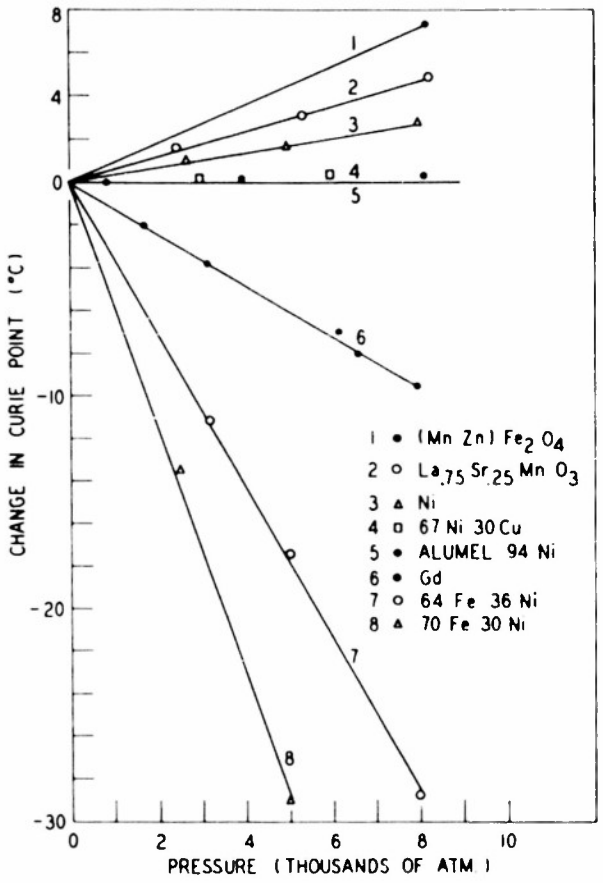

Fig. 9. Change of Curie point vs pressure for 8 samples measured in the liquid system.

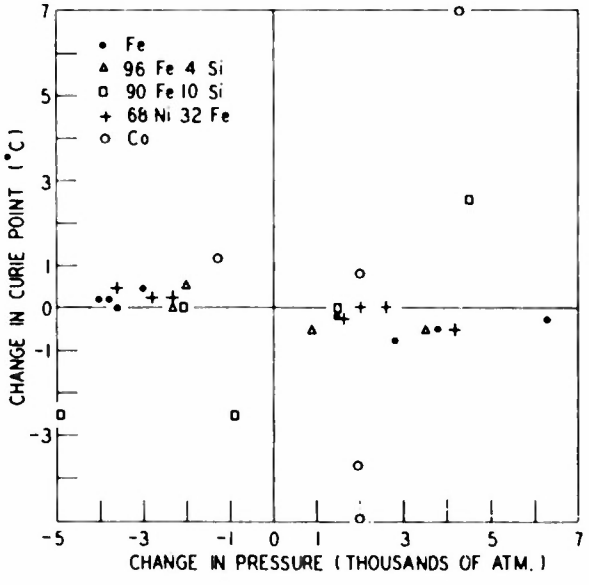

Fig. 10. Change of Curie point vs change of pressure for 5 samples measured in the gas system.

TABLE I

Change of Curie Point with Pressure

Sample	Approx. Curie temp.	Degrees change per 1000 Atm. (+ indicates increase)	Predicted Change
Fe	770	0 ±0.1	0.79 (Ref. 6) 5 to 10 (Ref. 11)
Co	1120	0 ±1	4.6 (Ref. 6)
Ni	360	+0.35 ±0.02	0.13 (Ref. 6) 0.05 (Ref. 13) 0.35 (Ref. 12)
Gd	16	-1.2 ±0.05	
96Fe 4Si	733	-0.1 ±0.1	
90Fe 10Si	615	+0.2 ±0.2	
Compensator 70Fe 30Ni	80	-5.8 ±0.2	5 (Ref. 11)
Invar 64Fe 36Ni	210	-3.6 ±0.1	
Permalloy 68Ni 32Fe	606	-0.1 ±0.1	
Monel	50	+0.07 ±0.03	0.06 (Ref. 9)
Alumel 94 Ni	143	+0.04 ±0.02	
$Mn_{1/2}Zn_{1/2}Fe_2O_4$	90	+0.9 ±0.04	
$La_{.75}Sr_{.25}MnO_3$	80	+0.6 ±0.04	

or for Co by Neel.

Table I lists the change per 1000 Atm of all samples, with an estimate of the experimental error based on the scatter in Figs. 9 and 10. This assumes a linear change of Curie point with pressure, and does not include any error resulting from the effect of pressure on the thermocouple. More detailed information on the probable error can be obtained from the curves of output vs temperature for each sample at different pressures, but these are not reproduced here because of space limitations.

Chemical Analysis of Samples

The Fe and Co were high purity samples obtained from the Institute's metallurgy section, and the Ni was a high purity sample (> 99.9%) obtained from Bell Telephone Labs. The Gd was prepared by A. Moskowitz under the direction of Dr. N. H. Nachtrieb and the largest impurity shown by spectroscopic analysis was 0.1% Fe.

No chemical analysis was obtained for the commercial alloys Monel, Alumel, Invar and Permalloy. The percentages shown in Table I are the usual percentages for these alloys.

The FeSi alloys reported as 96Fe 4Si and 96Fe 10Si were found to have 3.5% and 10.5% respectively of Si. The ferrite was found to be represented approximately by the formula $Mn_{1/2}Zn_{1/2}Fe_2O_4$ (the Mn was 3% short and the Zn was 5% short). The Compensator alloy contained 29.7% Ni. The for-

mula $La_{.75}Sr_{.25}MnO_3$ represents the proportions which went into the preparation of this sample—no analysis was made subsequently.

Discussion of Results

Fe and Fe-Si Alloys. Fe is of special interest because of the decrease of Curie point with pressure of 5 to 10 degrees for 1000 Atm predicted by Kornetzki, using volume magnetostriction measurements made between 20° C and 100° C. Smoluchowski[19] has also treated this problem and he calculated the volume dependence of the Weiss constant from the same data. His calculations are $N^{-1}\, dN/d\omega = 44.1$ at 20° C and $N^{-1}\, dN/d\omega = 32.2$ at 100° C, a marked decrease with rising temperature. If one takes the point of view that interatomic distance, D, is the important factor, and that the decrease of volume dependence with temperature is due to thermal expansion, then the conclusion is that the interaction curve rises sharply at the room temperature value of D in Fe, but has reached the top of the curve at 770° C, for which D is about 1% greater—hence no change of Curie point with pressure in the present experiment. If this is so, a large decrease of Curie temperature could be obtained with a pressure of 50,000 Atm, which would reduce the lattice constant to its room temperature value.

Because 50,000 Atm is not available the experiment was carried out on two Fe-Si alloys. Si reduces the lattice parameter of Fe, and magnetically appears to act as a diluent, leaving the magnetic moment of the Fe atom unchanged up to about 5% Si by weight. The Curie point is lowered, and the combination of reduced D and lower Curie point results in a value of D at the Curie point of the 10% Si alloy which is very nearly that of pure Fe at 20° C. If interatomic distance is the important parameter in magnetic interaction a large decrease of Curie point with pressure should have been observed in the 10% Si alloy, in view of the volume dependence shown by the magnetostriction data.

Cobalt. The result for Co (no change with pressure) is in contradiction to the prediction of Neel (a decrease of 4.6° per 1000 Atm). However, the temperature of 1120° C is far beyond the 580° C to which the pressure calibration of the thermocouple was carried, so the result cannot be regarded with the same certainty as those for the other samples.

Nickel. Although here again the result differs from Neel's prediction, there is rough agreement with predictions based on the volume magnetostriction and on the thermal expansion anomaly. Nickel satisfies all the requirements for good experimental accuracy. The Curie temperature is low enough so that the liquid system may be used, the drop in output occurs within 2°, and there is no significant change in permeability under pressure. Fig. 11 shows the output curves for several pressures.

Gadolinium. For this element the generalized interaction curves must predict an increase with pressure rather than the observed decrease. The inner incomplete shell is in this case the 4f shell with 7 electrons (a half-filled shell), and its small size results in a greater ratio of D/d and a greater value of D-d than for any of the transition metals, Fe, Co or Ni.

Compensator Alloy. This is similar to the alloy which Steinberger reported as becoming paramagnetic under pressure (at room temperature). Kornetzki also predicted a decrease of about 5° per 1000 Atm from volume magnetostriction measurements, which agrees with the results found here.

Some doubts about the effect of phase change in this system had been expressed.[20] However the changes with pressure were found to be instantaneous and reversible and proportional to the applied pressure; hence a

phase change cannot be responsible. X-ray powder pictures showed that the sample was in the 2-phase region; the amount of body-centered (α) phase was estimated to be about 5 or 10 per cent.

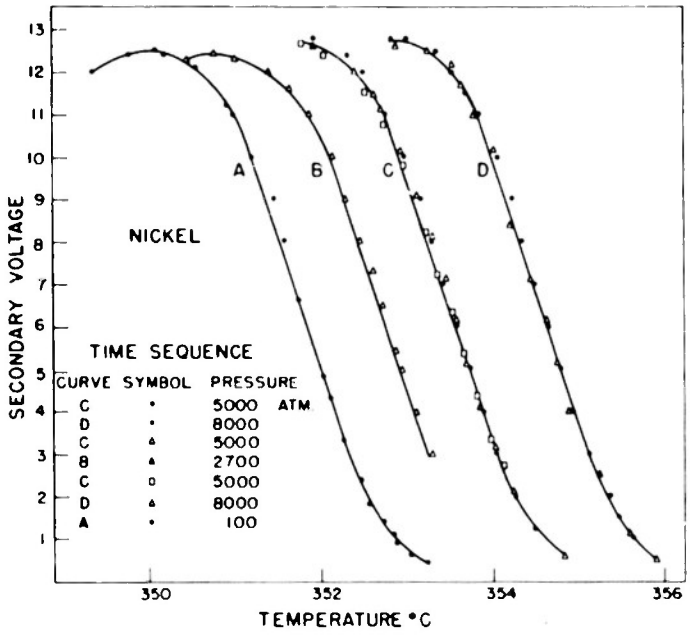

Fig. 11. Secondary voltage vs temperature for Ni at several pressures.

Invar. This alloy is close to Compensator in composition but is a single phase alloy (f.c.c.). The decrease of Curie point with pressure is smaller but of the same order of magnitude. The very abnormal thermal expansion gives a good indication of the result to be expected.

Permalloy. This is another Fe-Ni alloy, but one of the composition having scarcely any thermal expansion anomaly. Hence the negligible change of Curie point with pressure was to be expected.

Monel. The change here is in agreement with that found by Michels et. al.

$La_{.75}Sr_{.25}MnO_3$. For this ceramic type material (perovskita crystal structure) Zener[21] has proposed a formula relating conductivity and Curie point. It would therefore be interesting to compare change of Curie point with change of conductivity under pressure. However, the formula applies only in the temperature range in which the conductivity is metallic, which would be at low temperatures in this case, since the material is a semiconductor at room temperature.

V. Conclusions

The generalized interaction curves shown in Figs. 2 and 3 are not consistent with the results of this experiment. Apart from the objection to plotting the Curie point in Fig. 2 which was mentioned earlier, this curve would predict an increase of Curie point for Gd instead of a decrease, a large decrease for Fe instead of no change, and a larger increase for Ni than was observed.

Neel's predictions for Fe, Co and Ni are not confirmed. Fig. 3 does

not include Gd, but if the same rules had been used for placing it on the curve, Fig. 3 would also predict an increase. In fact, the only element for which both curves would predict the same change would be Gd, and the predicted change would be wrong.

The Forrer correlation would lead one to expect much larger changes than are observed. This suggests that the ferromagnetic range may be much wider than 10% of D in metals, and that the conduction electrons may play a role in the interaction, as outlined by Zener. If this is so it explains the failure of the generalized interaction curves also, as they would then be omitting an important parameter. The results on Fe and the Fe-Si alloys also tend to show that interatomic distance is not an all-important parameter.

One may still suppose that the interaction curve for a single element takes the form of Fig. 1. The fact that some large decreases of Curie point with pressure have been found but no large increases suggests that there may be a steep rise of the interaction curve as it crosses over from the antiferromagnetic region, but only a gradual fall at large D. This is supported by the fact that there are no large values of negative volume magnetostriction reported, nor large positive thermal expansion anomalies.

VI. Acknowledgments

The writer wishes to thank his sponsor, Dr. A. W. Lawson, for advice and discussions of the problem.

Thanks are due to various people for samples and assistance in the preparation of samples. Dr. R. M. Bozorth of Bell Telephone Laboratories supplied three of the samples. Dr. N. H. Nachtrieb and A. Moskowitz prepared the Gd and perovskite samples. Messrs. K. K. Ikeuye and E. Selmanoff prepared the FeSi alloy and gave assistance with other samples. Messrs. N. D. Nachtrieb and K. Lindholm assisted in preparing a number of samples.

This research was supported in part by the Office of Naval Research.

References

1. J. C. Slater, Phys. Rev. 36, 57 (1930).
2. A. Sommerfeld and H. A. Bethe, Handbuch der Physik, 2nd Ed., Vol. XXIV/2, p. 596.
3. C. Zener, Phys. Rev. 81, 440 (1951).
4. R. Forrer, Ann. phys. 7, 605 (1952).
5. R. M. Bozorth, "Ferromagnetism" (D. Van Nostrand Co. Inc. 1951); R. M. Bozorth, Bell System Tech. J. 19, 1 (1940).
6. L. Neel, "Le Magnetisme" Vol. 2, p. 65 (Univ. de Strasbourg 1939).
7. L. H. Adams and J. W. Green, Phil. Mag. 12, 361 (1931).
8. R. L. Steinberger, Physics 4, 153 (1933).
9. A. Michels et al., Physica 4, 1007 (1937). A. Michels and J. Strijland, Physica 8, 53 (1941).
10. F. Ebert and A. Kussman, Physik. Z. 39, 598 (1938).
11. M. Kornetzki, Physik. Z. 44, 296 (1943).
12. A. Michels and S. R. de Groot, Physica 16, 249 (1950).
13. J. C. Slater, Phys. Rev. 58, 54 (1940).
14. M. Kornetzki, Z. Physik 98, 289 (1935).
15. P. W. Bridgman, "The Physics of High Pressure" (Bell — 1949).
16. H. Yoder, Trans. Am. Geophys. Union 31, 827 (1950).
17. F. Birch, Rev. Sci. Inst. 10, 137 (1939).
18. David Lazarus, Phys. Rev. 76, 545 (1949).

19. R. Smoluchowski, Phys. Rev. 59, 309 (1941); 60, 249 (1941).
20. R. M. Bozorth,"Ferromagnetism", p. 726 (D. Van Nostrand Co. 1951).
21. C. Zener, Phys. Rev. 82, 403 (1951).

XIV

PUBLICATIONS
INSTITUTE FOR THE STUDY OF METALS

1946

On the Possible Use of Brownian Motion for Low Temperature Thermometry - A. W. Lawson and E. A. Long, Physical Review, 70, 220 (1946).

Further Remarks on the Possible Use of Brownian Motion in Low Temperature Thermometry - A. W. Lawson and E. A. Long, Physical Review, 70, 977 (1946).

A Theoretical Criterion for the Initiation of Slip Bands - C. Zener, Physical Review, 69, 128 (1946).

A Thermodynamic Criterion for the Fracture of Metals - A Criticism - C. Zener, Physical Review, 70, 225 (1946).

1947

A Low Temperature Transformation in Lithium - C. S. Barrett, Physical Review, 72, 245 (1947).

The Electron Microscope and its Application to Metals (chapter in Electronic Methods of Inspection of Metals, A.S.M., 1947) - C. S. Barrett.

Grain Growth in Alpha Brass - J. E. Burke, Journal of Applied Physics, 18, 1028 (1947).

The Formation of Uranium Hydride - J. E. Burke and C. S. Smith, Journal of the American Chemical Society, 69, 2500 (1947).

Spectrochemical Analysis by the Copper Spark Method - M. Fred, N. H. Nachtrieb and F. S. Tompkins, Journal of the Optical Society of America, 37, 279 (1947).

Experimental Evidence of the Viscous Behavior of Grain Boundaries in Metals - T. S. Kê, Physical Review, 71, 533 (1947).

Stress Relaxation Across Grain Boundaries in Metals - T. S. Kê, Physical Review, 72, 41 (1947).

On Simple Binary Solid Solutions - A. W. Lawson, Journal of Chemical Physics, 15, 831 (1947).

Note on the Efficiency of Radiation Shields - A. W. Lawson and R. Fano, Review of Scientific Instruments, 18, 727 (1947).

Proportioning Temperature Controller - D. Lazarus and A. W. Lawson, Review of Scientific Instruments, 18, 730 (1947).

On a Connection Between the Fountain Effect, Second Sound and Thermal Conductivity in Liquid Helium II - L. Meyer and W. Band, Physical Review, 71, 828 (1947).

Trends in Metallurgical Research - C. S. Smith, American Iron and Steel Institute (1947).

The Magnetic Quenching of Superconductivity - J. W. Stout, Physical Review, 71, 741 (1947).

Stress Induced Preferential Orientation of Pairs of Solute Atoms in Metallic Solid Solution - C. Zener, Physical Review, 71, 34 (1947).

A Defense of the Cauchy Relations - C. Zener, Physical Review, 71, 323 (1947).

Contributions to the Theory of Beta-Phase Alloys - C. Zener, Physical Review, 71, 846 (1947).

Mechanical Behavior of High Damping Metals - C. Zener, Journal of Applied Physics, 18, 1022 (1947).

1948

Second Sound and the Heat Conductivity in Helium II - W. Band and L. Meyer, Physical Review, 73, 226 (1948).

The Influence of Relaxation on the Two Velocity Field Model of Helium II - W. Band and L. Meyer, Physical Review, 74, 386 (1948).

A New Modification of Sodium - C. S. Barrett, American Minerologist, 33, 749 (1948).

X-Ray Diffraction (section in Metals Handbook, A.S.M., 1948) - C. S. Barrett.

Low Temperature Transformation in Lithium and Lithium-Magnesium Alloys - C. S. Barrett and O. R. Trautz, Trans. A.I.M.E. 175, 579 (1948); (T.P. No. 2346, Metals Technology, 1948).

The Nature of Strain Markings in Alpha-Brass - J. E. Burke and C. S. Barrett, Trans. A.I.M.E. 175, 117 (1948); (T.P. No. 2327, Metals Technology, 1948).

The Effect of Deformation on Grain Growth in Alpha-Brass - J. E. Burke and Y. G. Shiau, Trans. A.I.M.E., 175, 141 (1948).

Extension of De Barr's Analysis of Radiation Shielding - J. B. Garrison and A. W. Lawson, Review of Scientific Instruments, 19, 574 (1948).

Activity Coefficients in Alpha-Brass from Statistical Thermodynamics - L. Guttman, Trans. A.I.M.E., 175, 178 (1948).

Spectrographic Determination of Rare Earth Elements in Uranium Compounds - R. Hirt and N. H. Nachtrieb, Analytical Chemistry, 20, 1077 (1948).

The Elastic Constants of Beta-Brass - D. Lazarus, Physical Review, 74, 1726 (1948).

On the Structure of Grain Boundaries in Metals - T. S. Kê, Physical Review, 73, 267 (1948).

Internal Friction in the Interstitial Solid Solutions of C and O in Tantalum - T. S. Kê, Physical Review, 74, 7 (1948).

Stress Relaxation by Interstitial Atomic Diffusion in Tantalum - T. S. Kê, Physical Review, 74, 16 (1948).

Anelastic Properties of Iron - T. S. Kê, Trans. A.I.M.E., 176, 448 (1948).

Viscous Slip Along Grain Boundaries and Diffusion of Zinc in Alpha-Brass - T. S. Kê, Journal of Applied Physics, 19, 285 (1948).

Internal Friction and Precipitation in the Solid Solution of N in Tantalum - T. S. Kê, Physical Review, 74, 914 (1948).

A Contribution to the Discussion of the Paper: John Chipman, "Activities in Liquid Metallic Systems" - O. J. Kleppa, Discussions of the Faraday Society, 4, 109 (1948).

Relaxation Theory of Thermal Conduction in Helium II - L. Meyer and W. Band, Physical Review, 74, 394 (1948).

On the Relation Between Fountain Pressure and Heat Current in Helium II - L. Meyer and W. Band, Nature, 162, 67 (1948).

A Possible Explanation for the Anomolous Mechano-Caloric Heat Effects in the Supercritical Flow of He II Through Slits - Lothar Meyer and William Band, Physica (The Hague), XIV, 63 (1948).

Simultaneous Photography of Two Wave-Length Ranges in Spectrochemical Analysis - N. H. Nachtrieb, J. G. Conway, E. D. Wilson, and S. Wexler, Analytical Chemistry, 20, 282 (1948).

The Extraction of Ferric Chloride by Isopropyl Ether. Parts I and II - N. H. Nachtrieb and J. G. Conway (Part I); N. H. Nachtrieb and R. E. Fryxell (Part II), Journal of the American Chemical Society, 70, 3547 (1948).

Note on the Distribution of Sulfur Between Molten Iron and Slag - T. Rosenqvist, Trans. A.I.M.E., 176, 541 (1948).

Activities in Liquid Metallic Solutions. A Discussion to a Paper by John Chipman – T. Rosenqvist, Discussions Faraday Society, 4, 110 (1948).

The Temperature Coefficient of the Surface Tension of Liquid Metals – A. Skapski, Journal of Chemical Physics, 16, 386 (1948).

The Surface Tension of Liquid Metals – A. Skapski, Journal of Chemical Physics, 16, 389 (1948).

Grains, Phases and Interfaces: An Interpretation of Microstructure – C. S. Smith, Trans. A.I.M.E., 175, 15 (1948).

Characteristics of the Dropping Mercury Electrode in Fused Salts – M. Steinberg and N. H. Nachtrieb, Journal of the American Chemical Society, 70, 2613 (1948).

Second Order Transformations in Two Component Systems; Application to Solutions of Helium III in Helium IV – J. W. Stout, Physical Review, 74, 605 (1948).

Twinning in Tetragonal Alloys of Copper and Manganese – F. T. Worrell, Journal of Applied Physics, 19, 929 (1948).

On the Micromechanism of Fracture (chapter in Fracturing of Metals, A.S.M., 1948) – C. Zener.

Elasticity and Anelasticity of Metals – C. Zener (University of Chicago Press, 1948).

Theory of Strain Interaction of Solute Atoms – C. Zener, Physical Review, 74, 639 (1948).

1949

Anomalous Adsorption of Helium at Liquid Helium Temperatures – W. Band, Physical Review (Letter to the Editor), 76, 441 (1949).

Transport Phenomena in the Bose-Einstein Gas – W. Band, Physical Review, 75, 1937 (1949).

Non-Equilibrium Phenomena in Bose-Einstein Gas – W. Band, Physical Review, 76, 558 (1949).

Non-Equilibrium States in Helium II – W. Band and L. Meyer, Physical Review, 76, 417 (1949).

Transformations in Pure Metals (chapter in Phase Transformations in Solids, National Research Council) – C. S. Barrett, Wiley & Sons, N. Y.

The Crystallographic Mechanisms of Translation, Twinning and Banding (chapter in Cold Working of Metals, A.S.M., 1949) – C. S. Barrett.

X-Ray Microscopes - C. S. Barrett, Metal Progress, 55, 848 (1949).

Thermodynamic Relations of Immiscibility and Crystallization of Molten Silicates - T. F. W. Barth (Dept. of Geology) and T. Rosenqvist, American Journal of Science, 247, 316 (1949).

Some Factors Affecting the Rate of Grain Growth in Metals - J. E. Burke, Trans. A.I.M.E., 73, 180 (1949).

Fundamentals of Recrystallization and Grain Growth (chapter in Grain Control in Industrial Metallurgy, A.S.M., 1949). - J. E. Burke.

Non-Ferrous Metals (chapter in Marks Handbook of Mechanical Engineering) - J. E. Burke (in press).

Microsampling and Microanalysis of Metals - D. F. Clifton and C. S. Smith, Review of Scientific Instruments, 20, 583 (1949).

Preparation of Samples of Active Metals - D. F. Clifton, Review of Scientific Instruments, 20, 830 (1949).

The Influence of Temperature on the Affinity of Sulfur for Copper, Manganese, and Iron - E. M. Cox, M. C. Bachelder, N. H. Nachtrieb, and A. S. Skapski, Trans. A.I.M.E., 185, 27 (1949).

Precipitation Phenomena in the Solid Solutions of Nitrogen and Carbon in Alpha Iron Below the Eutectoid Temperature - L. J. Dijkstra, Trans. A.I.M.E., 185, 252 (1949).

A Nucleation Problem in Ferromagnetism - L. J. Dijkstra (Symposium on Thermodynamics, A.S.M., 1949).

Metallographic Examination of Zinc from Athens - Marie Farnsworth, C. S. Smith, and J. L. Rodda, Hesperia: Suppl. VIII, 126 (1949).

The Extraction of Gallium Chloride by Isopropyl Ether - R. E. Fryxell and N. H. Nachtrieb, Journal of the American Chemical Society, 71, 4035 (1949).

An Absolute Noise Thermometer for High Temperature and Pressure - J. B. Garrison and A. W. Lawson, Review of Scientific Instruments, 20, 763 (1949).

The Thermodynamical Treatment of Very Small Solid Solubilities - L. Guttman. Trans. A.I.M.E. 185, 740 (1949).

Structure and Nature of Kink Bands in Zinc - J. B. Hess and C. S. Barrett, Trans. A.I.M.E., 185, 599 (1949).

Grain Boundary Relaxation and the Mechanism of Embrittlement of Copper by Bismuth - T. S. Kê, Journal of Applied Physics, 20, 1226 (1949).

Grain Boundary Model and the Mechanism of Viscous Intercrystalline Slip - T. S. Kê, Journal of Applied Physics, 20, 276 (1949).

Apparatus for Measurement of Extremely High Internal Friction - T. S. Kê and M. Ross, Review of Scientific Instruments, 20, 795 (1949).

Analysis of the Temperature Coefficient of Shear Modulus of Aluminum - T. S. Kê, Physical Review, 76, 579 (1949).

Ultrasonic Velocities of Sound in Some Liquid Metals - O. J. Kleppa, Journal of Chemical Physics, 17, 668 (1949).

A Thermodynamic Study of Liquid Metallic Solutions. I. The System Lead-Gold - O. J. Kleppa, Journal of the American Chemical Society, 71, 3275 (1949).

An X-Ray Camera for Obtaining Powder Pictures at High Pressures - A. W. Lawson and N. A. Riley, Review of Scientific Instruments, 20, 763 (1949).

High Pressure Allotropic Modification of Cerium - A. W. Lawson and Lee-Ting Tang, Physical Review, 76, 301 (1949).

The Variation of the Adiabatic Elastic Constants of KCl, NaCl, CuZn, and Al with Pressure to 10,000 Bars - D. Lazarus, Physical Review, 76, 545 (1949).

Anomalous Adsorption of Helium at Liquid Helium Temperatures - E. A. Long and L. Meyer, Physical Review (Letter to the Editor), 76, 440 (1949).

Plastic Deformation Waves in Aluminum - A. W. McReynolds, Trans. A.I.M.E., 185, 32 (1949).

Effects of Stress and Deformation on the Martensite Transformation - A. W. McReynolds, Journal of Applied Physics, 20, 896 (1949).

Der gegenwärtige Stand des Helium II Problems - L. Meyer and W. Band, Die Naturwissenschaften, 36, 5 (1949).

Aluminum Overgrowths - T. N. Rhodin, Jr., Crystal Growth Symposium, Discussions of the Faraday Society, 5, 215 (1949).

Oriented Arrangements of Thin Aluminum Films on Ionic Substrates - T. N. Rhodin, Jr., Gordon Research Conference on Corrosion (1948), Trans. A.I.M.E., 185, 371 (1949).

Corrosion -- Review of Fundamentals - W. D. Robertson, Encyclopedia of Chemical Technology, 4, 487 (1949).

A Thermodynamic Investigation of the System Silver/Silver-Sulphide - T. Rosenqvist, Trans. A.I.M.E., 185, 451 (1949).

Determination of Preferred Orientation in Flat Transmission Samples Using a Geiger Counter X-Ray Spectrometer - L. G. Schulz, Journal of Applied Physics, 20, 1033 (1949).

A Direct Method of Determining Preferred Orientation of a Flat Reflection Sample Using a Geiger Counter X-Ray Spectrometer - L. G. Schulz, Journal of Applied Physics, 20, 1030 (1949).

The Structure and Growth of Evaporated LiF and NaCl Films on Amorphous Substrates - L. G. Schulz, Journal of Chemical Physics, 17, 1153 (1949).

Preferred Orientation in Rolled and Recrystallized Beryllium - A. Smigelskas and C. S. Barrett, Trans. A.I.M.E., 185, 145 (1949).

On Blowing Bubbles for Bragg's Dynamic Crystal Model - C. S. Smith, Journal of Applied Physics (Letter to the Editor), 20, 631 (1949).

Solid Nuclei in Liquid Metals - C. S. Smith, Trans. A.I.M.E., 185, 204 (1949).

Bergwerk und Probierbüchlein - C. S. Smith and A. Sisco, A.I.M.E., New York (1949).

Studies of Interface Energies in Some Aluminum and Copper Alloys - C. S. Smith and K. K. Ikeuye, Trans. A.I.M.E., 185, 762 (1949).

Solutions of He^3 and He^4 - J. W. Stout, Physical Review, 76, 864 (1949).

Paramagnetic Anisotropy of Manganous Fluoride - J. W. Stout and Maurice Griffel, Physical Review, 76, 144 (1949).

Precipitation from Solid Solution of Carbon and Nitrogen in α-Iron - C. Wert, Journal of Applied Physics, 20, 943 (1949).

Interstitial Atomic Diffusion Coefficients - C. Wert and C. Zener, Physical Review, 76, 1169 (1949).

Dynamics of Slip Bands (chapter in Cold Working of Metals, A.S.M., 1949) - C. Zener.

Theory of Growth of Spherical Precipitates from Solid Solution - C. Zener, Journal of Applied Physics, 20, 950 (1949).

Relation between Residual Strain Energy and Elastic Moduli - C. Zener, Acta Crystallographica, 2, 163 (1949).

Relaxation Phenomena in Metals - C. Zener, Physica, 15, 111 (1949).

1950

X-ray Analysis (chapter in Handbook of the American Society for Experimental Stress Analysis) - C. S. Barrett (1950).

Faults in the Structure of Copper-Silicon Alloys - C. S. Barrett, Trans. A.I.M.E., 188, 123 (1950).

Transformation Characteristics of a Lithium-Magnesium Alloy - C. S. Barrett and D. F. Clifton, Trans. A.I.M.E., 188, 1329 (1950).

The Crystallography of Cubic-Tetragonal Transformation in the Indium-Thallium System - J. S. Bowles, C. S. Barrett and L. Guttman, Trans. A.I.M.E., 188, 1478 (1950).

The Formation of Annealing Twins - J. E.Burke, Trans. A.I.M.E., 188, 1324 (1950).

Low Temperature X-ray Diffraction Apparatus - D. F. Clifton, Review of Scientific Instruments, 21, 339 (1950).

Effect of Inclusions on Coercive of Iron - L. Dijkstra and C. Wert, Physical Review, 79, 979 (1950).

Preparation of Single Crystals of Manganous Fluoride. The Crystal Structure from X-ray Diffraction. The Melting Point and Density - Maurice Griffel and J. W. Stout - Journal of the American Chemical Society, 72, 4351 (1950).

The Magnetic Anisotropy of Manganous Fluoride Between 12 and 295°K - Maurice Griffel and J. W. Stout, Journal of Chemical Physics, 18, 1455 (1950).

Crystal Structures and Transformations in Indium-Thallium Solid Solutions - L. Guttman, Trans. A.I.M.E., 188, 1472 (1950).

A Ferroelectric Curie Point in KTaO at Very Low Temperatures - J. K. Hulm, B. T. Matthias and E. A. Long, Physical Review, 79, 885 (1950).

The Ionization of Hydrogen in Metals - Irvin Isenberg, Physical Review, 79, 736 (1950).

The Virial Theorem and the Variation Principle - Irvin Isenberg, Physical Review, 79, 737 (1950).

Internal Friction of Metals at Very High Temperatures - T. S. Kê, Journal of Applied Physics, 21, 414 (1950).

Anomalous Internal Friction Associated with the Precipitation of Copper in Cold-Worked Al-Cu Alloys - T. S. Kê, Physical Review, 78, 420 (1950).

Internal Friction of Cold-Worked Metals at Various Temperatures - T. S. Kê, Trans. A.I.M.E., 188, 575 (1950).

A Study of Recrystallization and Grain Growth by Measurement of Internal Friction - T. S. Kê, Trans. A.I.M.E., 188, 581 (1950).

A Thermodynamic Study of Liquid Metallic Solutions. II. The System Tin-Gold - O. J. Kleppa, Journal of the American Chemical Society, 72, 3346 (1950).

Ultrasonic Velocities of Sound in Some Metallic Liquids. Adiabatic and Isothermal Compressibilities of Liquid Metals at their Melting Points – O. J. Kleppa, Journal of Chemical Physics, 18, 1331 (1950).

Ultrasonic Velocities of Sound at 12 Mc in Liquid Sulfur – O. J. Kleppa, Journal of Chemical Physics, 18, 1303 (1950).

A Diamond Bomb for Obtaining Powder Pictures at High Pressures – A. W. Lawson and Ting-Yuan Tang, Review of Scientific Instruments, 21, 815 (1950).

On Equations of State and the Phase Diagrams of Simple Binary Alloys – A. W. Lawson (chapter in Thermodynamics in Physical Metallurgy, A.S.M., Cleveland, 1950).

Thermal Expansion in Silver Halides – A. W. Lawson, Physical Review, 78, 185 (1950).

On Heat Conductivity in Liquids – A. W. Lawson, Journal of Chemical Physics, 18, 1421 (1950).

Superfluidity and Thermomechanical Effect in Adsorbed Helium II Film – Earl Long and Lothar Meyer, Physical Review, 79, 1031 (1950).

Effect of Pressure on the Low Frequency Dielectric Constant of Ionic Crystals – Sumner Mayburg, Physical Review, 79, 375 (1950).

The Reaction of Graphite with Oxygen, Carbon-Dioxide and Water Vapor – L. Meyer, Colloquium on the Combustion of Carbon, Nancy, France (1949), Journal Chimie Physique, 47, 328 (1950).

Principles and Practice of Spectrochemical Analysis – N. H. Nachtrieb, McGraw-Hill, New York (1950).

A Study of Amplitude-Dependent Internal Friction Arising from the Motion of Dislocations in Single Crystals of Copper – A. S. Nowick (Paper in Symposium on the Plastic Deformation of Crystalline Solids, O.N.R., Pittsburgh, 1950).

Studies of Copper Surfaces by Low Temperature Adsorption Isotherms – T. N. Rhodin, Jr., Journal of the American Chemical Society, 72, 4343 (1950).

Single Crystal Copper Surfaces – T. N. Rhodin, Jr., Journal of Applied Physics, 21, 971 (1950).

Low Temperature Oxidation of Copper. I. Physical Mechanism – T. N. Rhodin, Jr., Journal of the American Chemical Society, 72, 5102 (1950).

The Anisotropy of Nitrogen Adsorption on Single Crystal Copper Surfaces – T. N. Rhodin, Jr., Journal of the American Chemical Society, 72, 5691 (1950).

Preferred Orientation as a Factor in Intergranular Corrosion – W. D. Robertson, Trans. A.I.M.E., 188, 791 (1950).

Correlation of Ionic and Atomic Radii with the Heat of Hydration - W. D. Robertson, Journal of Chemical Physics, 18, 1365 (1950).

The Activity of Sulphur in Liquid Steel; The Influence of Copper - T. Rosenqvist and E. M. Cox, Trans. A.I.M.E., 188, 1389 (1950).

Accurate Thickness Measurements with a Fabry-Perot Interferometer - L. G. Schulz, Journal of the Optical Society of America (Letter to the Editor), 40, 177 (1950).

Interferometric Method for Accurate Thickness Measurements of Thin Evaporated Films - L. G. Schulz, Journal of the Optical Society of America, 40, 690 (1950).

Examination of Thin Overgrowths by Multiple Scattering of Electrons - L. G. Schulz, Journal of Applied Physics (Letter to the Editor), 21, 942 (1950).

Polymorphism of Cesium and Thallium Halides - L. G. Schulz, Journal of Chemical Physics (Letter to the Editor), 18, 996 (1950).

Experimental Study of the Change in Phase Accompanying Reflection of Light from Thin Evaporated Films - L. G. Schulz and E. J. Scheibner, Journal of the Optical Society of America, 40, 761 (1950).

A Decade for Metallurgical Science - C. S. Smith, Review for Metal Progress, October 1950.

Alloys of Copper and Iron - C. S. Smith and E. W. Palmer, Trans. A.I.M.E., 188, 1486 (1950).

Undercooling of Minor Liquid Phases in Binary Alloys - C. S. Smith and C. C. Wang, Trans. A.I.M.E., 188, 136 (1950).

Polarography in Fused Salts - Martin Steinberg and Norman H. Nachtrieb, Journal of the American Chemical Society, 72, 3558 (1950).

The Magnetic Anisotropy of α-$NiSO_4 \cdot 6H_2O$ between 13 and 295°K. A Torsion Balance for Magnetic Anisotropy Measurements - J. W. Stout and Maurice Griffel, Journal of Chemical Physics, 18, 1449 (1950).

Meissner Effect in Superconducting Alloys of Indium and Thallium - J. W. Stout and L. Guttman, Physical Review, 79, 396 (1950).

Phenomena Accompanying Precipitation from Solid Solutions of C and N in Alpha-Iron (chapter in Thermodynamics in Physical Metallurgy, A.S.M., 1950) - C. Wert.

Measurements on the Diffusion of Interstitial Atoms in B.C.C. Lattices - C. Wert, Journal of Applied Physics, 21, 1196 (1950).

Diffusion Coefficient of C.in α-Iron - C. Wert, Physical Review, 79, 601 (1950).

Solid Solubility of C in α-Iron, C. Wert, Trans. A.I.M.E., 188, 1242 (1950).

Interference of Growing Precipitate Particles, C. Wert and C. Zener, Journal of Applied Physics, 21, 5 (1950).

Ring Diffusion in Metals, C. Zener, Acta Crystallographica, 3, 346 (1950).

The Role of Statistical Mechanics in Physical Metallurgy, C. Zener, (chapter in Thermodynamics in Physical Metallurgy, A.S.M. 1950).

1951

BARRETT, C. S. (Section Editor for Metals), Structure Reports for 1947-48 (Vol. 11) International Union of Crystallography, N.V.A. Oosthoek's, Uitgevers MIJ, Utrecht (1951).

BOWLES, J. S., Metallographic Study of the Martensite Transformation in Lithium, Trans. A.I.M.E. 189, 44-6 (1951).

———, The Crystallographic Mechanism of the Martensite Reaction in Iron-Carbon Alloys, Acta Cryst. 4, 162-71 (1951).

BRAIDWOOD, R. J., J. E. BURKE, and NORMAN H. NACHTRIEB, Ancient Syrian Coppers and Bronzes, J. Chem. Educ. 28, 87-96 (1951).

BURKE, J. E. See Braidwood, R. J.

CHRISTY, R. W., and A. W. LAWSON, High Temperature Specific Heat of AgBr, J. Chem. Phys. 19, 517 (1951).

CLIFTON, DONALD F. See Kleppa, O. J.

DORFMAN, LEON M. See Gomer, Robert.

GOMER, ROBERT, Wall Reactions and Diffusion in Static and Flow Systems, J. Chem. Phys. 19, 284-9 (1951).

———, A Novel Method for the Estimation of Very Low Pressures, J. Chem. Phys. 19, 1072-3 (1951).

GOMER, ROBERT, and LEON M. DORFMAN, Concerning the Steric Factor of Free Radical Reactions, J. Chem. Phys. 19, 136 (1951).

HESS, JAMES B., A Modification of Cohen Procedure for Computing Precision Lattice Constants from Powder Data, Acta Cryst. 4, 209-15 (1951).

HSU, YEE-CHANG, Relation of Antiferromagnetic Structure to Binding Energies of Some b.c.c. Transition Metals, Phys. Rev. 83, 975-9 (1951).

HULM, J. K. See Matthias, B. T.

HULM, J. K., and B. T. MATTHIAS, New Superconducting Borides and Nitrides, Phys. Rev. 82, 273-4 (1951).

ISENBERG, IRVIN, Overlap Forces and Elastic Constants of Body-Centered Cubic Metals, Phys. Rev. 83, 637-40 (1951).

KEYES, ROBERT W., The Electrical Conductivity of Liquid Germanium, Phys. Rev. 84, 367-8 (1951).

KLEPPA, O. J. A Thermodynamic Study of Liquid Metallic Solutions, III. The Systems Bismuth-Gold and Thallium-Gold, J. Am. Chem. Soc. 73, 385-90 (1951).

KLEPPA, O. J. and DONALD F. CLIFTON, Low Temperature Instability of Intermetallic Phases, Acta Cryst. 4, 74 (1951).

KLEPPA, O. J. and J. A. WEIL, The Solubility of Copper in Liquid Lead Below 950°, J. Am. Chem. Soc. 73, 4848-52 (1951).

LAWSON, A. W. See Christy, R. W.; Smith, A. H.

LONG, EARL. See Meyer, Lothar; Strauss, A. J.

LONG, EARL, and LOTHAR MEYER, The Vapor Pressure of Liquid Helium at the Lambda-Point, Phys. Rev. 83, 860 (1951).

MATTHIAS, B. T. Ferroelectricity, Science 113, 591-6 (1951).

———, See also Hulm, J. K.

MATTHIAS, B. T. and J. K. HULM, New Ferroelectric Tartrates, Phys. Rev. 82, 108-9 (1951).

MEYER, LOTHAR. See Long, Earl; Strauss, A. J.

MEYER, LOTHAR, and EARL LONG, On the Thermo-Mechanical Effect in Adsorbed Layers of Helium II, Phys. Rev. 84, 551-2 (1951).

NACHTRIEB, NORMAN H. See Braidwood, R. J.; Saltman, William M.

NOWICK, A. S., The Production and Detection of a Non-Equilibrium Number of Vacancies in a Metal, Phys. Rev. 82, 551-2 (1951).

———, Anelastic Effects Arising from Precipitation in Aluminum-Zinc Alloys, J. Appl. Phys. 22, 925-33 (1951).

———, A Reinterpretation of Experiments on Intermetallic Diffusion, J. Appl. Phys. 22, 1182-6 (1951).

RADAVICH, JOHN, and CHARLES WERT, Study of Precipitates of C and N in Iron with an Electron Microscope, J. Appl. Phys. 22, 367-71 (1951).

RHODIN, T. N., JR., Low Temperature Oxidation of Copper. II. Reaction Rate Anisotropy, J. Am. Chem. Soc. 73, 3143-6 (1951).

RILEY, N. A. See Smith, A. H.

ROBERTSON, W. D. Molybdate and Tungstate as Corrosion Inhibitors and the Mechanism of Inhibition, J. Electrochem. Soc. 98, 94-100 (1951).

ROSENQVIST, TERKEL, A Thermodynamic Study of the Reaction CaS + $H_2O \rightleftharpoons CaO + H_2S$ and the Desulphurization of Liquid Metals with Lime, Trans. A.I.M.E. 191, 535-40 (1951).

SALTMAN, WILLIAM M., and NORMAN H. NACHTRIEB, Spectrographic Determination of Impurities in Gallium Chloride Solutions, Anal. Chem. 23, 1503-5 (1951).

SCHULZ, L. G., Growth of Alkali Halide Crystals from the Vapor Phase and from Solution onto Substrates of Mica, Acta Cryst. 4, 483-6 (1951).

———, Polymorphism of Cesium and Thallium Halides, Acta Cryst. 4, 487-9 (1951).

———, Polymorphism of RbBr, J. Chem. Phys. 19, 504 (1951).

———, The Effect of Phase Changes in White Light Interferometry, J. Opt. Soc. Am. 41, 261-4 (1951).

———, An Interferometric Method for the Determination of the Absorption Coefficients of Metals, with Results for Silver and Aluminum, J. Opt. Soc. Am. 41, 1047-51 (1951).

SISCO, ANNELIESE G., and CYRIL STANLEY SMITH, Lazarus Ercker's Treatise on Ores and Assaying, translated from the German edition of 1580, University of Chicago Press (1951).

SMITH, A. H., N. A. RILEY, and A. W. LAWSON, A Radiographic Method of Dilatrometry, Rev. Sci. Instr. 22, 138-40 (1951).

SMITH, CYRIL STANLEY. See Sisco, Anneliese G.

SNOW, A. I., The Outer Electron Configuration in Metallic Copper. J. Chem. Phys. 19, 1124-7 (1951).

———, The Experimental Determination of the Distribution of the Valence Electrons in Crystals, Acta Cryst. 4, 481-2 (1951).

STRAUSS, A. J., E. LONG, and L. MEYER, The adsorption of Helium on Fe_2O_3 at Temperatures Below 4.2°K, Proceedings of the International Conference on Low Temperature Physics, Oxford, 1951.

VAN VLACK, L. H., Intergranular Energy of Iron and Some Iron Alloys, J. Metals 3, 251-9 (1951).

WEIL, J. A. See Kleppa, O. J.

WERT, CHARLES. See Radavich, John.

ZENER, CLARENCE, Interaction Between the d-Shells in the Transition Metals, II. Ferromagnetic Compounds of Manganese with Perovskite Structure, Phys. Rev. 82, 403-5 (1951).

_____, Theory of D_o for Atomic Diffusion in Metals, J. Appl. Phys. 22, 372-5 (1951).

1952

ANDERSON, H. L., E. FERMI, E. LONG, R. MARTIN, and D. E. NAGLE, Total Cross Sections of Negative Pions in Hydrogen, Phys. Rev. 85, 934-5 (1952).

ANDERSON, H. L., E. FERMI, E. LONG, and D. E. NAGLE, Total Cross Sections of Positive Pions in Hydrogen, Phys. Rev. 85, 936 (1952).

BARRETT, C. S., "Imperfections from Transformation and Deformation," Chapter in Imperfections in Nearly Perfect Crystals, Wiley, N. Y. (1952) pp. 97-128.

_____, Structure of Metals, Second Edition, McGraw-Hill, N. Y. (1952).

_____ (Section Editor of Metals), Structure Reports for 1949 (Vol. 12) International Union of Crystallography, N. V. A. Oosthoek's, Uitgevers MIJ, Utrecht (1952).

_____. See also Bowles, J. S., and Hess, J. B.

BECK, LILIAN HEIKKINEN, and CYRIL STANLEY SMITH, The Copper-Zinc Constitution Diagram, Redetermined in the Vicinity of the β Phase by Means of Quantitative Metallography, Trans. A.I.M.E. 194, 1079-83 (1952).

BOWLES, J. S., and C. S. BARRETT, "The Crystallography of Transformations," Chapter I in Progress in Metal Physics, Interscience Publishers, N. Y. (1952).

CATALANO, EDWARD. See Nachtrieb, Norman H.

DUNICZ, BOLESLAW L. See Rosenqvist, Terkel.

DUNICZ, BOLESLAW L., and TERKEL ROSENQVIST, Determination of Microgram Quantities of Sulphide Sulphur, Anal. Chem. 24, 404-6 (1952).

FRYXELL, ROBERT E. See Nachtrieb, Norman H.

FRYXELL, ROBERT E., and NORMAN H. NACHTRIEB, Effect of Stress on Metal Electrode Potentials, J. Electrochem. Soc. 99, 495-503 (1952).

GOMER, ROBERT, Velocity Distribution of Electrons in Field Emission. Resolution in the Projection Microscope, J. Chem. Phys. 20, 1772-6 (1952).

GOMER, ROBERT, and JOHN K. HULM, Field Emission from Tantalum in the Normal and Superconducting State, J. Chem. Phys. 20, 1500-2 (1952).

GUTTMAN, LESTER. See Stout, J. W.

GUTTMAN, LESTER, and J. W. STOUT, Superconductivity in MgTl and LiBi, Proceedings of the NBS Semicentennial Symposium on Low-Temperature Physics, March 1951 (NBS Circular No. 519, October 1952) pp. 65-7.

HENNIG, G., and L. MEYER, Search for Low Temperature Superconductivity in Graphite Compounds, Phys. Rev. 87, 439 (1952).

HENRY, W. G., and G. V. RAYNOR, Superlattice Studies in the Systems Silver-Magnesium-Tin and Silver-Magnesium-Zinc, Can. J. Phys. 30, 412-21 (1952).

HESS, J. B., and C. S. BARRETT, Transformation in Cobalt-Nickel Alloys, Trans. A.I.M.E. 194, 645-7 (1952).

HULM, J. K., Heat Transfer in Superconducting Alloys, Proceedings of the NBS Semicentennial Symposium on Low-Temperature Physics, March 1951 (NBS Circular No. 519, October 1952) pp. 37-41.

_____. See also Gomer, Robert, and Matthias, B. T.

JACOBS, I. S., and A. W. LAWSON, An Analysis of the Pressure Dependence of the Dielectric Constant of Polar Liquids, J. Chem. Phys. 20, 1161-4 (1952).

JOHNSTON, W. G. See Meyer, Lothar.

JONES, W. M., JOSEPH GORDON, and E. A. LONG, The Heat Capacities of Uranium, Uranium Trioxide, and Uranium Dioxide from 15°K to 300°K, J. Chem. Phys. 20, 695-9 (1952).

KLEPPA, O. J., A Thermodynamic Study of Liquid Metallic Solutions. IV. Approximate Thermodynamic Data from the Phase Diagram for the Systems Copper-Bismuth, Copper-Lead, and Copper-Thallium, J. Am. Chem. Soc. 74, 6047-51 (1952).

_____, A. Thermodynamic Study of Liquid Metallic Solutions. V. The Systems Zinc-Bismuth and Zinc-Lead. J. Am. Chem. Soc. 74, 6052-6 (1952).

KUBO, RYOGO, Thermal Ionization of Trapped Electrons, Phys. Rev. 86, 929-37 (1952).

_____, The Spin-Wave Theory of Antiferromagnetics, Phys. Rev. 87, 568-80 (1952).

KURNICK, S. W., The Effects of Hydrostatic Pressure on the Ionic Conductivity of AgBr, J. Chem. Phys. 20, 218-28 (1952).

LAWSON, A. W. See Jacobs, I. S., and Nachtrieb, N. H.

LONG, EARL. See Anderson, H. L., Jones, W. M., and Meyer, Lothar.

LONG, EARL, and LOTHAR MEYER, Some Experiments on Flow in the Unsaturated Helium II Film, Phys. Rev. 85, 1030-5 (1952).

_____, Heat Conduction by the Unsaturated Helium II Film, Phys. Rev. 87, 153 (1952).

MATTHIAS, B. T., and J. K. HULM, New Superconducting Compounds, Proceedings of the NBS Semicentennial Symposium on Low-Temperature Physics, March 1951 (NBS Circular No. 519, October 1952) pp. 69-70.

_____, A Search for New Superconducting Compounds, Phys. Rev. 87, 799-806 (1952).

MEYER, LOTHAR. See Hennig, G., and Long, Earl.

MEYER, LOTHAR, and WILLIAM BAND, Theory of Superconductivity by M. von Laue, Translated. Academic Press, Inc., N. Y. (1952).

MEYER, LOTHAR, and EARL LONG, Phase Transitions in Adsorbed Films, Phys. Rev. 85, 1035-7 (1952).

MEYER, LOTHAR, G. S. PICUS, and W. G. JOHNSTON, The Electric Conductivity of Graphite at Liquid Helium Temperatures, Proceedings of the NBS Semicentennial Symposium on Low-Temperature Physics, March 1951 (NBS Circular No. 519, October 1952) pp. 249-52.

NACHTRIEB, NORMAN H. See Fryxell, Robert E.

NACHTRIEB, NORMAN H., EDWARD CATALANO, and JOHN A. WEIL, Self-Diffusion in Solid Sodium, I. J. Chem. Phys. 20, 1185-8 (1952).

NACHTRIEB, NORMAN H., and ROBERT E. FRYXELL, The Extraction of Ferric Chloride by Isopropyl Ether. III. J. Am. Chem. Soc. 74, 897-901 (1952).

NACHTRIEB, NORMAN H., JOHN A. WEIL, and EDWARD CATALANO, Preparation of Radioactive Sodium Metal by Exchange of Na^{23} and $Na^{22}Cl$, J. Am. Chem. Soc. 74, 264 (1952).

NACHTRIEB, N. H., J. A. WEIL, E. CATALANO, and A. W. LAWSON, Self-Diffusion in Solid Sodium. II. The Effect of Pressure, J. Chem. Phys. 20, 1189-94 (1952).

NOWICK, A. S., "Stress Relaxation Across Interfaces," Chapter in Metal Interfaces, American Society for Metals, Cleveland (1952) pp. 248-68.

_____, Anelastic Measurements of Atomic Mobility in Substitutional Solid Solutions, Phys. Rev. 88, 925-34 (1952).

PATERSON, M. S., The Effects of Lattice Imperfections on X-Ray Line Broadening, J. Appl. Phys. 23, 499-500 (1952).

_____, X-Ray Diffraction by Face-Centered Cubic Crystals with Deformation Faults, J. Appl. Phys. 23, 805-11 (1952).

PICUS, G. S. See Meyer, Lothar.

RAYNOR, G. V. See Henry, W. G.

ROBERTSON, W. D., Precipitation of Colloidal Ferric Oxide by Corrosion Inhibitor Ions, J. Phys. Chem. 56, 671-2 (1952).

ROSENQVIST, TERKEL. See Dunicz, Boleslaw L.

ROSENQVIST, TERKEL, and BOLESLAW L. DUNICZ, The Solid Solubility of Sulphur in Iron, Trans. A.I.M.E. 194, 604-8 (1952).

SCHULZ, L. G., Growth of Alkali Halides from the Vapor on Single Crystal Substrates of Alkali Halides, Acta Cryst. 5, 130-2 (1952).

_____, Overgrowth of Alkali Halides on $CaCO_3$ and $NaNO_3$, Acta Cryst. 5, 264-5 (1952).

_____, Oriented Overgrowths of Alkali Halides on Silver Substrates, Acta Cryst. 5, 266-8 (1952).

SMITH, CYRIL STANLEY, "Interfaces between Crystals." Chapter in L'Etat Solide. Report of 19th Solvay Conference on Physics, Brussels (1952) pp. 11-53.

_____, "Grain Shapes and Other Metallurgical Applications of Topology," Chapter in Metal Interfaces, American Society for Metals, Cleveland (1952) pp. 65-113.

_____, "Interphase Interfaces," Chapter in Imperfections in Nearly Perfect Crystals, Wiley, N. Y. (1952) pp. 307-401.

_____, Pure and Applied Science in American Metallurgy, Metal Progress, Jan. 1952, pp. 51-4.

_____. See also Beck, Lilian Heikkinen, and Williams, W. M.

SNOW, A. I., Neutron Diffraction Investigation of the Atomic Magnetic Moment Orientation in the Antiferromagnetic Compound CrSb, Phys. Rev. 85, 365 (1952).

_____, A. Method for Introducing Sublimable Material into a Vacuum System, Rev. Sci. Instr. 23, 246-7 (1952).

STEPHENSON, C. C., R. W. BLUE, and J. W. STOUT, The Nature of the Gradual Transition in NH_4Cl and ND_4Cl, J. Chem. Phys. 20, 1046-7 (1952).

STOUT, J. W. See Guttman, Lester, and Stephenson, C. C.

STOUT, J. W., and LESTER GUTTMAN, Superconducting Properties of Indium-Thallium Alloys, Proceedings of the NBS Semicentennial Symposium on Low-Temperature Physics, March 1951 (NBS Circular No. 519, October 1952) pp. 51-60.

_____, Superconductivity of Indium-Thallium Solid Solutions, Phys. Rev. 88, 703-12 (1952).

___ ___. The Electrical Resistivity of Indium-Thallium Solid Solutions, Phys. Rev. 88, 713-4 (1952).

UHLIR, ARTHUR, J., Thermal Conductivity of Fluid Argon and Nitrogen, J. Chem. Phys. 20, 465-72 (1952).

WALNUT, THOMAS, A Study of Selection Rules for Vibrational Spectra of Complex Crystals, J. Chem. Phys. 20, 58-62 (1952).

WEIL, JOHN A. See Nachtrieb, Norman H.

WILLIAMS, W. M., and CYRIL STANLEY SMITH, A Study of Grain Shape in an Aluminum Alloy and other Applications of Stereoscopic Microradiography, Trans. A.I.M.E. 194, 755-65 (1952).

ZENER, CLARENCE, "Theory of Diffusion in Metals," Chapter in Imperfections in Nearly Perfect Crystals, Wiley, N. Y. (1952) pp. 289-314.

1953

AZIZ, P. M., Radioactive Tracers in the Study of Pitting Corrosion on Aluminum, J. Electrochem. Soc. (in press).

_____. See also Barrett, C. S.

BARRETT, C. S., An Abnormal After-Effect in Metals, Acta Met. 1, 2-7 (1953).

_____, "X-ray Diffraction Techniques," Chapter in Modern Research Techniques in Physical Metallurgy, American Society for Metals, Cleveland (1953), pp. 72-94.

_____, After-Effects in Polycrystalline Cadmium, Trans. A.I.M.E. (in press).

_____. See also Broom, T.

BARRETT, C. S., P. M. AZIZ, and I. MARKSON, Torsional After-Effect Measurement and Applications to Aluminum, Trans. A.I.M.E. (in press).

BERRY, R. L., and G. V. RAYNOR, The Crystal Chemistry of the Laves Phases, Acta Cryst. 6, 178-86 (1953).

BOWERS, RAYMOND, The Adsorption of Gases at High Saturations: I. The Adsorption of Nitrogen, Argon, and Oxygen, Phil. Mag. 44, 467-84 (1953).

_____, The Adsorption of Gases at High Saturations: II. The Thickness of the Unsaturated Helium Film, Phil. Mag. 44, 485-96 (1953).

_____, Thickness of the Saturated Helium II Film, Phys. Rev. 91, 1016-7 (1953).

_____, The Thickness of the Saturated Helium II Film, Phil. Mag. (in press).

BOWERS, RAYMOND, and EARL A. LONG, A Microbalance Assembly for Adsorption Studies at Low Temperatures, Rev. Sci. Instr. (in press).

BROOKS, ALFRED A., A Thermodynamic Study of the Equilibrium 2Cu(s) + $H_2S(g) = Cu_2S$ (γ) + $H_2(g)$, J. Am. Chem. Soc. 75, 2464-7 (1953).

BROOM, T., and C. S. BARRETT, The Effect of Deformation on the Electrical Resistivity of Some Cobalt-Nickel Alloys, Acta Met. 1, 305-9 (1953).

CHRISTY, R. W., Creep of Silver Bromide at High Temperatures, Acta Met. (in press).

DIJKSTRA, L. J., and R. J. SLADEK, Effect of Alloying Elements on the Behavior of Nitrogen in α-Iron, Trans, A.I.M.E. 197, 69-72 (1953).

GIBBONS, DONALD F., The Plastic Deformation of Iron Between 300—77.2°K, Trans. A.I.M.E. (1953) 1245-50.

GOMER, ROBERT, Field Emission from Nickel Surfaces, J. Chem. Phys. 21, 293-303 (1953).

_____, Note on Field Emission, J. Chem. Phys. 21, 764 (1953).

_____, Work Function in Field Emission Chemisorption, J. Chem. Phys. 21, 1869-76 (1953).

_____, Preparation and Some Properties of Conducting Transparent Glass, Rev. Sci. Instr. 24, 993 (1953).

GOMER, ROBERT, and J. K. HULM, A Method for Studying the Mobility of Chemisorbed Films: Oxygen on Tungsten, J. Am. Chem. Soc. 75, 4114-5 (1953).

GOMER, ROBERT, and CYRIL STANLEY SMITH (Editors), Structure and Properties of Solid Surfaces, University of Chicago Press (1953).

GOMER, ROBERT, and DONALD A. SPEER, Molecular Images with the Projection Microscope. The Ionization Potential of Zinc Phthalocyanine, J. Chem. Phys. 21, 73-80 (1953).

GRACE, RICHARD E., Concentration Gradients Associated with Growing Pearlite. Trans. A.I.M.E. 197, 820-1 (1953).

GUTTMAN, LESTER. See Smith, Cyril Stanley.

GUTTMAN, LESTER, and JAMES R. ARNOLD, The Nonparticipation of He^6 in the Superfluidity of He^4, Phys. Rev. 92, 547-51.

HARDY, GEORGE F., and JOHN K. HULM, Superconducting Silicides and Germanides, Phys. Rev. 89, 884 (1953).

HULM, J. K., Thermal Resistivity of Mercury in the Intermediate State, Phys. Rev. 90, 1116 (1953).

_____, Low Temperature Dielectric Properties of Cadmium and Lead Niobates, Phys. Rev. 92, 504-5 (1953).

_____. See also Gomer, Robert; Hardy, George F.; and Matthias, B. T.

JAMIESON, JOHN C., Phase Equilibrium in the System Calcite-Aragonite, J. Chem. Phys. 21, 1385-90 (1953).

KEYES, ROBERT W., The Electrical Properties of Black Phosphorus, Phys. Rev. 92, 580-4 (1953).

KUBO, RYOGO, The Spin-Wave Theory as a Variational Method and its Application to Antiferromagnetism, Revs. Modern Phys. 25, 344-51 (1953).

LAWSON, A. W. See Smith, A. H.

LAWSON, A. W., and LOTHAR MEYER, Light Scattering in Liquid Helium, Phys. Rev. (in press).

LONG, EARL A. See Bowers, Raymond.

LONG, EARL, and LOTHAR MEYER, The Unsaturated Helium Film, Phil. Mag. Suppl. 2, 1-27 (1953).

_____, A Note on the Adsorption of Helium on Glass, Phil. Mag. 44, 788-9 (1953).

MARKSON, I. See Barrett, C. S.

MATARRESE, L. M. See Stout, J. W.

MATTHIAS, B. T., and J. K. HULM, Superconducting Properties of Cobalt Disilicide, Phys. Rev. 89, 439-41 (1953).

MEYER, LOTHAR, The Thickness of the Helium Film, Phys. Rev. (in press).

_____. See also Lawson, A. W., and Long, Earl.

NACHTRIEB, NORMAN H. See Saltman, William M.

NICHOLSON, M. E., Constitution of Iron-Boron Alloys in the Low Boron Range, Trans. A.I.M.E. (in press).

NOWICK, A. S., and R. J. SLADEK, Anelastic Measurement of Atomic Mobility under Non-Equilibrium Conditions, Acta Met. 1, 131-40 (1953).

PICUS, GERALD S., The Transfer Rate of the Liquid Helium II Film Near Zero Level Difference, Phys. Rev. 90, 719-20 (1953).

POCHAPSKY, T. E., Heat Capacity and Thermal Diffusivity of Silver Bromide, J. Chem. Phys. 21, 1539-40 (1953).

_____, Heat Capacity and Resistance Measurements for Aluminum and Lead Wires, Acta Met. (in press).

_____, Determination of Heat Capacity by Pulse Heating, Rev. Sci. Instr. (in press).

RAYNOR, G. V. See Berry, R. L.

RHODIN, T. N., JR., Physical Adsorption on Single Crystal Zinc Surfaces, J. Phys. Chem. 57, 143-8 (1953).

_____, "Surface Studies with the Vacuum Microbalance: Instrumentation and Low Temperature Application," Chapter in Advances in Catalysis, V, Academic Press, N. Y. (1953) pp. 39-117.

ROBERTSON, W. D., The Capacity of Polarized Platinum Electrodes in Hydrochloric Acid, J. Electrochem. Soc. 100, 194-201 (1953).

SALTMAN, WILLIAM M., and NORMAN H. NACHTRIEB, The Electrochemistry of Gallium, J. Electrochem. Soc. 100, 126-30 (1953).

SCHULZ, L. G., Optical Properties of Bismuth in the Near Infra Red, J. Opt. Soc. Am. 43, 406-7 (1953).

SLADEK, R. J., A New Thermal Resistivity Maximum in Superconducting Alloys, Phys. Rev. 91, 1280-1 (1953).

_____. See also Dijkstra, L. J., and Nowick, A. S.

SMITH, A. H., and A. W. LAWSON, The Velocity of Sound in Water as a Function of Temperature and Pressure, J. Chem. Phys. (in press).

SMITH, CYRIL STANLEY, Microstructure (1952 Campbell Memorial Lecture), Trans. Am. Soc. Metals 45, 533-75 (1953).

_____, Further Notes on the Shape of Metal Grains: Space-Filling Polyhedra with Unlimited Sharing of Corners and Faces, Acta Met. 1, 295-300 (1953).

_____, "Pure and Applied Science in Metallurgy." Chapter in: Proceedings of the American Iron and Steel Institute, N. Y. (1953), pp. 11-20.

_____, "Uranium." Chapter in: Modern Uses of Non-Ferrous Metals (C. H. Mathewson, ed.) A.I.M.E., New York (1953), pp. 464-77.

_____. See also Gomer, Robert.

SMITH, CYRIL STANLEY, and LESTER GUTTMAN, Measurement of Internal Boundaries in Three-Dimensional Structures by Random Sectioning. Trans. A.I.M.E. 197, 81-7 (1953).

SNOW, A. I. Magnetic Moment Orientation and Thermal Expansion of Antiferromagnetic CrSb, Revs. Modern Phys. 25, 127 (1953).

SPEER, DONALD A. See Gomer, Robert.

STOUT, J. W., Thermochemistry and the Thermodynamic Properties of Substances, Annual Review of Physical Chemistry 4, 1-22 (1953).

_____, The Thermodynamics of Reversible Galvanic Cells in which the Compositions of Some of the Phases Vary with Temperature, J. Chem. Phys. 21, 1829-30 (1953).

_____, Thermodynamics of Surface Adsorption, Acta Met. (in press).

STOUT, J. W., and EDWARD CATALANO, Thermal Anomalies Associated with the Antiferromagnetic Ordering of FeF_2, CoF_2, and NiF_2, Phys. Rev. (in press).

STOUT, J. W., and L. M. MATARRESE, Magnetic Anisotropy of the Iron-Group Fluorides, Revs. Modern Phys. 25, 338-43 (1953).

COMPLETE CONTENTS FOR 1953 ISSUES

Twenty-Eighth Quarterly Report

Twenty-Ninth Quarterly Report

Page

Thirty-First Quarterly Report